Ecole doctorale biologie santé 446 Lille

Université de Lille

THESE DE DOCTORAT

En vue de l'obtention du grade de Docteur en Science de l'Université de Lille

Aspects moléculaires et cellulaires de la biologie

Présentée par

ALICE CAPUZ

Production d'anticorps par des cellules non-immunitaires

Soutenue à Lille, le 05 décembre 2022

Directeur de Thèse : Pr. Michel SALZET. PRISM, INSERM U1192. Université de Lille.

Co-Encadrant : Dr. Franck RODET. PRISM, INSERM U1192. Université de Lille.

Membre du jury :

Président du jury : Pr. Patrick Vermersch. Univ. Lille, Inserm U1172 LilNCog. CHU Lille.

Rapporteur : Dr. Hélène Castel-Gandolfo. INSERM U1239. Université de Rouen.

Rapporteur : Dr. Virginie Redeker. MIRCen, CEA, CNRS UMR9199. Université Paris-Saclay.

Examinateur : Dr. Chiara Guerrera. SFR Necker INSERM US24. Université de Paris.

Examinateur : Dr. Philippe Marin. CNRS UMR5203, INSERM U1191. Université de Montpellier.

Examinateur : Pr. Vincent Sobanski. INFINITE, INSERM U1286. Université de Lille.

Citations

« Ne confonds pas ton chemin avec ta destination. Ce n'est pas parce que c'est orageux aujourd'hui que cela signifie que tu ne te diriges pas vers le soleil »

Anthony Fernando

« NOBODY's perfect »

Remerciements

Je tiens à adresser tout mon respect et mes sincères remerciements.

Au Professeur Michel SALZET, directeur du laboratoire PRISM, qui m'a accompagné et aidé tout au long de cette thèse. J'ai été ravie d'avoir travaillé en ta compagnie sur ce projet, car outre ton appui scientifique, tu as toujours été présent pour me soutenir et m'encourager.

Au Docteur Franck RODET, maître de conférences au laboratoire PRISM, qui a été présent pour toutes ces années. Je te remercie pour le temps que tu m'as accordé, pour toutes nos discussions et conseils scientifiques que nous avons pu partager.

Aux Dr. Helene Castel-Gandolfo, Dr. Virginie Redeker, Dr. Chiara Guerrera, Dr. Philippe Marin Pr. Vincent Sobanski, et Pr. Patrick Vermersch pour avoir accepté d'être membres de mon jury de thèse et pour leur temps accordés à l'évaluation de mon travail.

À l'ensemble des partenaires et des collaborateurs, dont le Dr Amélie Bonnefond et Mehdi Derhourhi avec qui j'ai pu travail sur ce sujet.

À Sylvain Osien, doctorant 3e année au Laboratoire PRISM, pour avoir été un véritable coéquipier dans les moments forts, comme dans les plus difficiles. Je te souhaite également une bonne soutenance.

À Soulaimane Aboulouard, ingénieur au laboratoire PRISM, qui m'a beaucoup soutenu pendant cette thèse. Tu as toujours été disponible pour m'apporter ton aide et tes conseils m'ont beaucoup aidée. Un grand merci pour les chocolats et les gâteaux qui ont été indispensables pour le moral.

À Marie Leleu, docteur et postdoctorant, pour ton amitié précieuse et ton soutien tout au long de ces années. Nous avons commencé cette histoire dès le master et depuis, tu as toujours été présente dans les bons et les mauvais moments. Je te souhaite le meilleur pour la suite.

À Rémy Le Beillant, Camille Hache et Alice Blanckaert, de véritables amis qui ont toujours été là pour me soutenir et m'encourager. Je vous souhaite de réussir tous vos futurs projets.

À toute ma famille et mon petit chat, pour m'avoir encouragé et aiguillé tout au long de ces années, et qui a toujours été présent, peu importe les difficultés.

A Kamel Bachiri, Tristan Cardon, Paul Chaillou, Etienne Coyaud, Lucille Darras, Marie Duhamel, Jean-Pascal Gimeno, Diego Gracia, Khodor Issa, Laurine Lagache, Estelle Laurent, Léa Ledoux, Christophe Lefebvre, Antonella Raffo Romero, Lucas Roussel, Diala Safar Kantar, Christelle Van Camp, Louise Vansteenkiste, Lydia Ziane Chaouche pour toutes nos discussions et vos conseils. Je vous souhaite de réussir tous vos projets et objectifs futurs.

Enfin, je tiens à remercier l'ensemble du laboratoire pour leur aide, leurs conseils et leur bonne humeur. J'ai pu non seulement avoir une vue sur le monde de la recherche, mais aussi une occasion d'acquérir les compétences nécessaires pour réussir dans cette voie. Ce fut une expérience très instructive. Je vous souhaite à tous une bonne réussite dans vos projets. Merci à vous tous.

Contributions scientifiques

- **Publications**

- Acceptées

The Antibody Dependant Neurite Outgrowth Modulation Response (ADNM) involvement in Spinal Cord Injury.
Capuz A, Karnoub MA, Osien S, Rose M, Mériaux C, Fournier I, Devos D, Vanden Abeele F, Rodet F, Cizkova1 D, Salzet M.
Front Immunol. 2022 Jun 16 ;13:882830. eCollection 2022. doi: 10.3389/fimmu.2022.882830.

PC1/3 KD Macrophages Exhibit Resistance to the Inhibitory Effect of IL-10 and a Higher TLR4 Activation Rate, Leading to an Anti-Tumoral Phenotype.
Rodet F, Capuz A, Ozcan BA, Le Beillan R, Raffo-Romero A, Kobeissy F, Duhamel M, Salzet M. Cells. 2019 Nov 22;8(12):1490. doi: 10.3390/cells8121490.

Deciphering molecular consequences of the proprotein convertase 1/3 inhibition in macrophages for application in anti-tumour immunotherapy.
Rodet F, Capuz A, Hara T, Van Meel R, Duhamel M, Rose M, Raffo-Romero A, Fournier I, Salzet M. J Biotechnol. 2018 Sep 20;282:80-85. Epub 2018 Jul 7. PMID: 29990570 doi: 10.1016/j.jbiotec.2018.07.002.

- En soumission

Heimdall, an alternative protein issued from a ncRNA related to kappa light chain variable region, is a key player in Astrocyte-to-neuron reprogramming
Osien S, Capuz A, Cardon T, Karnoub MA, Aboulouard S, Raffo-Romero A, Duhamel M, Cizkova D, Trerotola M, Devos D, Kobeissy F, Van den Abelle F, Bonnefond A, Fournier I, Rodet F, Salzet M. En revision à Frontiers in immunology

Astrocytes express aberrant immunoglobulins involved as gatekeeper of astrocytes to neuron conversion
Capuz A, Osien S, Karnoub MA, Aboulouard S, Laurent E, Coyaud E, Raffo-Romero A, Duhamel M, Bonnefond A, Derhourhi M, Trerotola M, El Yazidi-Belkoura I, Devos D, Zilkova M, Kobeissy F, Vanden Abeele F, Fournier I, Cizkova D, Rodet F, Salzet M. Soumis à Cell Death & Differentiation

- En préparation

Immunoglobulins production in glioblastomas and characterization of a new IgG5.
Capuz A, Osien S, Aboulouard S, Cardon T, Rodet F, Salzet M.

- **Congrès**

- Présentations orales

Structure Fédérative de Recherche Technologies de Santé et Médicament SFR-TSM, (14 décembre 2020), Faculté de Médecin et Pôle Recherche.

The European Graduate School of Neuroscience (EURON) Webinar (21 Janvier 2021), Maastricht.

Cancer and Cancer Treatments on Cognitive Functions: At the Era of Comprehensive Mechanisms (8 juillet 2022), Cancéro-pôle Nord Ouest, Paris.

European Euro biotechnology congress (5-7octobre 2022), Prague.

- Posters

Structure Fédérative de Recherche Technologies de Santé et Médicament SFR-TSM, (14 décembre 2020), Faculté de Médecine Pôle Recherche.

Structure Fédérative de Recherche Technologies de Santé et Médicament SFR-TSM, (29 mars 2022), Faculté de Médecin Pôle Recherche.

Comité EURON

- Représentante PhD au comité d'EURON
- Organisation PhD days2021
- Mise en place d'un Webinar / workshop avec l'ED Biologie Santé de Lille.

Enseignements

- 48h Travaux Pratiques en Immunologie, Licence 3, année 2020/2021
- 48h Travaux Pratiques en Immunologie, Licence 3, année 2021/2022
- CM / TD / TP d'immunologie, licence 3, année 2022/2023

Encadrement

1ère année :

- Marion Kretsch : M2 Proteomics, stage de 6 mois. Projet IgG5

2ème année :

- Hanane Touabi : M2 Omics, stage de 6 mois. Projet NOBODY / BARCODE

3ème année :

- Hind Lekam : M1 Omics, stage de 4 mois. Projet BARCODE
- Jade Ferrante : L3 BCP, stage de 1 mois. Projet BARCODE
- Julien Salzet : L1, stage de 2 mois. Projet BARCODE

Formations personnelles

- Anglais : Wall Street English, 3,5-7h/semaine, année 2020-2021
- Anglais : Wall Street English: 3,5-7h/semaine, année 2021-2022

Résumé en français

La moelle épinière est l'une des parties les plus importantes du système nerveux central (SNC). Cependant, celle-ci peut être sujette à des lésions allant de la contusion à la section, à la suite d'accidents de la route, d'agressions physiques, de chutes, etc. Malheureusement, aucun traitement efficace n'est réellement connu à ce jour. Dans ce contexte, il est important de caractériser les mécanismes moléculaires mis en jeu lors de cette physiopathologie. Pour cela, une étude protéomique spatio-temporelle sur des rats présentant une lésion de la moelle épinière (LME) a été réalisée. Celle-ci a permis de mettre en évidence que la région rostrale localisée en amont de la lésion synthétise des facteurs impliqués dans la neurogenèse ; alors que sur le site de lésion et la région caudale localisée en aval de la lésion, les facteurs produits sont de nature inflammatoire. De façon surprenante, cette étude a également montré que les sécrétomes issus des cultures organotypiques de ces différents segments de la LME contiennent des immunoglobulines Gamma (IgG), d'isotypes IgG1, IgG2A, IgG2B et IgG2C. Celles-ci apparaissent dès 12 h après lésion. Or, lors d'une réponse adaptative conventionnelle, la production d'IgG par les lymphocytes B nécessite 7 à 8 jours. Bien qu'actuellement, il soit considéré que seuls les lymphocytes B soient capables de produire des IgG, cette expression précoce soutient l'idée que ces Igs pourraient être produites par des cellules résidentes du SNC. Ainsi, le but de cette thèse a été d'identifier la source de ces Igs et de déterminer leur rôle lors d'une LME. Au cours de ce travail, nous avons montré que des Igs peuvent être produites au sein même du système nerveux central par les neurones et les astrocytes. En effet, à l'aide d'analyses multi-omiques, nous avons révélé l'expression constitutive des chaînes lourdes IgG2C et IgG2B dans les neurones et les astrocytes respectivement. Lorsque nous nous sommes intéressés à la chaîne lourde IgG2B dans les astrocytes, des études de surexpression et d'invalidation ont montré un rôle de cette IgG dans le maintien de l'identité des astrocytes. Ces Igs se sont révélées particulières, car elles ne présentent pas une forme classique, mais plutôt une forme aberrante. C'est-à-dire des parties variables et constantes aussi bien pour la chaîne lourde IgG que pour la chaîne légère Kappa qui sont produites de façon indépendante. Nous avons pu montrer par des études fonctionnelles que ces Igs présenteraient un rôle dans la conservation du phénotype astrocytaire et seraient impliquées dans la neurogénèse et la repousse neuritique. Ces nouvelles immunoglobulines peuvent être nommées les « Igs dérivées des cellules neurales ». Ces résultats renforcent les dernières recherches montrant que les Igs peuvent produire par d'autres cellules que les cellules B. En conclusion, l'ensemble de ces travaux a permis de mettre en évidence une nouvelle classe d'Igs issu de cellules non-B, ouvrant la porte à des recherches portant sur leurs rôles et leurs cibles au sein du SNC dans des conditions physiologiques normales ou physiopathologiques.

Abstract in English

The spinal cord is one of the most important parts of the central nervous system (CNS). However, the spinal cord can be subject to injury (SCI), ranging from contusion to severance, due to life events (motor vehicle or bicycle accidents, physical aggression, falls etc.). Unfortunately, no effective treatment is known to date. In this context, it is important to characterize the molecular mechanisms involved in this physiopathology. To this end, a spatio-temporal proteomic study on rats with a spinal cord injury (SCI) was carried out. This made it possible to highlight that the rostral region located upstream of the lesion synthesizes factors involved in neurogenesis; whereas at the lesion site and in the caudal region located downstream of the lesion the factors produced are inflammatory in nature. Surprisingly, this study also showed that the secretomes from organotypic cultures of these different segments of injured spinal cord contain Gamma immunoglobulins (IgG), of the isotypes IgG1, IgG2A, IgG2B and IgG2C. Surprisingly, these appear as early as 12 hours after injury. However, during a conventional adaptive response, the production of IgG by B lymphocytes requires 7 to 8 days. Although it is currently considered that only B lymphocytes can produce IgG, this early expression supports the idea that these IgGs could be produced by CNS resident cells. Thus, the aim of this thesis was to identify the source of these IgGs and to determine their role in SCI. In the course of this work, we have shown that Igs can be produced in the central nervous system by neurons and astrocytes. Indeed, using multi-omics analysis, we revealed the constitutive expression of IgG2C and IgG2B heavy chain in neurons and astrocytes respectively. When we focused on the IgG2B heavy chain in astrocytes, overexpression and invalidation studies showed a role for this IgG in maintaining astrocyte identity. These Igs were found to be peculiar in that they did not have a classical form, but rather an aberrant form. That is, independent variable and constant parts for both the IgG heavy chain and the Kappa light chain. We were able to show by functional studies that these Igs had a role in the conservation of the astrocytic phenotype and were involved in neurogenesis and neuritic regrowth. They can now be called “neural derivated Igs”. The current dogma is that Ig is produced by B lymphocytes (LB) during an immune response. Our work tends to show that B cells are no longer the only ones to produce these Igs. In conclusion, our work has identified a new class of non-B cell derived Igs, opening the door to research on their roles and targets in the nervous system under normal or pathophysiological conditions.

Sommaire

Liste des figures

Liste des abréviations

20-HETE = acide 20-hydroxyeicosatétraénoïque
AA = Acide arachidonique
Ac = Anticorps
ADCC = Antibody Dependent Cell Cytotoxicity
ADNM = Antibody Dependent Neurites Outgrowth Modulation
Altprot = protéines alternatives
Ang = Angiopoïétine
ARNnc = ARN non codant
ASIA = American Spinal Cord Injury Association
Asn = Asparagine
ATP = Adénosine Triphosphate
BHE = Barrière Hémato-Encéphalique
Ca2+ = Calcium
CD = Cluster de Différenciation
CD = Cluster de différenciation
CH = Constante Heavy / Constante Lourde
CL= Constant Light / Constante Légère
CMH-II = CMH de classe II
CPA = Cellules Présentatrices d'Antigènes
CPO / OCP = Cellules Progénitrices d'Oligodendrocytes / Oligodendrocytes progenitor cell
Ct = C terminal
DNA-PKc = DNA-dependent protein kinase, catalyticsubunit
EGF = Facteur de Croissance Epidermique
Eph = Ephrines
ET= Endothéline
Fab = Fragment Antigen-Binding / Fragment de Liaison à l'Antigène
Fc = / Partie Cristallisable
Fc = Fraction cristallisable
FcRn = récepteur Fc néonatal
FcYR = Fragment Crystallizable Gamma Receptor
FGF = Facteur de Croissance Fibroblastique
GFAP = Protéine Acide Fibrillaire Gliale
GLUT1 = transporteurs de glucose 1
GPCR = récepteurs sont couplés aux protéines G
GR = Glie Radiale
HO-1 = Oxygénase-1
Ig(s) = Immunoglobuline(s)
IgG = Immunoglobuline Gamma
K+ = Potassium
Ko = Knockout

LAM = Leucémie Myéloïde Aiguë
LB = Lymphocytes B
LCS / LCR = Liquide Cérébrospinal / Liquide Céphalorachidien
LME / SCI = Lésion de la Moelle Epinière / Spinal Cord Injury
LncARN = ARN non codant
ME = Moelle Epinière
MEGF10 = Multiple EGF-like-domains 10
MERTK = MER Tyrosine Kinase
MPT = Modification Post-Traductionnelle
NgR = récepteurs Nogo
Nt = N terminal
O2 = Oxygène
OCB = Bandes Oligoclonales
ORF = Open Reading Frame / lecture ouvert de référence
p75NTR = récepteur de la neurotrophine p75
PAMP / DAMP = Motifs Moléculaires Associés aux agents Pathogènes / aux Dangers
PAP = Processus Astrocytaires Périsynaptiques
PGE2 = Prostaglandine E2
pro-B = cellules B progénitrices
RefProt = Protéine de Référence
RhoAi = inhibiteur de RhoA
RNM = résonance magnétique nucléaire
ROS = Reactive Oxygen species
S1P = Sphingosine 1-Phosphate
SEP = Sclérose en Plaques
SNC / CNS = Système Nerveux Central / Central Nervous System
SPARC = Protéine Acide Riche en Cystéine Sécrétée
Tdt / DNTT = Terminal deoxynucleotidyl transferase
TGF-β = Facteur de Croissance Transformant β
TLR = Toll Like Receptor
VH = Variable Heavy / variable Lourde
VL = Variable light / variable Légère

Problématiques et objectifs

Le système nerveux central (SNC) présente deux parties bien distinctes, l'encéphale et la moelle épinière (spinale). Il est responsable de la réception, du traitement et de l'envoi de l'information nerveuse au reste du corps. Il est donc indispensable pour les fonctions motrices, sensorielles et cognitives de l'organisme. Le SNC est composé de neurones, de cellules gliales et de cellules immunitaires au sein des méninges (Macrophages et cellules T) (Kwon, 2022). Les neurones sont connus pour véhiculer l'information nerveuse à travers le système nerveux central et périphérique. Les cellules gliales, quant à elles, soutiennent les circuits neuronaux et interviennent dans l'homéostasie du SNC. Elles se divisent en différents types cellulaires : les épendymocytes, la microglie (ou cellules microgliales), les oligodendrocytes et les astrocytes. Les cellules astrocytaires sont les cellules les plus abondantes du SNC. Elles jouent un rôle majeur dans le SNC en régulant l'apport en nutriments, l'homéostasie du SNC, la transmission de l'information nerveuse au niveau des synapses ainsi que la formation synaptique. Par ailleurs, les astrocytes et la microglie peuvent également présenter une fonction immunitaire. Le système nerveux central a longtemps été considéré comme coupé du système immunitaire périphérique. Or, récemment, il a été montré qu'outre ses propres cellules immunitaires (la microglie), le cerveau assure aussi sa protection en permettant à des cellules T et des macrophages de circuler au niveau de sa périphérie à travers le liquide céphalorachidien (Kwon, 2022). Ainsi, il semble que le système nerveux central ne soit pas totalement dépourvu de cellules immunitaires, mais en héberge et communique avec celles-ci. Cependant, à ce jour, la fonction exacte de ces cellules au sein du système nerveux reste à définir.

Dans ce contexte, pour l'étude de la réponse immunitaire au sein du système, nous nous sommes intéressés à la lésion de la moelle épinière (LME). La moelle épinière est protégée par le canal rachidien et le liquide rachidien. Néanmoins, elle peut être sujette à des lésions irréversibles lors d'accidents de la vie, tels que des chutes, des agressions, des activités sportives traumatisantes ou encore lors de collision avec un engin motorisé. La LME peut être atteinte plus ou moins sévèrement et lésée à n'importe quel endroit de la colonne vertébrale. Une lésion au niveau de la région cervicale conduit à une tétraplégie avec une perte de motricité de l'ensemble du corps, alors qu'une lésion dans la région lombaire provoque une paraplégie avec une perte de motricité des membres inférieurs. Au cours de ces dernières

années, le nombre de LME a augmenté considérablement à la suite des changements des conditions de vie. Cette lésion conduit à deux phases distinctes. Lors de la première phase, le déplacement des vertèbres va entrainer une compression physique de la moelle épinière. Puis, une seconde phase va se mettre en place et évoluer en trois temps. Tout commence par une phase aigüe, où l'endommagement des vaisseaux sanguins conduit à la formation d'un hématome, une ischémie locale et une excitotoxicité. Ensuite, la phase subaiguë prend place, au cours de laquelle, l'excitotoxicité provoque une mort neuronale importante, un stress oxydatif ainsi que l'activation des astrocytes. Enfin, la phase chronique survient et se caractérise par la mise en place d'une réponse inflammatoire et la formation d'une cicatrice gliale. Malheureusement, aucun traitement ne s'est avéré efficace pour permettre une récupération des fonctions motrices et sensorielles du patient. Une des raisons expliquant la difficulté de mettre en place une telle stratégie thérapeutique est la méconnaissance des mécanismes moléculaires impliqués dans cette physiopathologie.

Dans ce contexte, des études, réalisées au sein de l'unité sur les premières heures de la lésion ont montré la mise en place d'une réponse inflammatoire qui se diffuse de part et d'autre de la lésion aux niveaux rostral et caudal. Celle-ci entraîne un changement de profil protéique 24heures après la lésion (Cizkova et *al.,* 2014 ; Devaux et *al.,* 2016). En effet, tout d'abord à 12h après lésion, un mélange des deux profils est observé. En revanche à 24h, des profils avec des marqueurs bien distincts ont été identifiés entre des régions éloignées de la lésion. Plus les régions sont éloignées, plus les profils montrent la présence de facteurs neurotrophiques, alors qu'au plus près de la lésion, des facteurs inflammatoires sont sécrétés. Une étude protéomique spatio-temporelle a été réalisée ensuite de 1 à 10 jours après la lésion sur les sécrétomes d'explants de moelle épinière lésée. Les résultats ont permis de mettre en évidence que seule la lésion et le coté rostral ont des capacités régénératrices dès 24h. Ces résultats ont pu être confirmés par des études histologiques et des tests biologiques. Ceci est dû à la présence des lymphocytes T régulateurs du côté rostral qui ont migré précocement, alors que le coté caudal est toujours inflammatoire. La production de facteurs anti-neurotrophiques du côté caudal explique également la différence observée entre les deux côtés de la lésion. Ce n'est qu'après 7 jours que les lymphocytes T régulateurs migrent du côté caudal. Pendant cette fenêtre de temps, les cellules microgliales activées produisent des acylcarnitines qui activent les macrophages infiltrants et attirent les astrocytes (Quanico *et al.,*

2018). La migration des astrocytes activés conduit par la suite à la formation de la cicatrice gliale (Quanico *et al.,* 2018). De façon intéressante, lors de cette étude, la présence d'immunoglobulines (Igs) de type IgG a également été mise en évidence dès 12h au niveau du site de lésion (Devaux et *al.,* 2017). La présence de ces Igs à des temps si précoces questionne sur leur origine cellulaire, puisque celle-ci n'est pas compatible avec la production par les lymphocytes B. En effet, les IgM sont les premiers anticorps produits par les lymphocytes B après 7 jours lors d'une première réponse immunitaire, alors que les IgG ne sont produites qu'après 48h lors d'une réponse secondaire.

La question de l'origine cellulaire de ces Igs a encore été renforcée lorsque nous avons pu mettre en évidence leur présence au sein de la moelle épinière non lésée. Ce résultat est très surprenant car la barrière hémato-encéphalique (BHE) empêche le passage de ces molécules dans le SNC. Cependant, la présence de cellules immunitaires au niveau des méninges permettant un dialogue croisé entre systèmes nerveux et immunitaire, ainsi que la présence de vaisseaux lymphatiques dans le cerveau sont à prendre en compte.

Ainsi, mon premier objectif de thèse a été d'identifier l'origine de ces Igs et de déterminer leurs possibles rôles au sein du SNC. Pour ce faire, j'ai d'abord réalisé des études protéomiques spatio-temporelles afin d'identifier les différentes immunoglobulines produites au cours d'une LME. Par la suite, des analyses multi-omics ont été effectuées sur des cellules neuronales pour rechercher l'expression d'Igs, ainsi que des différents récepteurs aux Igs. Ensuite, j'ai voulu déterminer quelle corrélation existerait entre les isotypes identifiés au cours du temps et la présence de leurs récepteurs. C'est ainsi que j'ai pu démontrer leurs possibles impacts sur la croissance neuritique et mettre en évidence l'existence d'une réponse de type Antibody Dependent Neurites outgrowth Modulation (A.D.N.M) au sein du système nerveux central en corollaire de la réponse Antibody Dependent Cell Cytotoxicity au sein du système immunitaire périphérique.

Cependant, au cours d'expériences d'immunofluorescence, les IgG ont été identifiés tant au niveau des neurones que des astrocytes (Devaux et *al.,* 2016, 2017). Mon second objectif a donc été de déterminer si cet autre type cellulaire pouvait être à l'origine de ces Igs. J'ai donc entrepris des recherches transcriptomiques et protéomiques de ces Igs au sein des astrocytes.

Puis, après avoir identifié le profil isotypique de ces cellules, j'ai voulu déterminer leurs cibles et leurs fonctions au sein du SNC et lors de la LME. Au cours de ces travaux, j'ai pu mettre en évidence l'existence d'une chaine variable kappa libre issue d'un ARN non-codant au sein des astrocytes, que j'ai baptisé Heimdall. Cette protéine alternative tout comme la chaîne lourde de l'IgG2B contrôle le phénotype astrocytaire. Néanmoins, les chaines lourdes et légères semblent avoir la faculté de s'associer soient en homodimères ou hétérodimères et participeraient à la reconnaissance d'antigènes. Le dogme ayant établi que seuls les Lymphocytes B sont capables de produire des anticorps est donc révolu.

L'ensemble de ces objectifs devaient permettre de répondre à la question suivante : existe-t-il des Igs au sein du système nerveux pouvant être produites par des cellules non-B et dont le rôle ne serait pas immunitaire mais dans le neurodéveloppement, la neurogénèse, la cognition ou la mémoire.

Introduction

A. Le système nerveux central (SNC)

I. Généralités

Chez les mammifères, le système nerveux central (SNC) régule les fonctions sensorielles, vitales et cognitives de l'organisme. Il est le centre d'intégration et de traitement de l'information nerveuse. Le SNC comprend deux structures principales : l'encéphale et la moelle épinière (**Figure 1**.

> L'encéphale

L'encéphale est situé en totalité dans la boîte crânienne. Il se divise en trois parties : le cerveau, le cervelet et le tronc cérébral. Le cerveau est la plus grande partie de l'encéphale. Il se compose du télencéphale, c'est-à-dire des hémisphères droit et gauche séparés par une scissure sagittale interhémisphérique et du diencéphale comprenant le thalamus, l'hypothalamus et l'épithalamus. Le cerveau régule notamment l'activité musculaire, le fonctionnement du système hormonal ainsi que les fonctions cognitives et sensorielles. Le cervelet vient du mot latin « cerebellum » qui signifie « petit cerveau ». Celui-ci se situe sous les hémisphères cérébraux et il permet principalement la coordination des mouvements du corps. Le tronc cérébral est quant à lui situé sous l'encéphale et à l'avant du cervelet. Il comprend le mésencéphale, le pont et le bulbe rachidien. Il est le lien entre l'encéphale et la moelle épinière (**Figure 1**) (MacVicar et *al.,* 2015).

> La moelle épinière ou moelle spinale (ME ou MS)

La moelle spinale (MS), anciennement appelée « moelle épinière (ME) », est constituée par l'ensemble des fibres nerveuses venant et allant vers le système nerveux périphérique. L'information nerveuse peut ainsi être transmise dans les deux sens. De ce fait, la ME présente deux types de nerfs distincts. Les nerfs afférents qui vont envoyer le message du corps vers le système nerveux central et les nerfs efférents qui vont à l'inverse transmettre les informations nerveuses à l'ensemble du corps. Ces fibres sont protégées par le canal rachidien. Celui-ci commence au niveau du tronc cérébral et s'étend jusqu'en bas de la colonne vertébrale. Le canal rachidien est composé d'un empilement de vertèbres cervicales, thoraciques, lombaires,

sacrées et coccygiennes (**Figure 1**. Cependant, le nombre de vertèbres est différent selon l'espèce. Par exemple, un être humain adulte possède 33 vertèbres (ou segments) dont 7 vertèbres cervicales (C1 à C7), 12 vertèbres thoraciques (T1 à T12), 5 vertèbres lombaires (L1 à L5), 5 vertèbres sacrées (S1 à S5) et 4 vertèbre coccygienne (Co1-Co4) (**Figure 1**. En revanche, le rat présente 34 paires vertébrales dont 8 vertèbres cervicales, 13 vertèbres thoraciques, 6 vertèbres lombaires, 4 vertèbres sacrées et 3 vertèbres coccygiennes.

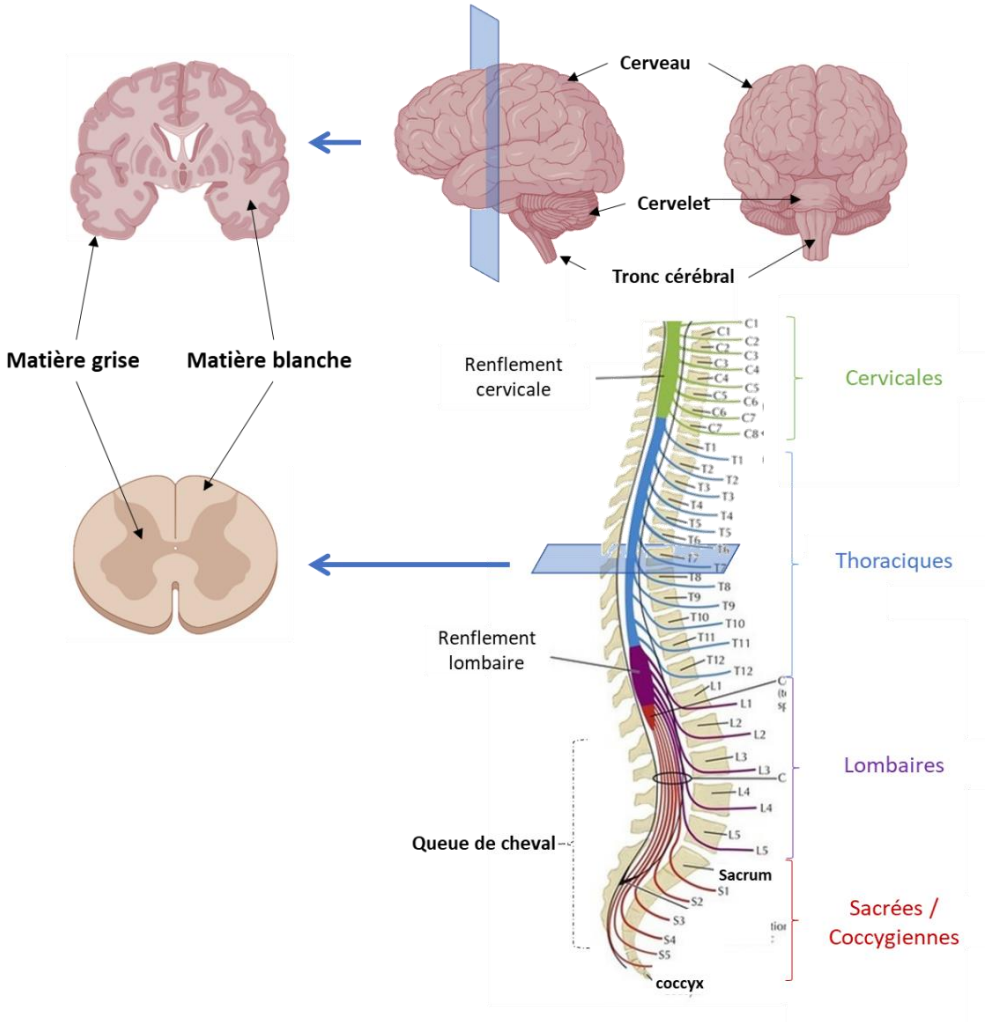

<u>Figure 1 :</u> Représentation anatomique du système nerveux central. L'encéphale est constitué du cerveau, du cervelet et du tronc cérébral. Ce dernier fait le lien entre le cerveau et la moelle épinière. Le système nerveux présente deux zones distinctes. La matière blanche, contenant les axones myélinisés des neurones et la matière grise composée des corps cellulaires des neurones. La moelle épinière est constituée de fibres nerveuses permettant la communication entre le cerveau et le reste du corps. Elle est protégée par un empilement de vertèbres cervicales, thoraciques, lombaires, sacrées et coccygiennes.

D'un point de vue externe, la moelle épinière présente une forme cylindrique et légèrement aplatie dans le plan coronal. De plus, il est possible d'observer deux zones plus volumineuses

au niveau des régions cervicales et lombo-sacrées. Celles-ci sont appelées les renflements (**Figure 1**). Ces renflements sont dus au passage d'une concentration plus importante de fibres nerveuses allant vers les différents membres du corps. Le premier renflement se trouve entre les segments C3 et T1 et il contrôle les membres supérieurs. Le second renflement, quant à lui, est situé entre les segments L1 et S2 et contrôle les membres inférieurs (**Figure 1**). Il est à noter que la moelle épinière ne s'étend pas sur la totalité de la colonne vertébrale. En effet, celle-ci va se diviser en une multitude de filaments nerveux appelée la queue de cheval (**Figure 1**).

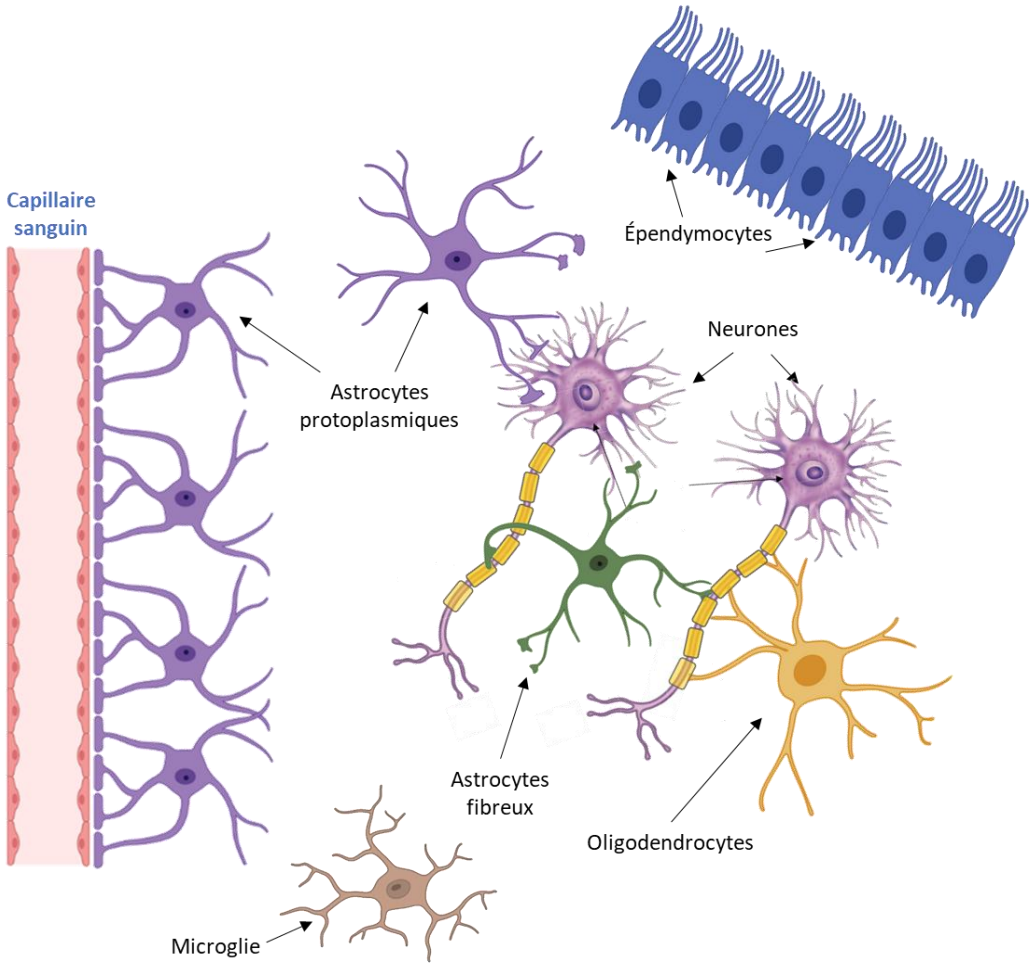

<u>Figure 2 :</u> Représentation des neurones et les cellules gliales dans le système nerveux central.

Une coupe sagittale de la moelle épinière révèle que celle-ci présente, au niveau interne, deux zones distinctes (**Figure 1**). Une première zone plus claire en périphérie qui correspond à la matière blanche. Celle-ci va contenir les prolongements axonaux des neurones fortement myélinisés. La gaine de myéline est une couche concentrique de membranes compactes qui accélère et assure la bonne transmission de l'information nerveuse. C'est la présence de la

myéline qui est responsable de cette couleur blanche. Au centre de la moelle spinale, on retrouve une seconde zone plus sombre en forme de « H » ou d'un papillon. Il s'agit de la matière dite grise (**Figure 1**). À l'inverse de la matière blanche, elle est constituée des corps cellulaires des neurones. Il est à noter que les deux zones sont inversées dans le cerveau.

II. Cellules du SNC

Le SNC régule les fonctions motrices, cognitives, sensorielles de l'ensemble du corps. Pour permettre ses différentes fonctions, il est composé d'une multitude de cellules présentant des rôles bien distincts. Parmi celles-ci, nous retrouvons en particulier les neurones et les cellules gliales. Les cellules gliales comprennent les astrocytes, les oligodendrocytes, la microglie et les épendymocytes (**Figure 2**).

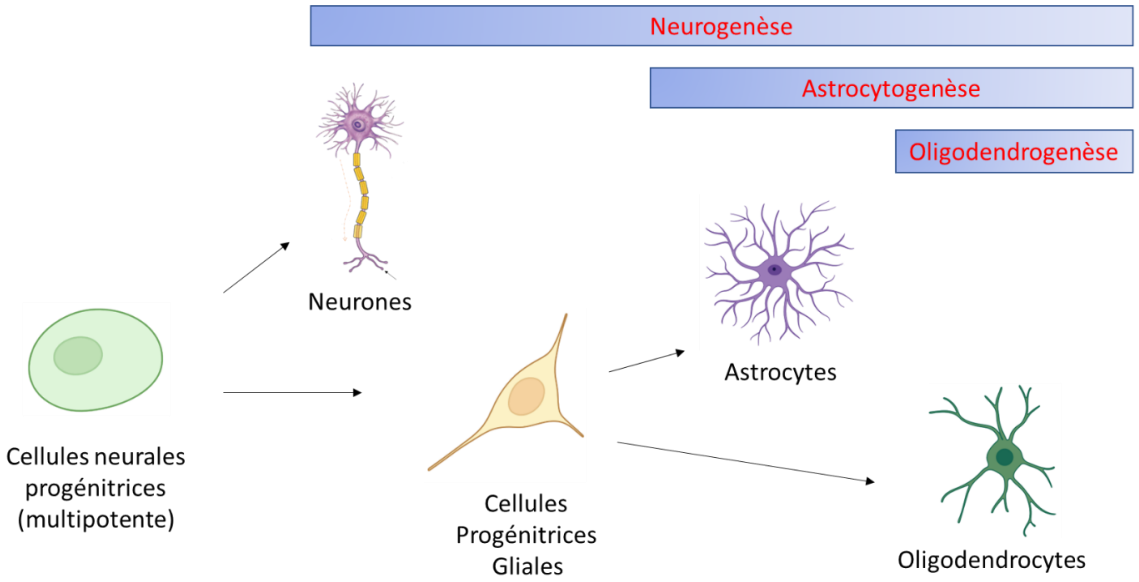

Figure 3 : Différenciation des cellules souches neurales en neurones et cellules gliales. Les cellules progénitrices vont se différencier en différents neurones, puis en fonction des facteurs gliaux exprimés, celles-ci vont se différencier vers un phénotype astrocytaire ou oligodendrocytaire.

A l'exception de la microglie, toutes les cellules du SNC proviennent de cellules souches neurales qui vont se différencier au cours de l'embryogenèse et même après la naissance. Ces cellules souches neurales sont des cellules multipotentes capables de s'auto-renouveler (**Figure 3**). Leur différenciation en neurones ou en cellules gliales ne se fait pas simultanément. Dans un premier temps, les cellules souches neurales sont situées dans zone ventriculaire du

tube neurale, où elles peuvent se différencier en sous-populations de neurones. C'est la neurogénèse. Ensuite, l'astocytogenèse se met en place au cours duquel les cellules souches ou cellules gliales radiale vont dériver en astrocytes à la suite de l'expression de facteurs astrogliaux. Enfin, l'oligodendrocytogenèse est réalisé peu de temps avant la naissance où les oligodendrocytes sont générés pour la formation de la myéline (**Figure 3**) (Chandrasekaran*et al.,* 2016 ; Tao et *al.,* 2016).

1) Les neurones

Les neurones constituent l'unité fondamentale du système nerveux central. Ceux-ci se composent de trois parties. Le corps cellulaire, ou également appelé soma, est la partie centrale du neurone. Il va traiter l'information nerveuse. Ensuite, le neurone présente deux prolongements, les dendrites en amont et les axones en aval. Les dendrites sont des processus courts qui vont recevoir l'information nerveuse et la transmettre sous forme de potentiels d'action au soma (**Figure 4**). L'axone est quant à lui un processus cellulaire très long qui va communiquer l'information nerveuse aux dendrites du neurone suivant au travers des synapses (**Figure 4** : **Les différents types de neurones**..

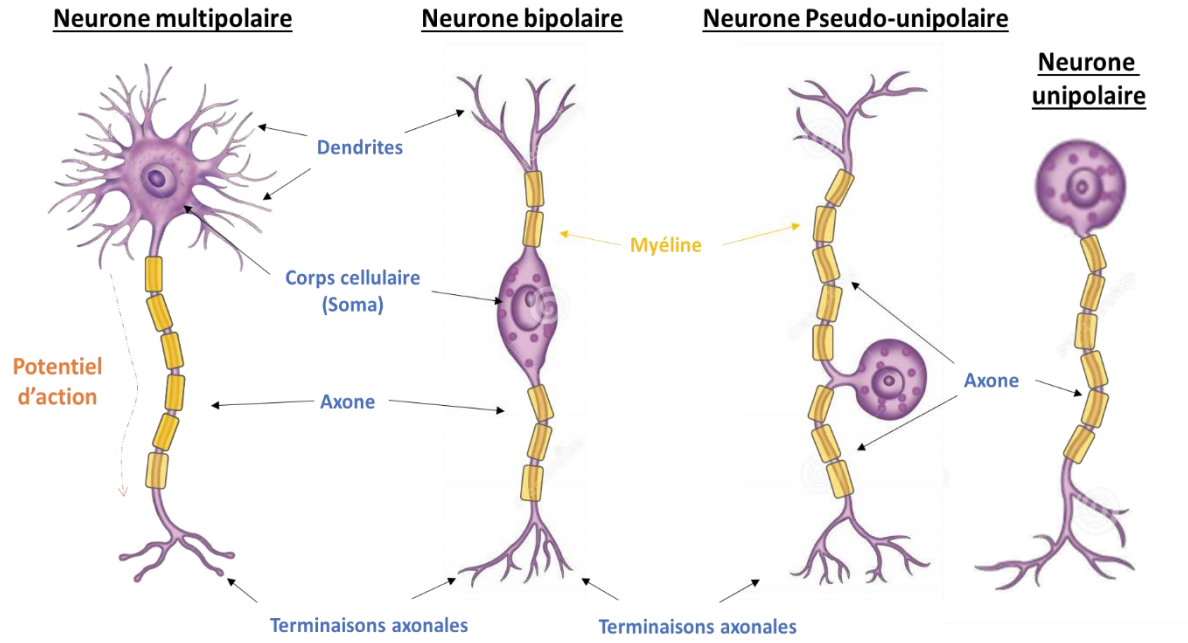

Figure 4 : Les différents types de neurones. Les neurones peuvent être classés en fonction du nombre de dendrites et d'axones qu'ils possèdent. Les multipolaires présentent plusieurs dendrites et un axone, les bipolaires ne possèdent qu'une dendrite et un axone, alors que les pseudo-unipolaires et les unipolaires ne contiennent qu'un axone. Les axones vont être myélinisés afin de faire circuler plus rapidement l'information nerveuse sous forme de potentiels d'action.

Ces cellules neuronales peuvent être classées en fonction de leur morphologie et plus particulièrement en fonction du nombre de prolongements qu'ils présentent. Trois grands types de neurones peuvent être ainsi distingués : les neurones unipolaires, qui présentent un seul axone qui va réceptionner l'information nerveuse provenant du corps ; les neurones bipolaires, avec un axone et une dendrite ; et enfin, les neurones multipolaires, qui vont présenter un axone et plusieurs dendrites comme les motoneurones et les interneurones (**Figure 4**).

Les différents types de neurones vont présenter des rôles différents dans le SNC. Certains d'entre eux comme les neurones sensitifs vont transmettre les informations du corps au SNC. Les interneurones, quant à eux, sont les neurones les plus abondants et sont chargés de relayer le message nerveux entre deux neurones. De plus, ces interneurones présentent une structure multipolaire leur permettant de recevoir plusieurs informations nerveuses en même temps, qu'ils vont unifier et transmettre à un autre neurone. Enfin, les neurones moteurs, appelés également motoneurones, transmettent le message nerveux au reste du corps. Ainsi, ils contrôlent par exemple, la contraction ou le relâchement des muscles.

Afin de permettre la transmission des potentiels d'action, l'axone du neurone pré-synaptique et une dendrite du neurone post-synaptique vont former une synapse. Les synapses se réalisent soit de façon chimique, soit de façon électrique. Dans le premier cas, les neurones utilisent des neurotransmetteurs. En fonction du type de neurotransmetteur utilisé, il est possible de distinguer différents types de neurones, tels que les neurones GABAnergiques, glutamatergiques ou encore cholinergiques. Dans le cas d'une synapse chimique, le neurone présynaptique va libérer des neurotransmetteurs dans la fente synaptique. Ceux-ci se fixent sur les récepteurs présents à la surface des neurones postsynaptiques qui s'activent alors. Cette activation provoque l'ouverture des canaux ioniques (calcium, potassium, sodium, ou chlore) et ainsi la genèse de potentiels d'action. À l'inverse des synapses chimiques, les synapses électriques ne vont pas utiliser de neurotransmetteurs. Dans leur cas, les neurones pré-synaptiques et post-synaptiques établissent des contacts directs et font passer instantanément des ions entre leurs canaux ioniques. Les synapses électriques fonctionnent ainsi plus rapidement que les synapses chimiques.

2) Les cellules gliales (ou névroglie)

Les cellules gliales constituent le type cellulaire majoritairement présent dans le SNC. Le terme « glie » vient du grec « glia » qui signifie glu. Elles ont été nommées ainsi, car elles assurent notamment le soutien structural du SNC. Cependant, de nos jours, plusieurs études ont montré que ces cellules présentent également d'autres fonctions indispensables au SNC, comme le maintien de son homéostasie ou la régulation du message nerveux (Zhou et al 2019). Les cellules gliales sont classées en différents types que sont les cellules épendymaires, les oligodendrocytes, la microglie et les astrocytes (**Figure 2**).

a) Cellules épendymaires / épendymocytes

Les épendymocytes ou cellules épendymaires ont une forme cubique et forment une couche cellulaire autour du canal de l'épendyme et des ventricules cérébraux. Elles sont responsables de la circulation du liquide cérébrospinal grâce à la mobilité de leurs cils (**Figure 2**).

b) Les oligodendrocytes

Les oligodendrocytes sont des cellules dérivées des cellules progénitrices d'oligodendrocytes (OPC). Ils présentent deux rôles distincts en fonction de leur localisation. Les oligodendrocytes présents dans la substance blanche vont être responsables de la formation et du maintien de la gaine de myéline qui entoure les axones des neurones. Cependant, contrairement à leur analogue dans le système nerveux périphérique, c'est-à-dire les cellules de Schwann, un oligodendrocyte peut synthétiser plusieurs gaines de myéline sur plusieurs axones. Les oligodendrocytes de la substance grise, quant à eux, régulent le métabolisme des neurones (**Figure 2**).

c) La microglie

Les cellules microgliales, ou microglie, sont définies comme les macrophages du SNC (**Figure 2**). Ces cellules présentent de grandes similitudes avec les monocytes du système immunitaire. Elles assurent la protection du SNC en combattant et en phagocytant les pathogènes. Par ailleurs, à la suite de la mort des cellules nerveuses, elles éliminent les débris cellulaires. De plus, elles régulent aussi les fonctions synaptiques, la plasticité synaptique et la neurogenèse adulte.

d) Les astrocytes

Les astrocytes sont les cellules gliales les plus abondantes du SNC. Elles représentent environ 20 à 40 % des cellules du cerveau, soit 1/3 de sa masse totale. Le nom « astrocyte » provient du grec « astron » ou du latin « astrum » qui signifie « étoile » ou « corps céleste ». Elles tiennent leur nom de leur forme très étoilée. Celle-ci est due à la présence d'une multitude de prolongements, appelés processus. Ces processus vont être classés en fonction de leur taille et de leur localisation. D'abord, il y a les branches qui sont les plus gros processus partant du soma de l'astrocyte (**Figure 5**). Ensuite, ces branches vont se diviser en processus plus fins appelés les rameaux. Ceux-ci vont également se diviser pour former des folioles ou des pieds terminaux (**Figure 5**). Les folioles, ou « processus astrocytaires périsynaptiques » (PAP), sont les processus les plus fins de l'astrocyte. Les PAP entrent en contact avec les synapses afin de moduler la transmission de l'information nerveuse entre deux neurones. Les pieds terminaux, quant à eux, établissent des contacts avec les vaisseaux sanguins pour réguler l'apport en nutriments dans le SNC (**Figure 5**).

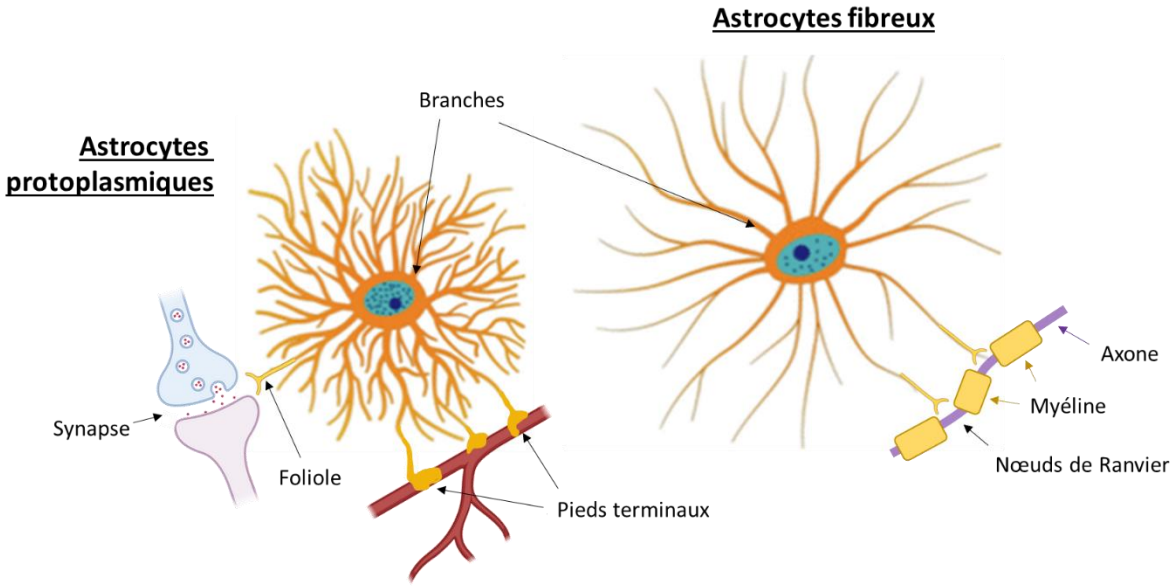

Figure 5 : Les astrocytes protoplasmiques et fibreux. Les astrocytes protoplasmiques vont avoir un grand nombre de processus courts. Ceux-ci entrent en contact avec les synapses pour moduler la transmission de l'information nerveuse ou les vaisseaux sanguins pour permettre l'apport de nutriments au SNC. Les astrocytes fibreux ont des processus très longs et moins ramifiés. Ils établissent des contacts avec les Nœuds de Ranvier afin de contrôler l'activité les canaux ioniques.

Ces cellules astrocytaires sont dérivées de cellules souches de la glie radiale (GR) issue de la zone ventriculaire du tube neurale (Han et *al.,* 2021). C'est à partir des mêmes cellules souches

progénitrices que se sont différenciés les neurones. Dans les premiers stades de développement, l'astrocytogenèse se met en place après la neurogenèse. Chez la souris, elle commence vers le 11^{e} jour embryonnaire (E11) au niveau de la moelle épinière et le 18^{e} jour (E18) au niveau du cerveau (Reemst *et al.,* 2016; Farhy-Tselnicker et *al.,* 2018; Hasel et *al.,* 2021). Au cours de la maturation des astrocytes, plusieurs voies de signalisation moléculaires vont être activées. Par exemple, la voie NOTCH est essentielle à la différenciation des astrocytes, car elle va induire l'expression de gènes astrocytaires et gliaux, tels que la GFAP et le facteur nucléaire NF1A (Akdemir et *al.,* 2020). Cependant, contrairement aux neurones, les astrocytes continuent de se développer après la naissance. Chez la souris, ils se différencient et poursuivent leur maturation jusqu'au 7^{e} jour postnatal (Reemst *et al.,* 2016; Farhy-Tselnicker et *al.,* 2018; Hasel et *al.,* 2021). De plus, il est intéressant de noter que les astrocytes sont des cellules mitotiques. Au cours de la vie, ces cellules gardent leur capacité à se diviser mais aussi de revenir à un état de cellules progénitrices en cas de traumatisme (Reemst *et al.,* 2016; Farhy-Tselnicker et *al.,* 2018).

Les astrocytes sont connus pour présenter une grande hétérogénéité aussi bien morphologique, biochimique que fonctionnelle. Au XIXe siècle, les études de Ramon y Cajal ont montré que les astrocytes pouvaient être classés en 2 grands types majoritaires en fonction de leur morphologie : les astrocytes protoplasmiques et les astrocytes fibreux (**Figure 5**) (Miller et *al.,* 1984)**.** Les astrocytes protoplasmiques, principalement retrouvés dans la matière grise présentent des milliers de processus très courts, ramifiés et très fins. Ceci leur confère un aspect « spongiforme » ou « touffu » avec un grand nombre de prolongements. Ainsi, ils peuvent établir plusieurs connexions en même temps avec notamment le corps cellulaire des neurones ou au niveau des synapses afin de moduler la transmission de l'information nerveuse. D'autres connexions au niveau des vaisseaux sanguins sont également retrouvées. Celles-ci contribuent à l'édification de la membrane BHE et à la régulation de l'apport en nutriments dans le SNC (**Figure 5**). Contrairement aux astrocytes protoplasmiques, les astrocytes fibreux sont quant à eux retrouvés dans la matière blanche. Ils présentent des prolongements plus longs, affilés et non ramifiés (**Figure 5**). Ces extensions plus longues possèdent une grande quantité de fibrilles, ou gliofibrilles. Celles-ci sont nécessaires pour la formation de la cicatrice gliale. De plus, les processus des astrocytes fibreux vont également moduler la transmission des potentiels d'action au niveau de Nœuds de Ranvier des neurones

en régulant la disponibilité des ions calciques ou sodiques (**Figure 5**) (Serwanski et *al.,* 2017). Il est à noter que ces sous-populations d'astrocytes sont localisées de façon stricte dans le système nerveux. En effet, l'étude menée par Emsley et son équipe montre que les astrocytes fibreux se retrouvent préférentiellement dans l'amygdale et dans le cône dorsal de la moelle épinière alors que les astrocytes protoplasmiques sont plutôt observés dans l'hypothalamus et l'hippocampe (Emsley et *al.,* 2006).

Bien que ces deux classes principales d'astrocytes aient pu être largement identifiées, celles-ci ne sont pas pleinement représentatives de l'hétérogénéité astrocytaire. En effet, d'autres types d'astrocytes ont été identifiés tels que les astrocytes périvasculaires, vêlés, radiaux, les cellules de Müller dans la rétine et les cellules gliales de Bergmann dans le cervelet. Toutes ces cellules expriment des marqueurs astrocytaires mais ne présentent pas la même morphologie ou les mêmes fonctions que ces dernières. En plus de cette hétérogénéité, il est intéressant de noter que les astrocytes présentent une « inhibition de contact » ou un « espacement des contacts » les uns par rapport aux autres. C'est-à-dire que des astrocytes de la même ou de différentes populations ne se chevauchent pas et maintiennent une distance dans le SNC. Cette régionalisation augmente ainsi le nombre de sous-types astrocytaires. Par exemple, les astrocytes protoplasmiques présents dans l'hippocampe vont être subdivisés en différents sous-types avec des profils transcriptomiques et biochimiques différents (Emsley et *al.,* 2006). Ainsi, en fonction de leur localisation et du sous type auxquels ces cellules appartiennent, les astrocytes ne vont avoir des rôles dans le SNC (Emsley et *al.,* 2006). Par ailleurs, les cellules astrocytaires vont avoir une densité variable en fonction de la localisation dans le SNC. En effet, une étude du nombre d'astrocytes a été réalisée à l'aide d'un marquage de la protéine acide fibrillaire gliale (GFAP), filament intermédiaire retrouvé au niveau du soma et des branches astrocytaires. Les résultats obtenus montrent que 10 astrocytes par mm^2 sont retrouvés dans le cortex, alors qu'en environ 80-90 et 500 astrocytes par mm^2 sont respectivement identifiés dans l'hypothalamus et l'hippocampe (Bushong *et al.,* 2002).

De nos jours, les astrocytes sont des cellules gliales connues pour assurer une multitude de fonctions majeures dans le système nerveux central (**Figure 6**). Outre, leur rôle de support structurel du SNC, elles contrôlent également le flux sanguin, l'homéostasie ionique, la

clairance des neurotransmetteurs, la régulation de la transmission de l'information nerveuse ainsi que la formation, la maturation et l'élimination des synapses. Par ailleurs, une fonction neuro-immunitaire de ces cellules a également été décrite (Araque et *al.,* 2014 ; Dallérac et Rouach, 2016).

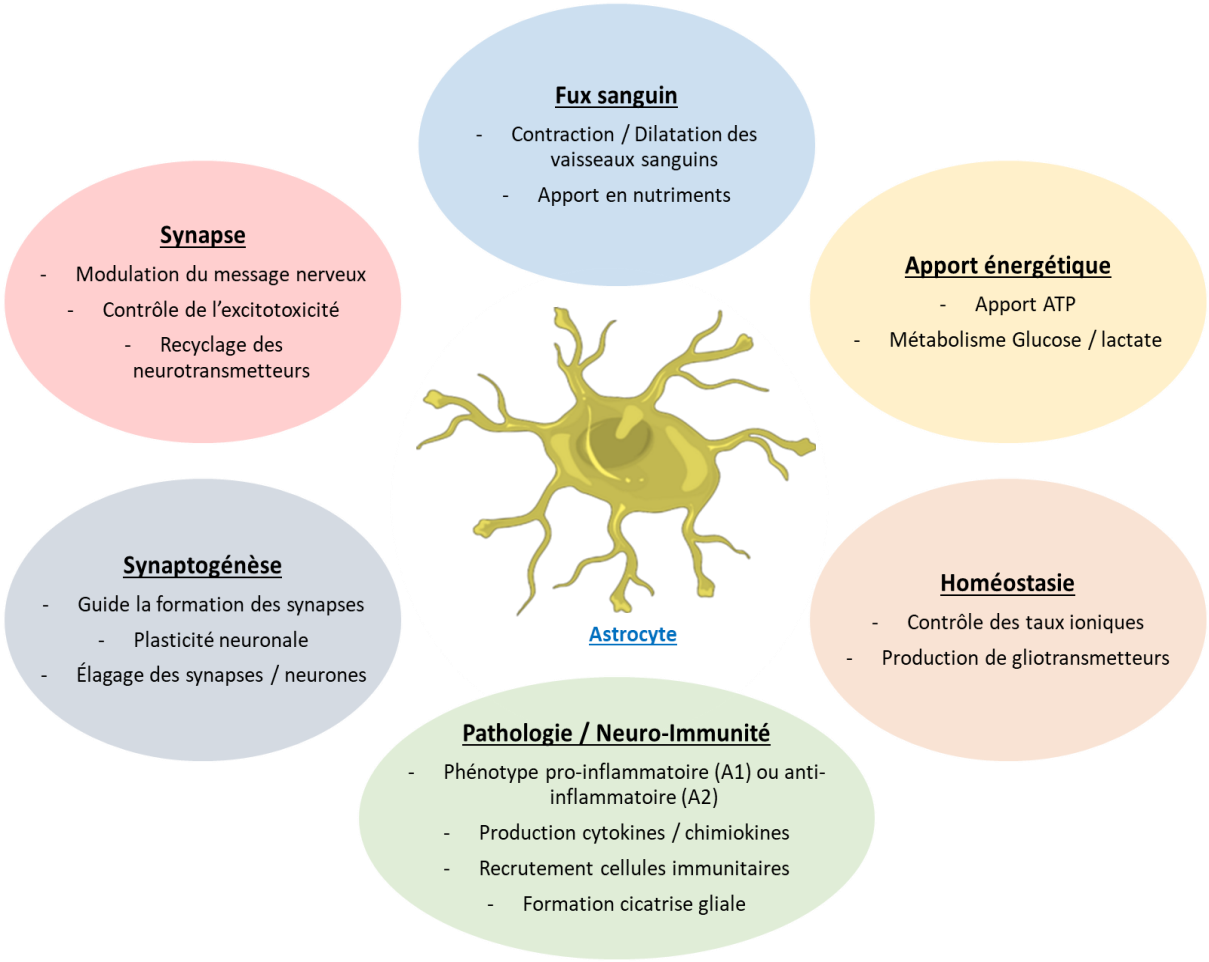

Figure 6 : Les grandes fonctions des astrocytes dans le SNC. Les astrocytes jouent un rôle primordial dans le système nerveux central, tel que la régulation du flux sanguin, l'apport d'énergie, la régulation de la synaptogenèse, etc.

- Contrôle du flux sanguin dans le système nerveux central par les astrocytes

L'activité cérébrale nécessite une quantité d'énergie très importante. Elle représente, à elle seule, environ 20 % de la consommation énergétique totale du corps. Cependant, cette activité doit être hautement régulée afin d'éviter une réduction énergétique qui impacterait négativement les transmissions synaptiques. Dans ce contexte, les astrocytes jouent un rôle majeur dans la régulation du flux sanguin cérébral dans le but d'approvisionner le système nerveux central en nutriments (**Figure 6**). Pour ce faire, les pieds terminaux des astrocytes

entrent en contact avec les vaisseaux sanguins et couvrent près de 99 % de leur surface totale (Takahashi, 2022). En fonction du taux d'oxygène (O_2) ou de potassium extracellulaire (K+), les astrocytes induisent la contraction ou la dilatation de ces vaisseaux. En effet, lorsque les astrocytes détectent un niveau d'O_2 extracellulaire relativement faible, un influx de Ca^{2+} survient dans le milieu intracellulaire. Cette augmentation de Ca^{2+} active la cellule, qui libère alors de la prostaglandine E2 (PGE2) dans le milieu extracellulaire. La sécrétion de cette molécule induit à son tour une dilatation des vaisseaux sanguins. À l'inverse, si les astrocytes détectent un haut niveau d'oxygène dans le milieu extracellulaire, ils libèrent de l'acide arachidonique (AA). L'AA ainsi libéré est alors converti en acide 20-hydroxyeicosatétraénoïque (20-HETE). Ce métabolite induit la diminution du niveau de Ca^{2+} intracellulaire dans les muscles lisses, ce qui provoque la contraction des vaisseaux sanguins (MacVicar et Newman, 2015). Par ailleurs, les astrocytes peuvent également moduler l'afflux sanguin en libérant du potassium (K^+). En effet, une concentration importante de K^+ dans le milieu extracellulaire entraîne un relâchement des cellules musculaires et ainsi une dilatation des vaisseaux sanguins. En revanche, un niveau trop élevé de K^+ provoque une dépolarisation des cellules musculaires et ainsi leur contraction. Il en résulte une vasoconstriction (MacVicar et *al.,* 2015).

- Apport énergétique au SNC par les astrocytes

Les astrocytes apportent également un soutien énergétique au système nerveux central. En effet, les neurones ont besoin d'une grande quantité d'ATP pour leur fonctionnement. Celle-ci s'élève à 50 % de l'ATP total du cerveau. Cependant, ces neurones n'ont pas la capacité d'en produire en si grande quantité. Ce sont les astrocytes qui vont assurer cet apport énergétique grâce à une glycolyse aérobie (**Figure 6**) (MacVicar et Newman, 2015). Pour cela, à l'aide des transporteurs de glucose 1 (GLUT1) présent à leur surface membranaire, les astrocytes vont récupérer le glucose circulant dans le sang. Le glucose peut être stocké sous forme de glycogène dans la cellule ou, dans 80-85 % des cas, métabolisé en pyruvate via des enzymes glycolytiques. Ce pyruvate est ensuite converti en lactate, qui est libéré dans le milieu extracellulaire afin d'être utilisé par les neurones. De plus, il a été montré que le transfert de lactate entre les astrocytes et les neurones n'a pas seulement un but énergétique. En effet, le lactate joue également un rôle essentiel dans la plasticité synaptique et ainsi l'amélioration de la mémoire à long terme. De plus, ce métabolite aurait également une fonction

neuroprotectrice lors d'un traumatisme cérébral (Allaman et *al.,* 2015; Beard et *al.,* 2022; Takahashi, 2022).

- Modulation de la transmission synaptique

Au cours de ces dernières années, il a été démontré que les astrocytes modulent également la transmission de l'information nerveuse (**Figure 6**). En effet, leurs processus astrocytaires périsynaptiques (PAP) entrent en contact avec les synapses dans le but de créer une communication bidirectionnelle « astrocyte – neurone ». Les astrocytes sont donc devenus le troisième élément important de la synapse, qui est alors caractérisé de « synapse tripartite » (Allen et Barres 2009 ; Ventura et Harris, 1999 ; Araque et *al*. 1999 ; Halassa et *al*. 2009 ; Santello et *al.,* 2012). Pour permettre cette communication, les astrocytes présentent un grand nombre de récepteurs à leur surface qui fixent les neurotransmetteurs libérés par les neurones dans la fente synaptique, tels que le GABA, le glutamate, la dopamine ou encore la sérotonine. Ces récepteurs astrocytaires sont couplés aux protéines G (GPCR) et l'induction des voies de signalisation intracellulaires associées conduit à l'activation de la cellule. Celle-ci provoque une augmentation du niveau de calcium intracellulaire de l'astrocyte, ce qui à son tour induit la libération de gliotransmetteurs comme le glutamate, la D-sérine et l'ATP/adénosine. Ces gliotransmetteurs ainsi libérés dans le milieu extracellulaire modulent alors l'activité des cellules neuronales environnantes (Allen et Eroglu, 2017; Noriega-Prieto and Araque, 2021). Par ailleurs, il est intéressant de noter que ces récepteurs aux neurotransmetteurs qui sont exprimés à la surface cellulaire des astrocytes présents au niveau de la synapse exercent également un rôle de clairance. En effet, lors de la survenue d'un message nerveux, le neurone pré-synaptique libère une grande quantité de glutamate au niveau de la fente synaptique. Si cette concentration n'est pas régulée, elle peut induire une excitotoxicité pour les cellules ou atteindre d'autres synapses avoisinantes et déclencher ainsi des potentiels d'action non voulus. Pour éviter cela, une partie de ce glutamate va être éliminée par les astrocytes, qui le convertissent alors en glutamine. La glutamine est ensuite renvoyée aux neurones pour être transformée en neurotransmetteur GABA. De plus, en capturant les neurotransmetteurs, les astrocytes régulent la disponibilité de ceux-ci au niveau de la fente synaptique, et modulent ainsi l'induction ou l'inhibition de potentiels d'action au niveau du neurone post-synaptique.

- Implication des astrocytes dans le développement des circuits neuronaux

Bien que les astrocytes jouent un rôle primordial dans l'homéostasie, la transmission synaptique ou dans la réponse neuroimmunitaire, les astrocytes sont également indispensables aux stades précoces du développement (**Figure 6**). En effet, ces cellules sont impliquées dans l'angiogenèse, la formation de la barrière hématoencéphalique, la vasculogenèse ainsi que la synaptogenèse (Griffiths, Bhutani et Stary, 2019). Par exemple, il a été montré que les astrocytes produisent différents facteurs guidant la neurogenèse. Parmi ceux-ci, l'expression astrocytaire de la laminine et de la fibronectine, deux glycoprotéines de la matrice extracellulaire, stimule et guide favorablement l'excroissance axonale. Ces deux facteurs sont captés par des structures sensorimotrices situées aux extrémités axonales, appelées les cônes de croissance. Au cours du développement, ces cônes de croissance permettent, en fonction des signaux extrinsèques, de moduler l'attraction ou la répulsion des axones et ainsi la construction correcte du circuit neuronal. Les récepteurs aux éphrines (Eph) sont également retrouvés au niveau de ces cônes de croissance axonaux. Ceux-ci exercent une fonction répulsive. En effet, la signalisation induite par l'éphrine permet la migration des axones neuronaux vers les organes cibles en repoussant l'axone loin du site d'activation. De plus, il a été montré qu'une sous population d'astrocytes de la moelle épinière exprime la sémaphorine-3a (sema3a) afin de contrôler la bonne organisation des circuits des motoneurones et des neurones sensoriels (Marquardt *et al.,* 2005; Molofsky *et al.,* 2014; Reemst *et al.,* 2016). En plus de guider la formation des circuits neuronaux, les astrocytes libèrent une multitude de facteurs angiogéniques tels que le VEGF l'angiopoïétine-1 (Ang-1), l'angiopoïétine-2 (Ang-2), l'endothéline-1 (ET-1) et l'oxygénase-1 (HO-1) régulant alors la formation et la stabilisation des vaisseaux sanguins (Reemst *et al.,* 2016).

- Modulation des astrocytes dans la synaptogenèse

Les astrocytes modulent également la formation, la maturation ou l'élimination des synapses (**Figure 6**). En 2011, Kucukdereli et son équipe ont montré que l'ajout d'astrocytes dans des cultures de neurones était indispensable pour permettre la formation de synapses et l'activation des cellules neuronales (Kucukdereli *et al.,* 2011). En effet, les astrocytes synthétisent des protéines synaptogènes et anti-synaptogènes, telles que la protéine Hevin et la protéine acide riche en cystéine sécrétée (SPARC). La protéine Hevin favorise la synaptogenèse et la maturation des synapses glutamatergiques (Perez-Catalan et *al.,* 2021).

De plus, cette protéine exerce également un impact positif sur la réparation du SNC à la suite d'une lésion. En revanche, la protéine SPARC, antagoniste de la protéine Hevin, inhibe la formation de synapses et aucune activité post-synaptique n'est détectée. Il a été observé chez les souris Knockout (KO) SPARC une synaptogenèse excitatrice plus importante (Perez-Catalan et *al.,* 2021). En plus de favoriser la synaptogenèse, les astrocytes ont aussi un rôle dans l'élagage des synapses (Reemst *et al.,* 2016). En effet, dès les premiers stades de développement et tout au long de la vie, les astrocytes phagocytent les synapses excessives ou aberrantes afin de redéfinir les circuits neuronaux. Pour ce faire, les astrocytes expriment des récepteurs phagocytaires, tels que Multiple EGF-like-domains 10 (MEGF10) et MER Tyrosine Kinase (MERTK) (Reemst *et al.,* 2016).

- Dédifférenciation des astrocytes en cellules pluripotentes

Les progéniteurs d'astrocytes gardent une capacité de dédifférenciation durant le développement et en fonction de l'environnement, ces progéniteurs gliaux peuvent revenir à l'état de cellules pluripotentes afin de se réorienter vers un autre type cellulaire (en astrocytes ou en neurones par exemple). Plusieurs voies de différenciation peuvent être observées dans les cellules souches neurales. Par ailleurs, les astrocytes immatures peuvent aussi se diriger vers un phénotype neuronal fonctionnel par l'expression de Neurog1, Neurog2 et Mash1. En effet, pour revenir à l'état pluripotent, les astrocytes subissent un changement épigénétique caractérisé par la mise sous silence des gènes astrocytaires et la réactivation des gènes progéniteurs. Pour ce faire, différents mécanismes moléculaires peuvent être mis en jeu, comme la modification post-traductionnelle des histones ou encore le changement d'expression de facteurs de transcription. En effet, il a été montré que l'acétylation des lysines de l'histone H3K9 permet de retourner vers un état pluripotent et donne à la cellule la capacité de se reprogrammer. De plus, il est intéressant de noter que cette acétylation diminue au cours de la différenciation et la maturation des cellules astrocytaires (Karmodiya *et al.,* 2012). Par ailleurs, il a été montré que l'acétylation de H3K9 et H3K14 est corrélée à l'activation des promoteurs de gènes neuronaux, tels que *Neurog1* et *Neurog2*. Ceci permet de rediriger la cellule vers un phénotype neuronal (Griffiths, Bhutani and Stary, 2019). A l'inverse, l'expression de l'histone méthyltransférase (Ezh2), qui catalyse la méthylation de l'histone H3K27 augmente fortement afin que les astrocytes ne maintiennent plus leur phénotype et redeviennent des cellules souches. Cette reprogrammation est intéressante, car les astrocytes

dédifférenciés ont la capacité de devenir des neurones glutamatergiques excitateurs sous l'influence de NeuroG2 ou des neurones GABAnergiques inhibiteurs sous Dlx2. Cette capacité de reprogrammation des astrocytes est très utilisée dans le cadre de stratégies thérapeutiques visant à traiter des pathologies du SNC telles que les maladies de Parkinson, d'Alzheimer ou encore à la suite d'un AVC. En effet, la maladie de Parkinson est caractérisée par la perte des neurones dopaminergiques. Ainsi, l'utilisation de la reprogrammation des astrocytes en neurones a permis une nette amélioration du comportement moteur. Par ailleurs, cette reprogrammation peut aussi être utilisée à la suite d'une lésion cérébrale ou une lésion de la moelle épinière. En effet, l'expression du facteur de transcription SOX2 a permis de convertir les astrocytes spinaux en neuroblastes, qui a leur tour, se sont redifférenciés en interneurones matures. De plus, ces interneurones présentent un état d'activation similaire aux neurones produits lors de la neurogénèse et édifient des synapses fonctionnelles (Su et *al.,* 2014).

- Rôle des astrocytes dans la réponse neuroimmunitaire

Pendant longtemps, le système nerveux central a été considéré comme immuno-privilégié (dépourvu de cellules immunitaires périphériques). En effet, il est admis que celui-ci est isolé du reste du corps par la BHE, empêchant ainsi l'entrée des cellules immunitaires. Cependant, il a été démontré que le SNC présente sa propre protection grâce à des cellules résidantes, telles que les cellules microgliales. Celles-ci sont considérées comme ayant la capacité de phagocyter, les rapprochant ainsi des macrophages, bien que leur origine embryonnaire soit différente (Ginhoux et Garel, 2018).Elles assurent la surveillance immunitaire du SNC et la phagocytose des pathogènes l'ayant infiltré ou encore des débris cellulaires générés à la suite de la mort des cellules nerveuses. Toutefois, des études menées au cours des vingt dernières années, ont également établi le rôle des astrocytes dans la réponse neuro-immunitaire. À partir d'analyses transcriptomiques ou protéomiques, il a pu être démontré que ces derniers s'activent lors de lésions traumatiques, de maladies neurodégénératives, d'infection, d'inflammation auto-immune ou encore lors d'une tumeur. Nous parlons « d'astrocytes réactifs » ou « d'astrocytose ». Cette activation dépend des signaux perçus de l'environnement par le grand nombre de récepteurs présent à leur membrane. En effet, selon la nature de ces signaux, les astrocytes présentent un phénotype immunitaire de type pro-inflammatoire (A1) ou anti-inflammatoire (A2). Par exemple, les signaux pro-inflammatoires, tels que le TNFα, IL-1β, et IL-17 activent les astrocytes afin de réguler et coordonner

l'inflammation. Dans le même contexte inflammatoire, les sphingolipides, qui sont des lipides présents à la surface membranaire, vont induire la voie NF-κB et ainsi orienter les astrocytes vers un phénotype A1. Il en résulte une production de cytokines et de chimiokines pro-inflammatoire. De plus, Linnerbauer et son équipe ont montré que la sphingosine 1-phosphate (S1P) joue un rôle important dans la régulation de la SEP et de l'EAE en induisant la translocation nucléaire de NF-κB (Linnerbauer, Wheeler et Quintana, 2020). D'autre part, les cellules astrocytaires expriment également des récepteurs aux motifs moléculaires associés aux agents pathogènes (PAMP) et aux dangers (DAMP), appelés Toll Like Receptor (TLR). Les TLRs sont connus pour entraîner la libération de molécules pro-inflammatoires ou anti-inflammatoires (Renaud et *al*., 2015; Gorina *et al.,* 2011; Linnerbauer, Wheeler et Quintana, 2020; Sofroniew, 2020; Han *et al.,* 2021).

Une autre étude a montré que la stimulation des astrocytes avec de l'IFN-γ induisait l'expression de la molécule du CMH de classe II (CMH-II). Ceci suggère que les astrocytes pourraient également exercer un rôle de cellules présentatrices d'antigènes (CPA). Par ailleurs, bien que les astrocytes soient activés par les signaux environnants, ils peuvent aussi réguler l'activité immunitaire des cellules avoisinantes en sécrétant des molécules telles que le facteur de croissance transformant β (TGF-β). La présence de TGF-β astrocytaire induit l'expression neuronale du C1q qui est impliqué dans la voie du complément (Bialas et Stevens, 2013). De plus, lors d'un traumatisme comme une lésion de la moelle épinière, les astrocytes au lieu d'entrer en apoptose s'activent et prolifèrent (Mallah *et al.,* 2021). En effet, ils perçoivent des signaux moléculaires indicateurs d'un traumatisme, tel que le facteur de croissance épidermique (EGF), le facteur de croissance fibroblastique (FGF) ou encore l'adénosine triphosphate (ATP). Ces molécules réinitient le cycle cellulaire des astrocytes matures qui ainsi s'activent et prolifèrent afin de former la cicatrice gliale.

III. Protection du SNC

Compte tenu du rôle crucial du système nerveux central, celui-ci va être très bien protégé des chocs et des risques d'infections. L'une de ces premières protections est conférée par sa structure elle-même. En effet, directement sur l'encéphale et la moelle épinière, trois couches de tissus cognitifs, appelés les méninges sont retrouvées. De l'extérieur vers l'intérieur, nous avons la dure-mère, l'arachnoïde et la pie-mère. Entre l'arachnoïde et la pie-mère, l'espace

sous-arachnoïdien laisse circuler le liquide cérébrospinal (ou liquide céphalorachidien (LCR). Ce liquide céphalorachidien, qui est sécrété par les plexus choroïdes, protège le SNC contre les chocs et constitue ainsi sa seconde protection. Il permet également de filtrer les débris générés au sein du SNC. Enfin, pour limiter l'entrée de cellules ou molécules qui pourraient lui être délétères, le SNC va être totalement enveloppé d'une barrière dite infranchissable, la BHE. Cette barrière est composée de cellules endothéliales aux jonctions très serrées, de péricytes, d'astrocytes et de cellules microgliales. Ainsi, de façon hautement contrôlée, elle ne laisse passer que des molécules présentant un faible poids moléculaire. La charge et la liposolubilité de ces molécules seront également des critères dirimants pour leur passage au travers de la BHE. De plus, cette barrière va complétement isoler le SNC du reste du corps, en empêchant l'entrée de cellules immunitaires, de cytokines ou d'espèces réactives qui pourraient déclencher une réponse neuro inflammatoire (Liddelow et Barres, 2017).

B. Lésion de la moelle épinière

I. Généralités

En cas de traumatisme vertébral tel qu'une fracture ou une luxation, la moelle épinière peut être sujette à des lésions, allant de la contusion à la section (Cizkova et *al.,* 2018). Une lésion de moelle épinière (LME) peut mener à la paralysie, selon le degré de sévérité et la localisation de la lésion (Pires et Pêgo, 2015). Une lésion de la partie basse du tronc au niveau des vertèbres lombaires ou thoraciques peut mener à une paraplégie des membres inférieurs. À l'inverse, une lésion de la partie supérieure du tronc au niveau des vertèbres cervicales est associée à une tétraplégie (**Figure 7**) (Alizadeh, Dyck et Karimi-Abdolrezaee, 2019). Dans la majorité des cas, les principales causes de lésion sont les accidents de la route, les chutes, des agressions ou encore des chocs lors d'activités sportives. Au cours des dernières années, le nombre de LME a largement augmenté avec une prédominance masculine. Selon l'organisation mondiale de la santé, entre 250 000 et 500 000 personnes dans le monde et par an sont atteintes de traumatismes médullaires (https://www.who.int/). La France, à elle seule, compte mille nouveaux cas par an, avec environ vingt patients à l'échelle lilloise. Au niveau économique, le coût à vie d'une LME représente environ 2,35 millions de dollars par patient (Alizadeh et *al.,* 2019). Bien qu'il existe différentes formes de lésion médullaire, la plus courante est la lésion compressive résultant d'une compression de la moelle épinière par les vertèbres qui se sont déplacées. Afin d'établir le niveau de sévérité de la lésion de la moelle

épinière, l'American Spinal Cord Injury Association (ASIA) a proposé une classification. Celle-ci prend en compte le degré de perte de la fonction sensorielle et de l'activité motrice ainsi que le niveau neurologique du patient et le niveau de récupération de la blessure.

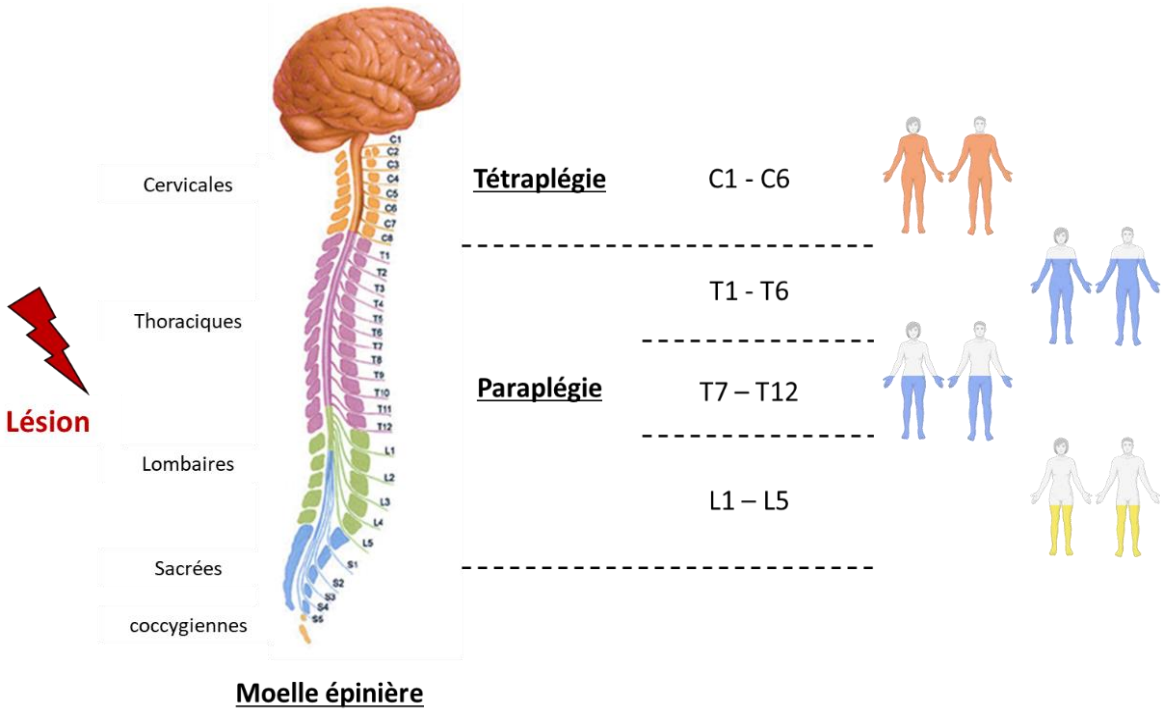

Figure 7 : Les différents niveaux de lésion de la moelle épinière. Une lésion de la LME au niveau des vertèbres cervicales entraine une tétraplégie alors qu'une lésion entre les vertèbres thoraciques et lombaires entraine une paraplégie des membres inférieurs du corps.

II. Physiopathologie

La lésion de la moelle épinière se déroule en deux phases principales :

La première phase est caractérisée par un traumatisme mécanique primaire dû au déplacement des vertèbres (**Figure 8**). En effet, dans la majorité des cas, il n'y a pas de coupure nette de la moelle épinière. Ce sont les vertèbres ou fragments d'os déplacés qui provoquent une compression, une lacération et/ou un cisaillement de la moelle épinière. La durée et le degré de compression va déterminer la gravité et l'issue de la lésion (**Figure 8**).

<u>Figure 8 :</u> Compression de la moelle épinière par le déplacement de vertèbres. IRM d'une lésion de la moelle épinière engendrée par le déplacement des vertèbres cervicales.

Après cette phase mécanique, une seconde phase se met en place en trois temps : la phase aiguë, la phase subaiguë et la phase chronique (**Figure 9**). Lors de la phase aigüe, les vaisseaux sanguins vont être endommagés par la compression, ce qui conduit à la création d'un hématome au site lésionnel. Puis, cet hématome entraîne la formation d'un œdème et d'une ischémie locale (Rowland et *al.,* 2008 ; Alizadeh, Dyck et Karimi-Abdolrezaee, 2019). La privation en oxygène induit une importante mort cellulaire au site lésionnel, causant une libération importante de glutamate. Une très haute concentration de glutamate dans le milieu extracellulaire va alors créer une excitotoxicité pour les cellules avoisinantes. En effet, le glutamate qui est un neurotransmetteur excitateur du SNC, va se lier aux récepteurs NMDA ou AMPA présents sur les cellules neuronales et gliales et déclencher une entrée importante de calcium (Ca^{2+}) dans celles-ci. Cependant, la mitochondrie de la cellule ne peut pas prendre en charge une si grande quantité de Ca^{2+}, ce qui va provoquer un déséquilibre ionique, la production de radicaux libres, une déficience en ATP et finalement la mort cellulaire. Par la suite, l'apoptose et la démyélinisation des neurones initient la phase subaiguë. Lors de cette mort neuronale, un relargage important de protéines intracellulaires dans le milieu extracellulaire va survenir et conduire à l'activation des astrocytes (**Figure 9**).

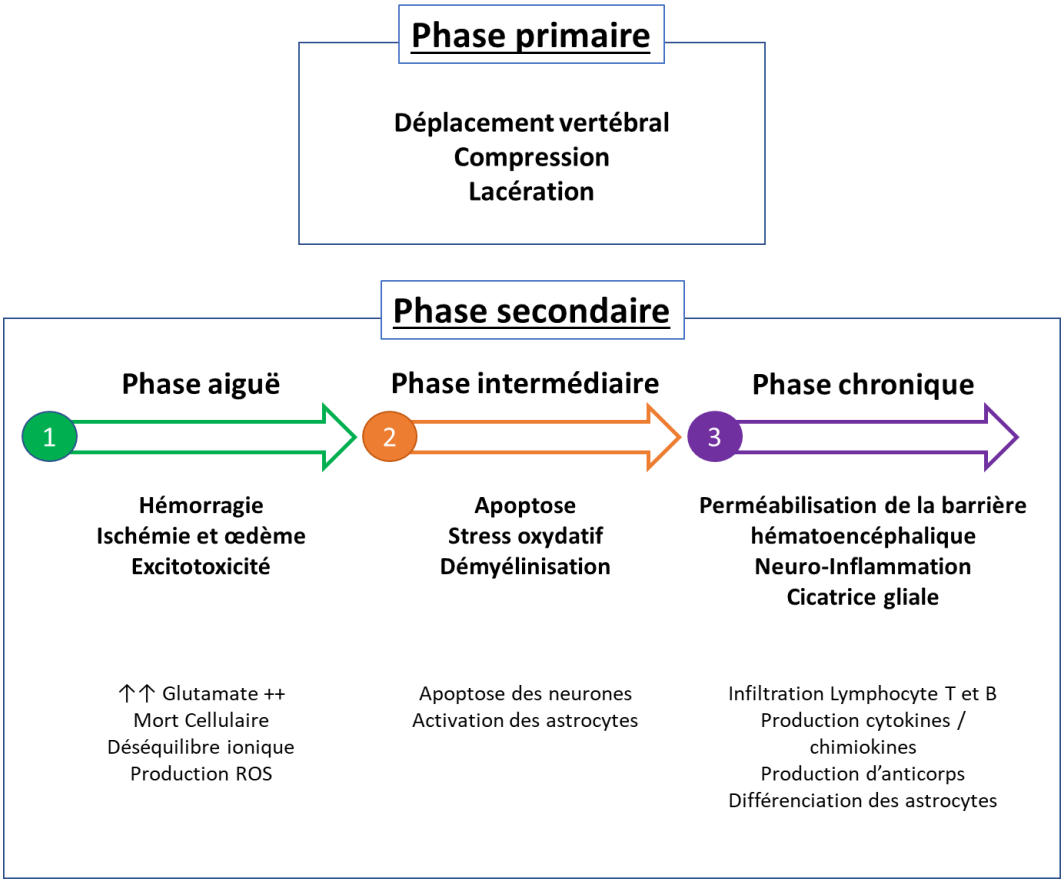

Figure 9 : Physiopathologie de la lésion de la moelle épinière au cours du temps. La LME peut se diviser en deux grandes phases. La première se caractérise par le déplacement de vertèbres qui engendre une compression et une lacération des vaisseaux sanguins. Puis une seconde phase en trois temps se met en place. D'abord la phase aigüe se met en place avec une hémorragie qui va provoquer un œdème et une ischémie locale. La diminution d'oxygène entraine une augmentation du niveau de glutamate extracellulaire qui provoque une excitotoxicité. Cet environnement toxique initie la phase intermédiaire avec l'apoptose des cellules neuronales et avoisinantes. Par la suite, lors de la phase chronique, la perméabilisation de la barrière hématoencéphalique entraine l'infiltration de cellules immunitaires au site lésionnel qui vont déclencher une neuro-inflammation.

À la suite de cette activation, les cellules astrocytaires vont libérer des cytokines et des chimiokines qui vont entraîner la perméabilisation de la barrière hémato-encéphalique (BHE). Cette ouverture permet l'infiltration de cellules immunitaires sur le site lésionnel telles que les neutrophiles, la microglie ainsi que les lymphocytes T et B. Une réponse neuro-inflammatoire très complexe se met alors en place et marque le début de la phase chronique (**Figure 9**) (Alizadeh et *al.,* 2019; Cizkova *et al.,* 2020). Les lymphocytes T et B ayant ainsi infiltré le site lésionnel vont produire des molécules pro-inflammatoires et des anticorps, ce qui accentue la dégénérescence cellulaire et tissulaire. Cependant, afin de rétablir l'intégrité de la BHE et l'homéostasie tissulaire, les astrocytes activés vont proliférer et migrer vers le site

lésionnel. Une fois arrivés au niveau du site lésionnel, la production de filaments intermédiaires astrocytaires augmente et conduit à la formation de la cicatrice gliale. Cette cicatrice va permettre d'isoler la lésion et de limiter sa propagation aux tissus sains. Néanmoins, cette barrière gliale présente aussi des inconvénients puisqu'elle va empêcher la régénération de la moelle épinière.

III. Traitements

Le premier acte thérapeutique va être de réaliser une neurochirurgie afin de décompresser et de stabiliser la moelle épinière le plus rapidement possible lors de la phase primaire. Celle-ci n'a pas pour but de permettre la récupération des fonctions sensorielles ou motrices, mais seulement de limiter les complications graves qui pourraient subvenir à la suite d'une compression prolongée. Après cette chirurgie, selon le stade d'avancement de la lésion médullaire, différentes thérapies peuvent être mises en place telles que des thérapies pharmacologiques, non pharmacologiques ou encore des transplantations cellulaires (Alizadeh et *al.,* 2019). En effet, un traitement pharmacologique va être privilégié lors de la phase aiguë alors qu'un traitement avec des tissus nerveux et/ou des facteurs neurotrophiques sera plutôt privilégié lors du stade chronique.

Les traitements médicamenteux les plus couramment utilisés sont :

- Le Riluzole, un neuroprotecteur, qui va bloquer les récepteurs du glutamate. Celui-ci va réduire l'excitotoxicité et ainsi diminuer la mort cellulaire dépendante du calcium. Depuis 2014, des essais cliniques sont en cours et montrent que cette neuroprotection permet des améliorations fonctionnelles au niveau du site lésionnel.

- Le Kétorolac, un analgésique et anti-inflammatoire non stéroïdien (AINS), va réduire l'agression ischémique lors de la phase aiguë. Il va ainsi diminuer la mort neuronale et l'activation des astrocytes. Cependant, des études ont montré que l'efficacité du traitement au Kétorolac pour permettre une amélioration des fonctions motrices dépend du moment d'administration (Hsieh et *al.,* 2005; Bagriyanik et *al.,* 2008; Dong et *al.,* 2013).

- La Minocycline, qui est déjà connue comme agent neuroprotecteur dans plusieurs maladies neurodégénératives. Cet antibiotique anti-inflammatoire va réguler la

production de cytokines pro-inflammatoires et de radicaux libres par la microglie et les neutrophiles infiltrants. Les derniers essais cliniques MASC « Minocycline in Acute Spinal CordInjury » ont montré qu'un traitement à la minocycline lors de la phase aiguë de la LME permet une amélioration motrice significative en fonction du site de lésion. En effet, le traitement n'a eu aucun effet chez les patients atteints de lésions médullaires cervicales alors que celui-ci s'est trouvé plus efficace chez des patients ayant une lésion médullaire thoracique (Arnold et Hagg, 2011; Casha *et al.,* 2012).

- Le Fingolimod (FTY720), un agoniste des récepteurs de la sphingosine, induit une lymphopénie. En effet, un traitement au FTY720 dès la phase aiguë a permis de diminuer l'infiltration de lymphocytes T. Ce traitement réduit également l'accumulation d'astrocytes au site lésionnel. FTY720 limite ainsi l'inflammation chronique et permet une récupération de la fonction motrice (Norimatsu et *al.,* 2012).

- Le magnésium (Mg^{2+}), qui est largement connu pour ses propriétés neuroprotectrices dans de nombreuses maladies neurodégénératives du système nerveux central. Il va entrer en compétition avec les ions calcium pour les récepteurs N-méthyl-D-aspartate (NMDA), et ainsi empêcher l'activation des astrocytes réactifs (Kaptanoglu *et al.,* 2003).

- Des médicaments anti-inflammatoires sont également testés. La Méthylprednisolone (MPSS), un corticostéroïde anti-inflammatoire utilisé pour améliorer le flux sanguin et diminuer le taux de calcium extracellulaire. La Gacyclidine (GK-11), un antagoniste non compétitif des récepteurs NMDA, qui agit comme agent neuroprotecteur contre l'apoptose des oligodendrocytes. Cependant, les agents anti-inflammatoires se sont avérés efficaces uniquement lors de la phase aiguë de la lésion.

- De nombreux autres traitements basés sur des facteurs de croissance ou des composés anti-inflammatoires naturels sont par ailleurs en cours d'essai et ont montré des résultats intéressants (Alizadeh et *al.,* 2019).

Malheureusement, à ce jour, l'ensemble de ces traitements reste encore inefficace pour une récupération complète des fonctions motrices et sensorielles de la moelle épinière. Ainsi, il

est important de mieux comprendre la physiopathologie de la lésion dans le but d'établir de nouvelles thérapies.

IV. Modèle de la lésion de moelle épinière chez le rat

Pour mieux comprendre les mécanismes biologiques survenant lors d'une lésion de la moelle épinière, plusieurs modèles animaux ont été développés. Par exemple, de grands mammifères tels que les chiens, les chats ou les primates peuvent être utilisés mais cela reste très rare. En effet, leur utilisation est soumise à des restrictions éthiques très strictes. De plus, ces animaux nécessitent des soins post-opératoires et un hébergement très coûteux. C'est pourquoi, au cours de ces dernières années, les modèles de LME sur les rongeurs ont largement été privilégiés. En effet, en plus d'être moins coûteux, le risque d'infections post-chirurgicales reste faible et leur prise en charge thérapeutique est très facile. Par ailleurs, des études par IRM sur la LME chez le rat ont montré de grandes similarités électrophysiologiques, fonctionnelles et/ou morphologiques par rapport à une LME retrouvée chez l'homme (Devaux *et al.,* 2016, 2017; Cizkova et *al.,* 2020; Metz *et al.,* 2000).

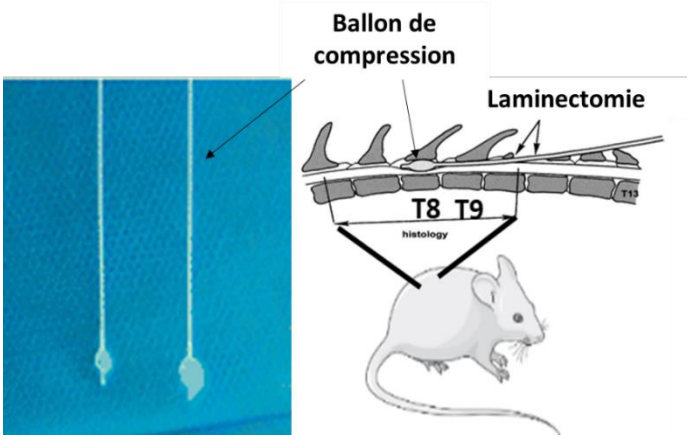

Figure 10 : Modèle de lésion de la moelle épinière. Ballon de compression et représentation d'une laminectomie avec insertion d'un ballonnet de compression au niveau des vertèbres thoraciques 8 et 9 (T8-T9).

Au niveau cellulaire, les astrocytes humains et de rongeurs diffèrent sur plusieurs points. Les astrocytes protoplasmiques humains sont 2,55 fois plus grands avec des processus 2,6 fois plus longs et plus complexes que ceux des rongeurs. Cependant, il peut aussi y avoir des caractéristiques communes entre les deux espèces. Tout comme chez la souris et le rat, les

astrocytes humains vont présenter une régionalisation bien définie selon leur sous type (Oberheim et *al.,* 2009). Les lésions de la moelle épinière sont réalisées chez le rat par laminectomie et à l'aide d'un cathéter de Fogarty de 2 French (**Figure 10**). Il consiste à insérer un ballonnet de compression dans l'espace péridural ou sous-dural à travers un petit trou pratiqué vers la vertèbre T10 (Tarlov, Klinger et Vitale 1953). Le ballonnet est ensuite avancé crânialement jusqu'aux vertèbres T8-9 (**Figure 10**). Une fois en place, celui-ci est gonflé avec 15 µl de solution saline pendant 5 minutes afin de mimer une compression vertébrale (Yeo *et al.,* 2004; Chung *et al.,* 2013). Ce modèle présente ainsi une paraplégie complète avec une récupération fonctionnelle progressive. Cependant, il est possible d'utiliser différents volumes ou temps de compression pour obtenir différents degrés de dommages de la ME (Yeo et *al.,* 2004; Chung et *al.,* 2013).

V. Présence d'immunoglobulines lors d'une lésion de la moelle épinière

Étant donné, le rôle majeur de la réponse inflammatoire lors de la LME, le laboratoire PRISM s'est focalisé sur la compréhension des mécanismes moléculaires impliqués lors de celle-ci. Pour ce faire, le laboratoire a réalisé des études protéomiques spatio-temporelles afin d'identifier les différents facteurs mis en jeu (Devaux *et al.,* 2017; Cizkova *et al.,* 2018). Celles-ci ont montré que la région rostrale, localisée en amont de la lésion, produit des facteurs impliqués dans la neuritogénèse, alors qu'au niveau de la lésion et de la région caudale située en aval de la lésion, ce sont des facteurs inflammatoires qui sont libérés. Néanmoins, les profils moléculaires ont montré l'existence d'une neuritogenèse tant du côté rostral que caudal. Seuls les segments de part et d'autre de la lésion diffèrent au cours du temps. En effet, à 12h après la lésion, le profil moléculaire est identique entre la région rostrale et caudale, alors qu'à 24 heures après la lésion, une orientation vers environnement inflammatoire se réalise à la région caudale et s'amplifie à 3 jours (Cizkova *et al.,* 2014; Devaux *et al.,* 2016, 2017). Ce changement d'orientation peut s'expliquer par l'arrivée massive de lymphocytes T régulateurs dans les premières heures du côté rostral, mais pas du côté caudal où il faut attendre après 7 jours. Cette différence temporelle empêche une neuritogénèse coordonnée de part et d'autre de la lésion. L'analyse fine des facteurs produits au sein des segments (rostral et caudal) a permis de mettre en évidence, de façon surprenante, la présence d'immunoglobulines de type chaînes lourdes IgG et de chaînes légères Kappa et Lambda dès 12h après la lésion (Devaux et *al.,* 2016). L'analyse par Western-Blot a également montré une quantité plus importante d'Igs

dans le sécrétome d'explants de moelle épinière 12h après lésion, et ce, principalement au niveau du site lésionnel (Cizkova et *al.,* 2018; Devaux et *al.,* 2017). Cette présence d'IgG est surprenante, étant donné que ces isotypes d'anticorps, n'interviennent que 7 jours après une première infection ou 3 jours lors d'une seconde infection. Ces résultats posent donc la question de l'origine cellulaire de ces Igs.

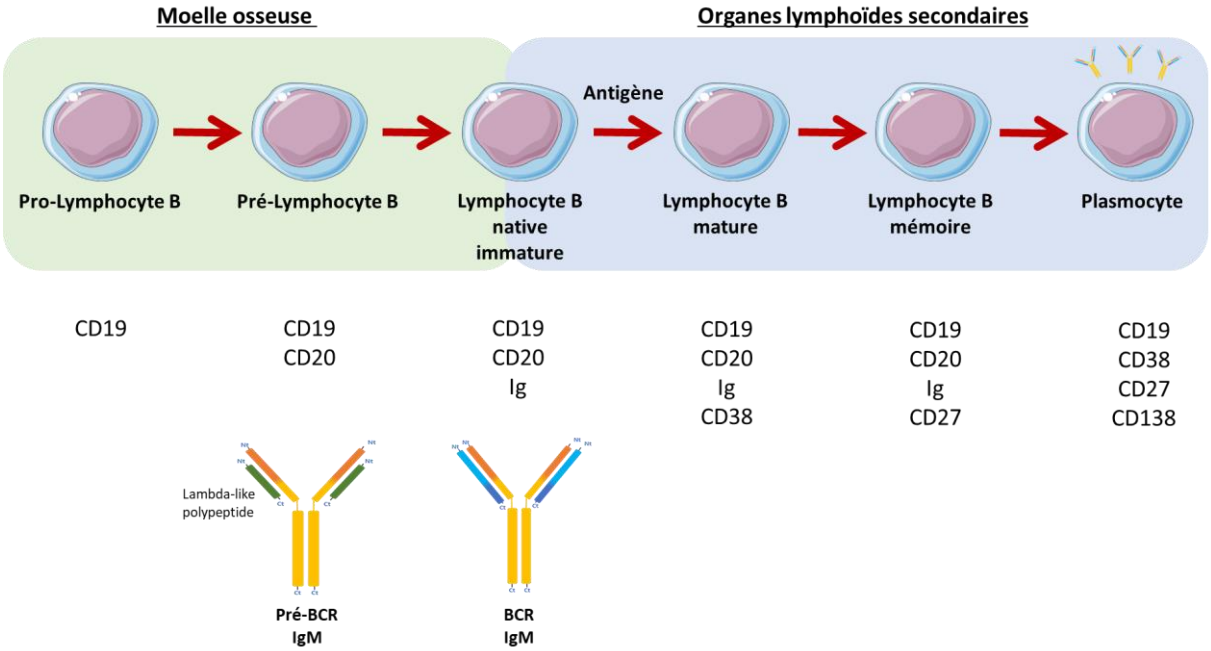

Figure 11 : Différenciation des lymphocytes B. les Lymphocytes B prennent naissance dans la moelle osseuse. Elles se différencient dans la moelle osseuse, puis migrent vers les organes lymphoïdes secondaires pour rencontrer l'antigène et devenir mature.

C. Les immunoglobulines (Igs)

I. Généralité

Les êtres vivants sont continuellement en contact avec des agents pathogènes tels que les bactéries, les virus ou les levures. L'organisme est protégé contre ces agressions par son système immunitaire. En cas d'infection, la réaction immunitaire se met en place et se déroule selon deux phases séquentielles majeures. Dans un premier temps, la réponse immunitaire innée va se mettre en place de façon rapide et non strictement spécifique. Si celle-ci n'est pas suffisante, la réponse adaptative se met alors en place dans un second temps et ciblera de manière spécifique le pathogène. Cette dernière va faire intervenir différentes cellules immunitaires dont les lymphocytes B. Les lymphocytes B, ou cellules B, sont responsables de la réponse immunitaire humorale spécifique. Ils se développent dans la moelle osseuse à

partir des cellules souches hématopoïétiques. Ces dernières forment des progéniteurs lymphocytaires communs (CLP) dont une partie deviendra les premières cellules B progénitrices (pro-B). Celles-ci matureront ensuite en cellules pré-B qui exprimeront à leur surface le marqueur de différenciation CD20. Les pré-B deviendront des cellules B immatures, puis des cellules B matures naïves. Les LB naïfs migreront ensuite vers les organes lymphoïdes secondaires, où ils rencontreront l'antigène et produiront alors des anticorps (Ac) dirigés spécifiquement contre celui-ci. Cette réponse est dite humorale (**Figure 11**).

II. Structure d'une immunoglobuline

Les anticorps, aussi appelés immunoglobulines, sont des glycoprotéines constituées par l'association de quatre chaînes polypeptidiques, c'est-à-dire de deux chaînes lourdes identiques de 50 kDa et de deux chaînes légères identiques de 25 kDa, reliées entre elles par des ponts disulfures (Espinosa et *al.,* 2010). Chaque chaîne présente une partie constante du côté C terminal (Ct) et une partie variable du côté N terminal (Nt).

La chaîne légère possède une seule région variable (VL) et constante (CL) tandis que la chaîne lourde possède un domaine variable (VH) et 3 à 4 domaines pour la partie constante (CH1 à CH3 ou CH4) (**Figure 12**). Par ailleurs, une zone charnière (Hinge, en anglais) permettant la flexibilité de l'Ac est présente entre le CH1 et le CH2 de la chaîne lourde. L'anticorps peut distinguer deux fragments. Le fragment de liaison à l'antigène (Fab) en 5' est formé de la chaîne légère entière et de la région variable et du CH1 de la chaîne lourde. Le second fragment est la partie cristallisable (Fc). Celle-ci est constitué de l'association des CH2 et CH3 (ou CH4) des deux chaînes lourdes (**Figure 12**). L'association des parties variables forme une structure moléculaire 3D, appelée le paratope et qui reconnait spécifiquement l'épitope d'un antigène donné (**Figure 12**). Sur ce principe, une très grande diversité de paratopes est nécessaire pour cibler un très grand nombre d'antigènes différents. Une telle variabilité est alors générée par un mécanisme de recombinaison somatique aléatoire, appelé la recombinaison V(D)J.

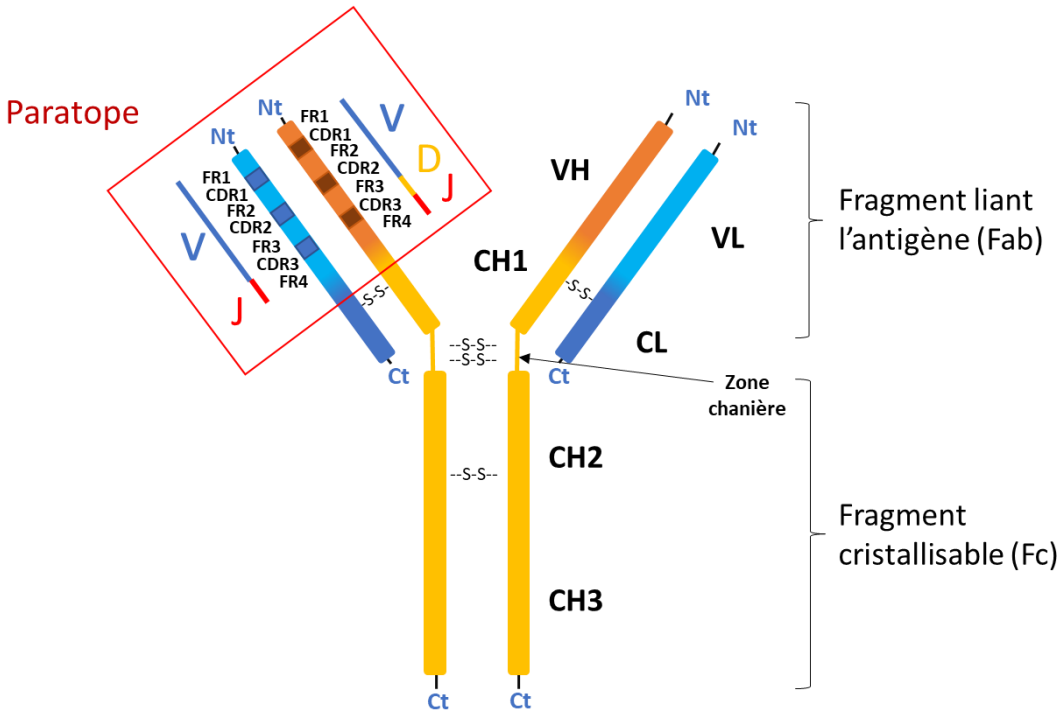

Figure 12 : Structure d'un anticorps (Ac). Aussi appelés immunoglobulines, les Ac sont des glycoprotéines constituées de deux chaînes lourdes identiques et de deux chaînes légères identiques, reliées entre elles par des ponts disulfures (Espinosa et *al.,* 2010). Chaque chaine présente une partie constante du côté C terminal (Ct) et une partie variable du côté N terminal (Nt). La chaîne légère possède une région variable (VL) et constante (CL), alors que la chaîne lourde est composée d'un domaine variable (VH), d'une zone charnière et de 3 à 4 domaines constants (CH1 à CH3 ou CH4). L'association des parties variables forme un paratope qui lie spécifiquement un antigène donné. VL: variable light; CL: constant light; VH: Variable heavy; CH: constant heavy (Light = légère; Heavy = lourde).

III. Recombinaison V(D)J

Cette recombinaison se caractérise par un réarrangement génique du segment V (variable) avec un segment D (diversité) et J (jonction) dans le cas des chaînes lourdes et V et J dans le cas des chaînes légères (**Figure 13**). Chaque exons V, D et J est flanqué par des séquences de recombinaison très conservées, appelées RSS « recombination signal sequences ». Ces RSS sont constitués d'un heptamère palindromique très conservé (CACAGTG), suivi d'une séquence intercalante non conservée de 12 ou 23 nucléotides, puis d'un nonamère également conservé (ACAAAAACC). Il est important de noter qu'un RSS avec une séquence intercalante de 12 nucléotides ne peut être recombinée qu'avec un RSS de 23 nucléotides. C'est la règle 12-23. Celle-ci permet de contrôler correctement le réarrangement génique des exons V-D-J pour la chaîne lourde et V-J pour la chaîne légère. Elle empêche ainsi l'appariement entre deux mêmes segments et contrôle l'ordre de recombinaison. Par exemple, pour le locus de la chaîne

lourde, elle empêche la survenue d'un réarrangement V-J et assure le réarrangement tout d'abord DJ puis V-DJ (**Figure 13**).

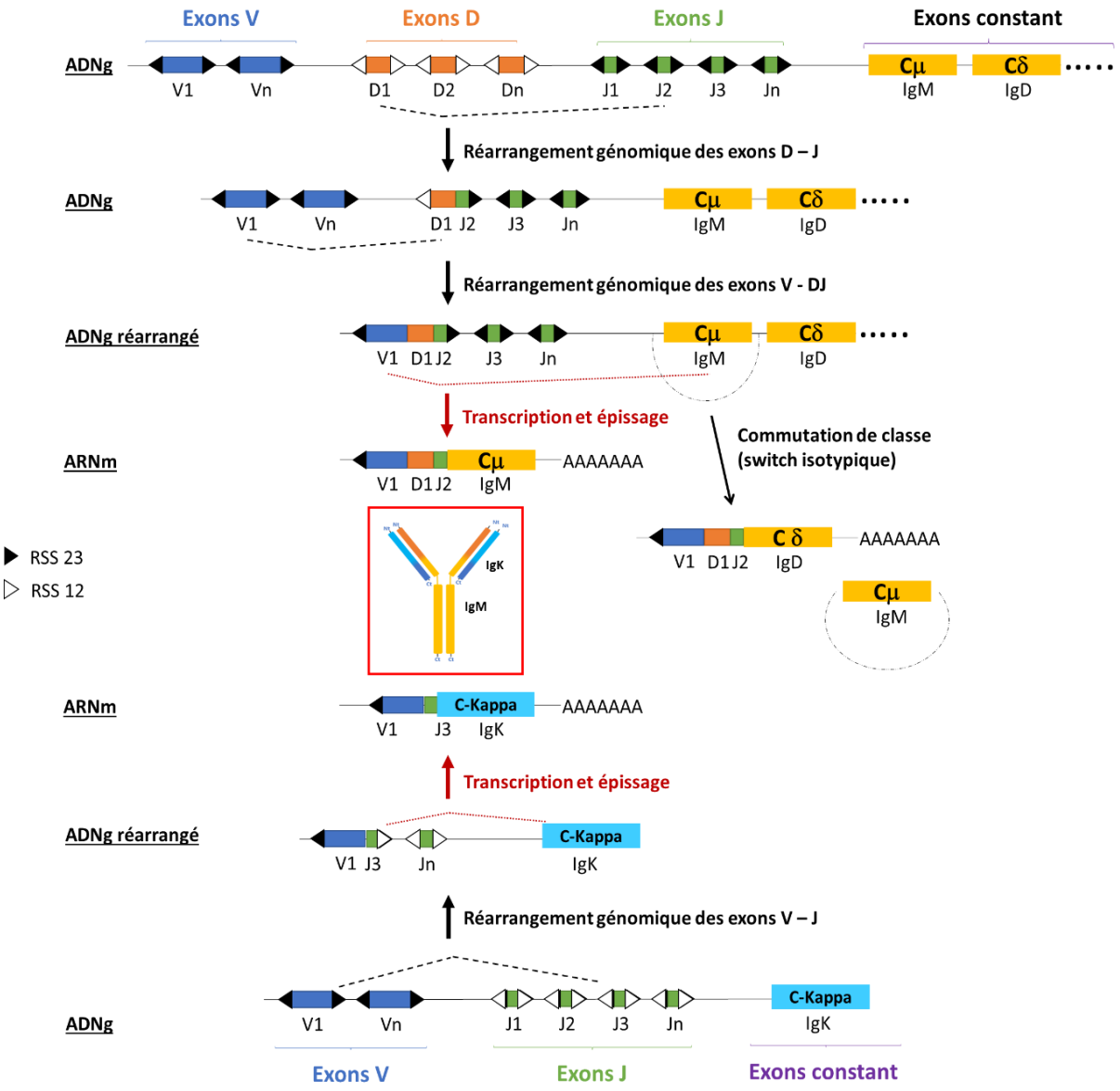

<u>Figure 13 :</u> Recombinaison des exons V – (D) – J de la partie variable de l'Ig et commutation de classe.(Kaeser and Chun, 2020). Réarrangement génomique des segments Variable (V), de Diversité (D) et de Jonction (J) avec la partie constante de la chaîne lourde IgM ou IgA. Réarrangement génomique des segments Variable (V) et de Jonction (J) avec la partie constante de la chaîne légère Kappa (IgK).

Ce processus V(D)J fait intervenir un complexe enzymatique particulier (**Figure 14**). Dans un premier temps, les deux transposases RAG1 et RAG2 se lient au niveau des séquences RSS 12-23 des exons sélectionnés et clivent l'ADN. Puis, pour initier le processus de réparation, KU70 et KU80 induisent la formation d'épingles à cheveux et cassent les extrémités clivées. Ensuite,

la protéine kinase ADN dépendante (DNA-PKCs) et l'endonucléase Artemis sont recrutées pour ouvrir ces épingles à cheveux et permettre à la Terminal deoxynucleotidyl transferase (Tdt, ou nouvelle nomenclature DNTT) d'ajouter aléatoirement des nucléotides. Cette addition de nucléotidiques permet d'accroître la diversité des séquences des anticorps synthétisés, nous parlons de diversité jonctionnelle. Par la suite, la DNA Ligase IV, l'XRCC4 ainsi que Cermunnos - XLF relient les deux segments ensemble (**Figure 14**) (Kuby et al. 2008).

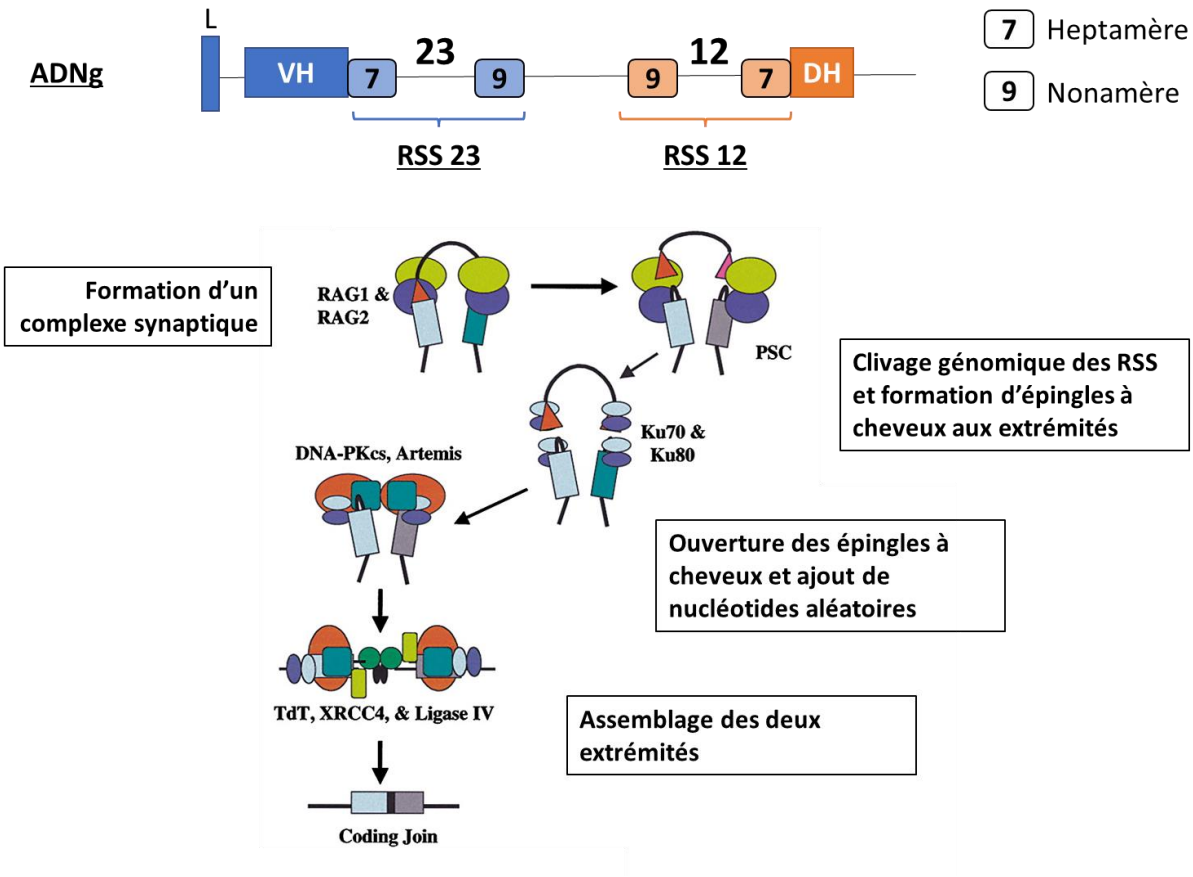

Figure 14 : Mécanisme enzymatique de la recombinaison V(D)J. Les enzymes Rag1 et Ra2 vont cliver l'ADNg au niveau des RSS. Par la suite, Ku70, Ku80, DNA-PKc et Artemis coupent ces épingles à cheveux afin de permettre à la TdT, XRCC4 et la Ligase IV d'assembler les deux extrémisés (Adapté à partir de Bassing, Swat and Alt, 2002).

Par ce mécanisme, une multitude de combinaisons V - (D) - J peut alors être générée et conduit à une grande diversité combinatoire. Le locus génique ainsi recombiné est ensuite transcrit afin de synthétiser un l'ARN pré-messager correspondant. Cependant, les segments VDJ pour la chaîne lourde et VJ pour la chaîne légère sont toujours séparés des exons codant la région constante C de l'anticorps par un intron (**Figure 13**). Celui-ci est retiré lors de l'épissage du pré-ARNm, ce qui permet de joindre le segment V(D)J au segment constant. La traduction des

messagers conduit à la synthèse de chaînes lourdes et légères qui s'associeront pour former l'anticorps (**Figure 13**).

IV. Isotypes et fonctions

a) Chaines légères

Pour la chaine légère, il existe 2 isotypes différents que sont les chaines légères Kappa (IgK) et Lambda (IgL). Ces chaines sont codées par des gènes situés sur deux locus différents. Le gène IgK se situe sur le chromosome 2 chez l'humain et 4 chez le rat, alors que le locus IgL se trouve sur le chromosome 22 chez l'humain et 11 chez le rat. Chaque chaîne légère présente un poids moléculaire de 25 kDa. Par ailleurs, il est intéressant de noter que la chaine IgK est préférentiellement produite par rapport à la chaine lambda. Cela est dû à une sélection allélique majoritaire qui a lieu lors du développement du LB. Les cellules pré-B vont d'abord présenter un réarrangement VDJ-constante pour la chaîne lourde. Seule la chaîne d'IgM est synthétisée à ce stade et va être associée à une chaîne polypeptide Lambda-Like en attendant la sélection de la chaîne légère. Cette dernière commence par un réarrangement VJ-constante sur le locus Kappa. Si aucun réarrangement n'est productif et sélectionné, c'est le locus Lambda qui est réarrangé. Si aucun des deux locus n'est fructueux, la cellule B entre en apoptose. Au cours de la synthèse des anticorps, les chaines légères sont produites en quantité plus importante que les chaines lourdes. Il y a donc une partie de ces chaines légères qui n'est pas utilisée pour la formation de l'anticorps. Celles-ci seront retrouvées de façon libre dans le sang et seront éliminées par les urines au cours des jours suivants. Le dosage du taux de ces chaines libres peut être utilisé comme marqueur prognostique pour certaines maladies comme la « protéinurie de Bence - Jones ». Elles sont aussi observées dans certaines hémopathies, telles que les gammapathies, le myélome, la maladie de Waldenström ou encore l'amyloïdose.

b) Chaines lourdes

Les Igs peuvent être classées en isotypes ou sous-classes en fonction du gène codant la partie constante de la chaine lourde. Ces gènes sont retrouvés au niveau du locus IgH sur le chromosome 14 chez l'humain et 6 chez le rat. Ils sont organisés dans l'ordre suivant : 5'-Cμ-Cδ-Cγ3-Cγ1-Cψε-Cα1-Cψγ-Cγ2-Cγ4-Cε-Cα2- 3', et codent respectivement pour IgM, IgD, IgG3,

IgG1, IgEHP, IgA1, IgGHP, IgG2, IgG4, IgE et IgA2. IgEHP et IgGHP sont considérés comme des pseudogènes. De plus, chacun de ces isotypes va jouer un rôle et une structure définis.

	IgA	IgD	IgE	IgM	IgG1 / IgG2 / IgG3 / IgG4
				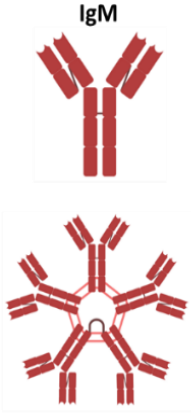	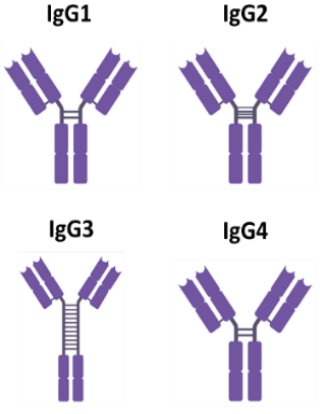
Chaine	α	δ	ε	μ	γ
Poids moléculaire	170 - 385 kDa	150 kDa	190 kDa	180 - 900 kDa	150 – 160 kDa
Activation du complément	-	-	-	+	+
Fonction	Protection des muqueuses Sécrétée dans les mucus	Antigène récepteur membranaire	Réactions allergiques et parasitaires	Réponse primaire non spécifique Recepteur membranaire	Réponse secondaire spécifique (adaptative)

Figure 15 : Les différents Isotypes d'immunoglobulines et leurs caractéristiques. Les 5 classes d'immunoglobulines représentée avec leurs caractéristiques structurales et fonctionnelles.

Pour la chaîne lourde, il existe 5 isotypes :

- IgM (Mu). Les IgM représentent en moyenne 10 % des immunoglobulines sériques. La partie constante de la chaîne lourde d'une IgM est composée de 4 domaines constants (CH1 à CH4). Ce sont les premières immunoglobulines produites lors de l'ontogenèse des cellules B et lors d'une première infection. Celles-ci vont présenter une faible spécificité pour l'antigène. De plus, elles peuvent être synthétisées sous deux formes : soit sous forme monomérique présentée à la membrane pour servir de récepteur antigénique ; soit sous forme pentamérique constituée par l'association de 5 IgM reliés entre elles par une petite chaîne J. Cette forme pentamérique est sécrétée dans la circulation afin de servir pour la surveillance de l'organisme. Elle conduit à une forte activation de la voie du complément.

- IgD (Delta). Les IgD sont majoritairement exprimées sous forme monomérique et à la surface membranaire des LB. Elles vont former des récepteurs à l'antigène, avec les

protéines CD79a et CD79b. Pour les lymphocytes B matures, elle est coexprimée avec l'IgM et représente environ 1% des protéines de la membrane plasmique.

- IgA (Alpha). Les IgA sont, quant à elles, retrouvées sous forme dimérique dans la salive ou encore les sécrétions nasales et gastrointestinales. Elles présentent deux sous-classes distinctes que sont les IgA1 et IgA2. Elles vont protéger les muqueuses en empêchant les pathogènes de se lier aux cellules épidermiques.

- IgE (Epsilon). Les IgE sont des anticorps principalement associés aux réactions allergiques et parasitaires. Cette immunoglobuline epsilon présente une demi-vie d'environ deux jours. Elles sont essentiellement retrouvées au niveau de la peau, du tube digestif mais aussi des amygdales et du tractus respiratoire.

- IgG (Gamma). Les immunoglobulines Gamma, ou IgG, sont les anticorps les plus abondamment synthétisés. Elles sont produites principalement lors d'une réponse secondaire adaptative et elles vont permettre une protection de l'organisme à long terme de par une demi-vie très longue. Elles ont un poids moléculaire d'environ 150-170 kDa. Chez l'humain, elles sont réparties en quatre sous-classes selon leur ordre croissant d'abondance : IgG1, IgG2, IgG3 et IgG4 codées respectivement par les gènes Cγ1, Cγ2, Cγ3 et Cγ4 (Vidarsson, Dekkers and Rispens, 2014). À quelques différences près, ces différentes IgG vont avoir des séquences protéiques très proches. Par exemple, elles se différencient majoritairement au niveau du domaine CH2, zone de fixation de la molécule du complément C1q et par la flexibilité de la zone charnière. Elles vont aussi présenter des différences par rapport à leur spécificité de liaison à l'antigène, leur taux d'expression, leur demi-vie ainsi que leur fonction. En effet, l'IgG1 est produite en réponse à des antigènes protéiques solubles ou membranaires et elle peut activer tous les récepteurs FcγR et la voie du complément. L'IgG2 est quant à elle principalement synthétisée à la suite de la présence de polysaccharides membranaires dérivés de bactéries ayant infecté l'organisme. Cependant, elle ne présente pas la même capacité que l'IgG1 pour se lier aux récepteurs FcγR et activer la voie du complément. Ces deux IgG ont une demi-vie similaire d'environ 21 jours. Les IgG3 sont

particulièrement retrouvées lors d'une infection virale. Ce sont des anticorps hautement pro-inflammatoires et qui ont une forte habilitée à activer les fonctions effectrices. Par conséquent, elle est l'IgG qui se fixe le mieux aux récepteurs FcγR. Pour éviter une réponse excessive, les IgG3 ont une durée de vie plus courte d'environ 7 jours. C'est aussi l'IgG qui présente la plus grande région charnière, ce qui lui confère un poids moléculaire plus important de 170 kDa. Enfin, l'IgG4 est principalement produite lors d'une inflammation chronique. Par exemple, elle est exprimée avec l'IgE lors d'une réponse allergique ou encore lors de tumeur présentant des antigènes cancéreux sur une longue période. L'IgG4 présente une région charnière très petite de 12 acides aminés et une demi-vie de 21 jours comme les IgG1 et IgG2. Cette Ig ne présente pas une grande affinité pour les récepteurs FcγR et n'active pas la voie du complément. Dans ces conditions, même si le rôle de ces IgG4 n'est pas encore bien connu, elles peuvent être exprimée pour bloquer les fonctions effectrices des autres IgG par compétition ou fixation aux IgG (Crescioli *et al.,* 2016).

Le changement entre les classes d'Igs implique un mécanisme appelé, la commutation de classe (ou switch isotypique). Celle-ci fait intervenir l'enzyme AID (Activation-Induced cytidine Deaminase) (**Figure 13**). Au cours de ce processus, l'AID remplace les exons Cμ (IgM) par les exons Cγ ou Cα ou Cδ ou Cε codant respectivement pour IgG, IgA, IgD ou IgE. Le type de commutation de classe réalisé dépend de la nature des cytokines et chimiokines présentes dans le microenvironnement cellulaire. Par exemple, la stimulation du Toll-like Receptor 4 (TLR4) avec des lipopolysaccharides (LPS) va favoriser une commutation de classe vers l'isotype IgG2 ou IgG3 alors qu'une stimulation au LPS conjointement avec de l'IL-4 va orienter la commutation de classe vers l'IgG1 ou l'IgE. En revanche, au cours de ce processus, la région variable VDJ qui avait été sélectionnée va être conservée et inchangée. Il est important de noter qu'au cours d'une réponse immunitaire, les Ac ne sont pas produits simultanément par les lymphocytes B. En effet, lors d'une réponse primaire, les IgM sont produits en très grandes quantités dès 72 heures, alors que les IgG ne sont produites qu'après 7 jours et en plus faible quantité. A l'inverse, lors d'une réponse secondaire, ce sont les IgG qui seront produites de façon très importante dès 72 heures pour permettre une meilleure reconnaissance de l'antigène.

A la fin du XXe siècle, Takahashi et son équipe ont identifié une nouvelle IgG5 (ou IgGHP) qui est synthétisée à partir d'un gène défini comme un pseudogène. Cette IgG présente une forte homologie de séquence avec l'IgG1. Ce pseudogène est localisé en amont du gène codantl'IgG2 et présente une structure classique avec l'alternance exons/introns ainsi que des sites d'épissage et de polyadénylation bien conservés. En revanche, cette pseudo-IgG ne présente pas de région répétitive dans les 10 kb permettant les cassures chromosomiques nécessaire à la commutation de classe. Bien que ce gène présente un super enhancer 3' RR1 à environ 16 kb en amont de l'exon codant le CH1 de l'IgG5, la grande distance les séparant ne permet pas un épissage normal. Ainsi, du fait qu'IgG5 ne présente pas de région switch canonique, la possibilité que ce gène s'exprime a longtemps été controversée. En réalité, Dalloul et son équipe montrent que son expression fait intervenir un mécanisme non conventionnel. À la suite de différentes analyses transcriptomiques, plusieurs sites accepteurs ont été trouvés directement en amont du gène, suggérant une recombinaison non canonique. De plus, leur étude montre que plusieurs transcrits d'IgG5 avec une diversité de région VDJ a pu être observés. Par la suite, ils ont également confirmé la production de la protéine. D'un point de vue structural, l'IgG5 possède une région charnière plus petite et présentant une séquence spécifique. Sous sa forme complète IgG5 possède des propriétés fonctionnelles similaires aux autres IgGs, telles que la capacité d'activer la voie du complément et la réponse de cytotoxicité à médiation cellulaire dépendante des anticorps (ADCC). Cependant, l'IgG5 présente une séquence charnière particulière lui donnant la possibilité d'être clivé en fragment Fc et Fab. Ces fragments présenteraient un rôle de régulateur et immunosuppressive en entrant en compétition de l'effet effectrice des autres IgG (Dalloul, 2018).

Comme nous avons pu le voir précédemment, les Igs peuvent exister sous forme membranaire ou sous forme sécrétée, pour former des récepteurs à la membrane cellulaire ou circuler dans le sang. Cela est réalisé par un épissage alternatif de l'exon S « sécrétée » ou des exons M1 et M2 « membranaire 1 et membranaire 2 » (**Figure 16**). Ces deux formes permettent d'activer différents mécanismes immunitaires comme la voie du complément, l'opsonisation ou encore la voie ADCC. Pour la voie ADCC, l'anticorps se lie à l'antigène avec son paratope du côté N-terminal, alors que sa partie Fc se fixe sur des récepteurs spécifiques présents à la surface de différentes cellules immunitaires, appelés récepteur FcR.

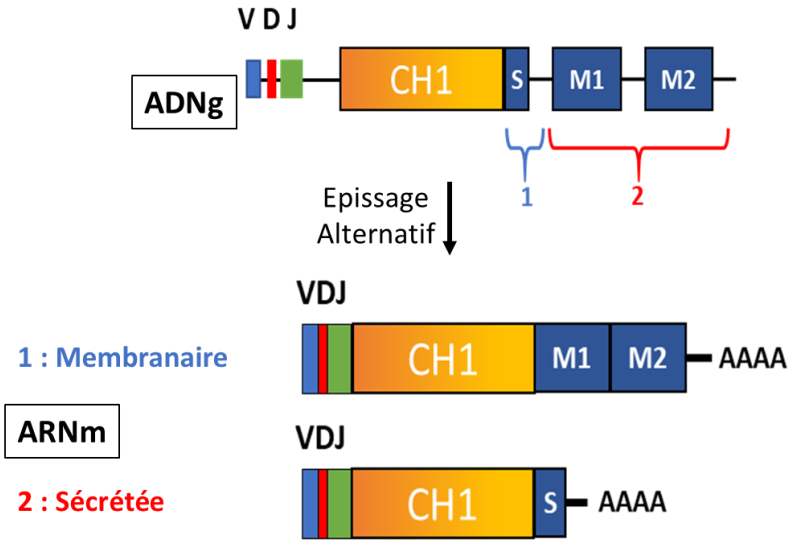

Figure 16 : Epissage alternatif entraînant la forme membranaire ou sécrétée de l'Ig. Un épissage alternatif avec l'exon « S » entraine l'expression de la forme sécrétée, alors que l'épissage avec les exons « M1 » et « M2 » entraîne la forme membranaire de l'immunoglobuline.

V. Récepteurs FcR : les récepteurs FcYR des IgGs

Les récepteurs Fc sont des protéines transmembranaires présentes à la surface de différentes cellules immunitaires telles que les cellules dendritiques, les macrophages, les neutrophiles, les cellules Natural killer (NK) ou encore les lymphocytes B. Ces récepteurs ont la capacité de reconnaître la partie CH2 et la région charnière des immunoglobulines afin de moduler de la réponse immunitaire. Il existe plusieurs classes de récepteurs pour chaque isotype d'Igs. Les IgG se lient aux récepteurs FcYR, les IgE à FcεR, les IgA à FcαR (CD89), et les IgM à FcμR.

Parmi ces récepteurs, seuls ceux reconnaissant les IgGs seront présentés dans cette partie. Au total, 6 classes et sous-classes de récepteurs FcYR ont été identifiées de nos jours à savoir FcYRI (CD64), FcYRIIA (CD32a), FcYRIIB (CD32b), FcYRIIC (CD32c) FcYRIIIA (CD16a), et FcYRIIIB (CD16b). Outre ces récepteurs, notons qu'il existe aussi le récepteur FcR néonatal (FcRn) qui est principalement retrouvé au niveau du placenta au niveau duquel il assure le transport des IgGs maternelles au fœtus. Chacun de ces récepteurs va présenter des affinités différentes pour chacune des sous-classes d'IgGs. Comme présenté dans la figure 16, FcYRI (CD64) va plutôt avoir une haute affinité pour les IgGs monomériques telles que l'IgG1 et l'IgG3 (**Figure 17**). En revanche, il va rarement lier les IgG2 et IgG4. À l'inverse, bien que FcYRII ait une préférence particulière pour les IgG2, les récepteurs CD32 et CD16 auront globalement une

plus faible affinité pour les IgGs (**Figure 17**). L'affinité de liaison des IgGs aux différents récepteurs dépend en partie des glycosylations présentes au niveau de leur domaine CH2. En effet, une glycosylation plus importante va créer un encombrement stérique et ainsi réduire la capacité de l'IgG à se lier au récepteur. D'autre part, les récepteurs FcYR vont aussi avoir une fonction distincte en exerçant un rôle activateur ou inhibiteur de la réponse inflammatoire. En effet, les récepteurs CD64, CD32a, CD32c et CD16 présentent un motif d'activation basé sur la tyrosine (ITAM) qui va induire l'activité phagocytaire, la réponse ADCC ou la production de molécules inflammatoires (**Figure 17**). En revanche, le récepteur CD32b présente un motif inhibiteur (ITIM) qui va empêcher l'activité phagocytaire et l'activité effectrice (**Figure 17**) (Fanger et *al.,* 1996; Raghavan et *al.,* 1996; Nimmerjahn et *al.,* 2006). En plus d'activer des voies immunitaires, ces récepteurs contrôlent également d'autres processus immunomodulateurs tels que la régulation de la maturation des cellules dendritiques, de l'activation des lymphocytes B ou encore le recrutement de cellules inflammatoires (**Figure 17**) (Nimmerjahn et *al.,* 2006).

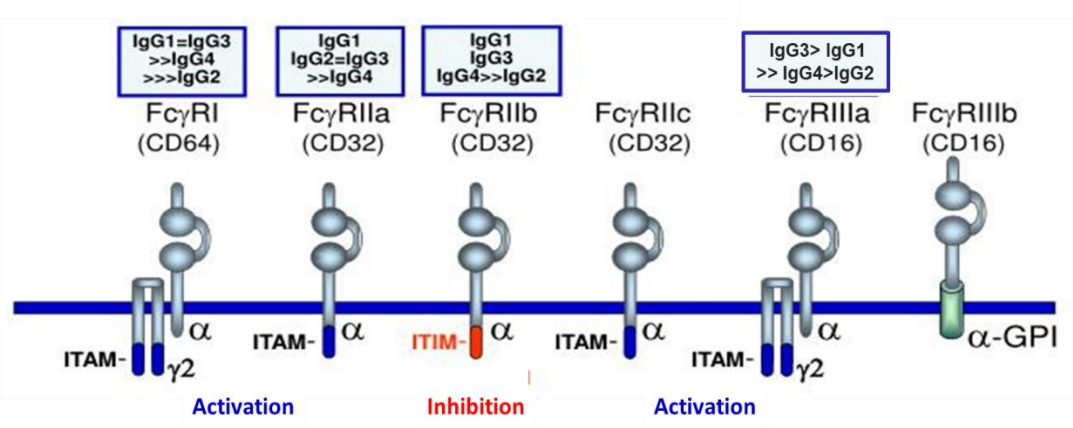

Affinité	Forte	Faible	Faible	Faible	Faible	Faible
Fonction	Phagocytose Activation de la voie cytotoxique	Phagocytose Dégranulation par les éosinophiles	Inhibition des lymphocyte B Inhibition phagocytose Inhibition de la production de cytokines	Phagocytose	Activation de la voie ADCC Induction de la production de cytokines	Induction de la lyse microbienne

Figure 17 : les différents isotypes, les récepteurs et les fonctions des Igs. Les récepteurs CD64, CD32 a et c, ainsi que les récepteurs CD16 présentent un domaine ITAM avec un rôle d'activation des voies effectrices. A l'inverse, le récepteur CD32b présentent un domaine ITIM menant à l'inhibition des fonctions effectrices. Chaque récepteur présente une affinité différente pour sous-classes d'IgG, ainsi que des fonctions distinctes.

VI. Glycosylations des Is

Les fonctions effectrices des anticorps peuvent être influencées par des modifications post-traductionnelles. Parmi celles-ci, la glycosylation a un effet important sur l'immunogénicité, la solubilité et la demi-vie de l'anticorps. Les IgGs présentent un site de N-glycosylation hétérogène localisé au niveau de l'asparagine 297 sur la région CH2 de la chaîne lourde. Le corps de base de ces N-glycanes est composé de deux N-acétyl glucosamines (GlcNAc) et trois résidus mannoses (Man) sur lesquels différents monosaccharides ou acides sialiques peuvent se fixer. De plus, pour 90% des IgGs sériques, un fucose peut se lier en alpha 1,6 du GlcNAc, ce qui diminue leur capacité à induire la réponse ADCC et à se lier au récepteur FcγRIIIa (Raju et *al.,* 2008).

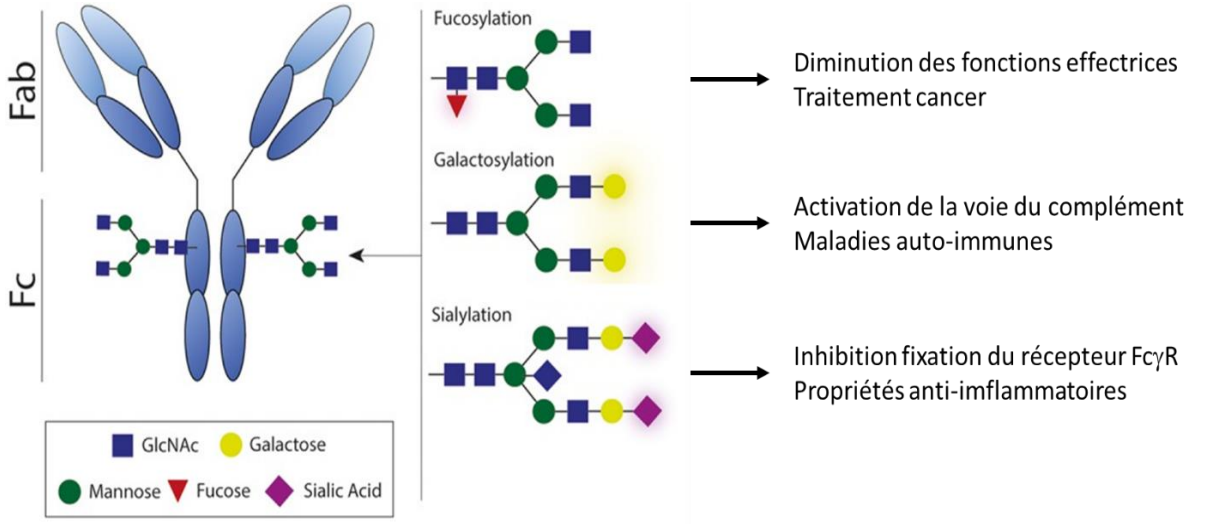

Figure 18 : Glycosylation des anticorps. L'ajout de fucose ou d'acides sialiques diminue les fonctions effectrices, alors que la présence de galactose augmente la voie du complément.

Les anticorps fucosylés se sont révélés immunoprotecteurs (Van Erp *et al.,* 2019). Raju et son équipe ont étudié plus précisément l'influence que ces sucres terminaux exercent sur la fonction de l'anticorps. Ainsi, ils ont montré que la présence d'acide sialique, de fucose, de N-acétylglucosamine ou de mannose en position terminale du N-glycane influence la capacité de liaison de l'anticorps aux récepteurs FcγR (**Figure 18**) (Raju et *al.,* 2008 ; Van Erp et *al.,* 2019). Des niveaux plus élevés d'acides sialiques sont associés à une fonction anti-inflammatoire. Ces acides entrainent une diminution de la voie ADCC du fait d'une liaison plus faible de l'IgG au FcγRIIIa présent à la surface des cellules NK (Scallon *et al.,* 2007). En outre, la présence d'acides sialiques en position terminale augmente la demi-vie de l'anticorps (**Figure 18**). La présence d'un galactose, quant à lui, permet une activation plus forte de la voie

du complément de par la liaison entre l'IgG et le C1q. En revanche, celle-ci est réduite lorsqu'un groupement de mannoses se trouve en position terminale (Raju et *al.,* 2008).

Le dogme, disant que les Igs sont uniquement réalisées par les lymphocytes B, est déjà bien controversé. En effet, des Igs dérivés du cancer ont été mis en évidence (Cui *et al.,* 2021).

D. Igs dérivées du cancer

I. Identification des Igs cancéreuses

De plus en plus d'études ont montré la production de chaînes lourdes et légères d'immunoglobulines par différents types de cancers, liquides ou solides. Celles-ci ont été nommées les Igs dérivées du cancer.

C'est en 1996 que les immunoglobulines cancéreuses ont été identifiées pour la première fois dans la leucémie myéloïde liquide (LAM) et différents cancers épithéliaux. Cependant, du fait du dogme considérant que seules les cellules B produisent des Igs, celles-ci ont été considérées comme des Ig-likes et non comme de véritables immunoglobulines. De plus, une étude réalisée en 1998 a pu démontrer l'expression des gènes codant pour les régions constantes des chaînes lourdes d'IgD, d'IgM, d'IgG1, d'IgG3, d'IgE et d'IgA dans différentes lignées de cancers non hématopoïétiques (Kimoto et *al.,* 1998). C'est seulement après les années 2000 que l'expression d'IgGs a été confirmée aussi bien au niveau transcriptomique que protéomique dans plusieurs lignées ou tissus cancéreux, comme les cancers du sein, de l'estomac, ou encore du côlon (Babbage *et al.,* 2006; Yang *et al.,* 2013; Li *et al.,* 2016; Jiang *et al.,* 2019). Néanmoins, bien que la chaîne lourde d'isotype IgG soit majoritairement identifiée dans un grand nombre de cancers, d'autres isotypes ont également pu être retrouvés. En effet, des études par immunohistochimie ou spectrométrie de masse ont révélé la synthèse de la chaîne lourde d'IgA par des lignées du cancer du sein, du col de l'utérus ou encore de la bouche (Cui *et al.,* 2021). L'expression de la chaîne lourde d'IgM a été, quant à elle, observée dans les cas de la leucémie myéloïde aiguë et le cancer du larynx (Cui *et al.,* 2021). Concernant les chaînes légères, il est intéressant de constater que c'est la chaîne kappa qui est le plus couramment retrouvée dans différentes cellules cancéreuses. La chaîne Lambda n'a été identifiée que dans le cancer de l'œsophage (**Figure 19**) (Chen et *al.,* 2007; Cui *et al.,* 2021). Il est à noter que ces Igs cancéreuses sont localisées dans le cytoplasme ou à la surface cellulaire,

ce qui suggère que celles-ci pourraient être synthétisées soit sous forme sécrétée, soit sous forme membranaire (**Figure 19**) (Qiu *et al.,* 2003; Chen et *al.,* 2007; Hu *et al.,* 2011; Niu *et al.,* 2012).

Types de malignité	Isotypes d'Ig détectés	Ratio positif chez les patients (%)	Lignées cellulaires positives	Fonctions biologiques	Signification clinique
Cancer du sein	IgG	81	MCF-7, MDA-MB-231, SKBR3, T47D, ZR75-1, MDA-435	Favorise la croissance, favorise l'évasion immunitaire de la tumeur	Sous-type histologique, métastase, stade clinique
	IgA	97	SKBR3, MCF-7, MDA-MB-231, Bcap37	N / A	Métastase ganglionnaire
Cancer du poumon	IgG	66	A549, NCI-H520, SK-MES-1, Calu-6, H441	Favorise la croissance, favorise l'invasion et la migration	Envahissement local, différenciation tumorale, métastase ganglionnaire, pronostic
Cancer du colon	IgG	55	HT-29, LoVo, SW480, HCT116, SW1116	Favorise la croissance, favorise la migration et l'invasion	Différenciation tumorale, stade TNM, métastase ganglionnaire, infiltration inflammatoire
Cancer du pancréas	IgG	87	HC48, SW1990, AsPC-1, BxPC-3, MIA PaCa-2, PANC-1, T3M4, CFPAC-1, HPAF	Inhibe l'activité cytotoxique des cellules NK, inhibe l'apoptose, favorise la croissance, favorise la migration et l'invasion, induit l'inflammation	Différenciation tumorale, chimiorésistance, métastase, pronostic
Cancer du foie	IgG	N / A	BCL-7402, HepG2, Hep3B, Hep-2	Favorise la croissance, favorise la migration, inhibe l'apoptose	N / A
Cancer de l'estomac	IgG	44	MGC-803, MKN28, AGS, BGC-823, SGC-7901	Favorise la croissance, favorise la migration et l'invasion	Pronostic
Cancer de l'oesophage	IgG, Igκ, Igλ	77	Eca109, SHEEC	N / A	Différenciation tumorale, corrélation avec Ki67
Cancer du col de l'utérus	IgG, IgA	N / A	HeLa, C-33A, CA33, ME-180	Favorise la croissance, inhibe la fonction effectrice des cellules NK, induit une inflammation	N / A
	Igκ	78	HéLa	Favorise la transformation maligne	N / A
Cancer des ovaires	IgG	N / A	CaOV3, SK-OV-3, OC-3-VGH	Favorise la croissance, favorise la migration et l'invasion	N / A
Cancer de la prostate	IgG, Igκ	92	PC3, DU145, LNCaP	Favorise la croissance, favorise l'invasion et la migration, inhibe l'apoptose	Différenciation tumorale
Cancer de la vessie	IgG	75-91	T24, BIU-87, 5637, JE	Favorise la croissance, favorise la migration et l'invasion, inhibe l'apoptose	Différenciation tumorale, récidive
Cancer du rein	IgG	90	786-O, ACHN, Caki-1, 293	Favorise la croissance, favorise la migration et l'invasion, inhibe l'apoptose	Différenciation tumorale, stade clinique, pronostic
Cancer du nasopharynx	IgA, Igκ	N / A	CNE1, HNE2	Favorise la croissance, favorise la transformation maligne	N / A
Cancer du larynx	IgM	63	HEp2	N / A	Métastase ganglionnaire, stade clinique, pronostic
Cancer de la bouche	IgG, IgA	86	WSU-HN6, CAL27	Favorise la croissance, la migration et l'invasion, inhibe l'apoptose	N / A
Cancer des glandes salivaires	IgG	52-60	SACC-83	Favorise la croissance, médie la motilité, régule l'EMT	Invasion nerveuse, métastase, pronostic
Cancer de la thyroïde	IgG	80	N / A	N / A	Diagnostic différentiel, métastase ganglionnaire
Cancer de la parathyroïde	IgG	78	N / A	N / A	Diagnostic différentiel, récidive, pronostic
Tumeur des tissus mous	IgG	97	A673, U-2OS, HT1080	N / A	Différenciation tumorale
Leucémie aiguë myéloïde	IgG	79	HEL, NB4, HL-60, OCI-AML3, THP-1	Favorise la croissance, inhibe l'apoptose	Différenciation tumorale, pronostic
	IgM	50	THP-1, OCI-AML3, HL-60, U937, HEL, KG-1, NB4	Favorise la croissance	N / A
	Igκ	94	HEL, HL-60, KG-1, NB4, OCI-AML3, THP-1	Favorise la migration	N / A

Figure 19 : Identification des immunoglobulines dans différents lignées cancéreuses et leurs fonctions. (Cui et *al.,* 2021).

II. Structures des Igs dérivées du cancer

Dans la majorité des cas, ces Igs présentent une structure similaire à celles produites par les lymphocytes B. Cependant, il a été démontré qu'elles pouvaient également être produites avec des séquences tronquées et / ou présenter un profil de glycosylation aberrant. Cette synthèse d'Igs tronquées a notamment pu être démontrée en 2011 lorsque des Western-blots contre les chaînes IgA et Kappa ont été réalisés sur dans différentes lignées cellulaires cancéreuses. En effet, les résultats obtenus ont montré que celles-ci avaient des poids moléculaires bien inférieurs à ceux des Igs produites par les LB. De plus, la détection de ces deux chaînes à la même taille (60 – 70 kDa) dans des extraits protéiques membranaires a permis de montrer que ces deux chaînes pouvaient s'associer pour former un anticorps tronqué présent à la membrane plasmique. Par ailleurs, l'observation d'Igs à d'autres poids moléculaires de 130, 110, 80 et 40 kDa soutient l'idée que ces chaînes d'Igs tronquées peuvent s'associer les unes aux autres (Hu et *al.,* 2011). Ainsi, Hu et son équipe montrent que les cellules cancéreuses produisent différentes formes d'association d'Igs tronquées (**Figure 20**) (Hu et *al.,* 2011). L'expression de telles formes tronquées n'est pas seulement observée dans les cellules cancéreuses mais peut aussi l'être dans les Lymphocytes B, dans lesquels des Igs peuvent être synthétisées avec une délétion de la partie variable ou de la région CH1 (**Figure 20)** (Komori et *al.,* 1995).

Après s'être intéressé à la partie constante, des études se sont ensuite portées sur l'identification de parties variables afin de pouvoir identifier les antigènes de ces Igs dérivées du cancer. En 2009, Zheng et son équipe démontrent que différentes cellules cancéreuses isolées par microdissection laser produisent une diversité de parties variables, même si une prévalence quant à l'expression de certains exons V-D-J était observée (Zheng *et al.,* 2009). Par ailleurs, ils ont aussi recherché si des mutations génétiques au niveau de la partie variable pourraient également être retrouvées dans les cellules tumorales. Pour rappel, dans les lymphocytes B, ces mutations sont principalement générées au niveau des CDR par l'enzyme AID. Cependant, l'expression du gène codant cette enzyme n'a pas été observée dans les cellules cancéreuses (Zheng *et al.,* 2009). Enfin, ils ont observé que la commutation de classe ne se déroulait pas de la même manière que dans les LB. En effet, dans les LB, le changement isotypique de la chaîne lourde conserve normalement la partie variable V(D)J. Cependant, aucun transcrit codant les isotypes IgG ou IgM et présentant la même partie variable n'a pu

être identifié dans les cellules cancéreuses (Zheng *et al.,* 2009). Toutefois, Duan et son équipe ont montré la production de deux parties variables libres et dépourvues de peptide signal dans des hybridomes murins (Duan et *al.,* 1994).

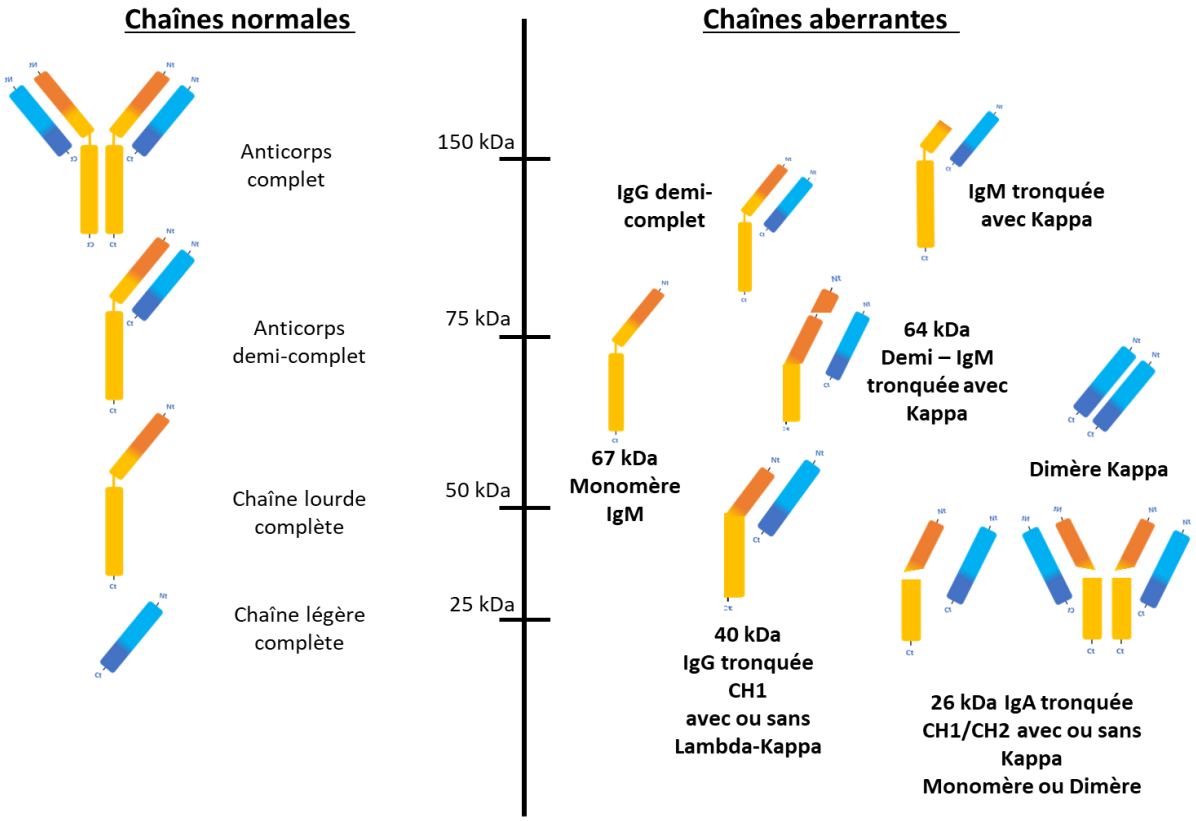

Figure 20 : Immunoglobulines aberrants. Les différentes immunoglobulines tronquées possibles dans le cancer avec leur masse moléculaire.

Parallèlement, des recherches ont montré que les Igs dérivées du cancer présentent un profil de glycosylation aberrant. Or, dans le cas des anticorps produits par les lymphocytes B, la glycosylation est importante car elle permet de moduler leur fonction. Il est donc indispensable d'identifier les différentes modifications post-traductionnelles (MPT) que subissent les Igs dérivées du cancer. Pour ce faire, l'anticorps monoclonal RP215 d'abord utilisé pour identifier un marqueur tumoral, s'est avéré reconnaitre les Igs dérivées du cancer. En effet, son paratope reconnaît la N-glycosylation de l'asparagine 162 (Asn162) présentant une modification de l'acide sialique située au niveau du domaine CH1 de la chaîne lourde (Tang *et al.,* 2018). Cette modification est retrouvée spécifiquement sur les IgGs dérivées du cancer. De plus, il a été montré qu'un traitement avec le RP215 permet d'induire l'apoptose des

cellules cancéreuses, suggérant ainsi que celui-ci pourrait bloquer la fonction des IgG cancéreuses. Par ailleurs, une étude a montré que la présence de cette glycosylation peut inhiber l'infiltration et la prolifération des lymphocytes T effecteurs dans les tissus tumoraux, ce qui favorise la croissance tumorale (Wang *et al.,* 2020). Une autre étude a également démontré que les Igs sialylées favorisent la survie, la migration et la croissance *in vivo* des cellules du carcinome épidermoïde du poumon (LSCC) (Tang *et al.,* 2018).

III. Fonctions

Il est intéressant de noter que les Igs cancéreuses ne présentent pas un caractère immunologique comme ses homologues dérivés des lymphocytes B. Celles-ci réguleraient plutôt la prolifération, la migration et l'invasion des cellules cancéreuses (Cui *et al.,* 2021). En 2013, Wang et ses collègues ont montré qu'*in vitro* et *in vivo*, l'inhibition d'IgGs diminue la croissance et la prolifération cellulaire des cellules cancéreuses. Ceci serait dû à un arrêt du cycle cellulaire en phase S. Ils ont aussi montré que les IgG seraient impliquées dans la production de ROS, indispensable pour la croissance et la prolifération des cellules cancéreuses (Wang *et al.,* 2013). Par ailleurs, la production de chaînes lourdes IgG et de la chaîne légère kappa est corrélée avec un caractère plus malin de la tumeur (Li *et al.,* 2012) (Yang *et al.,* 2013). Dans le même sens, Li et son équipe ont montré que ces Igs cancéreuses sont impliquées dans l'échappement au système immunitaire. Elles rentrent en concurrence avec les Igs issues des LB pour les récepteurs des cellules effectrices et empêchent ainsi l'activation de la voie ADCC (Li *et al.,* 2012).

VII. Immunoglobulines dans le système nerveux central

L'expression de certains récepteurs FcYR a été observée à la surface cellulaire de neurones et de cellules gliales de la moelle épinière. Ainsi, le FcYRIII présent à la surface de la microglie régule la libération de chimiokines et l'induction de l'activité phagocytaire (Raghavan et *al.,* 1996). Par ailleurs, la stimulation du récepteur FcYRI présent à la surface des neurones sensoriels induit une augmentation de la concentration de Ca^{2+} intracellulaire et ainsi à leur activation marquée notamment par la libération de neurotransmetteurs (Andoh et *al.,* 2004). De même, il a été montré que les microglie du SNC expriment des FcγR permettant la phagocytose de pathogènes après leur opsonisation (Aloisi, 2001). Cependant, l'activation de ces récepteurs au niveau du SNC est plutôt surprenante car elle nécessite la présence locale

d'Igs. Or, les anticorps du fait de leur taille importante (150-170 kDa) ne peuvent pas traverser la BHE.

La question en suspens est donc l'origine de ces IgGs au niveau de la moelle épinière. Dans plusieurs pathologies neuro-inflammatoires telles que la sclérose en plaques (SEP), des auto-anticorps ont été trouvés dans le SNC. Ces IgG se sont révélées être présentes au niveau intrathécale. L'une des caractéristiques de ces IgG intrathécales est de former des bandes oligoclonales (OCB), ce qui suggère une diversité assez limitée d'anticorps et par conséquent un nombre défini d'antigènes ciblés correspondants. Alors que la SEP est essentiellement caractérisée par l'existence de lésions inflammatoires et démyélinisantes multifocales (les plaques de SEP), les OCB se développent en quasi-absence de cellules B dans ces lésions inflammatoires. En effet, les OCB sont considérées comme les produits de cellules B expansées de façon clonale dans le LCR. Cependant, de grandes quantités d'IgG peuvent être éluées des plaques de SEP dans lesquelles les cellules B sont absentes. En outre, dans une étude récente analysant des échantillons de LCR provenant de 115 patients atteints de SEP, il a été calculé que 3,2 milliards de cellules B seraient nécessaires pour générer des quantités aussi importantes d'IgG intrathécales (30 mg dans 500 ml de LCR) (Beseler *et al.,* 2017). Or, étant donné le nombre estimé de lymphocytes B circulants dans le LCR, la part d'IgGs que ceux-ci produiraient ne compterait que pour moins de 0,1 % des niveaux d'IgGs présents dans le cerveau des personnes atteintes de SEP. Une telle constatation suggère donc que ces IgGs intrathécales ne seraient pas produites par des lymphocytes B intrathécaux. L'origine de ces IgGs est donc débattue. Une des hypothèses serait qu'elles seraient produites par des cellules du système nerveux central lui-même.

Des travaux plus anciens soutiennent cette hypothèse d'une origine plutôt centrale que périphérique de ces IgGs. En effet, celles-ci ont été détectées dans les tissus cérébraux de différentes espèces animales (Upender *et al.,* 1997; Huang *et al.,* 2008) et dans le liquide céphalo-rachidien (LCR) dans des conditions tant physiologiques que pathologiques (Reiber et *al.,* 1998). Les IgGs atteignent le LCR par transfert passif à travers la barrière hémato-encéphalique (BHE) ou par absorption par les terminaisons axonales des motoneurones se projetant en dehors de la BHE avec transport rétrograde vers le SNC (Mohamed *et al.,* 2002). Cela implique également que les IgG ont trouvé leurs récepteurs (FcR) dans le SNC.

L'expression du récepteur Fc néonatal (FcRn) a été signalée au niveau de la microvasculature cérébrale et de l'épithélium du plexus choroïde (Schlachetzki et *al.,* 2002). Zhang et Pardridge ont démontré dans un modèle de souris que le FcRn ne médiait que le transport inverse des IgG du cerveau vers la circulation systémique et non le transport de la circulation systémique vers le SNC. Enfin, Huang et al. 2008 ont démontré à l'aide d'expériences d'immunohistochimie, d'hybridation *in situ* et de Western-blot que l'ARNm et les protéines IgGs sont présents dans les neurones cérébraux néonataux et adultes de la souris, en particulier dans les neurones dopaminergiques (Huang *et al.,* 2008). Les IgGs pourraient être produites par les neurones et la microglie du SNC et par le système nerveux périphérique (Zhang *et al.,* 2013). Par des expériences *in vitro*, il a été montré que l'exposition au complément (C5a) provoquait l'apoptose de cultures primaires de neurones couplée à une augmentation significative des taux d'IgGs. La neutralisation de ces IgGs avec des anticorps dirigés contre ceux-ci augmenterait cette apoptose et ce, à un stade précoce de la culture. L'ensemble de ces résultats suggère donc que les IgGs dérivées des neurones pourraient protéger les neurones de l'apoptose précoce et de la mort cellulaire induite par l'activation du complément (Zhang *et al.,* 2013).

Par ailleurs, des études d'immunofluorescence menées par le laboratoire suite à une lésion de la moelle épinière chez le rat ont mis en évidence la présence d'IgGs dans les neurones et les astrocytes (Devaux *et al.,* 2016, 2017). Ces expériences avaient été réalisées à la suite d'un traitement avec un anticorps dirigé contre le marqueur de différenciation CD20 (anti-CD20) spécifique aux Lymphocytes B (LB) et ce, une heure après lésion. Ce traitement permettait d'exclure la présence de LB infiltrants. Ces résultats suggèrent clairement que ces IgGs pourraient être produites par les neurones et les astrocytes eux-mêmes bien qu'à ce stade leur recapture à partir de la circulation sanguine ou du LCR ne peut pas être exclue. Ainsi, le but de ma thèse a été d'identifier l'origine cellulaire de ces IgGs et de déterminer leur fonction potentielle dans différents conditions physiologiques ou pathologiques.

Chapitre 1 : Modulation de l'excroissance des neurites par les anticorps (ADNM) d'origine neurale lors d'une lésion de la moelle épinière

Introduction

Il est largement admis que la LME se divise en deux phases principales (**Figure 9**). Lors de la phase primaire, la moelle épinière subit un traumatisme mécanisme causé par le déplacement des vertèbres. Celles-ci exercent alors une force compressive ou lacèrent et cisaillent la ME. Lors de la phase secondaire, les mécanismes cellulaires et moléculaires se mettent en place. Cette phase secondaire évolue alors en trois temps avec la phase aiguë, subaiguë et chronique (**Figure 9**). Ainsi, la compression excessive de la moelle épinière entraîne la formation d'un hématome au site lésionnel provoquant à son tour une ischémie locale, un œdème et une mort cellulaire importante. Cette dernière génère l'accumulation de débris cellulaires, de glutamate, de potassium et d'ATP dans le milieu extracellulaire conduisant à une excitotoxicité pour les cellules avoisinantes (**Figure 9**). Parallèlement, la rupture de la barrière hématoencéphalique conduit à l'invasion du site lésionnel par des cellules immunitaires et ainsi à la mise en place d'une réponse inflammatoire. Cette invasion commence avec le recrutement des neutrophiles et de la microglie 24h après la lésion, puis avec celui des monocytes et macrophages circulants 3 jours après la lésion. Il faut noter que les lymphocytes T régulateurs arrivent progressivement à l'épicentre de la LME seulement après 7 jours post-lésion. L'environnement inflammatoire devient le point central de la phase chronique et empêche une régénération fonctionnelle (Cizkova et *al.,* 2020).

Afin de mieux comprendre au niveau moléculaire pourquoi cette réaction inflammatoire empêche la réparation de la ME, une étude protéomique spatio-temporelle a été réalisée par le laboratoire en utilisant un modèle de lésion de la moelle épinière chez le rat. Pour cela, la moelle a été récupérée à différents temps à la suite de la lésion et coupée en sections de 1 cm, donnant les régions rostrales 2 et 1 en amont de la lésion, le site lésionnel et les régions caudales 1 et 2 en aval de la lésion (**Figure 21**). Le contenu protéique de ces différents segments a alors été analysé par LC-MS/MS. Les résultats obtenus révèlent une régionalisation protéique entre les différents segments (Cizkova et *al.*, 2014 ; Devaux et *al.,* 2016 ; Devaux et *al.,* 2017 ; Cizkova et *al.,* 2018). En effet, après 3 jours de lésion, les segments rostraux (R1 et

R2) et le segment caudal (C2) qui est le plus éloigné du site lésionnel, synthétisent des facteurs de croissance neuritique ainsi que des facteurs recrutant des cellules immunitaires présentant un phénotype anti-inflammatoire. Ceci permet de créer un environnement favorable à la repousse neuritique de part et d'autre de la lésion (Cizkova et *al.,* 2014). À l'inverse, de très nombreux facteurs conduisant à une réaction pro-inflammatoire ont été identifiés au niveau du site lésionnel et du segment Caudal 1. Parmi ces facteurs, des cytokines pro-inflammatoires, des éléments des voies Memo1-RhoA-Diaph1 et RhoA-Rocket d'immunoglobulines ont été caractérisés (Devaux et *al.,* 2016).

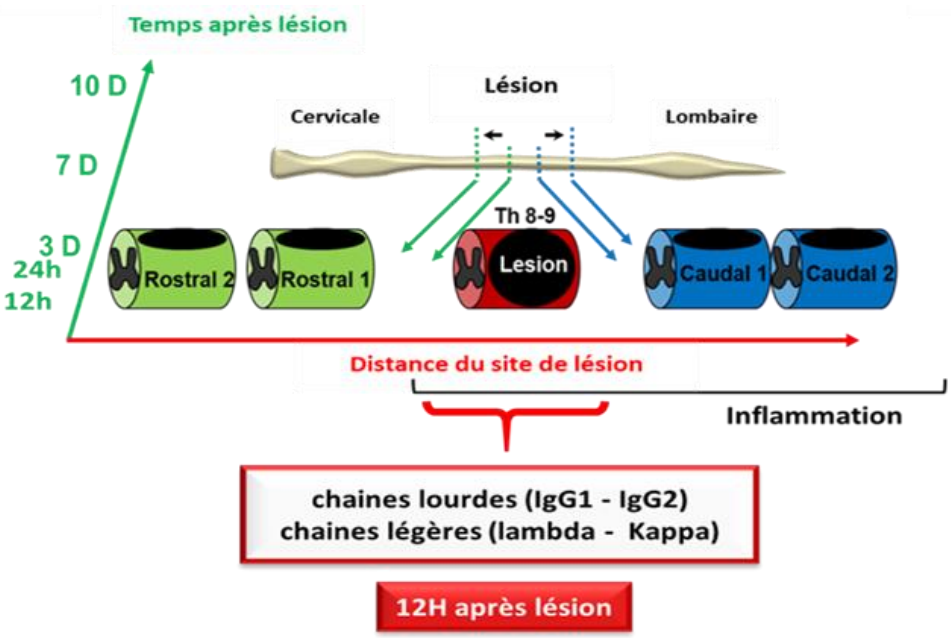

<u>Figure 21 :</u> Présence des chaines lourdes IgG et des chaines légères Lambda et Kappa au site lésionnel dès 12h après lésion.

La voie RhoA-Rock est impliquée dans plusieurs processus cellulaires tels que la régulation de l'organisation du cytosquelette par la formation de fibres d'actine, la contractilité de l'actomyosine, le développement cellulaire, le contrôle transcriptionnel ou encore la maintenance du cycle cellulaire (Zaoui *et al.,* 2008). Par ailleurs, des études montrent que cette voie contrôle également la croissance axonale. En effet, son activation a été corrélée avec la perte des cônes de croissance des neurones et ainsi l'inhibition de la croissance axonale. De plus, il a été montré que la voie RhoA-Rock est activée dès la première heure suivant une lésion de la moelle épinière et que son activation est maintenue jusqu'à 7 jours après la lésion. L'initiation de cette voie est fortement liée à la mise en place d'une

excitotoxicité et ainsi à une importante mort neuronale. La voie RhoA est généralement déclenchée par trois inhibiteurs de croissance associés à la myéline tels que Nogo, la glycoprotéine oligodendrocyte-myéline (OMgp) ou encore le protéoglycane de sulfate de chondroïtine (CPSG). Lors d'une LME, les astrocytes réactifs produisent de tels protéoglycanes et conduisent ainsi à la formation d'une cicatrice gliale. Lorsque le CPSG est libéré dans le milieu extracellulaire, il se lie aux récepteurs Nogo1 (NgR1) et Nogo3 (NgR3). Ces récepteurs s'associent alors avec le récepteur de la neurotrophine p75 (p75NTR) afin d'activer la voie RhoA/Rho kinase par une cascade de phosphorylation. Il en résulte l'inhibition de la croissance et/ou de la réparation des neurites et ainsi un blocage de la régénération de la ME (Wu et Xu, 2016). A contrario, l'inhibition de cette voie par divers composés permet généralement la repousse axonale et ainsi une récupération fonctionnelle. Le composé le plus utilisé est l'exoenzyme C3 transférase qui est issue de la bactérie *Clostridium botulinum*. Les propriétés physico-chimiques de cette enzyme ont été modifiées afin de lui permettre de passer les membranes cellulaires et ainsi inhiber la voie RhoA. Elle est alors appelée BA-210 ou Cethrin. En effet, la C3 transférase ribosyle la protéine RhoA sur le résidu Aspargine 41 entrainant son inactivation (Wilde et *al.,* 2002). Actuellement, le BA-210 est en essai clinique de phase I et II et montre des résultats prometteurs. Lorsque le laboratoire a utilisé ce traitement dès la phase aiguë de la lésion de la ME chez le rat, une excroissance neuritique et une reconnexion synaptique ont été observées (Devaux et *al.,* 2017). Cependant, cette régénération n'est pas complète. Certains facteurs semblent limiter cette régénération nerveuse au sein de la zone de lésion. Nous avons donc recherché ces facteurs et nous avons pu mettre en évidence de façon surprenante la présence de chaines lourdes IgG et les chaines légères Lambda et Kappa dans le milieu conditionné du segment du site lésionnel dès 3 jours après lésion. Or, celles-ci ont été caractérisées alors qu'un traitement avec un anticorps dirigé contre le CD20, marqueur de lymphocytes B, avait été réalisé 1h après la lésion (Devaux *et al.,* 2016). Ce traitement anti-CD20 empêche le recrutement de ces cellules B en induisant leur apoptose par divers mécanismes tels que l'activation de la voie du complément, la voie ADCC ou l'induction de l'apoptose (Boross et Leusen, 2012). De plus, des expériences d'immunofluorescence utilisant des anticorps dirigés contre les IgG et NeuN qui est un marqueur des neurones montrent la présence de ces IgG dans le cytoplasme des neurones. Pour certains neurones, ces IgG ne sont détectées qu'au niveau de leur membrane plasmique. A ce stade, l'ensemble de ces résultats suggère que ces IgG puissent se lier à un récepteur

présent à la membrane cellulaire afin d'être internalisées dans la cellule ou soient produites par les neurones eux-mêmes (Devaux et *al.,* 2016). Cette dernière possibilité est soutenue par une nouvelle étude protéomique réalisée sur des explants de moelle épinière collectés à un temps plus précoce après la lésion, à savoir 12h, et toujours à la suite d'un traitement avec un anti-CD20. En effet, à ce temps, les IgG1 et IgG2 ainsi que les chaînes légères Kappa et lambda ont de nouveau été mises en évidence (**Figure 21**). La présence d'IgGs à un temps aussi précoce n'est pas cohérente avec une réponse adaptative classique impliquant les lymphocytes B. En effet, comme mentionné précédemment, les IgG sont normalement produites après deux semaines par les LB ou au cours d'une seconde infection. Par ailleurs, lorsque que les rats subissant la LME sont traités avec un inhibiteur de RhoA (RhoAi), une augmentation des taux d'IgG2B et d'IgG2C dans les segments lésionnels et caudaux est observée. Ceci suggère qu'une commutation de classe des IgG1 en IgG2 soit induite quand la voie RhoA est inhibée (Devaux *et al.,* 2017). Compte tenu du rôle favorable exercé par RhoAi sur la croissance neuritique, ce résultat laisse également penser que ces IgG puissent jouer un rôle sur la régénération nerveuse.

Dans ce contexte, la présence d'anticorps 12h après la lésion et l'effet de RhoAi sur leur synthèse posent donc d'emblée la question de leur origine cellulaire ainsi que de leur rôle lors d'une lésion de la moelle épinière.

Objectifs

Le premier travail de cette thèse a été de réaliser des études spatio-temporelles à la suite d'une LME dans le but d'identifier les différentes voies moléculaires impliquées au cours du processus physiopathologique. Un intérêt plus particulier s'est porté sur la recherche des différents profils isotypiques des immunoglobulines produites au cours de cette LME. De plus, nous avons également recherché l'origine cellulaire de ces Igs et leur fonction.

Résultats

Au cours de ce travail, la présence des différentes classes d'IgG a été montrée dans les explants de moelle épinière lésée ou non ainsi que dans leurs sécrétomes de 12h à 10 jours. De plus, la quantification relative réalisée révèle que les taux de ces différentes sous-classes varient en fonction de leur localisation par rapport au site de lésion mais aussi au cours du temps. En

effet, les IgG1, IgG2 (A, B) et IgM sont observés tout au long de la cinétique de temps alors que les IgG2C apparaissent à 12h après lésion et disparaissent à partir de 3 jours à la suite de la LME tout comme la partie variable de la chaine lourde (**Figure 21**). Par ailleurs, il est intéressant de noter qu'à 12hpost-lésion le traitement avec RhoAi favorise la production et la sécrétion de l'isotype IgG2C.

Lors des recherches précédentes du laboratoire, les IgG avaient été détectées au niveau du cytoplasme et de la membrane plasmique des neurones. C'est pourquoi, nous avons cherché à déterminer si ces IgG pourraient être produites par les neurones eux-mêmes. Pour ce faire, plusieurs banques transcriptomiques ont été obtenues à partir de la base de données Sequence Read Archive (SRA). Celles-ci ont été générées par séquençage à haut débit d'ARN à partir de cultures primaires de neurones sensoriels isolés des ganglions de la racine dorsale (DRG) de rat. Ainsi, l'expression des gènes codant les parties constantes des chaînes lourdes IgG1, IgG2(A, B) et IgM ainsi que des chaînes légères Kappa et Lambda dans l'explant DRG a été démontrée. De plus, plusieurs transcrits codant des parties variables V(D)J associées ou non aux parties constantes des chaînes IgG2 et Kappa ont également été identifiés suggérant l'expression d'immunoglobulines entières. Parallèlement, une étude transcriptomique par RT-PCR a été réalisée sur la lignée cellulaire de neurones sensoriels de rat DRG ND7/23 et la lignée neurale dopaminergique de rat N27 non différenciée. Seule l'expression du gène codant la chaîne lourde IgG2C a été mise en évidence dans les cellules N27.

Par la suite, nous avons voulu déterminer si ces cellules pouvaient synthétiser des Igs présentant une diversité de parties variables. La survenue d'une telle diversité est permise grâce au processus de recombinaison V(D)J qui implique un complexe enzymatique particulier dont RAG1 et RAG2 sont les premières enzymes recrutées (**Figure 14**). Ainsi, par RT-PCR, l'expression de *Rag1* n'a été observée que dans les cellules N27 alors que celle de *Rag2* a été mise en évidence dans les deux lignées cellulaires. Il est important de noter que les enzymes RAG génèrent des coupures importantes de l'ADN, c'est pourquoi, l'expression de leurs gènes est hautement régulée au cours du développement et du cycle cellulaire. Ces données montrent que les neurones sont une nouvelle source d'Igs et que celles-ci pourraient y être synthétisées avec une variabilité.

Nous avons ensuite cherché à déterminer quel serait le rôle de ces IgG d'origine neuronale. Lors d'une réaction immunitaire, les IgG sont particulièrement impliquées dans le mécanisme de cytotoxicité à médiation cellulaire dépendante des anticorps (ADCC). En effet, le paratope de l'IgG reconnaît l'épitope d'un antigène alors que la partie Fc de l'IgG se lie à des récepteurs présents sur les différentes cellules immunitaires. Les récepteurs mis en jeu sont les FcγR. Ceux-ci sont divisés en différentes sous-classes : FcYRI (CD64), FcYRIIA (CD32a), FcYRIIB (CD32b), FcYRIIC (CD32c) FcYRIIIA (CD16a), et FcYRIIIB (CD16b) (**Figure 17**). Pour commencer, nous avons démontré par RT-PCR l'expression des gènes codant les récepteurs CD16 et CD32dans les cellules DRG ND7/23. La synthèse des récepteurs au niveau protéique a ensuite été confirmée par Western-blot. De plus, un traitement de ces neurones DRG avec des lipopolysaccharides, pour mimer l'état inflammatoire observé au cours de la LME, induit une synthèse plus importante de ces deux récepteurs. Dans le système immunitaire, CD32b est connu pour jouer un rôle inhibiteur puisqu'il est le seul à avoir un motif ITIM sur son domaine cytoplasmique alors que CD16 présente quant-à-lui des motifs activateurs ITAM. C'est pourquoi, l'expression de ces deux récepteurs aux fonctions opposées est importante. Afin de déterminer le rôle de ces IgG et des récepteurs FcγR dans les neurones, différentes stimulations ont été réalisées avec un anti-CD16, un anti-CD32 et/ou un isotype IgG2. Il est à noter que les anticorps anti-CD16 et anti-CD32 ne bloquent pas l'activité des récepteurs mais les trans-activent. Ceci est démontré par la libération de calcium par le RE. En absence d'IgG2, nous avons montré que seule l'activation de CD16 induit une croissance des neurites et est concomitante avec une augmentation de la libération du calcium au sein de la cellule. Lors de l'activation simultanée de CD16 et de CD32b, l'augmentation de la croissance des neurites est maintenue, ce qui montre que l'activation de CD16 peut être suffisante pour surmonter l'effet inhibiteur potentiel de CD32b. Cependant, lorsque l'activation de CD32b est induite par l'IgG2 l'effet exercé par CD16 et CD32 sur la croissance des neurites est perdu. L'ensemble de ces résultats suggère que les IgG peuvent moduler la croissance des neurites par l'activation du CD16 et du CD32. Ce processus mis en jeu a été nommé « Antibody Dependent Neurite Outgrowth Modulation » (ADNM) et il pourrait être un précurseur de la réponse neuro-inflammatoire dans des conditions pathologiques.

frontiers | Frontiers in Immunology

ORIGINAL RESEARCH
published: 16 June 2022
doi: 10.3389/fimmu.2022.882830

The Antibody Dependant Neurite Outgrowth Modulation Response Involvement in Spinal Cord Injury

Alice Capuz[1†], Mélodie-Anne Karnoub[1†], Sylvain Osien[1†], Mélanie Rose[1], Céline Mériaux[1], Isabelle Fournier[1,2], David Devos[3], Fabien Vanden Abeele[4], Franck Rodet[1], Dasa Cizkova[1,5,6] and Michel Salzet[1,2*]*

[1] Université de Lille, Inserm U1192, Laboratoire Protéomique, Réponse Inflammatoire et Spectrométrie de Masse (PRISM), Lille, France, [2] Institut Universitaire de France, Paris, France, [3] Université de Lille, Inserm U1172, CHU-Lille, Lille Neuroscience Cognition Research Centre, Lille, France, [4] Université de Lille, Inserm U1003, Laboratory of Cell Physiology, Villeneuve d'Ascq, France, [5] Institute of Neuroimmunology, Slovak Academy of Sciences, Bratislava, Slovakia, [6] Centre for Experimental and Clinical Regenerative Medicine, University of Veterinary Medicine and Pharmacy in Kosice, Kosice, Slovakia

OPEN ACCESS

Edited by:
George Smith,
Temple University, United States

Reviewed by:
Dengbing Yao,
Nantong University, China
Songlin Zhou,
Nantong University, China

***Correspondence:**
Michel Salzet
michel.salzet@univ-lille.fr
Dasa Cizkova
dasa.cizkova@uvlf.sk

[†]These authors share first authorship

Specialty section:
This article was submitted to Multiple Sclerosis and Neuroimmunology, a section of the journal Frontiers in Immunology

Received: 24 February 2022
Accepted: 02 May 2022
Published: 16 June 2022

Citation:
Capuz A, Karnoub M-A, Osien S, Rose M, Mériaux C, Fournier I, Devos D, Vanden Abeele F, Rodet F, Cizkova D and Salzet M (2022) The Antibody Dependant Neurite Outgrowth Modulation Response Involvement in Spinal Cord Injury. Front. Immunol. 13:882830. doi: 10.3389/fimmu.2022.882830

Spinal cord injury (SCI) represents a major medical challenge. At present, there is still no cure to treat it efficiently and enable functional recovery below the injury site. Previously, we demonstrated that inflammation determines the fate of the physiopathology. To decipher the molecular mechanisms involved in this process, we performed a meta-analysis of our spatio-temporal proteomic studies in the time course of SCI. This highlighted the presence of IgG isotypes in both spinal cord explants and their secretomes. These IgGs were detected in the spinal cord even if no SCI occurred. However, during the time course following SCI, abundance of IgG1 and IgG2 subclasses (a, b, c) varied according to the spatial repartition. IgG1 was clearly mostly abundant at 12 h, and a switch to IgG2a was observed after 24 h. This IgG stayed predominant 3, 7, and 10 days after SCI. A protein related to IgM as well as a variable heavy chain were only detected 12 h after lesion. Interestingly, treatment with RhoA inhibitor influenced the abundance of the various IgG isotypes and a preferential switch to IgG2c was observed. By data reuse of rat dorsal root ganglion (DRG) neurons RNAseq datasets and RT-PCR experiments performed on cDNA from DRG sensory neurons ND7/23 and N27 dopaminergic neural cell lines, we confirmed expression of immunoglobulin heavy and light chains (constant and variable) encoding genes in neurons. We then identified CD16 and CD32b as their specific receptors in sensory neuron cell line ND7/23 and their activation regulated neurites outgrowth. These results suggest that during SCI, neuronal IgG isotypes are released to modulate neurites outgrowth. Therefore, we propose a new view of the SCI response involving an antibody dependent neurite outgrowth modulation (ADNM) which could be a precursor to the neuroinflammatory response in pathological conditions.

Keywords: spinal cord injury acute phase, inflammation, astrocytes, shot gun proteomic, neurite outgrowth, neuronal antibodies, autoantibodies, immunoglobulin

INTRODUCTION

The spinal cord and the brain form the central nervous system (CNS). It supports all nerves, coming from or going to the peripheral nervous system. It is protected by the spinal canal, formed by the articulation of cervical, thoracic, and lumbar vertebrae. This is why vertebral fracture or luxation can lead to spinal cord injury (SCI), from concussion/contusion to section (1). The clinical consequences of these lesions are terrible, as they lead, according to the level, either to paraplegia or tetraplegia, which can be complete or incomplete. According to the literature, the incidence ranges between 19.4 patients per year in Europe, and 51 patients per year in North America (2). This represents not only an epidemiologic issue, but also a social and economic burden, since the population affected is mostly represented by young men with a mean age of 40 years old. The SCI etiologies gather car crashes (31.47%), falls (25.29%), gunshot wounds (10.42%), motorcycle crashes (6.80%), and diving (4.67%) (2).

Although a fundamental understanding has been obtained through various modeling studies, there is still a lack of knowledge about the pathophysiology of SCI. It has been established that everything starts with a primary mechanic traumatism by compression, laceration, distraction, or shearing (3). This induces vascular lesions that lead to the formation of a hematoma at the lesion site, which itself causes local ischemia, edema, and cell-regulated cell death such as apoptosis (3). Moreover, the blood spinal cord barrier is disrupted, which initiates the secondary extension of the lesion through the attraction of inflammatory cells, the accumulation of cytokines and vasoactive proteins. Finally, cell death is responsible for the accumulation of cellular debris, potassium, and ATP, leading to a cytotoxic environment. Then pro-inflammatory M1 microglial cells and phagocytes infiltrate this cytotoxic environment resulting in toxic oxidative stress to adjacent neurons (3). In our laboratory, a previous study focused on subacute inflammatory response after SCI demonstrated that after 3 days, the inflammatory response was intense at the lesion site and in downstream caudal 1 segment. Indeed, high amounts of cytokines and immunoglobulins were detected and the Rho-Rock and Memo1-RhoA-Diaph1 pathways were activated (4, 5). On the contrary, more caudally and distally from the central lesion, we have rather detected neurite outgrowth proteins and chemokines attracting first neutrophils, then T regulatory cells, and anti-inflammatory M2 microglial cells. This created a favorable environment for neurite outgrowth on both sides of the lesion (4).

Several innovative treatments currently being tested inhibit ligands known to engage the Rho-Rock pathway in neurons. These notably include chondroitin sulfate proteoglycans, myelin associated glycoprotein (MAG), oligodendrocyte myelin glycoprotein (OMGP), and neurite outgrowth inhibitor A (NOGO-A). For example, anti-NOGO-A antibodies delivered in the cerebrospinal fluid have been used in phase I clinical trials (6, 7) with promising results. Also, in pre-clinical studies, chondroitinase ABC was shown to partially block the Rho-Rock-mediated inhibition of neurite outgrowth and glial scar formation within the lesion (8). Finally, a RhoA inhibitor (RhoAi), called Cethrin (9, 10), has been assessed in a phase I and phase IIa clinical trial in patients with cervical SCI, and was found to improve functional repair (11). A phase IIb is foreseen. However, we have recently shown that the mechanisms triggered 12 h after the lesion were completely different from those observed after 1 day of injury. At 12 h after SCI, rostral and caudal segments showed no molecular difference but were distinct from the injury site (12). Repetitive delivery of RhoA inhibitor significantly increased the synaptogenesis and promoted neuritogenesis and neurite outgrowth through the cavity (12). However, a week after lesion, a plateau appeared which blocked the achievement of the biological processes and the neuronal reconnection. Among the proteins that may be involved in this inhibition, IgG1 and IgG2 isotypes represent good candidates. Indeed, we observed their presence in SCI secretome as early as 12 h after the lesion (4, 12). Then, we confirmed their presence in neurons and astrocytes 24 h after SCI even after preventive treatment with anti-CD20 (4, 12). In this context, we decided to identify these immunoglobulins between 12 h and 7 days after SCI. A meta-analysis was performed with MaxQuant software, in two rows. First analysis was performed against the SCI data (4) at several times (12 h, 1 day, 3 days, 7 days, and 10 days), and with several segments including rostral (R3, R2, R1), lesion (L), and caudal (C1, C2, C3). We then studied their expression and that of their specific receptors in neurons as well as their activity related to neurite outgrowth.

MATERIALS AND METHODS

Reagents

All chemicals were obtained with the highest purity available. Water, acetonitrile (ACN), formic acid (FA), and trifluoroacetic acid (TFA) were purchased from Biosolve B.V. (Valkenswaard, the Netherlands). DL-dithiothreitol (DTT), HEPES, ES FBS, thiourea, iodoacetamide (IAA), tri-reagent, isopropanol, chloroform, glucose, and agarose were purchased from Sigma Aldrich. Lys-C/Trypsin enzymatic mixture, DNase RQ1, deoxyribonucleotides (dNTPs), RNAsin® ribonuclease inhibitor, RNase H, GoTaq® G2 Hot Start Taq polymerase kit, molecular weight markers, PGEM-T Easy Vector System II®, T4 DNA ligase, and *E. coli* strain JM109 were purchased from Promega (France). Random primers, Superscript® III kit, phosphate buffered saline (PBS), Dulbecco's modified Eagle's medium (DMEM), RPMI 16140, fetal bovine serum (FBS), L-glutamine, penicillin and streptomycin, GeneJET Gel Extraction kit, Alexa Fluor® 647-conjugated goat anti-rat IgG, Alexa Fluor® 488-conjugated donkey anti-rabbit, Alexa Fluor® 488-conjugated donkey anti-mouse, melon Gel IgG Spin Purification Kit and Zeba Spin Desalting Columns (7K MWCO), Dynabeads Protein G, and enhanced chemiluminescence kit were obtained from Life Technologies (Milan, Italy). RhoA inhibitor was obtained from Cytoskeleton, Inc. (Denver, CO). All primers used were purchased from Eurogentec. The QiAquick PCR Purification kit was purchased from Qiagen®. The NucleoSpin® Plasmid kit was

purchased from Macherey Nagel. Urea was purchased from Euromedex. Mouse anti-GFAP, mouse anti-NeuN, Amicon ultracentrifugal filter 10K, and ZipTip C18 were purchased from Millipore. Mouse anti-CD16 and rabbit anti-CD32 were obtained from Santa Cruz Biotechnology. Peroxidase-conjugated goat anti-rat IgG was obtained from Thermofisher scientific, peroxidase-conjugated goat anti-mouse IgG and peroxidase-conjugated goat anti-rabbit IgG were obtained from Jackson ImmunoResearch (West Grove, PA). Ultrapure lipopolysaccharides (LPS-EB) were bought from *In vivo*Gen (Toulouse, France). PNGase F was bought from New England's Biolabs (US).

Experimental Design and Statistical Rational

Spinal cord segments and their conditioned media during time course of experiments were collected from at least 3 rats. For the proteomic statistical analysis of conditioned media, as a criterion of significance, we applied an ANOVA significance threshold of $P<0.05$, and heat maps were generated. Normalization was achieved using a Z-score with a matrix access by rows. Western blot analyses were performed twice in duplicate. Other experiments such as molecular biology, neurites outgrowth, and calcium measurements were conducted in triplicate. For neurite outgrowth experiments, statistical significance was assessed with a t-test using Graph pad PRISM software. Values of $P < 0.05$ were considered statistically significant (*P value of < 0.05, **P value of < 0.01, ***P value of < 0.001).

Secretome Preparation

All studies were carried out on adult male Wistar rats with the agreement and according to the rules laid down by the institutional committee for the protection of animals of the Slovak University of Science and by the European Directive 2010/63 on the use of the animals for research purposes, as well as with the Slovak animal welfare laws Nos. 377/2012 and 436/2012. Some of the animals underwent spinal cord injury at Th8-Th9 level by the balloon compression method, performed after laminectomy. Other animals, called "control" did not undergo compression but a simple laminectomy. Some also received treatment with RhoA inhibitor, injected at the lesion site at the time of the lesion. Rats were sacrificed after isoflurane anesthesia, 12 h (3 rats not treated with RhoA inhibitor and 3 rats treated with RhoA inhibitor) or 24 h (5 rats) after injury. Spinal cords were extracted by injection of sterile saline buffer and divided into 1-cm long segments, on both sides of the lesion, which level was macroscopically verified. It was therefore possible to obtain a lesion segment, 2 rostral segments, and 2 caudal segments, each segment being cut into two fragments of 0.5 cm. These fragments were then cultured for 12 h and 24 h in DMEM at 37°C and 5% CO_2. Conditioned media thus obtained were called secretomes.

Preparation of Intact Spinal Cord

Rats were sacrificed after isoflurane anesthesia. The spinal cord was extracted by injection of sterile saline buffer and immediately frozen as a whole.

Cell Line

The rat dorsal root ganglion (DRG) cell line ND7/23 and N27 dopaminergic neural cell line were purchased from Sigma-Aldrich. ND7/23 cells were obtained by PEG mediated cell fusion between the mouse neuroblastoma (N18 tg 2) and the rat dorsal root ganglion neurons. ND7/23 cell line was grown in DMEM medium supplemented with 10% fetal bovine serum, 1% L-glutamate, 100 U/ml penicillin, and 100 µg/ml streptomycin, at 37°C in a humidified atmosphere (5% CO_2). N27 cells were cultivated in RPMI 1610 supplemented with 10% embryonic FBS, 1% L-glutamate, 100 U/ml penicillin, and 100 µg/ml streptomycin, at 37°C in a humidified atmosphere (5% CO_2).

Protein Extraction

To extract the proteins, ND7/23 DRG cells were resuspended in RIPA buffer (150 mM NaCl, 50 mM Tris, 5 mM EGTA, 2 mM EDTA, 100 mM NaF, 10 mM sodium pyrophosphate, 1% Nonidet P-40, 1 mM PMSF, and 1X protease inhibitors) and subjected to three sonications of 5 s with a step on ice for 30 s between each sonication. Then the samples were centrifuged at 14,000 x g for 20 min at 4°C. The supernatant containing the proteins was collected. To determine protein concentration in the samples, Bradford assay was used.

As a first step to purify antibodies from spinal cord lesion segment withdrawn 7 days after injury (SCI 7D-L), proteins were extracted from 50 mg of tissue resuspended in RIPA buffer and submitted to the same procedure as described above. Seven days were chosen to mimic the dynamic of the inflammatory response that occured 7 days after lesion.

To conduct shotgun proteomics analysis on non-injured spinal cords, control spinal cords as well as on rostral, lesion, and caudal spinal cord segments collected 12 h after SCI, protein extraction was performed as follows. Tissues were cut to obtain small fragments of 1 mm thick and grinded in liquid nitrogen. Powders were resuspended in CHAPS lysis buffer (CHAPS 3.5%, Tris-HCl and DTT, pH 10), mixed thoroughly and subjected to sonication during 20 min. Samples were heated at 95°C during 5 min and centrifuged at 15,000 x g during 5 min at 4°C. Supernatants containing proteins were then collected.

Immunoglobulin Enrichment Procedure From SCI 7D-L Protein Extracts

To purify antibodies from protein extracts of SCI 7D-L obtained after RIPA extraction, ammonium sulfate precipitation was carried out on 500 µg of proteins according to the protocol of the Melon Gel IgG Purification Kit, with a few modifications. Briefly, saturated ammonium sulfate solution was prepared by dissolving 7.61 g ammonium sulfate in 10 mL milliQ water. Then, one volume of saturated ammonium sulfate solution was added to one volume of sample in order to have 50% ammonium sulfate. The sample was incubated during 4 h at 4°C, and centrifuged at 3000 x g for 20 min at 4°C. The supernatant was then removed and the pellet was resuspended in a volume of milliQ water, equivalent to the original sample volume. The resuspended pellet containing the purified antibodies was desalted thanks to the Zeba Spin

Desalting Columns according to manufacturer's instructions. Column's caps were removed and the column was placed in a 2.0-mL collection tube, prior to centrifugation at 1500 x g for 1 min in order to remove the storage solution. A washing step was performed by adding 300 µL of milliQ water to the column, and centrifugation at 1500 x g for 1 min. The washing process was repeated two more times. Ensuing these steps, sample was carefully added to the center of the column, and centrifuged at 1500 x g for 2 min in order to collect the desalted sample. Melon Gel IgG Purification was then conducted according to the manufacturer's instructions. Purification Buffer and Melon Gel IgG Purification Support were equilibrated for 15 min at room temperature. During this time, the sample volume was completed to 500 µL with purification buffer. Then, 500 µL of slurry was dispensed into a spin column placed in a microcentrifuge tube, and centrifuged for 1 min at 4000 x g. The flow-through was discarded afterward, and two washes were performed by adding 300 µL of purification buffer and centrifugation at 4000 x g for 10 s. The flow-through was discarded again, and the sample was loaded into the column. The column was mixed end-over-end for 5 min at room temperature, in order to bind the nonspecific proteins to the resin. The bottom cap was removed, the top cap was loosed, and centrifugation was performed at 4000 x g for 1 min to collect the purified antibodies in a new collection tube. After melon gel purification, the sample was digested after reduction, alkylation, and deglycosylation.

Reduction, Alkylation, Deglycosylation, and Trypsic Digestion of Samples Obtained After Melon Gel IgG Purification

Reduction was performed by the addition of DTT 200 mM to the sample, in order to have a final concentration of 50 mM, and the sample was incubated at 56°C for 1 h. Then, the sample was loaded into an Amicon 10K to change the buffer and retain the proteins on the membrane. To do that, approximately 450 µL was loaded into the column, centrifugation at 14,000 x g was done for 15 min, and flow-through was discarded. This step was performed four times in order to load the entire sample, since the maximum capacity of the Amicon was 500 µL. Then the washes step was performed by the addition of 200 µL NH_4HCO_3 50 mM to the column, centrifugation at 14,000 x g for 15 min, and flow-through removal. Alkylation was then performed by the addition of 100 µL IAA 50 mM, mixed briefly at 600 RPM, and incubated in the dark for 20 min. Then centrifugation was performed at 14,000 x g for 15 min, and two washes were performed by the addition of 200 µL NH_4HCO_3 50 mM, centrifugation at 14,000 x g for 15 min, and flow-through removal. Ensuing these steps, deglycosylation with PNGase F was carried out. PNGase F was prepared with NH_4HCO_3 50 mM (1:99, v/v), and a volume of this solution was added to the sample in order to have 10% of diluted PNGase F in the final sample. Then, the sample was mixed briefly at 600 RPM and incubated overnight at 37°C. The next day, two washes were performed by the addition of 200 µL NH_4HCO_3 50 mM to the column, centrifugation at 14,000 x g for 15 min, and flow-through removal. After the addition of 40 µL of Trypsin (20 ng/µL in NH_4HCO_3 50 mM), the sample was mixed briefly at 600 RPM and incubated overnight at 37°C. The addition of trypsin quenched the reaction with PNGase F. The next day, the column was placed in a new collection tube and 40 µL NH_4HCO_3 50 mM were added. A centrifugation was performed at 14,000 x g for 10 min to collect the digested sample. Trypsin digestion was then quenched with TFA 1%. Finally, the sample was dried in the SpeedVac and desalted with ZipTip C18 before HPLC-MS/MS analysis.

Reduction, Alkylation, and Trypsic Digestion of Secretomes From Spinal Cord Segments Treated Or Not With RhoA Inhibitor Collected 12 h and 24 h After SCI

Secretomes were deposited on 0.22-µm syringe filters. After filtration, denaturation of the proteins contained in the secretomes was performed with Urea 6 M and HEPES 40 mM. Reduction was then carried out with DTT 10 mM at 56°C for 40 min. Afterward, alkylation was conducted with IAA 55 mM for 40 min at room temperature and obscurity. Thiourea 100 mM was added to stop the reaction and digestion was performed overnight at 37°C with Lys-C/Trypsine (30 µg/mL). Addition of TFA 0.5% stopped the reaction. Finally, samples were dried in the SpeedVac and desalted with ZipTip C18 before HPLC-MS/MS analysis.

Reduction, Alkylation, and Trypsic Digestion of Protein Extracts From Non-Injured Spinal Cords, Control Spinal Cords As Well As Rostral, Lesion, and Caudal Spinal Cord Segments Collected 12 h After SCI

A total of 30 µl of each sample was loaded into an Amicon 30K and 200 µL of UA buffer (Urea 8 M, Tris-HCl 0.1 M pH 8.5) were added. Samples were centrifuged at 14,000 x g for 15 min and flow-through was discarded. Alkylation was conducted with 100 µL of IAA 55 mM. UA buffer was then added and samples were centrifuged at 14,000 x g for 15 min. This step was repeated three times. Ammonium bicarbonate (AB) buffer was then added and samples were centrifuged three times at 14,000 x g for 15 min. Digestion was performed overnight at 37°C with Lys-C/Trypsine (30 µg/mL). After centrifugation at 14,000 x g for 10 min, 500 µL of NaCl and TFA 0.5% were added. Finally, samples were dried in the SpeedVac and desalted with ZipTip C18 before HPLC-MS/MS analysis.

SDS-PAGE and In Gel Digestion

To identify immunoglobulins in secretomes of segments R1, L, and C1 collected 12 h and 24 h post SCI, 2.5 µg of proteins of each sample were separated on a 12% SDS-polyacrylamide gel (SDS-PAGE). Gels were colored overnight at room temperature with Coomassie blue and in gel digestion was eventually carried out. Bands of interest were cut in small pieces of approximately 1 mm square and placed in new microtubes. Then 300 µl of milliQ water were added to the gel pieces and mixed for 15 min. Then 300 µL of ACN were added and the samples were mixed for 15 min. The supernatant was removed afterward, and 300 µL of NH_4HCO_3 100 mM were added to the gel pieces. After an agitation of 15 min, supernatants were removed. A total of 300

µl of ACN/NH_4HCO_3 100 mM (1/1, v/v) were added. After an agitation of 15 min, supernatants were discarded. As a final wash, 100 µL ACN were added to the gel pieces and an agitation of 10 min was carried out. Band pieces should become white and shrinked. Then ACN was removed and band pieces were dried in the SpeedVac for 10 min. Reduction was performed on the band pieces by the addition of 50 µL/band DTT 10 mM in NH_4HCO_3 100 mM, and incubation at 56°C for 1 h. Following this step, 50 µL/band IAA 50 mM in NH_4HCO_3 100 mM were added to the gel pieces and samples were incubated for 30 min in the dark at room temperature. Then supernatants were removed and 300 µL NH_4HCO_3 100 mM were added and mixed for 15 min. Supernatants were removed again, and 300 µL ACN/NH_4HCO_3 20 mM (1/1, v/v) were added to the band pieces and mixed for 15 min. Ensuing this agitation, supernatants were removed and a final wash with 100 µL ACN was performed with an agitation during 10 min. Band pieces should become white and shrinked. ACN was removed from the samples and band pieces were dried for 10 minutes in the SpeedVac. Digestion was then performed. Then 50 µl of Trypsin (20 ng/µL) were added to the band pieces, and incubation at 37°C was performed overnight. The next day, after an addition of 50 µL of ACN, samples were incubated at 37°C for 30 min and mixed for 20 min. The supernatants containing the peptides were transferred afterward to new microtubes. After an addition of 50 µL of 1% FA, band pieces were mixed for 20 min, and the supernatants were collected in the new microtubes from the previous step. This last step was carried out four times in total. Afterward, 150 µL ACN were added to the band pieces, followed by an agitation during 10 min. The supernatants were collected and added to the tubes containing the peptides. The peptides were finally dried in the SpeedVac and desalted with ZipTip C18 prior to HPLC-MS/MS analysis.

HPLC-MS/MS

An online reversed-phase chromatography was used to separate the sample, through a Thermo Scientific Proxeon easy nLC1000 equipped with a Proxeon trap column (100 µm ID x 2 cm, Thermo Scientific) and a C18 packed-tip column (Acclaim PepMap, 75 µm ID x 15 cm, Thermo Scientific). Peptides were separated with an increasing amount of ACN (2%-40% over 60 min) at a flow rate of 300 nL/min. The peptides were electrosprayed directly from the analytical column and a voltage of 1.7 kV was applied *via* the liquid junction of the nanospray source. The chromatography system was coupled to the mass spectrometer Thermo Scientific Q-exactive programmed with a top 10 data-dependent mode for all the samples. The resolving power was 70,000 FWHM (m/z 400), in a positive mode and using an AGC target of 3^{e6}. Default charge state was set at 2, unassigned and +1 charge states were rejected and dynamic exclusion was enabled for 25 s. The scan range was set to 300-1600 m/z. For $ddMS^2$, the scan range was between 200 and 2000 m/z, 1 microscan was acquired at 17,500 FWHM and an isolation window of 4.0 m/z was used.

MS Data Analysis

The MS data from secretomes were analyzed through MaxQuant 1.6.2.6 using the Andromeda search engine. Proteins and peptides were searched against a custom databank composed of the complete proteome of Rattus norvegicus (29,961 entries, July 2018) from the Uniprot database. Carbamidomethylation was set as a static modification, and methionine oxidation was set as a variable modification. For samples subjected to the deglycosylation step, asparagine to aspartate was also set as a variable modification. Parameters were set to 1 peptide per protein, 2 miss cleavages, with a strict FDR of 0.01. The mass tolerance was 10 ppm for the precursors, and 0.6 ppm for the fragments. Relative, label-free quantification was performed using the MaxLFQ algorithm integrated in MaxQuant software, with the default parameters. LFQ intensity was logarithmized (log2[x]). Proteins only identified with modified peptides and potential contaminants were removed. The MS data from neuron samples were analyzed through Proteome Discoverer 2.2. Proteins and peptides were searched against the same custom databank as for the secretome samples, in order to identify the VHH. Carbamidomethylation was set as a static modification, and methionine oxidation was set as a variable modification. For samples subjected to the deglycosylation step, asparagine to aspartate was also set as a variable modification. Parameters were set to 1 peptide per protein, 3 miss cleavage, with no limitation for FDR to identify all the potential peptides in the sample. Mass tolerance was also 10 ppm for the precursors and 0.6 ppm for the fragments.

Alignments of Peptidic Sequences

For the alignments of the variable parts of the antibodies, and for some of the constant parts of the antibodies, peptides were identified in different entries of the protein databank because of a high variability in the peptidic sequences. To align all the peptides obtained by MS, entries of the same part of the antibodies were aligned first in MultiAlin (http://multalin.toulouse.inra.fr/multalin/), then the consensus was used to perform the alignments. All the peptides identified were directly highlighted on the consensus sequence to compare peptides identified in all the samples.

Western Blots

To detect the presence of immunoglobulins in secretomes of segments R1, L, and C1 collected 12 h and 24 h after SCI, Western blots were performed (n=2). To determine protein concentration in the samples, the Bradford method was used. Twelve percent acrylamide gels were loaded with 2.5 µg of proteins from each sample. After migration, proteins were transferred to a nitrocellulose membrane. Membranes were saturated for 1 h in a solution of PBS-Tween 0.1% containing 5% non-fat dry milk and incubated overnight at 4°C with peroxidase-conjugated goat anti-immunoglobulins (0.08 µg/mL). After intensive washes with PBS-Tween 0.1%, chemiluminescence revelation was performed. Membranes were then dehybridized for 30 min with 0.2 M citric acid solution. After intensive washes with PBS-Tween 0.1%, membranes were again saturated and incubated overnight at 4°C with a primary mouse anti-GFAP antibody (1:1000). After intensive washes with PBS-Tween 0.1%, membranes were incubated with a peroxidase-conjugated goat anti-mouse

antibody (0.03 µg/mL). After intensive washes with PBS-Tween 0.1%, chemiluminescence revelation was performed.

To detect the presence of immunoglobulins in secretomes of segments R1, L, and C1 from rat treated with RhoA inhibitor, injected at the lesion site at the time of the lesion and collected 12 h after SCI, Western blots were performed (n=2). Secretomes of segments R1, L, and C1 from rat not treated with RhoA inhibitor and collected 12 h after SCI served as controls. To determine protein concentration in the samples, the Bradford method was used. Twelve percent acrylamide gels were loaded with 2.5 µg of proteins of 12 h samples. After migration, proteins were transferred to a nitrocellulose membrane. Membranes were saturated for 1 h in a solution of PBS-Tween 0.1% containing 5% non-fat dry milk and incubated overnight at 4°C with peroxidase-conjugated goat anti-immunoglobulins (0.08 µg/mL). After intensive washes with PBS-Tween 0.1%, chemiluminescence revelation was performed.

To detect FC gamma receptor CD16 in DRG ND7/23 cells, an immunoprecipitation was carried out. Anti-CD16 diluted at 1:100 in PBS-Tween 0.02% was added to Dynabeads Protein G and incubated for 4 h. Afterward, 1 mg of protein extracts from ND7/23 cells treated or not with 200 ng/mL of LPS was added and incubated overnight at 4°C. After intensive washes with PBS-Tween 0.02%, Protein G beads were eluted with glycine 50 mM pH 2.8 and Tris buffer pH 7.4 was added to neutralize the pH. Proteins eluted were separated by SDS-PAGE and transferred onto nitrocellulose membranes. After saturation for 1 h with the blocking buffer (PBS-Tween 0.1% containing 5% BSA), the membranes were incubated overnight at 4°C with mouse anti-CD16 (1:500) diluted in the blocking buffer. After intensive washes with PBS-Tween 0.1%, membranes were incubated with peroxidase-conjugated goat anti-mouse (0.03 µg/mL). After intensive washes with PBS-Tween 0.1%, chemiluminescence revelation was performed.

To detect FC gamma receptor CD32 in ND7/23 DRG cells, 40 µg of total cell extracts were analyzed by Western blotting. Proteins were separated by SDS-PAGE and transferred onto nitrocellulose membranes. After saturation for 1 h with the blocking buffer (PBS-Tween 0.1% containing 5% BSA), the membranes were incubated overnight at 4°C with rabbit anti-CD32 (1:500) diluted in blocking buffer. After intensive washes with PBS-Tween 0.1%, membranes were incubated with peroxidase-conjugated goat anti-rabbit (0.08 µg/mL). After intensive washes with PBS-Tween 0.1%, chemiluminescence revelation was performed.

Spinal Cords Sections and Immunofluorescence

Spinal cords were collected and fixed in 4% paraformaldehyde. They were then submerged in sucrose baths of increasing concentration of 10 to 30% over 3 days before being included in 2% cellulose and frozen at -80°C. Samples were then cut with a cryostat in 20-µm thick sections. For IHC, sections were dried in a desiccator for 5 min, followed by antigen retrieval in Tris-HCl 20 mM pH 9 by 30 s microwaves treatment. Sections were then rehydrated by 3 baths of phosphate buffer (PBS 1X), before saturation in PBS 1X containing 1% BSA buffer, 1% ovalbumin, 0.05% triton, and 1% normal donkey serum. Alexa Fluor® 647-conjugated goat anti-rat IgG (4µg/mL) and mouse anti-NeuN (1:500) were then added followed by an overnight incubation at 4°C. Sections were then washed 3 times with PBS 1X, before incubation for 1 h at 37°C with Alexa Fluor® 488-conjugated donkey anti-mouse IgG (2 µg/mL). After intensive washes with PBS 1X, coverslips were mounted using Dako fluorescent mounting medium.

CD16 and CD32b Immunostaining and Fluorescence Quantification

To detect Fc gamma receptors, 35,000 ND7/23 cells were grown on coverslips and treated or not beforehand with LPS (200 ng/ml) and RhoA inhibitor (1 µg/mL) for 24 h. The cells were fixed with paraformaldehyde 4% (PAF) for 10 min, washed in PBS1X (phosphate buffered sodium 1X), and quenched with glycine 50 mM. After cell membrane permeabilization with 0.2% Triton X-100 for 10 min, cells were immersed in a blocking buffer (PBS 1x containing 1% bovine serum albumin, 1% ovalbumin, 1% NDS) for 1 h. The cells were then incubated overnight at 4°C with rabbit anti-CD32 (1:100) or mouse anti-CD16 (1:100) diluted in the blocking buffer. Washes with PBS 1x were performed and followed by 1 h incubation at 37°C with Alexa Fluor® 488-conjugated donkey anti-rabbit or Alexa Fluor® 488-conjugated donkey anti-mouse diluted at 2 µg/mL in the blocking buffer. The cells were further washed with PBS 1X and nuclei were stained with Hoechst 33,342 (1:10 000). After a final wash in PBS 1X, coverslips were mounted using Dako fluorescent mounting medium. Fluorescent stained cells were analyzed using a confocal microscope (Zeiss LSM700) and the quantification was performed by ImageJ software. To that end, 10 fields representative of the wells were selected for each condition and circularity, area, and mean fluorescence as well as the background of each cell presented in the field were measured. Fluorescence intensity was calculated with the total corrected cellular fluorescence (TCCF) equation = integrated density – (area of selected cell × mean fluorescence of background readings). The results are presented as means ± SD. The statistical significance was evaluated through Student's t-test and values of $p < 0.05$ were considered statistically significant (*p-value of <0.05).

Investigation of the Biological Effects of Fc Gamma Receptors in ND7/23 DRG Cells

To study the role of CD16 and CD32 receptors, ND7/23 DRG cells were placed in serum-free medium containing 1% L-glutamate, 100 U/ml penicillin, and 100 µg/ml streptomycin. Afterward, cells were treated for 1 h with 1 µg/mL of RhoA inhibitor and then incubated for 24 h with rabbit anti-CD32 (1:600), mouse anti-CD16 (1:100), and mouse anti-GFAP (1:500). Mouse anti-GFAP displayed an IgG2 isotype and served as a control of Fc gamma receptors activation. Following these treatments, neurites length was measured through Image J software and the statistical significance was evaluated with a t-test using Graph pad PRISM software. Values

of $P < 0.05$ were considered statistically significant (*P value of < 0.05, **P value of < 0.01, ***P value of < 0.001).

Calcium Homeostasis Analysis in ND7/23 DRG Cells

ND7/23 DRG cells were treated with rabbit anti-CD32 (1:500) and mouse anti-CD16 (1:500) for 24 h and loaded with 2.5 µM Fura-2 AM. After intensive washes with culture medium, fluorescence intensity of Fura-2 in cells was recorded at 340 and 380 nm using MetaFluor Software. The ratio F340/F380 was calculated to evaluate the variations in cytosolic Ca^{2+} concentrations. After 100 s of monitoring, 1 µM of thapsigargin was added to induce Ca^{2+} efflux from the ER. This led to the activation of store-operated channels (SOCs) located at the plasma membrane increasing Ca^{2+} intake into the cells.

Transcriptomic Studies

To study *Fcgr3* (*CD16)* expression in ND7/23 DRG, RNA were extracted from ND7/23 cells stimulated with 200 ng/mL of LPS using Tri Reagent according to the manufacturer's instructions. Two micrograms of RNA were treated with 2 units of DNase RQ1 and retro-transcribed using the SuperScript® III kit. To perform RT-PCR experiments, the following primers were used: Rat *Fcgr3* (forward primer: 5′- CAC AGT CAA TGA CAG TGG -3′; reverse primer: 5′- TTG GAC ACA TGC ATT GTC -3′). cDNA amplification was performed using GoTaq polymerase and 40 cycles at 95°C/30 s, 60°C/1 min, and 72°C/1 min. Amplicons were then purified, subcloned into pGEM-T easy vector, and sequenced.

To study Rat *IgG2c* gene expression in N27 and ND7/23 cell lines, RNA were extracted from ND7/23 or N27 cells using Tri Reagent according to the manufacturer's instructions. Two micrograms of RNA were treated with 2 units of DNase RQ1 and retro-transcribed using the SuperScript® III kit. To perform RT-PCR experiments, the following primers were used: Rat *IgG2C* (forward primer: 5′- TCC GTG AAG CTC TCT TGT GC-3′; reverse primer: 5′- ATG GAG GCC TGG GAG GGA CGG -3′).

To study *Rag1* and *Rag2* gene expression in DRG cells (ND7/23) and N27 cell line, cells were stimulated 24 h with 10^{-4} M of H_2O_2. DRG cells were also stimulated with secretome from lesion segment collected 1 day after SCI. RNA were extracted using Tri Reagent according to the manufacturer's instructions. Two micrograms of RNA were treated with 2 units of DNase RQ1 and retro-transcribed using the SuperScript® III kit. To perform RT-PCR experiments, the following primers were used: Rat *Rag1* (forward primer: 5′- GGC CAT CCG TGT CAA TAC CT-3'; reverse primer: 5′- ACC GAA CTG CCT TTT CTG GA-3′), *Rag2* (forward primer: 5′- GCC TTC TAC CCA AAG AAC CAC-3'; reverse primer: 5′- ACA GTC CCG TTT CCC ATG TT-3′), *Actin* served as referent gene (forward primer: 5′- TTG TAA CCA ACT GGG ACG ATA TGG-3'; reverse primer: 5′- GAT CTT GAT CTT CAT GGT GCT AGG-3′).

RNASeq Data Reuse Analyses

RNAseq libraries were obtained from the Sequence Read Archive (SRA) database. SRX11310972 corresponded to the dorsal root ganglion (DRG) explant. By contrast SRX7119488 and SRX10720738 were obtained from primary neurons from DRG. A blast search was carried out on each databank to identify CD markers and immunoglobulin heavy and light chains. Initially, the search was carried out with a maximum of 100 reads for the expressed genes and a second analysis was carried out with 500 reads. The alignment allowed the identification of reads at the 5' end. Those reads covered the complete constant chain as well as the V(D)J region. This was confirmed using the IgBlast tool. The reads encoding a variable part linked to a constant part were aligned with a kappa light chain constant part.

RESULTS

In a past study proteins involved in the Memo-RhoA-Diaph1 and Rho-Rock pathways were identified in both lesion and caudal 1 segment on Day 3 to 10 post-SCI. On the opposite, rostral 1 segment was characterized by a pro-regenerative inflammatory profile favoring the attraction of neutrophils and T regulatory cells as well as a polarization of macrophages/microglia toward a repair promoting M2 phenotype (12). Accordingly, in these segments, many proteins promoting neurogenesis (neurotrimin, neurofascin, semaphorins) and synaptogenesis (septins, syntaxins, synapsins) were characterized. Such proteomic profiles contributed to settle a pro-neurite outgrowth medium on both parts of the lesion (12). Unfortunately, these phenomena were not only asynchronous but hampered by the development of a repair-inhibiting process that took place within the lesion itself and the adjacent caudal segment (thereafter referred to as the C1 segment). In these segments, activation of the Rho-Rock pathway, pro-inflammatory signals, glial scar-promoting molecules prevented the neurite outgrowth process initiated both in the adjacent rostral segment and the distal caudal one. Our objective was therefore to provide a precise description of time- and segment-specific inflammatory events and to identify new immune-related therapeutic targets in SCI. To prove that our model was well suited to assess the impact of inflammation during SCI, we first performed *in vivo* experiments using the anti-inflammatory agent, FK506 (12). Results showed that FK506 slightly improved synaptogenesis and neuritogenesis as revealed by anti-synaphysin I and anti-GAP43 labelling and increased the BBB score from 2 to 8 ± 2 in 2 weeks compared to untreated SCI rats. These results reflected that inflammation modulation could improve the BBB score and synaptogenesis but not neurite outgrowth (12). Therefore, it was not sufficient to greatly improve the regeneration process. In these conditions, we decided to deeply analyze the events occurring at early stages of the lesion, that is, 12 h and 24 h after SCI.

Spatio-Temporal Organization of Inflammatory Response and Neurogenesis at the Acute Stage of SCI

We studied the protein content of secretomes collected from Rostral 1 and 2 (R1, R2), lesion (L) and caudal 1 and 2 (C1, C2) spinal cord slices extracted 12 h or 24 h after SCI. After in solution digestion of secretome proteins, we proceeded to a nanoLC-HRMS in MS/MS mode analysis (**Supplementary Data 1**; **Figure 1** and **Table 1**). Collected data were analyzed, multi-samples tests were performed, and a hierarchical clustering was obtained (**Figure 1**). Two main branches detected. The first isolated lesion secretomes (12 h and 24 h) from secretomes of other segments. In lesion secretomes (Cluster 1), the more abundant proteins were inflammatory proteins (CRP, CXCL1, 2,3, interleukin 6), complement proteins (Cfi, C5, C1qc, C1r, C1s, C1qbp, C1q, C2, C3, C4, Cfp, C8g, C8a, C9, C6, Cs), calreticulin, metalloproteinase inhibitors 1 and 2, cathepsins B and D (**Figure 1** and **Table 1**). Of note, secretomes from C1 at 24 h clusterized with the secretomes of lesion segments, which confirmed and extended our previous data showing that, at later time points, lesion and C1 caudal segments harbored similar proteomic profiles (Cluster 2) (**Figure 1** and **Table 1**). Overexpression of complement components that were characteristics of innate immune response was initially restricted to the lesion segment before spreading essentially in the C1 segment between 12 h and 24 h and thus the acute phase of SCI-associated inflammation. Secretomes from other segments were partially clusterized depending on the time course and location. Thus, secretomes from rostral and caudal segments collected 12 h after SCI were enriched in neurogenesis inhibitors such as Nogo and neuroendocrine-specific protein (NSP) (Cluster 3) (**Figure 1** and **Table 1**). On the opposite, after 24 h, proteins promoting neurogenesis (Robo 1 and 2, Plexin B1, Semaphorins 6d and 4b, neuronal cell adhesion molecule 1 and 2 (Ncam1 and Ncam2)) were highly represented in secretomes from caudal and rostral segments (**Figure 1** and **Table 1**). It is especially interesting to notice that the intensity of the inflammatory response raised between 12 h and 24 h, as well as the proteomic profiles of rostral and caudal segments changed in this time window. Proteomic study performed during the acute phase at 12 h and 24 h also demonstrated the presence of immunoglobulins. Immunoglobulins found were IgG (IgG1, IgG2a, IgG2b, IgG2c) (**Supplementary Table 2**). Of note, IgGs were abundantly detected in spinal cord slices at early time points following SCI. We previously showed the presence of IgGs in the supernatants of SC slices at 3 days (3 D), 7 days (7 D), and 10 days (10 D) after SCI (4). Since B-cells were not detected in the spinal cord parenchyma during SCI we concluded that yet unknown mechanisms supported the uptake and subsequent release of IgGs from spinal cord slices (4). Their presence at such an early time (12 h) was surprising, and knowing that IgGs, depending on their subtype, have different receptors and functions, such as the ability to fix complement, we decided to focus our study on these immunoglobulins. We thus performed an in-depth analysis to further decipher the time-course of IgGs release from SC slices during SCI.

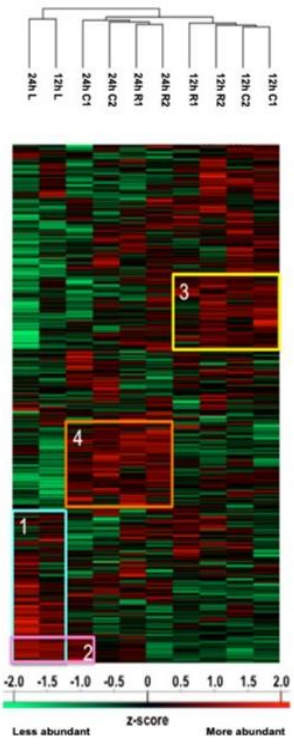

FIGURE 1 | Heatmap illustrating hierarchical clustering obtained after analysis of digested peptides isolated in secretomes from spinal cord segments collected 12 h and 24 h after SCI. Four clusters are highlighted. Cluster 1 corresponds to the inflammatory proteins' accumulation in lesions. Cluster 2 demonstrates that the proteomic profile of C1 starts to cluster with lesions after 24 h. Clusters 3 and 4, respectively, represent proteins more abundant in other segments at 12 h (neurite outgrowth inhibition) and at 24 h (synaptogenesis and neurogenesis proteins).

Meta-Analysis of the SCI Data

Except in shark and camel, where minibodies have been identified as dimers of shortened heavy chain of immunoglobulins (13–16), most vertebrate species display antibodies composed of four polypeptidic chains, two heavy chains and two light chains, linked by disulfide bonds (17). Heavy chains are subdivided in four domains, Variable Heavy (VH) and Constant Heavy (CH1, CH2, and CH3), whereas light chains are subdivided in two domains, Variable (VL) and Constant (CL) (17). In the variable domains (VH and VL), hypervariable regions (CDR for complementary determining regions) and variable regions (FR for framework) are present, determining the paratope of the antibody. Meta-analysis performed on triplicate data from shot gun proteomic based on spatio-temporal study of spinal cord injury from 12 h to 10 days, gave evidence of IgGs isotypes with a sequence coverage of 48,52% (4, 5, 12). The most abundant were IgGs, especially IgG2a and IgG2B, but constant kappa light chain was also found with high LFQ values (**Supplemetary Table 2**). Indeed these immunoglobulins as well as the Lambda constant chain were detected in the secretome regardless of the time after lesion and

TABLE 1 | Label free quantification (LFQ) values of proteins found in 12 h and 24 h secretomes.

Protein	Uniprot reference	12h R1	12h L	12h C1	24h R1	24h L	24h C1
Immune Response							
C5	**A0A096P6L9**	27.105	30.753	27.1991	29.8638	31.133	28.256
Complement facteur I	**A0A0G2K135**	28.6862	31.4865	29.1756	30.9452	31.9867	30.7474
C1q C	**P31722**	27.2059	27.5941	27.5216	28.0868	28.9265	27.5725
C8g	**D3ZWD6**	25.4009	29.3109	25.6515	28.2115	29.3498	27.933
C6	**F1M7F7**	26.2006	28.4164	25.2068	26.0326	28.8182	26.0147
C9	**Q62930**	29.3776	32.0729	28.8857	30.5028	32.8296	29.9725
C9	**Q62930**	29.3776	32.0729	28.8857	30.5028	32.8296	29.9725
Cfb	G3V615	27.5889	29.7907	28.1228	28.8318	30.2445	29.0034
Cfd	**P32038**	25.8039	29.2837	26.1685	27.3739	29.4617	26.6487
C1s	**G3V7L3**	25.9108	26.0894	0	0	26.1576	25.6268
C1q B	**P31721**	26.8409	27.8129	27.6312	27.3534	27.9999	27.1107
C3	**M0RBF1**	34.5677	35.9915	34.1207	35.4205	36.3782	34.9085
C1q binding protein	**O35796**	27.1542	28.7074	28.0595	28.183	28.7206	28.348
C4	**Q6MG90**	28.7578	31.2414	27.9086	29.5244	21.1205	30.2756
Complement C1q A	**P31720**	26.8299	28.2033	27.1038	28.0575	28.9744	28.2956
C8	**D3ZWD6**	25.4009	29.3109	25.6515	28.2115	29.3498	27.933
C2	**Q6MG73**	27.4799	29.0364	0	28.0699	29.841	27.8886
C1q receptor	**Q9ET61**	0	0	0	0	24.3473	24.4574
CRP	**P48199**	27.3319	29.1611	26.934	28.2882	29.9143	25.7745
Cathepsin D (ctsd) protease	**P24268**	29.5102	29.6845	30.016	29.7627	30.1024	29.5429
Cathepsin B (ctsb) protease	**P00787**	30.6649	31.0627	30.869	31.1476	31.5995	30.7585
Metalloproteinase 1 inhibitor	**P30120**	31.2912	31.3888	30.293	30.0952	32.0704	30.4234
Metalloproteinase 2 inhibitor	**P30121**	25.1333	26.2628	26.013	26.0498	26.7354	26.3374
Axonal Guidance							
Roundabout homolog 1 Robo 1	O55005	25.5019	25.6818	25.5182	25.4674	25.7368	26.0018
Protein Robo2	**Q9QZI3**	26.7878	25.2904	25.377	27.5075	26.8033	28.6504
Neuronal cell adhesion molecule	**A0A0G2K329**	32.237	32.0057	31.8815	32.527	31.8527	32.2182
Neural cell adhesion molecule 1	**P13596**	33.6315	33.5348	33.7206	34.7838	34.0443	35.0052
Protein Ncam2	A0A0G2K7P9	29.2571	28.2036	29.191	30.695	29.7085	30.0036
Contactin 4	Q62845	0	0	0	22.7805	0	24.6327
Contactin 6	P97528	0	0	0	24.2783	0	24.4514
Semaphorin 6d	A0A0G2JZC4	0	0	0	24.0672	0	24.8241
Semaphorin 4b	F1LSV0	26.4542	26.0691	26.504	26.7882	25.5816	26.8069
Plexin B1	D3ZDX5	28.3156	28.2094	28.5334	29.5902	27.9306	29.0632
		35_37	32_35	29_32	26-29	23-26	20-23

The color shading corresponds to the various LFQ values assigned after our protomics analysis.

the segment. Of note, some immunoglobulins (IgG1, IgG2a, IgG2b, constant kappa and lambda light chains) were also identified in the segments from the control group (**Supplemetary Table 2**). For IgG2a, the most part of the identified peptides whatever the conditions covered the CH2 and CH3, and one single peptide was detected in CH1 (**Supplementary Data 2**). For IgG2B, CH2 was mostly covered and one peptide in CH3 was found regardless of the time and the spatial localization (**Supplementary Data 2**). Concerning the Lambda chain, almost 93% of the constant part was identified (**Table 2** and **Supplementary Data 1).** It is interesting to note that IgM and IgG2c were also identified but almost exclusively at 12 h after the lesion. This means that these Igs were not natively present in the spinal cord and their release was therefore induced by the lesion (**Supplemetary Table 2** and **Supplementary Data 2**). Indeed, IgG2c and IgM-like proteins were mostly detected in secretomes from lesion and rostral segments at 12 h and then in lesion and caudal segments at 1 D. This fits with the slide from rostral to caudal segments previously demonstrated in whole proteomic studies (4). This time window is clearly unusual for IgM production which appears normally 6 to 7 days after trauma. We also observed that IgG2c diseapered afterward and IgM slightly decreased from 3 D and its production stayed centered at the lesion site. For IgM, different peptides covering various parts of the heavy chain were identified (**Supplementary Data 2**). At this time window (12 h, 24 h), we also identified a heavy variable part with a coverage of 54% (**Table 2** and **Supplementary Data 1**). At the lesion site 12 h after SCI,

variable parts of Kappa and Lambda light chains were also detected. Lambda V then disappeared whereas Kappa V spread in all segments at 24 h and then disappeared. Only 40% of the VL were identified whereas almost 80% of the VK were characterized (**Table 2** and **Supplementary Data 2**). To assess more accurately the spatio-temporal evolution of immunoglobulin levels in the secretomes after SCI, their LFQ values were normalized to those quantified in the secretomes of controls (non-lesioned spinal cord) (**Figure 2A**). This confirmed that abundance of IgG1, IgG2a, IgG2b, and IgG2c increased between 5 to 15 times from 12 h to 24 h in Rostral 1, Lesion and Caudal 1 segments. Moreover, at 24 h, the levels of IgGs increased only in the Caudal 2 segment. These levels began to decrease from 3 days and became low at 7 days for all these IgGs. However, IgG2a had the tendency to remain higher than other IgGs from 24 h to 10 days. Moreover, this analysis revealed again that immunoglobulins showed a trend to be higher at the lesion site.

To complete our study, Western blot analyses with anti-IgG were carried out on secretomes of Lesion, Rostral 1, and Caudal 1 segments harvested 12 h and 24 h after SCI. These experiments were conducted in denaturing and reducing conditions (**Figures 2Ba**). Two biological duplicates were loaded on each gel. These experiments confirmed the presence of heavy and light chains detected at 50 kDa and 25 kDa, respectively. In gel digestion was also performed in parallel and validated the identity of these bands as heavy and light chains (**Supplementary Data 3**). Previously, during our proteomic analysis, we detected constant levels of GFAP in these secretomes (12). Therefore, we decided to use this protein as an internal control during our Western blot experiments. The intensity of heavy and light chain bands was quantified and normalized to those of GFAP. Even if no significant differences were found, heavy and light chains showed again a trend to be higher at the lesion site, especially at 24 h after SCI (**Figure 2Bb**).

Immunoglobulins Are Detected in the Normal CNS

As described above, we identified immunoglobulins within the control spinal cords. This raised the question of the origins of these immunoglobulins released in the spinal cord under steady state conditions. The release of immunoglobulins from SC slices could be a consequence of the experimental setting since tissue slicing and subsequent short-term organotypic cultures are likely to alter the physiological behavior of neural cells. To address this issue, we extracted proteins from a freshly frozen intact spinal cord, thus avoiding any culture bias, and found similar results (**Figure 2C** and inset **Table 3**). Since neural cells express receptors binding the constant fraction (Fc) of immunoglobulins (18), one may propose that the presence of IgGs in spinal cord neural cells is primarily conditioned by their transport from blood to brain and their subsequent internalization and release by neural cells. However, intriguingly, a survey of the mouse brain atlas showed that mRNA expression of IgG1 and IgG2 classes in distinct CNS regions including the spinal cord, cerebellum, and hippocampus in both juvenile and adult mice (http://mouse.brainmap.org/) (**Supplementary Figure S1A**). Altogether these results support that immunoglobulins are present in the basal state in the spinal cord.

TABLE 2 | Sequence coverage in the SCI data from the different isotypes and regions of immunoglobulins from secretome 1 day after lesion.

Isotype	Coverage (%)
IgG1	51.23
IgG2A	66.46
IgG2B	41.74
IgG2C	34.65
IgM	31.52
Heavy V	53.96
Lambda C	93.27
Lambda V	39.34
Kappa C	41.51
Kappa V	79.51

Identification of Immunogobulins in SCI Tissues

Antibodies are mostly identified from biological fluids and mass spectrometry using shot gun proteomic (19) or top-down proteomic (20, 21) has highly contibuted in that direction. By contrast, immunoglobulins in complex samples such as tissues are more difficult to characterize. In order to further isolate and characterize IgGs in tissues, IgG enrichments may be necessary. Conventional enrichment of IgGs in complex samples is based on affinity chromatography with protein A, protein G, or antigen, and can be followed by mass spectrometry analysis (22). However, a new alternative technique named the Melon gel is also possible but it is mainly used to purify IgGs from serum. More precisely, the Melon gel is not an enrichment technique but is based on negative selection using a resin that captures all proteins except IgGs. To the best of our knowledge, this technique is used exclusively on serums and not on protein from tissue extracts (23–25). So it was decided to test Melon gel on protein extracts from tissue as well. Enrichment procedures using ammonium sulfate precipitation and Melon gel purification were performed on protein extracts from the spleen as a contol and a spinal cord lesion segment withdrawn seven days after injury (SCI 7D-L) (**Figure 3** and inset **Table 4** and **Supplementary Data 3**). After the MS analysis with MaxQuant, IgG were detected, confirming the efficiency of the enrichment procedure. Constant Lambda and Kappa light chains, as well as Kappa V were detected in both the spleen and SCI 7D-L as we previously found in secretome. Concerning immunoglobulin heavy chains, only IgG2A and IgG2B were detected in SCI 7D-L (**Figure 3**; inset **Table 4**). To extend our study, we validated the presence of immunoglobilins in SCI tissue by immunofluorescence (**Figure 3**). Co-labeling was performed with anti-NeuN (neuronal marker) and anti-IgG on sections of lesion segments from spinal cord collected 24 h after lesion (**Figures 3A–C**). This revealed that cells around the lesion site stained with anti-IgG were neurons since they were also labelled with anti-NeuN. We previously demonstrated the impact of RhoA pharmacological inhibition on neurites outgrowth and synaptogenesis (12). This was confirmed by shotgun proteomics performed on rostral, caudal, and lesion segments collected 12 h after lesion with or without treatment with RhoA inhibitor

(**Supplementary Figure 3**). This revealed that inflammatory proteins and immunoglobulins were more abundantly present in the lesion site with or without RhoAi treatment (Cluster 1). By contrast, Cluster 2 showed proteins involved in synaptogenesis which were more highly detected after RhoAi treatment. Cluster 3 represented proteins involved in neurite outgrowth such as CNTF, contactin, neural cell adhesion molecule L1, Stathmin, Neurofascin, Neurotrimin, and Dynactin. These proteins were more abundantly detected in R1 and C1 segments without RhoAi treatment. We therefore evaluated at an early stage after SCI, the impact of such RhoA inhibition (RhoAi) on IgG levels released from spinal cord explants (**Supplementary Data 5**).

RhoA Inhibition Increased IgG Release From Spinal Cord Explants

RhoA inhibitor was injected at the lesion site at the time of lesion and SCI explants were collected at an early stage after SCI, that is, 12 h. A shot gun proteomic analysis was then conducted on secretomes from the various segments (**Figure 4Aa**). The LFQ values obtained for IgG were compared to those measured in secretomes of SCI explants from rats untreated with RhoA inhibitor. This revealed that RhoAi treatment increased the release of the various IgG isotypes considered in this study. In section R2, C1, and C2, fold changes reached 3 to 4, whereas in R1 and lesion fragment, fold changes reached 2 to 3. Western blot analysis in reducing conditions reconfirmed the presence of IgG in these secretomes (**Figure 4B**). Afterward, semi-quantitative analysis of IgGs in spinal cord tissue sections confirmed the impact of RhoAi treatment in R1, C1, and lesion segments (**Figure 4Ab**). Interestingly, while IgG1 and IgG2C were the most prevalent isotypes in the spinal cord secretomes of untreated injured animals, IgG2A was the most abundant IgG isotype in the spinal cord secretome of RhoAi-treated injured animals, especially at the lesion site (**Figure 4A**). Besides IgG2A, we also observed an isotype-specific effect of RhoAi treatment for other IgGs. After treatment with RhoA inhibitor, IgG2C as well as IgG1 highly increased in the secretome of the lesion segment while conversely IgG2C was not detected in R1, decreased in the lesion and was predominant in C1. IgG2A greatly increased in the lesion (**Figure 4A**). These results indicate that RhoAi treatment induced an isotypic commutations (systemic or local) and/or an isotype-specific mechanism of capture and release of IgGs by neuronal cells.

Neurons Produce IgG

To determine if these IgG were synthesized or recaptured by neurons, a transcriptomic approach was undertaken in dorsal root ganglia (DRG) ND7/23 cell line stimulated with LPS to mimic an inflammatory condition as observed at the lesion site. Moreover, the same approach was performed in the non-differentiated N27 dopaminergic neural cell line (N27). Transcripts from the spleen serve as a positive control. By RT-

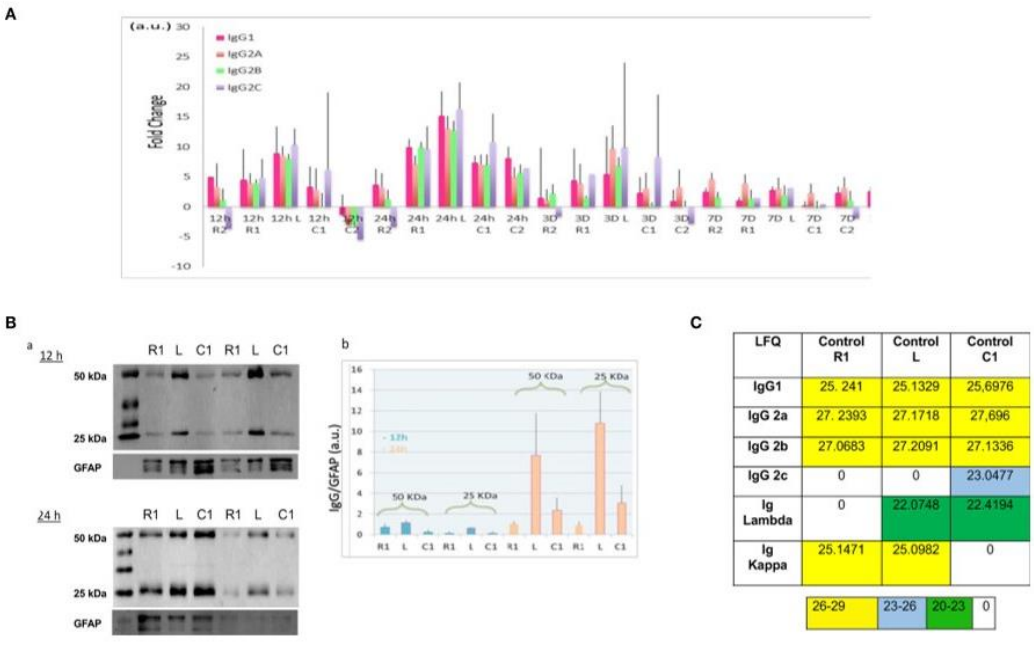

FIGURE 2 | **(A)** Ratio of IgG according to time course after SCI and spinal cord segment. Rationalization was performed by comparison with the control (non-lesioned spinal cord). **(B)** (a) Western blot of 12 h and 24 h secretomes, with anti-immunoglobulin antibodies. (b) Histogram illustrating the immunoglobulin level in function of time and segment was obtained by ImageJ software. Results rationalization was carried out using GFAP. **(C)**. Inset **Table 3**. Immunoglobulin rates in control spinal cord. (LFQ: label free quantification).

PCR, we amplified the whole IgG2c ORF in N27 cells as another source of neural cells. Cloning was performed and sequencing confirmed that this gene was expressed in N27 cells demonstrating the neural origin of these immunoglobulins (**Figure 5A**). These results are in line with recent data showing the expression of the genes encoding IgG3 and IgM in murine spinal and supraspinal neurons (26). Allen Brain Atlas confirms in mouse the presence of IgG3 and IgH-VS107 immunoglobulin chains in the cortex and hippocampus regions (**Supplementary Figures 1A, B**) or spinal cord (**Supplementary Figure 2**). Analyses of RNAseq Sequence Read Archive data from rat DRG neurons confirmed the expression of immunoglobulins heavy and light chains (constant and variable) (**Figure 5B**; **Supplementary Table 1** and **Supplementary Data 4**). We identified constant IgG1, IgG2(a, b), and IgM heavy chains as well as Kappa and Lambda light chains in DRG explant. IgG2(a, b), IgM, and Kappa chains were also detected in primary culture of DRG neurons. Several V(D)J chains were also identified associated with constant IgG2(a, b) chains and Kappa chains (**Figure 5B**). Taken together, the presence of immunoglobulins in neurons is comforted. Moreover, it is well known that the proteins of the immunoglobulin superfamily (IgSF) are implicated in various stages of brain development, including neuronal migration, axon pathfinding, target recognition, and synapse formation as well as the maintenance and function of neuronal networks in the adult (27). To support Ig production by neurons, we studied in DRG and N27 cells the expression of genes coding the RAG1 and RAG2 enzymes controlling V(D)J recombination. Since during SCI or other brain trauma, an important amount of neuronal death is observed, we thus mimic this process by using H_2O_2 treatment (28). Under that condition, *Rag1* expression was only observed in N27 cells whereas *Rag2* mRNA was detected in both cell lines (**Figure 5C**). Since *Rag1* expression may be induced by specific factors produced after SCI, DRG cells were cultivated in the presence of secretome of the lesion segment collected 1 day after lesion representing the acute phase of inflammation after SCI (**Figure 5C**) (12). In such conditions, *Rag1* expression was observed. These results suggest that neurons produce a variability of immunoglobulins through V(D)J recombination.

Identification of FcγRs (CD16, CD32) in DRG ND7/23 Neurons

In the immune system, immune response modulation by IgGs involves the antibody-dependent cell-mediated cytotoxicity (ADCC) mechanism (29). In this context, IgGs through their paratopes recognize their target and label the cells to be destroyed. For this purpose, cytotoxic immune cells recognize the bound IgGs through their constant region. This recognition involves FcγR such as CD64, CD32, and CD16 expressed at the cell surface of cytotoxic cells. For a long time, it was considered that the expression of these receptors was restricted to immune cells. However, recent studies have demonstrated the presence of FcγR I (CD64) at the cell surface of glial cells such as microglia and astrocytes (30). More

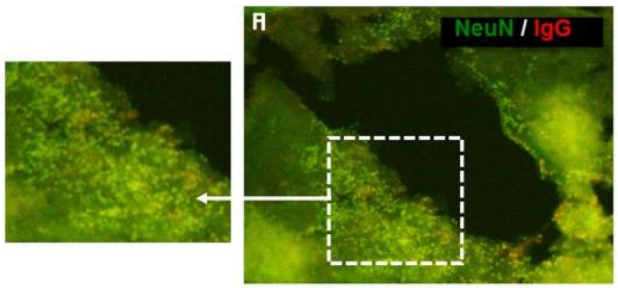

	Tissue	
	Spleen LPS	SCI 70-L
VHH	NaN	22.9
IgG1	NaN	NaN
IgG2A	31.2	32.5
IgG2B	30.8	30.2
IgG2C	29.1	NaN
IgM	30.7	NaN
Heavy V	NaN	25.1
J chain	NaN	NaN
Kappa C	29.9	30.0
Kappa V	26.4	25.4
Lambda C	28.1	28.6
Lambda V	NaN	24.3

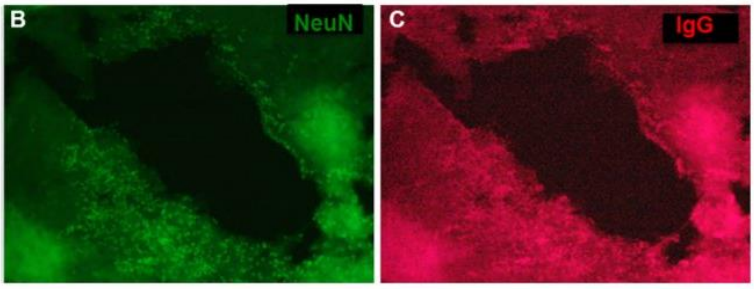

FIGURE 3 | The immunofluorescence performed on a section of lesion segment from the spinal cord revealed a colocalization **(A)** between NeuN (**(B)**, green, Alexa Fluor® 488) and IgG (**C**, red, Alexa Fluor® 647) (20X objective). Inset **Table 4**. Sequence coverage in the SCI data from the different isotypes of immunoglobulins from SCI tissues at 7 days after lesion and spleen from rat stimulated with LPS as control.

recently, Zhang and collaborators also established that FcγRI, but not FcγRII (CD32) and FcγRIII (CD16), was also expressed in a subpopulation of primary sensory neurons (31). Allen Brain Atlas indicated that Igs are colocalized with CD16 and CD32b in the same mouse brain regions (**Supplementary Figures 1C, D**). At a first step, to demonstrate the expression of CD16 and CD32 receptor, we used transcriptomic and Western blot approaches in DRG ND7/23 cells (**Figure 6**). A RT-PCR experiment was carried out to amplify *Cd16* transcripts. A positive fragment was obtained, and sequencing confirmed the expression of this gene in DRG ND7/23 cells (**Figures 5A**, **6B**). These results are in line with RNAseq analyses performed on rat DRG (**Figure 5** and **Supplementary Table 1**). To confirm the expression of CD16 at the protein level, Western blot experiment was conducted after immunoprecipitation with an anti-CD16 performed on protein extracts from DRG ND7/23 cells stimulated or not with LPS (**Figure 6C**). LPS stimulation was used to mimic an inflammatory condition as observed during SCI. In both conditions, a band close to 30 KDa and corresponding to CD16 was revealed. An additional band close to 52 KDa was also observed. It has been described that efficient cell expression of CD16 requires its interaction with a dimer of Fcer1g (29). Fcer1g mass is close to 10 KDa. Therefore, the band around 52 KDa observed in our experiment may correspond to CD16 bound to Fcer1g dimer. Altogether, this confirmed the expression of CD16 in DRG ND7/23 cells. Interestingly, under LPS treatment the intensity of the bands increased compared to the control condition. This pinpointed that the inflammatory environment mimicked by LPS regulated CD16 expression in sensory neurons (**Figures 6C**). To test the activation of CD16 with anti-CD16, intracellular calcium release (32) was registered (**Figure 6D**). The result obtained confirmed its activation. To identify the CD32b receptor in DRG cells, Western blot analysis was also conducted and revealed a band at 34 KDa matching with its molecular weight (**Figure 7A**). This receptor is known as the only inhibitory receptor of the FcγR family since it's the only one to display the ITIM motif on its cytoplasmic domain. These results are in line with RNAseq data (**Supplementary Table 1**). Moreover, we observed that RhoA inhibition increased IgG release by SCI explants (**Figure 7A**). In macrophages, it has been shown that CD32b expression was also increased by LPS treatment (33). Therefore, to determine if RhoA inhibition treatment combined with LPS could modulate the expression of CD16 and CD32 in DRG ND7/23 cells, we studied their expression profile by immunofluorescence (**Figure 7B**). Under LPS and/or RhoAi treatments, the intensity of CD16 immunostaining increased remarkably compared to the control condition. In fact, this intensity was 4%, 40%, and 63% higher for LPS, RhoAi, and the combined LPS+ RhoAi treatments, respectively. In comparison to the control condition, the intensity of CD32 staining was also enhanced by 52%, 72%, and 88% for LPS, RhoAi, and LPS+ RhoAi treatments, respectively (**Figure 7B**). These results suggested the potential involvement of those factors in the upregulation of CD16 and CD32 expression. Moreover, even if anti-CD16 and anti-CD32 were employed at the same concentration, the detection threshold for anti-CD32 was lower. Indeed, in comparison with anti-CD32, the intensity of fluorescence measured with anti-CD16 was 67%, 33%, 30%, and 38% more

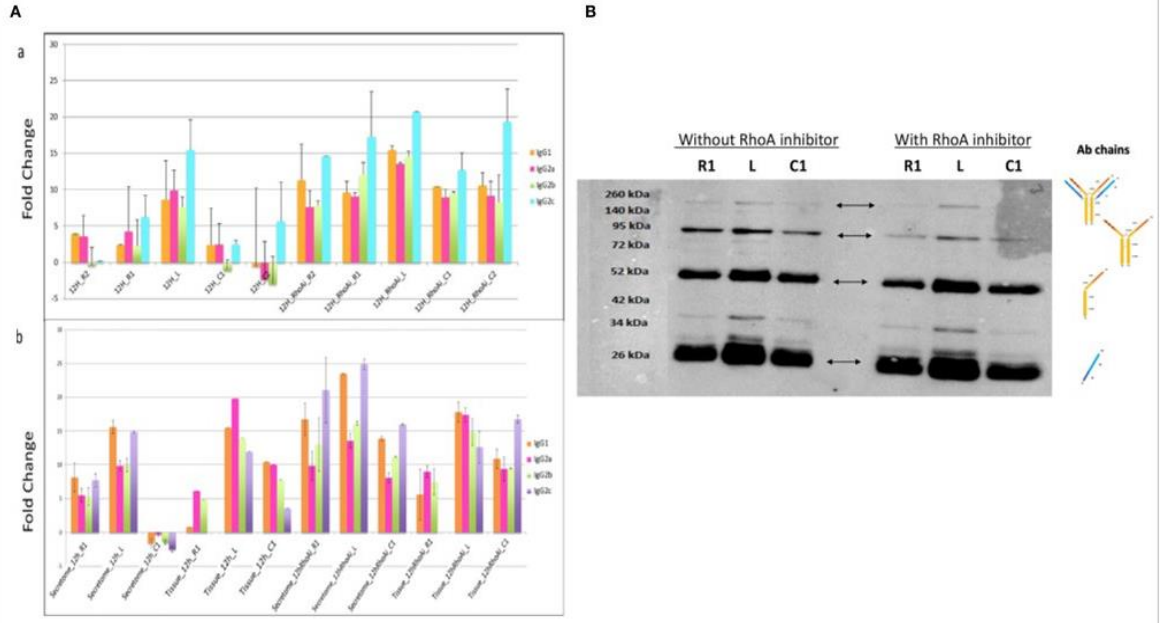

FIGURE 4 | **(A)** (a) Fold change between IgG isotypes in secretome from the different segments collected 12 h after SCI and treatment with RhoA inhibitor. (b) Fold change of IgG isotypes between tissue and secretome. **(B)** Detection by Western blot of IgG chains in secretomes from rostral, caudal, and lesion segments collected 12 h after lesion and treatment with RhoA inhibitor.

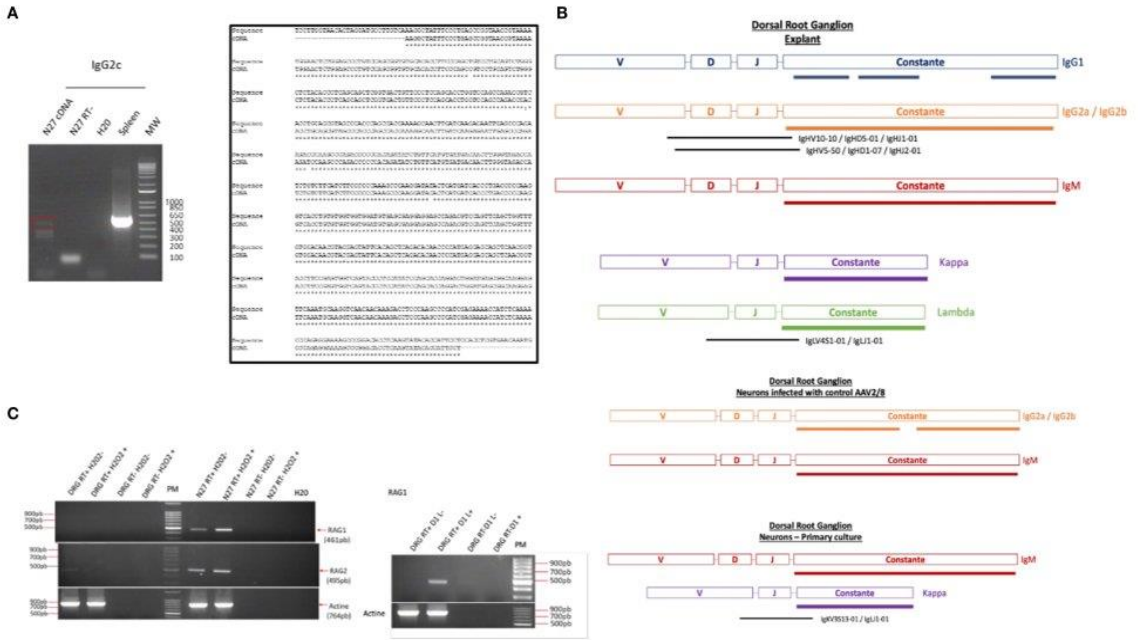

FIGURE 5 | **(A)** RT-PCR amplification of IgG2c in spleen and N27 cells was confirmed by sequencing. **(B)** Reads coding immunoglobulin constant heavy and light chains as well as variable parts were identified in DRG explant or DRG primary neurons by survey on RNaseq data B (**Supplementary Data 4** and **Supplementary Table S1**) **(C)** Amplification of *Rag1* and *Rag2* mRNA in DRG and N27 cells was carried out by RT-PCR in presence of H_2O_2 to induce neuronal death, as observed during the spinal cord injury. Since expression of RAG1 encoding gene was not observed under these conditions, DRG cells were cultivated in the presence of secretome of lesion segment from 1 day after SCI following by RT-PCR. As a control to exclude genomic DNA contamination, the experiment was also carried out on a negative reverse transcriptase sample (RT-), H_20, negative control.

intense for the control, LPS, RhoAi, and LPS+ RhoAi treatments, respectively (**Figure 7B**). This showed that the expression of CD16 was higher than CD32 under both basal and stimulated conditions. Since RhoAi modulated neurite outgrowth, synaptogenesis (12), and increased IgG release in the spinal cord as well as the expression of CD16 and CD32 in the sensory neurons (**Figures 7B, C**), we investigated the possibility that activation of these Fc receptors in DRG ND7/23 cells could modulate neurite outgrowth.

Antibody Dependent Neurite Outgrowth Modulation (ADNM) Responses

Before performing neurite outgrowth assays, we confirmed that unlike anti-CD16 (**Figure 6D**), anti-C32 did not stimulate intracellular calcium release (**Figure 7D**). To test the impact of CD16 and CD32b activation with their specific antibodies on neurite outgrowth, DRG sensory neurons were incubated with anti-CD16 and/or anti-CD32 in the presence of IgG2 isotype (**Figure 7E**). In comparison with the DMEM control condition, the percentage of neurite outgrowth was higher after CD16 activation while CD32b activation had no effect. Moreover, activation of both CD16 and CD32b also led to an increase of the percentage of neurite outgrowth. Keeping in mind that CD32b is known as the only inhibitory receptor of the FcγR family, this showed that CD16 activation could prevail and be sufficient to overcome a potential inhibitory effect exerted by CD32b. To test if CD32b could exert such an inhibitory effect on neurite outgrowth, a stronger activation of CD32b was triggered by the addition of a treatment with IgG2 isotype (**Figure 7E**). In its presence, we observed that whatever the conditions, the percentage of neurite outgrowth remained close to the one observed in control conditions with DMEM or IgG2 treatment. In comparison with CD16 activation combined with CD32b activation, the percentage of neurite outgrowth was significantly reduced when DRG cells were incubated in the presence of IgG2 isotype + anti-CD16 +/- anti-CD32. Therefore, the activation of CD32b by IgG2 isotype prevented CD16 from triggering neurite outgrowth. Altogether, these results suggest that various IgG according to their isotypes could modulate neurite outgrowth through the activation of CD16 and CD32b. We named this process antibody dependent neurite outgrowth modulation (ADNM) (**Figure 8**).

DISCUSSION

Autoimmune diseases affect about 5%–7% of the world population and 3% of these autoimmune diseases involve pathogenic CNS-reactive autoantibodies (34). Neural repertoires, defined as the whole

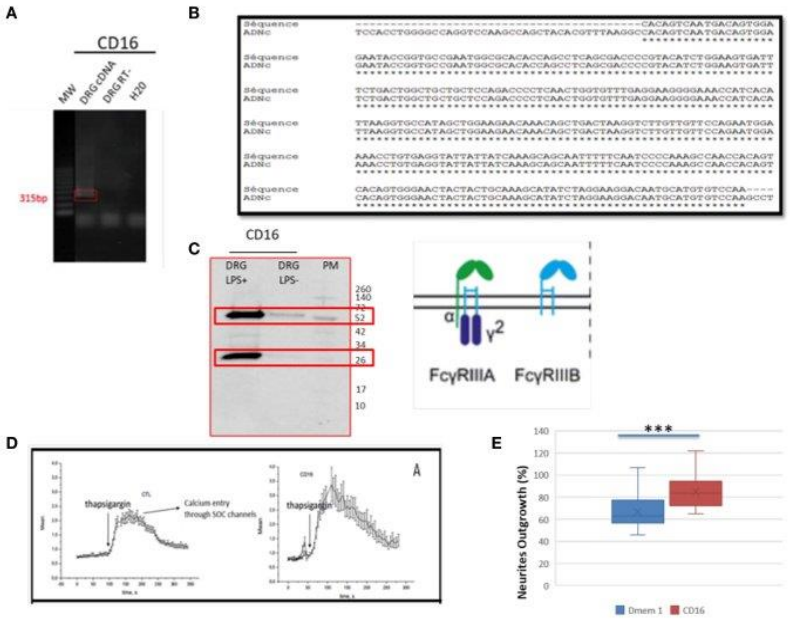

FIGURE 6 | Identification of FcγRIII receptors in sensory neurons. **(A)** RT-PCR amplification of *Cd16* mRNA. **(B)** Sequence alignment of the nucleic acid sequence. **(C)** Western blot analysis to detect CD16 in DRG cells treated with LPS. **(D)** CD16 activation by specific antibody in TG-activated SOCE conditions impacts Ca^{2+} homeostasis. Quantification of the results are presented in the left panel for the controls and in the right panel for CD16 activation. **(E)** Neurite outgrowth in DRG ND7/23 cells in the presence of anti-CD16 activating CD16. ***P value of < 0.001.

of neural populations and synaptic circuits supporting the cognitive and sensorimotor functional repertoires (35), express brain autoantigens such as myelin and synapse-derived proteins (glutamate decarboxylase (GAD2), acetylcholine receptor (AchR), and acetylcholine esterase (AchE)) (36). Interestingly, some brain autoantigens involved in major CNS functions are targeted in non-CNS autoimmune disorders. Such autoantigens, proposed to be named brain super autoantigens (35), notably include HSP60 and TROVE2, which are two major autoantigens in rheumatoid arthritis and lupus, respectively. HSP60 (*hspd1*) plays a major role in the control of synaptic neurotransmitter release and mutations in *hspd1* gene are responsible for autosomal recessive spastic paraplegia disease (37). Similarly, SNP variants of *trove2* gene (also knowns as RNA binding protein Ro60 autoantigen) have been associated with higher emotional memory capacity in healthy human subjects (36). It is thus thinkable that pathological autoimmunity in general is preferentially targeted toward brain autoantigens and reflects the distortion and/or the amplification of a physiological process in which autoimmunity supports cognition and CNS homeostasis (35). Favoring this view, in multiple sclerosis (MS) disease, a recent clinical study on 176 patients identified a large panel of autoantibodies recognizing more than 30 neuronal or glial autoantigens (38). Similarly, a number of neuropsychiatric disorders like autism spectrum disorder are accompanied by the synthesis of CNS-reactive antibodies (39). Independently from any consideration on their actual role, autoantibodies are thus emerging as a new generation of biomarkers in CNS disorders, ranging from neurotrauma to neuropsychiatric or neurodegenerative diseases (39). Interestingly, although brain-derived autoantigens might not be immunogenic under physiological conditions, several pathology-associated events might drive CNS-targeted autoimmunity. These notably comprise the occurrence of immunogenic post-translational modifications and the co-release by neural cells of brain autoantigens and danger signals. In TBI, autoantibodies are directed against a repertoire of CNS self-antigens (proteins) including GM1 gangliosides, myelin-associated glycoprotein, α-amino-3-hydroxy-5-methyl-4-isoxazolepropionic acid (AMPA), and N-methyl-D-aspartate (NMDA) glutamate receptors, and β-III-tubulin and nuclear antigens (34, 39–41). Moreover, immunocytochemistry studies performed with monoclonal antibodies as well as fragment antigen binding (Fabs) at the level of the CNS have shown the presence of immunoglobulin isotypes (IgG1, 2A, 2B, 2C), Kappa and Lambda chains (42, 43). In normal rat brain, IgG are detected, and this level reached a higher amount after head injury (44). *In situ* hybridization experiments depicted in mouse Brain Atlas also revealed the presence of such immunoglobulins encoding transcripts (IgG and IgM) in hippocampus, cortex, and spinal cord. Moreover, during spinal cord injury (SCI), traumatic brain injury (TBI) and a multitude of other CNS pathological conditions such as multiple sclerosis (MS), an intrathecal synthesis of IgGs is observed (45). The origin of such intra-CSF (cerebrospinal fluid) IgGs is still debated. The two main current hypotheses are that IgGs

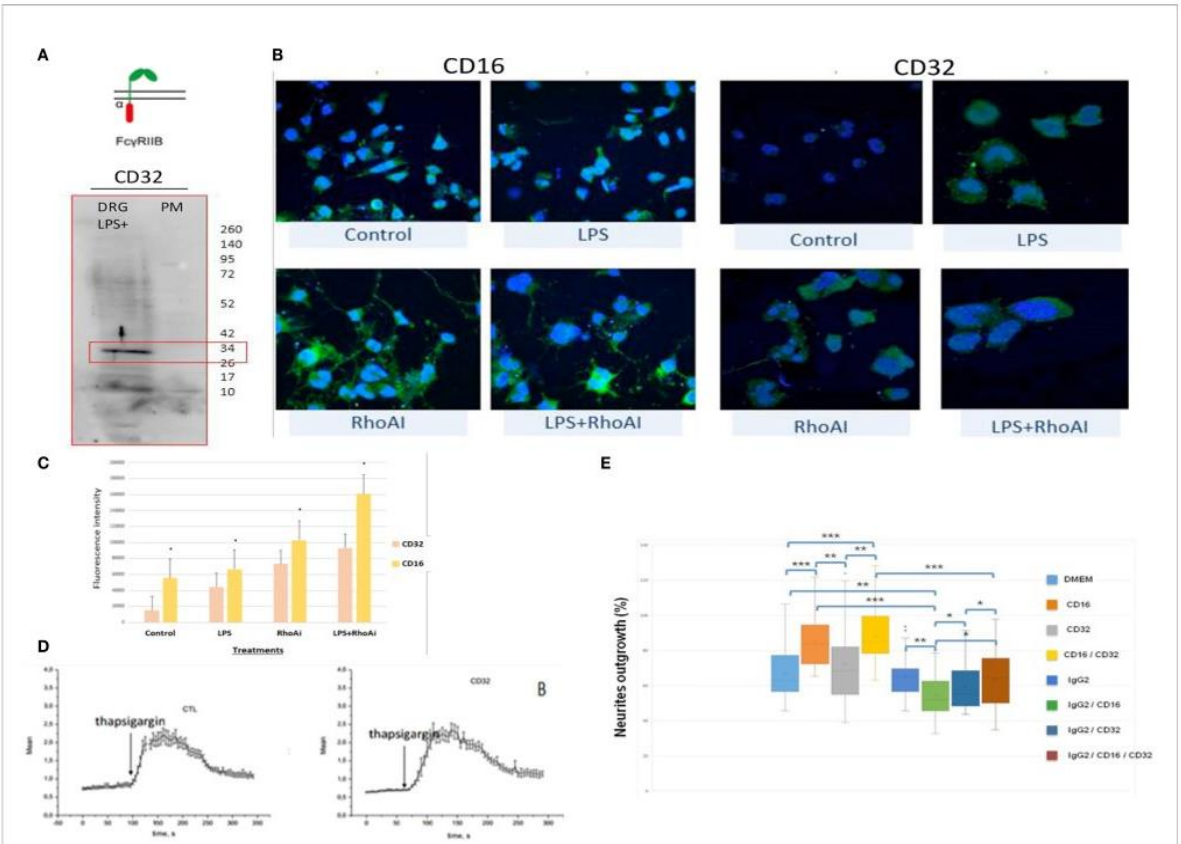

FIGURE 7 | FcγRIIB receptor identification in sensory neurons. **(A)** Western blot revealing CD32b receptor in DRG cells. **(B)** Immunofluorescence performed with anti-CD16 or anti-CD32 on DRG cells stimulated with LPS and/or RhoAi. Nuclei were counterstained with DAPI (blue). **(C)** Quantification of CD16 and CD32b immunofluorescence in DRG ND7/23 cells after RhoAi and/or LPS treatments. **(D)** CD32b activation by specific antibody in TG-activated SOCE conditions does not impact Ca^{2+} homeostasis. Quantification of the results are presented in the left panel for the controls and in the right panel for CD32 activation. **(E)** Neurites outgrowth in DRG ND7/23 cells in the presence of specific CD16 or CD32b activating antibody or CD16 and CD32b activating antibody with or without anti-GFAP. Mouse anti-GFAP displayed an IgG2 isotype and served as a control of Fc gamma receptors activation. *P value of < 0.05, **P value of < 0.01, ***P value of < 0.001.

are produced locally by CNS-invading B-cells or are somehow transported from blood to CNS. In several neuroinflammatory pathological disorders, including notably MS, a hallmark of intrathecal IgGs is to form oligoclonal bands (OCBs), which suggests a rather limited diversity of antibodies and, consequently, a finite number of corresponding targeted antigens. While MS pathology is essentially characterized by the existence of multifocal inflammatory and demyelinating lesions (the MS plaques), OCBs develop in the quasi-absence of B-cells in inflammatory lesions. Indeed, OCBs are considered the products of clonally expanded B cells in the cerebrospinal fluid (CSF), representing the sum of contributions from B cells in the brain. However, large amounts of IgGs can be eluted from MS plaques in which lymphocytes are absent. Interestingly, in a recent study analyzing CSF samples from 115 MS patients, it was calculated that 3.2 billion lymphocytes would be necessary to generate such large amounts of intrathecal IgG levels (30 mg in 500 ml CSF) (46). CSF-circulating lymphocytes were estimated to account for <0.1% of the IgG levels in MS brains. Such a finding is thus compatible with the possibility that intrathecal IgGs might not derive from intrathecal B-cells (46). Supporting this fact, the neuronal distributions of IgG are found in motor neurons in brainstem nuclei including trigeminal motor nucleus, facial nucleus, and hypoglossal nucleus (43) and confirmed recently by transcriptomics analyses in mice spinal neurons (26) as well as our immunofluorescence experiments (4) on rat spinal cord. The present study is in line with these results. Our proteomic data establish that IgG2A and IgG2B are present in the spinal cord in control and the level is similar in the time course of SCI. On the contrary, the protein related to IgM is only expressed 12 h to 24 h after lesion. This time window is not compatible with a B cell production since IgM are produced 7 to 10 days after antigen recognition. Accordingly, we demonstrated the expression of IgG2 isotypes encoding genes through RT-PCR experiments performed on CDNA from rat N27 dopaminergic neural cell line and data reuse of RNAseq datasets obtained from rat primary culture of DRG neurons. While a pathogenic role has been generally assigned to CNS

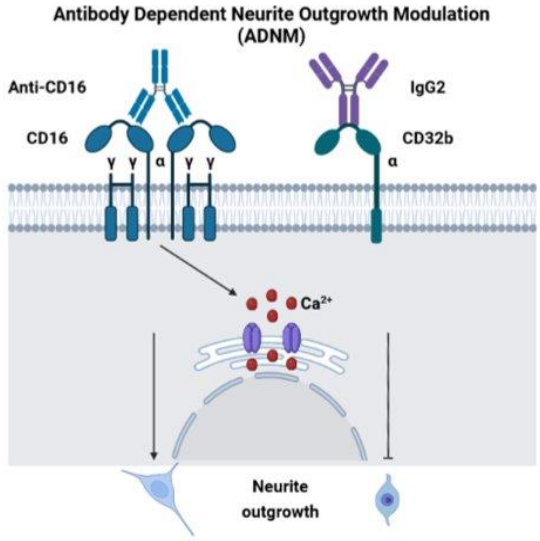

FIGURE 8 | Antibody dependent neurite outgrowth modulation (ADNM). CD16 activation with anti-CD16 induces calcium release from RE and triggers neurite outgrowth. On the contrary, C32b activation by IgG2 isotype prevents CD16 from triggering neurite outgrowth.

autoantibodies, a neuroprotective function of natural IgG autoantibodies has also been suggested. In this line, several studies have shown that binding of such antibodies to the surface of neurons through FCγR enhances remyelination and modulate neuronal apoptosis (47–52). Consistently, our results demonstrate that CD16 (FcγRIII) activation also modulates neurite outgrowth. Taken together, all these data show that autoantibodies have two sources of production, peripheric, that is, B-cells and central. However, our results suggest that these autoantibodies may not only be involved in immune responses like those of B-cells but may also modulate neurite outgrowth. In this context, the crosstalk play between CD16 and CD32b activation in neurite outgrowth process evoked an antibody dependent neurite outgrowth modulation (ADMN). This mechanism could be seen as a counterpart of the antibody dependent cell cytotoxicity (ADCC) observed during the inflammatory response and involving the same receptors. Indeed, while CD16 activation favors neurite outgrowth, CD32b activation inhibited it. The balance between activation and inhibition could be fine-tuned by the nature of the various IgG isotypes released after trauma as we observed during SCI. Moreover, we cannot also exclude that among the immunoglobulin released, some could be involved in inflammation since the VHH found at 12 h presents sequence homology with a nanobody directed against RON protein. RON is a macrophage-stimulating protein receptor and is related to c-MET receptor tyrosine kinase. In the brain RON is expressed on tissue-resident macrophages including microglia (53). An *in vivo* deletion of the ligand binding domain of Ron (Ron−/−) promotes inflammatory (M1) and limits a reparative (M2) macrophage activation. These results are in line with its expression found at 12 h at the lesion site (54). The possiblitiy that anti-RON could activate microglia 12 h after lesion also fits with previous data obtained on microglia activation studies (5). These results can also be correlated with previous studies performed by the Popovich group, which showed that mice lacking heavy chain of immunoglobulins (IgH-6 KO) have an improved locomotor function and reduced spinal pathology compared to wild-type mice after SCI, suggesting a pathogenic role for antibodies (40, 55). The intraspinal pathology caused by B cells in wild-type mice is due in part to antibody-mediated ligation of Fc receptors and complement activation. But even though intraspinal B cell clusters and autoantibodies are maintained indefinitely in injured mouse spinal cord, there is no proof that these immune responses cause protracted neurological deterioration. A precipitous decline in function would be registered in both mice as B cells became activated and autoantibodies were synthesized. B cells and autoantibodies would respond to proteins that are newly expressed in growing axons, remyelinating oligodendrocytes, stem cells, or new endothelia. In that case, little or no additional gain of function beyond that achieved prior to the onset of the autoimmune response would be expected, which is not the case. In fact, in animal models of SCI, spontaneous recovery of function is registered after a period of weeks or months post-injury. Taken together, results in wild-type animals tend to show that autoantibodies are not only involved in pro-inflammatory response but also in neuroregeneration. Unfortunately, the IgH-6 KO model fails to confirm this hypothesis because the invalidation blocks the two possible sources of IgG production in the same manner if the IgGs are synthesized by the same mechanism (VDJ recombination). All this evidence supports that IgGs and their receptors are involved in neurite outgrowth modulation. This interesting change of paradigm constitutes a ground-breaking advance in the field of both neuroscience and immunology. The story appears even more complex since CNS immunoglobulins seem to have various cellular origins. Indeed, the diversity of immunoglobulins identified during our study, that is, reuse of RNAseq datasets obtained from DRG explants and proteomics analysis performed on injured spinal cord, does not fit with the restricted number of IgG isotypes found in DRG sensory neurons. In line with such an assumption, our previous immunofluorescence experiment performed on injured spinal cord slices also revealed a staining in astrocytes (4, 12). A survey of "Geodatasets" (https://www.ncbi.nlm.nih.gov/gds/), the NIH-compiled bank of mRNA expression studies, focused specifically on the mRNA profile of spinal cord astrocytes under inflammatory conditions confirmed that astrocytes were a second source of neural IgGs. Indeed, we found one relevant study in which astrocytes derived from mice suffering from experimental allergic encephalomyelitis were cell-sorted at different time points and assessed about their RNA profiles. Surprisingly, when we reused the supplementary data provided in this work by Itoh and collaborators we found that the mRNA species showing the highest fold changes in EAE spinal astrocytes as compared to control spinal cord astrocytes were indeed mRNAs coding for IgG2c and kappa chains or junction chains (56) (**Supplementary Figure 4**). Now the challenge is to clarify the function of these CNS immunoglobulins.

DATA AVAILABILITY STATEMENT

The datasets used for analysis and the annotated MS/MS spectra were deposited at the ProteomeXchange Consortium (http://proteomecentral.proteomexchange.org) via the PRIDE partner repository with the dataset identifier PXD004639.

ETHICS STATEMENT

All studies on animals were reviewed and approved by the institutional committee for the protection of animals of the Slovak University of Science and conformed to the European Directive 2010/63 on the use of the animals for research purposes, as well as with the Slovak animal welfare laws Nos. 377/2012 and 436/2012.

AUTHOR CONTRIBUTIONS

Conceptualization, MS. Methodology, AC, M-AK, CM, SO, FA, FR, DC, IF, and MS; Software MS; Validation, M-AK, DC, and MS; Formal analysis, MS and DC. Investigation, DC and MS; Resources, DC, IF, and MS; Data curation, MS, AC, M-AK, and SO; Writing – Original Draft MS. Writing - Review and Editing, IF, FR, DD, DC, and MS; Supervision, FR, DC, and MS; Project Administration, DC and MS; Funding Acquisition, DC, IF, and MS. All authors contributed to the article and approved the submitted version.

FUNDING

This research was supported by funding from Ministère de l'Enseignement Supérieur, de la Recherche et de l'Innovation (MESRI), Institut National de la Santé et de la Recherche Médicale (Inserm), I-SITE ULNE (Nobody Project), and Université de Lille. The authors would like to thank Raphaël Decaudin for his contribution to this manuscript.

SUPPLEMENTARY MATERIAL

The Supplementary Material for this article can be found online at: https://www.frontiersin.org/articles/10.3389/fimmu.2022.882830/full#supplementary-material

Supplementary Table 1 | Sequence read archive data from rat dorsal root ganglion explant and primary culture of DRG neurons revealed the expression of genes coding immunoglobulin heavy and light chains as well as cluster of differentiation markers.

Supplementary Figure 1 | (A) *IgG3*, **(B)** *IgH-Vs107*, **(C)** *Cd32b*, and **(D)** *CdD16* mRNA expression in the hippocampus and in the cerebellum of mice according to the Allen Brain Atlas, mRNA expression.

Supplementary Figure 2 | (A) *IgG3* mRNA expression in the spinal cord; **(B)** of mice according to the Allen Brain Atlas, mRNA expression.

Supplementary Figure 3 | Heatmap illustrating hierarchical clustering obtained after analysis of digested peptides isolated from rostral, caudal, and lesion segments collected 12 h after lesion and treatment with RhoA inhibitor. Cluster 1 corresponds to the inflammatory proteins and immunoglobulins. Cluster 2 contains proteins involved in synaptogenesis, and Cluster 3 proteins are involved in neurite outgrowth.

Supplementary Figure 4 | Rodent mRNA species after NGS sequencing showing the highest fold changes in EAE spinal astrocytes as compared to control spinal cord astrocytes *IgHa*, *Ig Kappa c*, *J Chain*, and *Cd32b* mRNA have been identified in astrocytes from the spinal cord and the cortex.

REFERENCES

1. Wyndaele M, Wyndaele JJ. Incidence, Prevalence and Epidemiology of Spinal Cord Injury: What Learns a Worldwide Literature Survey? *Spinal Cord* (2006) 44:523–9. doi: 10.1038/sj.sc.3101893
2. Chen Y, Tang Y, Vogel LC, Devivo MJ. Causes of Spinal Cord Injury. *Top Spinal Cord Inj Rehabil* (2013) 19:1–8. doi: 10.1310/sci1901-1
3. Cizkova D, Murgoci AN, Kresakova L, Vdoviakova K, Cizek M, Smolek T, et al. *Understanding Molecular Pathology Along Injured Spinal Cord Axis: Moving Frontiers Toward Effective Neuroprotection and Regeneration*. United-Kingdom: IntechOpen (2017).
4. Devaux S, Cizkova D, Quanico J, Franck J, Nataf S, Pays L, et al. Proteomic Analysis of the Spatio-Temporal Based Molecular Kinetics of Acute Spinal Cord Injury Identifies a Time- and Segment-Specific Window for Effective Tissue Repair. *Mol Cell Proteomics MCP* (2016) 15:2641–70. doi: 10.1074/mcp.M115.057794
5. Cizkova D, Le Marrec-Croq F, Franck J, Slovinska L, Grulova I, Devaux S, et al. Alterations of Protein Composition Along the Rostro-Caudal Axis After Spinal Cord Injury: Proteomic. *Vitro Vivo analyses. Front Cell Neurosci* (2014) 8:105. doi: 10.3389/fncel.2014.00105
6. Freund P, Schmidlin E, Wannier T, Bloch J, Mir A, Schwab ME, et al. Nogo-A-Specific Antibody Treatment Enhances Sprouting and Functional Recovery After Cervical Lesion in Adult Primates. *Nat Med* (2006) 12:790–2. doi: 10.1038/nm1436
7. Freund P, Schmidlin E, Wannier T, Bloch J, Mir A, Schwab ME, et al. Anti-Nogo-A Antibody Treatment Promotes Recovery of Manual Dexterity After Unilateral Cervical Lesion in Adult Primates–Re-Examination and Extension of Behavioral Data. *Eur J Neurosci* (2009) 29:983–96. doi: 10.1111/j.1460-9568.2009.06642.x
8. DePaul MA, Lin CY, Silver J, Lee YS. Combinatory Repair Strategy to Promote Axon Regeneration and Functional Recovery After Chronic Spinal Cord Injury. *Sci Rep* (2017) 7:9018. doi: 10.1038/s41598-017-09432-6
9. Ulndreaj A, Badner A, Fehlings MG. Promising Neuroprotective Strategies for Traumatic Spinal Cord Injury With a Focus on the Differential Effects Among Anatomical Levels of Injury. *F1000Res* (2017) 6:1907. doi: 10.12688/f1000research.11633.1
10. Thibault-Halman G, Rivers CS, Bailey CS, Tsai EC, Drew B, Noonan VK, et al. Predicting Recruitment Feasibility for Acute Spinal Cord Injury Clinical Trials in Canada Using National Registry Data. *J neurotrauma* (2017) 34:599–606. doi: 10.1089/neu.2016.4568
11. Fehlings MG, Wilson JR, Frankowski RF, Toups EG, Aarabi B, Harrop JS, et al. Riluzole for the Treatment of Acute Traumatic Spinal Cord Injury: Rationale for and Design of the NACTN Phase I Clinical Trial. *J Neurosurg Spine* (2012) 17:151–6. doi: 10.3171/2012.4.AOSPINE1259
12. Devaux S, Cizkova D, Mallah K, Karnoub MA, Laouby Z, Kobeissy F, et al. RhoA Inhibitor Treatment At Acute Phase of Spinal Cord Injury May Induce Neurite Outgrowth and Synaptogenesis. *Mol Cell Proteomics MCP* (2017) 16:1394–415. doi: 10.1074/mcp.M116.064881
13. Nguyen VK, Su C, Muyldermans S, van der Loo W. Heavy-Chain Antibodies in Camelidae; a Case of Evolutionary Innovation. *Immunogenetics* (2002) 54:39–47. doi: 10.1007/s00251-002-0433-0
14. Leslie M. Small But Mighty. *Science* (2018) 360:594–7. doi: 10.1126/science.360.6389.594

15. Flajnik MF, Deschacht N. Muyldermans S. A Case of Convergence: Why did a Simple Alternative to Canonical Antibodies Arise in Sharks and Camels? *PloS Biol* (2011) 9:e1001120. doi: 10.1371/journal.pbio.1001120
16. Conrath KE, Wernery U, Muyldermans S, Nguyen VK. Emergence and Evolution of Functional Heavy-Chain Antibodies in Camelidae. *Dev Comp Immunol* (2003) 27:87–103. doi: 10.1016/S0145-305X(02)00071-X
17. Murphy K, Weaver C. Janeway's Immunobiology. *Garland Sci* (2016) 9:1–855. doi: 10.1201/9781315533247
18. Fuller JP, Stavenhagen JB, Teeling JL. New Roles for Fc Receptors in Neurodegeneration-the Impact on Immunotherapy for Alzheimer's Disease. *Front Neurosci* (2014) 8:235. doi: 10.3389/fnins.2014.00235
19. Nirmalan NJ, Harnden P, Selby PJ, Banks RE. Development and Validation of a Novel Protein Extraction Methodology for Quantitation of Protein Expression in Formalin-Fixed Paraffin-Embedded Tissues Using Western Blotting. *J Pathol* (2009) 217:497–506. doi: 10.1002/path.2504
20. Nemeth-Cawley JF, Tangarone BS, Rouse JC. "Top Down" Characterization is a Complementary Technique to Peptide Sequencing for Identifying Protein Species in Complex Mixtures. *J Proteome Res* (2003) 2:495–505. doi: 10.1021/pr034008u
21. Fornelli L, Ayoub D, Aizikov K, Liu X, Damoc E, Pevzner PA, et al. Top-Down Analysis of Immunoglobulin G Isotypes 1 and 2 With Electron Transfer Dissociation on a High-Field Orbitrap Mass Spectrometer. *J Proteomics* (2017) 159:67–76. doi: 10.1016/j.jprot.2017.02.013
22. Prądzińska M, Behrendt I, Spodzieja M, Kołodziejczyk AS, Rodziewicz-Motowidło S, Szymańska A, et al. Isolation and Characterization of Autoantibodies Against Human Cystatin C. *Amino Acids* (2016) 48:2501–18. doi: 10.1007/s00726-016-2271-7
23. Konno N, Sugimoto M, Takagi T, Furuya M, Asano T, Sato S, et al. Changes in N-Glycans of IgG4 and its Relationship With the Existence of Hypocomplementemia and Individual Organ Involvement in Patients With IgG4-Related Disease. *PloS One* (2018) 13:e0196163. doi: 10.1371/journal.pone.0196163
24. Mills JR, Barnidge DR, Murray DL. Detecting Monoclonal Immunoglobulins in Human Serum Using Mass Spectrometry. *Methods* (2015) 81:56–65. doi: 10.1016/j.ymeth.2015.04.020
25. Blanc MR, Anouassi A, Ahmed Abed M, Tsikis G, Canepa S, Labas V, et al. A One-Step Exclusion-Binding Procedure for the Purification of Functional Heavy-Chain and Mammalian-Type γ-Globulins From Camelid Sera. *Biotechnol Appl Biochem* (2009) 54:207–12. doi: 10.1042/BA20090208
26. Scheurer L, Das Gupta RR, Saebisch A, Grampp T, Benke D, Zeilhofer HU, et al. Expression of Immunoglobulin Constant Domain Genes in Neurons of the Mouse Central Nervous System. *Life Sci alliance* (2021) 4:1–9. doi: 10.26508/lsa.202101154
27. Maness PF, Schachner M. Neural Recognition Molecules of the Immunoglobulin Superfamily: Signaling Transducers of Axon Guidance and Neuronal Migration. *Nat Neurosci* (2007) 10:19–26. doi: 10.1038/nn1827
28. Whittemore E, Loo D, Watt J, Cotmans C. A Detailed Analysis of Hydrogen Peroxide-Induced Cell Death in Primary Neuronal Culture. *Neuroscience* (1995) 67:921–32. doi: 10.1016/0306-4522(95)00108-U
29. Aicheler RJ, Wang EC, Tomasec P, Wilkinson GW, Stanton RJ. Potential for Natural Killer Cell-Mediated Antibody-Dependent Cellular Cytotoxicity for Control of Human Cytomegalovirus. *Antibodies* (2013) 2:617–35. doi: 10.3390/antib2040617
30. Ulvestad E, Williams K, Vedeler C, Antel J, Nyland H, Mørk S, et al. Reactive Microglia in Multiple Sclerosis Lesions Have an Increased Expression of Receptors for the Fc Part of IgG. *J Neurol Sci* (1994) 121:125–31. doi: 10.1016/0022-510X(94)90340-9
31. Zhang J, Niu N, Li B, McNutt MA. Neuron-Derived IgG Protects Neurons From Complement-Dependent Cytotoxicity. *J Histochem Cytochem* (2013) 61:869–79. doi: 10.1369/0022155413504196
32. Lajoie L, Congy-Jolivet N, Bolzec A, Gouilleux-Gruart V, Sicard E, Sung HC, et al. ADAM17-Mediated Shedding of FcγRiiia on Human NK Cells: Identification of the Cleavage Site and Relationship With Activation. *J Immunol* (2014) 192:741–51. doi: 10.4049/jimmunol.1301024
33. Nimmerjahn F, Ravetch JV. Fcgamma Receptors: Old Friends and New Family Members. *Immunity* (2006) 24:19–28. doi: 10.1016/j.immuni.2005.11.010
34. Diamond B, Honig G, Mader S, Brimberg L, Volpe B. Brain-Reactive Antibodies and Disease. *Annu Rev Immunol* (2013) 31:345–85. doi: 10.1146/annurev-immunol-020711-075041
35. Nataf S. Autoimmunity as a Driving Force of Cognitive Evolution. *Front Neurosci* (2017) 11:582. doi: 10.3389/fnins.2017.00582
36. Nataf S. Evolution, Immunity and the Emergence of Brain Superautoantigens. *F1000Res* (2017) 6:171. doi: 10.12688/f1000research.10950.1
37. Hansen J, Svenstrup K, Ang D, Nielsen MN, Christensen JH, Gregersen N, et al. A Novel Mutation in the HSPD1 Gene in a Patient With Hereditary Spastic Paraplegia. *J Neurol* (2007) 254:897–900. doi: 10.1007/s00415-006-0470-y
38. Prineas JW, Parratt JDE. Multiple Sclerosis: Serum Anti-CNS Autoantibodies. *Mult Scler* (2017) 24(5):1352458517706037. doi: 10.1177/1352458517706037
39. Kobeissy F, Moshourab RA. Autoantibodies in CNS Trauma and Neuropsychiatric Disorders: A New Generation of Biomarkers. *In: Brain Neurotrauma: Molecular Neuropsychological Rehabil Aspects (ed Kobeissy FH)* (2015). 29:1–47.
40. Ankeny DP, Guan Z, Popovich PG. B Cells Produce Pathogenic Antibodies and Impair Recovery After Spinal Cord Injury in Mice. *J Clin Invest* (2009) 119:2990–9. doi: 10.1172/JCI39780
41. Poletaev A, Boura P. The Immune System, Natural Autoantibodies and General Homeostasis in Health and Disease. *Hippokratia* (2011) 15:295.
42. Kozlowski GP, Sterzl I, Nilaver G. Localization Patterns for Immunoglobulins and Albumins in the Brain Suggest Diverse Mechanisms for Their Transport Across the Blood-Brain Barrier (BBB). *Prog Brain Res* (1992) 91:149–54. doi: 10.1016/S0079-6123(08)62329-8
43. Aihara N, Tanno H, Hall JJ, Pitts LH, Noble LJ. Immunocytochemical Localization of Immunoglobulins in the Rat Brain: Relationship to the Blood-Brain Barrier. *J Comp Neurol* (1994) 342:481–96. doi: 10.1002/cne.903420402
44. Tanno H, Nockels RP, Pitts LH, Noble LJ. Breakdown of the Blood-Brain Barrier After Fluid Percussive Brain Injury in the Rat. Part 1: Distribution and Time Course of Protein Extravasation. *J neurotrauma* (1992) 9:21–32. doi: 10.1089/neu.1992.9.21
45. Kobeissy F, Moshourab RA. Autoantibodies in CNS Trauma and Neuropsychiatric Disorders. In: *Brain Neurotrauma: Molecular, Neuropsychological, and Rehabilitation Aspects* (ed Kobeissy FH) (2015) Chapter 29:1–47.
46. Beseler C, Vollmer T, Graner M, Yu X. The Complex Relationship Between Oligoclonal Bands, Lymphocytes in the Cerebrospinal Fluid, and Immunoglobulin G Antibodies in Multiple Sclerosis: Indication of Serum Contribution. *PloS One* (2017) 12:e0186842. doi: 10.1371/journal.pone.0186842
47. Wootla B, Denic A, Watzlawik JO, Warrington AE, Rodriguez M. Antibody-Mediated Oligodendrocyte Remyelination Promotes Axon Health in Progressive Demyelinating Disease. *Mol Neurobiol* (2016) 53:5217–28. doi: 10.1007/s12035-015-9436-3
48. Bieber AJ, Warrington A, Pease LR, Rodriguez M. Humoral Autoimmunity as a Mediator of CNS Repair. *Trends Neurosci* (2001) 24:S39–44. doi: 10.1016/S0166-2236(01)00007-8
49. Mitsunaga Y, Ciric B, Van Keulen V, Warrington AE, Paz Soldan M, Bieber AJ, et al. Direct Evidence That a Human Antibody Derived From Patient Serum can Promote Myelin Repair in a Mouse Model of Chronic-Progressive Demyelinating Disease. *FASEB J* (2002) 16:1325–7. doi: 10.1096/fj.01-0994fje
50. Vargas ME, Watanabe J, Singh SJ, Robinson WH, Barres BA. Endogenous Antibodies Promote Rapid Myelin Clearance and Effective Axon Regeneration After Nerve Injury. *Proc Natl Acad Sci* (2010) 107:11993–8. doi: 10.1073/pnas.1001948107
51. Wright BR, Warrington AE, Edberg DE, Rodriguez M. Cellular Mechanisms of Central Nervous System Repair by Natural Autoreactive Monoclonal Antibodies. *Arch Neurol* (2009) 66:1456–9. doi: 10.1001/archneurol.2009.262
52. Schwartz M. "Tissue-Repairing" Blood-Derived Macrophages are Essential for Healing of the Injured Spinal Cord: From Skin-Activated Macrophages to Infiltrating Blood-Derived Cells? *Brain Behav Immun* (2010) 24:1054–7. doi: 10.1016/j.bbi.2010.01.010
53. Dey A, Allen JN, Fraser JW, Snyder LM, Tian Y, Zhang L, et al. Neuroprotective Role of the Ron Receptor Tyrosine Kinase Underlying Central Nervous System Inflammation in Health and Disease. *Front Immunol* (2018) 9:513. doi: 10.3389/fimmu.2018.00513
54. Cizkova D, Devaux S, Le Marrec-Croq F, Franck J, Slovinska L, Blasko J, et al. Modulation Properties of Factors Released by Bone Marrow Stromal Cells on Activated Microglia: an. *Vitro study Sci Rep* (2014) 4:7514. doi: 10.1038/srep07514

55. Ankeny DP, Popovich PG. B Cells and Autoantibodies: Complex Roles in CNS Injury. *Trends Immunol* (2010) 31:332–8. doi: 10.1016/j.it.2010.06.006
56. Itoh N, Itoh Y, Tassoni A, Ren E, Kaito M, Ohno A, et al. Cell-Specific and Region-Specific Transcriptomics in the Multiple Sclerosis Model: Focus on Astrocytes. *Proc Natl Acad Sci* (2018) 115:E302–9. doi: 10.1073/pnas.1716032115

Conflict of Interest: The authors declare that the research was conducted in the absence of any commercial or financial relationships that could be construed as a potential conflict of interest.

Publisher's Note: All claims expressed in this article are solely those of the authors and do not necessarily represent those of their affiliated organizations, or those of the publisher, the editors and the reviewers. Any product that may be evaluated in this article, or claim that may be made by its manufacturer, is not guaranteed or endorsed by the publisher.

Conclusion

Ces recherches ont permis de mettre en évidence la présence de différents sous-types d'IgG au cours d'une lésion de la moelle épinière. De façon surprenante, ces Igs ont été observées alors que la moelle épinière a été préalablement traitée avec un anti-CD20 induisant l'apoptose des lymphocytes B. Dans ces conditions, nous avons observé que l'IgG2C est l'isotype préférentiellement retrouvé et sa sécrétion est favorisée par le traitement avec l'inhibiteur de la voie RhoA. L'ensemble de ces résultats suggère une autre source productrice d'anticorps que les lymphocytes B. À la suite d'expériences d'immunofluorescence révélant un marquage des IgG dans le cytoplasme et la membrane plasmique dans les neurones, des recherches ont été entreprises sur deux lignées neurales. Ainsi, nous avons pu montrer l'expression de la chaîne lourde d'IgG2C dans une lignée neurale dopaminergique N27 non différenciée. De plus, une méta-analyse de type BLAST sur des banques de RNAseq réalisées sur des neurones sensoriels DRG a montré l'expression des gènes codant les chaînes lourdes IgG et IgM ainsi que les chaînes légères Kappa et Lambda. Lors de ce travail, nous avons aussi démontré que ces IgG moduleraient la croissance des neurites via l'activation des récepteurs CD16 et CD32b. Ce processus, que nous avons nommé « Antibody Dependent Neurite Outgrowth Modulation », serait impliqué lors de la lésion de la moelle épinière afin de moduler la repousse neuritique.

En prenant en compte les connaissances déjà obtenues sur la lésion, il est possible que l'abondance relative de chaque isotype ainsi sécrété au cours du temps conditionne la repousse ou non des neurites. En effet, lors d'études précédentes réalisées par le laboratoire, il a été montré qu'au niveau de la lésion, une modification du contenu protéique survenait conduisant au passage d'un profil favorable à la neuritogenèse vers un profil pro-inflammatoire défavorable. Comme nous savons que les isotypes ont des affinités différentes pour les récepteurs FcR, il est possible qu'un isotype soit exprimé spécifiquement dans le but de favoriser ou non la croissance neuritique. La possibilité de conserver l'isotype IgG1 favoriserait la repousse neuritique. Le laboratoire a développé une stratégie thérapeutique via l'utilisation d'un biomatériau, l'alginate dans lequel a été greffé des facteurs de croissance et des exosomes de cellules souches de la moelle osseuse (Devaux et *al.,* 2017; Cizkova et *al.,* 2018, 2020). Des résultats prometteurs ont été obtenus non seulement chez le rat mais aussi chez le chien (Cizkova *et al.,* 2020; Vikartovska *et al.,* 2020). Nos résultats pourront servir à

compléter ce biomatériau afin de faire un pont neurologique permettant de refaire basculer plus précocement le segment caudal vers un profil neurogénique.

Chapitre 2 : Les astrocytes synthétisent des immunoglobulines aberrantes : La fin du dogme stipulant que les lymphocytes B sont la seule source d'immunoglobulines.

Introduction

Lors d'une LME, les astrocytes s'activent et prolifèrent dans le but de former une cicatrice gliale tout autour du site lésionnel. Cependant, bien que cette barrière physique permette de limiter l'étendue de la lésion aux régions avoisinantes, celle-ci empêche la régénération axonale et donc la récupération fonctionnelle et sensorielle de la moelle épinière. Le laboratoire PRISM a mis en évidence que les astrocytes étaient attirés par les cellules microgliales lors de la LME. En effet, celles-ci produisent des médiateurs lipidiques tels que les acylcarnithines (Quanico et *al.,* 2018, Mallah et *al.,* 2021). Le dialogue cellules microgliales et astrocytes conduit ces derniers à exprimer un phénotype de type A2 en produisant des facteurs activant la gliogenése (Mallah et *al.,*2021). Étant donné le rôle important des astrocytes dans la LME et le fait que nous ayons montré l'expression d'Igs au sein des neurones sensoriels. Cependant, la grande diversité des isotypes identifiés dans le sécrétome de la LME n'est pas cohérent par une production unique par les neurones. Une autre source cellulaire pourrait donc produire ces isotypes. Lors d'études réalisées sur la LME à la suite d'un traitement avec l'anti-CD20, nous avons mis en évidence un immunomarquage au sein des astrocytes (Devaux et *al*. ,2016). Nous avons donc émis l'hypothèse que les astrocytes pourraient également produire des Igs.

Objectifs

L'objectif de ce travail a tout d'abord été d'identifier le répertoire d'immunoglobulines généré par les astrocytes de rat, de caractériser intégralement leurs transcrits, d'identifier leurs cibles et rechercher leurs fonctions.

Résultats

Pour réaliser ce travail, des études multi-omiques ont été entreprises en utilisant la lignée d'astrocytes de rat DI TNC1 et des cultures primaires d'astrocytes isolées de moelles épinières et de cortex de rats âgés de 3 jours. Les résultats obtenus démontrent que ces cellules

produisent des parties variables ainsi que les parties constantes des chaînes lourdes IgG et IgM, les légères Kappa et Lambda sous forme libre. La machinerie de la recombinaison V(D)J complète permettant de générer la diversité des Igs a également été mis en évidence. Parmi l'ensemble des isotypes retrouvés, la partie constante de la chaîne lourde IgG2B est retrouvée de façon constitutive tant sous sa forme membranaire que sécrétée. Il en est de même de la partie constante de la chaîne légère kappa. Par ailleurs, la caractérisation de la séquence complète des transcrits par RACE-PCR révèle qu'à l'inverse de ce qui est observé dans les lymphocytes B, les chaînes constantes de ces Igs sont synthétisées de façon libre sans être associées à une partie variable. Les Igs astrocytaires sont donc produites sous des formes tronquées semblables à celles des Igs dérivées des cellules cancéreuses (Hu *et al.,* 2011). En effet, le messager codant la partie constante de la chaîne lourde IgG2B ne présente pas de séquence codant une partie variable à son extrémité 5', mais une séquence Kozak localisée directement en amont de l'exon codant le domaine CH1. De façon similaire, le transcrit codant la partie constante de la chaîne légère Kappa ne possède qu'une séquence RSS et un exon J au niveau de son extrémité 5'. De même, les transcrits codant les parties variables synthétisées dans les astrocytes contiennent les séquences codant la séquence Leader mais ne présentent pas les exons codant pour les régions D et J. Afin de confirmer la fonctionnalité de la séquence Kozak identifiée dans le messager *Igg2b*, la surexpression de celle-ci a été entreprise dans les astrocytes. Les expériences d'immunofluorescence réalisées confirment sa synthèse et mettent en évidence sa localisation au niveau de la membrane de vésicules intracellulaires. La caractérisation de l'interactome proximal par BioID de cette IgG2B suggère que l'IgG2B est : (i) N-glycosylée par le complexe OST ; (ii) adressée à la membrane plasmique par des vésicules contenant le complexe ATPase ; et (iii) ; se comporte partiellement comme SLC3A2 (CD98hc) par son association avec LAT1 et sa capacité à recruter ILKAP qui régule potentiellement les voies de signalisation en aval. Il sera particulièrement intéressant d'étudier si l'interaction proximale IgG2B - LAT1 se produit de manière concomitante avec TMEM57 et C2CD2L, au cœur d'une plateforme de signalisation cellulaire potentiellement nouvelle. Il est également à noter que TMEM57 (MACO-1) est connue chez C. elegans pour être impliquée différentes fonctions neuronales. En effet, cette protéine régulait l'oubli de l'adaptation olfactive à l'alcool isoamylique, qui est un odorant attractif perçu par différents types de neurones sensoriels (Arellano-Carbajal *et al.,* 2011; Kitazono *et al.,* 2017). Chez l'homme, MACO-1 est exprimé au sein des progéniteurs neuronaux en particulier lors de la

consolidation de la mémoire au sein de l'hippocampe (Poplawski, 2014). Afin de préciser la fonction de cette IgG2B, l'invalidation de son gène dans les astrocytes a été réalisée par CRISPR-Cas9. Les résultats obtenus montrent que l'inhibition de cette chaîne lourde conduit à la dédifférenciation des cellules astrocytaires en cellules progénitrices neurales via une activation de la voie BMP/YAP1/TEAD3. Cependant, sa surexpression renforce les voies impliquées dans la gliogenèse via une signalisation CRTC1-CREB-BDNF et oriente vers un profil pro-inflammatoire. La protéine YAP (yes-associated protein) est un cofacteur transcriptionnel clé qui est régulé négativement par la voie Hippo. Cependant, son rôle dans le cerveau n'est pas clair. YAP semble réguler la différenciation et la prolifération des astrocytes néocorticaux. YAP est indétectable dans les neurones mais sélectivement exprimée dans les cellules souches neurales (CSN) et les astrocytes. Dans les NSC, cette protéine est nécessaire à la différenciation astrocytaire néocorticale, sans rôle apparent dans l'auto-renouvellement ou la différenciation neuronale. Cependant, YAP dans les astrocytes est nécessaire pour la prolifération astrocytaire. Les souris knockout (KO) Yap (Yap1), knockout conditionnel Yap-nestin et knockout conditionnel Yap-GFAP présentent moins d'astrocytes néocorticaux et une prolifération astrocytaire altérée et par conséquent, la mort des neurones néocorticaux (Huang *et al.,* 2016). D'un point de vue mécanique, YAP est activé par BMP2 et YAP actif/nucléaire est crucial pour l'induction et la stabilisation de SMAD1 par BMP2 et la différenciation astrocytaire. La voie BMP2-YAP-SMAD1 sous-tend la différenciation astrocytaire dans le néocortex de la souris en développement. Dans notre étude, cette voie est activée lors de l'inhibition de la partie constante de la chaine lourde d'IgG2B. De plus, nos expériences d'électrophorèse bidimensionnelles couplées à des immuno-blots ont révélé que ces Igs astrocytaires reconnaissent des antigènes particuliers tels que les filaments intermédiaires et la protéase sérine 1 (PRSS1). Ces derniers seraient impliqués dans le développement des astrocytes et dans la conversion astrocytes - cellules souches neurales (Staflin et *al.,* 2009). L'ensemble de ces résultats montre que l'IgG2Bsynthétisée sous forme aberrante est impliquée dans la conservation de l'identité des astrocytes et que son inhibition conduit à la conversion vers un phénotype de cellules souches neurales. Ceci établit également la fin du dogme stipulant que les lymphocytes B sont la seule source d'immunoglobulines.

Astrocytes express aberrant immunoglobulins

involved as gatekeeper of astrocytes to neuronal progenitor conversion

Alice Capuz[1*], Sylvain Osien[1*], Mélodie Anne Karnoub[1], Soulaimane aboulouard[1], Estelle Laurent[1], Etienne Coyaud[1], Antonella Raffo-Romero[1], Marie Duhamel[1], Amélie Bonnefond[2], Mehdi Derhourhi[2], Marco Trerotola[3], Ikram El Yazidi-Belkoura[4], David Devos[5], Monika Zilkova[6], Firas Kobeissy[7], Fabien Vanden Abeele[8], Isabelle Fournier[1,9], Dasa Cizkova[1,6,10], Franck Rodet[1**], Michel Salzet[1,9**]

[1]Univ. Lille, Inserm, U-1192 - Laboratoire Protéomique, Réponse Inflammatoire et Spectrométrie de Masse-PRISM, F-59000 Lille, France

[2]Univ. Lille, Inserm UMR1283, CNRS UMR8199, European Genomic Institute for Diabetes (EGID), Institut Pasteur de Lille, CHU de Lille, 1 place de Verdun, 59000 Lille, France.

[3]Laboratory of Cancer Pathology, Center for Advanced Studies and Technology (CAST), University 'G. D'Annunzio', Chieti, Italy; Department of Medical, Oral and Biotechnological Sciences, University 'G. d'Annunzio', Chieti, Italy.

[4]Université de Lille, CNRS, UMR 8576 - UGSF - Unité de Glycobiologie Structurale et Fonctionnelle, F-59000, Lille, France.

[4]Université de Lille, INSERM, U1172, CHU-Lille, Lille Neuroscience Cognition Research Centre, 1 place de Verdun, 59000, Lille, France.

[6]Institute of Neuroimmunology, Slovak Academy of Sciences, Dúbravská cesta 9, 845 10 Bratislava, Slovakia

[7]Department of Biochemistry and Molecular Genetics, Faculty of Medicine, American University of Beirut. Lebanon.

[8]Université de Lille, INSERM U1003, Laboratory of Cell Physiology, 59650 Villeneuve d'Ascq, France.

[9]Institut Universitaire de France, 75005 Paris.

[10]Centre for Experimental and Clinical Regenerative Medicine, University of Veterinary Medicine and Pharmacy in Kosice, Kosice, Slovakia

***Authors contributed equally to the work.**

**** Co-Last and Co-Corresponding author**: Pr. Michel Salzet, [1]Univ. Lille, INSERM, U1192 - Laboratoire Protéomique, Réponse Inflammatoire et Spectrométrie de Masse-PRISM, F-59000 Lille, France, email: Michel.salzet@univ-lille1.fr Tel.: +33-320-4194; Fax: +33-320-4354. Franck Rodet ([1]Univ. Lille, INSERM, U1192 - Laboratoire Protéomique, Réponse Inflammatoire et Spectrométrie de Masse-PRISM, F-59000 Lille, France, email : Franck.rodet@univ-lille.fr

Abstract

Using multi-omics analyses including RNAseq, RT-PCR, RACE-PCR, and shotgun proteomic with enrichment strategies, we demonstrated that newborn rat astrocytes produce neural immunoglobulin constant and variable heavy chains as well as light chains. However, their edification is different from the ones found in B cells and resembles to aberrant immunoglobulins as observed in several cancers. Moreover, the complete enzymatic V(D)J recombination complex has also been identified in astrocytes. In addition, the constant heavy chain is also present in astrocytes adult rats, whereas in primary astrocytes from human fetal astrocytes we identified constant and variable kappa chains as well as the substitution lambda chains known to be involved in pre-B cells. To gather insights into the function of these neural IgG, CRISPR-Cas9 IgG2B constant heavy chain (IgH6), overexpression, proximal labeling of rat astrocytes IgH6 and targets identification though 2D gels were performed. In CRISPR-Cas9 IgG2B KO, over-expression of factors involved in hematopoietic cells, neural stem cells and the regulation of neuritogenesis have been identified. Moreover, overexpression of IgG2B in astrocytes induces the CRTC1-CREB-BDNF signaling pathway know to be involved in gliogenesis whereas CRISPR-Cas9 IgG2B KO triggers the BMP/YAP1/TEAD3 pathway activated in astrocytes dedifferentiation into neural progenitors. Proximal labeling (BioID) experiments revealed that IgG2B is N-glycosylated by the OST complex, addressed to vesicles membranes containing the ATPase complex; and behaves partially like CD98hc through its association with LAT1. Proximity-dependent biotin labeling (BioID) experiments suggests that proximal IgG2B-LAT1 interaction occurs concomitantly with MACO-1 and C2CD2L, at the heart of a potentially novel cell signaling platform. Finally, we demonstrated that these chains are synthesized individually and associated to recognize specific targets. Indeed, intermediate filaments and PRSS1 involved in astrocytes fate constitute targets for these neural IgG. Taken together, we established that aberrant neural IgG chains could be play a role as gatekeepers of astrocytes to neural progenitor conversion and are potential new targets for neurodegenerative diseases.

Key words: Astrocytes, Proteogenomic, RNAseq, Proteomic, Inflammation, Neurogenesis, Neurite Outgrowth, BioID, CRISPR-CAS9, Immunoglobulins, Neuronal Progenitor, Astrocytes - Neuron conversion

Introduction

Immunoglobulin superfamily (IgSF) proteins are implicated in diverse steps of brain development, including neuronal migration, axon pathfinding, target recognition, and synapse formation [1]. High diversity and function of transmembrane and secreted members of IgSF proteins have been reported in brain [1]. There are about 500 non-antibody, non-T cell receptor (TCR) IgSF proteins encoded by the human genome [2]. Among the role of membrane IgSF, neurite extension, neuronal migration, and synaptic plasticity are the most known [3]. Among these IgSF, Thy-1 [4] is of particular interest. Thy-1 presents sequence homology with the variable part of the immunoglobulin heavy chain. Neuronal Thy-1 interaction with the astrocyte αvβ3-integrin–syndecan-4 receptor pair triggers the formation of focal adhesions and stress fibers in astrocytes via RhoA activation [5]. This interaction stabilizes neuronal connections and suppresses axonal regrowth after injury in the astrocyte-rich areas of the adult central nervous system [6]. Recently, the expression of immunoglobulin constant domain genes in neurons of the mouse central nervous system have been demonstrated[7]. The identified IgG3 and IgM membrane forms lack the variable immunoglobulin regions. The corresponding IgG3 and IgM transcripts lack the canonical B-cell transcription initiation site, while alternative transcription start sites have been identified. In our recent work on motor neurons, we also identified IgG2B and IgG2C transcripts, their Fc receptors (CD16 and CD32b) as well as the recombination genes (RAG1 and RAG2) [8]. We established the involvement of CD16 and CD32b in antibody-dependent neurite outgrowth modulation (ADNM) response. Moreover, in astrocytes, we identified alternative proteins issued from long non-coding RNA encoding a variable light chain (so-called Heimdall) and a variable heavy chain [9]. We demonstrated that the Heimdall protein was involved in astrocytes phenotype control [9]. Its inhibition led to neuronal phenotype switch by expression of neuronal progenitor stem cells, neurite outgrowth factors, and induced astrocytes prolongments similar to neurites [9].

Taken together, evidence support that true immunoglobulin chains seems to be expressed in non-B cells. To understand whether a complete mechanism involving antibodies production also occurs in astrocytes like in B-cells, we investigate by pan-transcriptomic, proteomic to establish the complete repertoire of IgG chains. The variable heavy chain (IgVH) transcript does not contain the D and J chains but a leader and an RSS sequence, whereas the Heavy constant chain of IgG2B (IgH6) mRNA starts with a 5’ Kozak sequence and ends with a 3’ sequence

coding a transmembrane domain. The constant kappa chain transcript contains a 5' RSS sequence followed by a joining chain and the *Ighk* sequence whereas the variable kappa light chain starts with a 5' leader sequence followed by the *Igvk* and a 3' RSS sequence. We then established the expression of the V(D)J recombination complex in astrocytes. This complex is characterized by a gene rearrangement of the V (variable) segment, the J (junction) segment, and the D (diversity) segment for the heavy chain and the V (variable) segment and the J (junction) segment for the light chain in B cells. In the literature, this V(D)J process sets up a whole enzymatic complex. Finally, we investigated their function in astrocytes using CRISPR-Cas9, over-expression, proximal labeling using BioID, epitopes targeting methods and thus established these astrocytic IgGs could be involved as gatekeepers of astrocytes-neuronal progenitor conversion.

Results

Primary cell culture devoid of B cells

We previously detected the presence of IgG in astrocytes from sections of the injured spinal cord [10]. This experiment was performed 24h after anti-CD20 treatment to exclude the presence of B-cells. However, resident B cells like plasmocytes can still be there [11]. Thus, to exclude recaptured IgGs by astrocytes from blood circulation, we decided to perform our study on primary astrocyte cultures (spinal cord and cortex) from 3 days old rat pups. Rat pups 3 days old are devoid of B cells [12]. We also used a cell line of rat astrocytes (DI TNC1). All these astrocytes (primary cultures or cell line) were stimulated or not with 200 ng/mL of lipopolysaccharides (LPS) or a cocktail of cytokines to mimic the inflammation that occurs during spinal cord injury [10, 13, 14]. Moreover, to ensure that our cultures were devoid of B-cells, RT-PCR was performed to amplify *Cd*20 transcripts (**Figure 1A**). cDNA from the spleen served as an internal control. In primary astrocytes and DI TNC1 cell lines, no amplification was obtained for *Cd*20 mRNA (**Figure 1A**). This was confirmed by RNAseq analyses. In RNAseq, only 16 reads were aligned with the first three exons of Ms4a1 (chromosome 1: 227,429,596-227,441,442 positions encoding for the CD20) in astrocytes from the cortex and none from the ones of the spinal cord (**Figure 1A', Supp Data 1**). Thus, the coverage of all exons was not observed for *Cd*20, suggesting that *Cd*20 was not expressed in the astrocytes. Its expression was also analyzed by Western blot and no 33-37 kDa bands corresponding to CD20 were

observed in astrocytes contrary to B cells (**Figure 1B**). Moreover, no reads were observed for plasmacytic marker CD19 in RNAseq (**Figure 1A''**). By contrast, RT-PCR experiments performed with primers directed against the cDNA sequence encoding for the Glial fibrillary acidic protein (GFAP), an astrocyte marker, allowed the amplification of a fragment of interest the expected size 1,292 bp (**Supp. Figure 1A**). The nature of the transcript was confirmed by sequencing and RNAseq. Alignment with the *Gfap* gene on chromosome 10: 90,988,762-91,001,435 showed a complete and deep coverage with a depth of around 100,000 reads for the cortex and 45,000 reads for the spinal cord (**Figure 1A'''**). FACS was performed on rat blood with anti-CD45R and CD45-RA and confirmed the presence of B cells in the blood (**Figure 1C**). Surprisingly, some cortex and spinal astrocytes exhibited staining with CD45R and CD45RA. However, triple staining confirmed that these cells were GFAP positive (**Figure 1C**). Additional RNAseq analyses allowed the comparison between CD markers of the different B cell populations and astrocyte markers. This revealed that astrocytes are CD19, CD23, CD27, and CD52 negative but express some plasmocyte markers such as CD38 and CD138 (**Figure 1D**). Altogether, this points out the existence of a subpopulation of astrocytes sharing some common features with plasmocytes. To verify the astrocytic nature of the cells, detection of GFAP by western blot was carried out and confirmed the presence of its band at 55 kDa (**Supp. Figure 1B**). Moreover, additional bands corresponding to cleaved forms of GFAP were also detected which is in line with previous reports from literature [15]. Supporting the fact that specific sub-population of astrocytes exist, recent data reveal the presence of an astrocyte-like population in the spleen [16, 17]. Our data support that study determined a faint GFAP expression in the spleen lymphoid center. Although smaller, the bands obtained at 40 and 45 kDa could correspond to truncated form of GFAP (**Supp. Figure 1B**).

Immunoglobulin chains Identification

As a first step to demonstrate the presence of immunoglobulin chains in astrocytes, we performed immunocytochemistry (ICC) and immunofluorescence (IF) experiments on rat primary cortex and spinal astrocytes. ICC using an anti-IgG associated with peroxidase revealed immunoreactivity in normal astrocytes (**Figure 2A**) which is increased when stimulated with LPS **(Figure 2B).** We noticed that under LPS stimulation, the number of astrocytes reactive to anti-IgG is higher and the immunolabelling is present in the cell body of the astrocytes but also at the level of their prolongments **(Figure 2B).** Similar results were

obtained using immunofluorescence experiments performed on astrocytes from the spinal cord. Immunofluorescence for IgG (Green) was detected in cell bodies (close to the nucleus) and in prolongments of astrocytes without treatment (**Figure 2C**). Co-localization with GFAP (Red) confirmed the fact that these cells were astrocytes in both cortex and spinal cord (SC) (**Figure 2D-2F"**). To be sure that the presence of IgG was not due to recapture from blood during the isolation procedure, we also conducted this analysis on rat DI TNC1 astrocyte cell line. The staining for IgG was also observed which confirmed the ability of astrocytes to produce IgG (**Figure 2G**) as neurons [8]. The labeling appeared in granular structures scattered in the cytoplasm suggesting the possibility to be secreted (**Figure 2G**). To confirm the ability of astrocytes to produce IgG, we performed a pan-transcriptomic and proteomic analyses of the primary cultures and the cell line during normal and after LPS stimulation. After RNAseq analyses, MagicBlast alignment was performed against a specific bank containing all sequences coding for each V (Variable), D (Diversity), J (Junction) exons and heavy and light chain referenced in IMGT immunoglobulin database [18] for the *Rattus norvegicus*. It confirmed that reads corresponded to Ig constant part of heavy and light chains. Among them, 63 reads and 3 trinity corresponding to *Igg2b*; 30 reads for *Ighm* and 9 reads and 1 trinity for *IgK* were identified in spinal astrocytes (**Supp. Data 1**). Only 2 reads for *Igg2b*, 26 reads and 1 trinity of *Ighm*, 6 reads and 1 trinity for *Igg2a* and 4 reads and 1 trinity for *IgK* were found in astrocytes from the cortex (**Supp. Data 1**). These results were then validated by RT-PCR performed on cDNA from primary culture of cortex or spinal astrocytes as well as DI TNC1 cell line (**Figures 2H**). To mimic an inflammation as observed during the time course of SCI [13, 19], the cells were stimulated with LPS and for 24h or 48h with a cocktail of cytokines (**Figures 2H**). cDNA from the spleen served as a positive control. The primers used were deduced from peptides identified by proteome analysis after purification processes using Ig enrichment procedure [20]. For IgG2b, these peptides were VDKKVERRNGGIGHKCPTCPTCHK, ALPSPIEKTISKPKGLVR, KNTEPVMDSDGSFFMYSKLNVERSR (**Supp. Figure 2**). Some of these peptides were previously identified in SCI [20]. Another round of RT-PCR allowed the amplification of the complete constant heavy chain. The size at 1,001 bp corresponded to the mRNA that did not contain the sequence coding for the transmembrane (TM1) or (TM2) domains (**Figure 2H**) while the fragments at 1,209 bp exhibited TM1 and TM2 coding sequences (**Figure 2I, Supp. Figure 2**). These results suggest that a transmembrane form of IgG2B is produced in astrocytes. We then performed a 5'-RACE-PCR to identify the complete transcript (**Figure 2J**). Surprisingly, no VDJ

coding sequences associated with the constant heavy chain cDNA were identified. However, bioinformatic analyses revealed the presence of a Kozak sequence directly before Exon1 flanking the IgG2B constant chain coding sequence (**Figure 2J and 2K**). Constructs were performed including this Kozak sequence, the sequence coding for the IgG2B transmembrane form followed by the Flag tag sequence (**Figure 2L**). These constructs were overexpressed in DI TNC1 cells and Western blot analyses confirmed the expression of the construct at the predicted size of 50 kDa at 24h and slightly in 48h and 72h after transfection (**Supp. Data 2**). This band was not detected after transfection of the empty vector (EV), showing the specificity of the detection. These results confirmed support that IgG2B was synthesized as a free constant heavy chain. Even if no VDJ sequences associated with IgG2B coding sequence were detected, we previously discovered by proteomic analysis alternative proteins corresponding to free variable Heavy chain and Kappa light chains (Data not shown). Thus, we investigated our RNAseq data to identify these free variable chains. Several of them were detected (IGVH1-31*01, IGHV5-43*01, IGVH7-16*01) and some were confirmed by RT-PCR performed on cDNA from rat primary cortex and spinal astrocytes (**Figure 3A, Supp. Figure 3**). Interestingly, no stop codon in the 3' end (IgHV5-43.01 IgHV1.31.01 or IGVH7-16*01) was found. Moreover, IGVH7-16*01 exhibits an RSS sequence at its 3' end meaning that it is a free variable chain (**Figure 3A**). From previous proteomic analyses, several peptides were identified and covered parts of the IGVHs. RT-PCR that was performed against the sequences coding these variable parts validate their expression (**Supp. Figure 3A**). By contrast, using a forward primer directed against the sequences coding these variable parts and an antisense primer directed against the IgG2B encoding sequence, no amplification was observed. Therefore, these variable parts are not linked to IgG2B heavy chain (IgH6), however we cannot conclude whether they are associated with another isotype or if they are free chains.

We then investigated if free variable light chains were also produced. We previously established their existence by discovering from long coding RNA, two variable Kappa chains [9]. We thus also investigated their presence from classical mRNA. We retrieved from our RNA seq data, several free variable kappa light chains with a coding leader sequence in the 5' position (IGKV3S9*01, IGKV19S1*0) (**Figure 3B, Supp. Data 1**). At the genomic level, an intronic sequence separates the leader sequence (L1) and (L2) attached to the exon coding the variable heavy chain. Their association occurs during pre-mRNA splicing. Thus, its presence in our

sequence without any intronic sequence demonstrates that the variable sequences identified is a true transcript and is not linked to genomic amplification. Moreover, IGKV8S6*01 presents a RSS sequence in 3' position (**Figure 3B, Supp. Data 1**). We also amplified by RT-PCR the complete sequence coding the constant Kappa chain from DI TNC1 cells treated or not with LPS or a cytokine mix, as well as in rat primary spinal and cortex astrocytes (**Figure 3Ca**). We then conducted 5' RACE-PCR on a cDNA library from DI TNC1 cells (**Figure 3Cb**). This revealed the presence of a 5' RSS sequence followed by a joining sequence associated directly with the *Igk* sequence (**Figure 3Cc**). Thus, the complete schematic representation of astrocytic IgG2B is presented in **Figure 3C'**. IgK were identified in rat primary spinal and cortex astrocytes and proteomic analyses confirmed their translation (**Supp. Figures 4A**). On the contrary, the Lambda chain encoding sequence was only amplified in rat primary cortex and DI TNC1 astrocytes (**Figure 3Da and 3Db**). Furthermore, from our RNAseq database and RT-PCR analyses, we also identified IgM encoding sequence in rat primary spinal and cortex astrocytes stimulated by LPS (**Figure 3E, Supp. Figure 4B**). In astrocytes from adult rats, we also identified the sequences coding IgG2B and a variable IgVH chain corresponding to IGVH7-16*01, found in astrocytes isolated from pups (**Supp. Figure 4Ca and 4Cb**). In primary astrocytes from Human embryos, we identified transcripts related to IgG1 isotype, and heavy constant and light chains (**Supp. Figure 4Cc)**. Interestingly, our previous results on the alt IgKV, named Heimdall protein, a free variable kappa light chain, established that the chains were associated, and formed aberrant antibodies as observed in cancer cells [21].

Recombination enzymatic complex

Even though we only detected aberrant Ig, we investigated whether astrocytes exhibit the classic enzymatic machinery involved in V(D)J recombination. Indeed, in the first step, the two transposases RAG1 and RAG2 will bind to the recombination signal sequences (RSS) 12-23 that flank the selected V, D or J genes to cleave the DNA. Then, to initiate the repair process, KU70 (XRCC5) and KU80 (XRCC6) will form hairpins and break the ends of these RSS segments. Then, DNA-dependent protein kinase (DNA-PKCs) and Artemis endonuclease (DLREC1c) are recruited to open these hairpins and allow Terminal deoxynucleotidyl transferase (Tdt, or new nomenclature DNTT) to add nucleotides randomly. This nucleotide addition adds more diversity to antibody synthesis, called junctional diversity. Finally, DNA Ligase IV (LIG4), XRCC4 and Cemunnos-XLF (NHEJ1) link the two segments together [22]. RT-PCR experiments followed

by sequencing allowed the identification of all the sequences coding these enzymes (**Figure 4**). This was confirmed at the protein level by proteomic analyses performed on primary astrocyte cultures (**Supp Data 3**). The fact that few variable light and heavy chains were identified questions the role of this machinery in pups astrocytes used in this study *i.e.* V(D)J recombination or DNA repair. However, it cannot be excluded that this machinery is expressed for IgG diversity at a later developmental stages of astrocytes like in lymphopoiesis of B cells.

The Function of the constant Heavy chain of IgG2b

We then aimed to investigate the function of IgG2B constant heavy chain (IgH6). For this purpose, a CRISPR-Cas9 invalidation of *IgG2B* encoding gene was performed on the rat astrocyte DI TNC1 cell line. This invalidation was performed on two regions of the IgG2B coding sequence using two different sgRNAs. They will be referred to as *IgH6*-1 and *IgH6*-2. Uninfected cells as well as cells infected with an empty vector or a sgRNA directed against a non-target sequence *Trop-2* (T2) known to not be expressed in astrocytes were used as controls. We performed a comparison with our previous CRISPR-Cas9 targeting the sequence coding for a free kappa variable light chain named Heimdall (KO2) (data not shown). After invalidation, the cells were harvested, and the proteins were extracted for shotgun proteomics. For *IgH6*-1 KO cells, 71 exclusive proteins were found whereas 73 proteins were exclusively identified in *IgH6*-2 KO cells (**Figure 5A, Supp. Data 4**). Interestingly, among the proteins identified in *IgH6*-1 KO cells, we found Yap1, Tead3, Mcc, Kmt2d, and Ddhd2, which are known to be associated with neural progenitor cells [23] (**Supp. Figure 5A**). We also characterized proteins related to hematopoietic cells (FRG1, Pir), apoptosis regulations (Casp3, Cdk11b, Bax) or neuritogenesis (Plxna1, Rock1, Magi3, Tbl1x). In *IgH6*-2 KO cells, we identified proteins known as polarizing players in brain development (LLGL1, Atxn2) [24, 25] or related to neural stem cells (Gpc4, MAPK). We also identified Akt2, known to be implicated in survival growth and cell proliferation like Pfdn1. Moreover, 30 of the proteins identified were found in organelles and 28 were membrane-bound organelle proteins (**Supp. Figure 5B**). After shotgun proteomics, we applied an ANOVA test with a significance threshold of $p < 0.01$. A heatmap depicting the proteins showing a significant difference in LFQ expression between the different conditions was created. One main cluster was identified with *IgH6*-1 KO and *Igh6*-2 KO compared to control conditions (empty vector (EV), *Trop2* KO, control cells with or without polybrene treatment). (Of note, *Heimdall* KO (KO2) colocalized with *IgH6* KO). This

suggests that this free kappa variable light chain and free IgG2B heavy chain control the same biological processes (**Figure 5B, Supp. Data 5**). This cluster representing the over-expressed proteins in *IgH6* and *Heimdall* KO conditions encompassed proteins involved in transcription regulation of TP53, metabolism, cell cycle, and neuronal system, and developmental biology. Moreover, Reactome analyses established the involvement of these proteins in transcription, oncogenesis, cell cycle and stress response. Taken together, functional enrichment analyses of the specific clusters found for *IgH6* KO followed by Gene Set Enrichment Analysis (GSEA) [26] associated with Cytoscape [27] were in line with the previous analyses (**Figure 5C**). Most of the proteins are linked to cell proliferation, cell cycle, cell growth, associated with BMP receptor signaling (including Smad2, Smad9), morphogenesis and embryonic development related to neuronal stem cells progenitors (**Figure 5C**). Taken together, IgG2B seems to regulate astrocytes at the level of the cell cycle, transcription, and to maintain the phenotype by regulating transcription factors involved in neuronal cell reprogramming and growth. When *Igh6* is KO then astrocytes can be reprogrammed to switch in neurons as we previously demonstrated for the free variable kappa light chain, Heimdall [9].

IGH6 overexpression impact on DI TNC1 cells

Three constructions have been realized. The first one consisted of the one already described in (**Figure 2J**), consisted of the Kozak sequence followed by the *IgH6* and the Transmembrane domain with a Flag tag at the end of the construct (**Supp. Figure 6A**). The second construct is the same as the previous one without the TM domain and the third one, consisted only of the Kozak sequence and the TM domain with the flag sequence. The Western blot performed in non-reducing conditions revealed for the first construction presence of a specific band near a size of 60 kDa in both DI TNC1 and at 24h of LPS stimulation, slightly found in EV condition, but absent at 48h and 72h of LPS-stimulation. A second band close to 140 kDa is detected slightly at 24h and EV and highly at 48h but absent in DI TNC1 and 72h. The Last one is at a size close to 260 kDa and is only present at 24h and 48h of LPS-stimulation. Compared to the second construction without the TM domain, band of 60 kDa is only found in 24h, 48h, 72h, and EV. The one of 150 kDa is found in DI TNC1, 24h, 48h and 72 h and absent in EV. The one close to 260 KDa is only expressed at 24h of LPS-stimulation. Taken together, it seems that the IgH6 chain can associate itself but also with the light chain (IgKV and IgGV) as we already demonstrated in anti-IgKV Western blot of LPS-stimulated extracts in reducing conditions of

primary cultures of spinal or cortex astrocytes (**Supp. Figure 6B**) [9]. Moreover, Western blot analyses in reducing conditions with anti-IgKV of secretomes of LPS-stimulated CRISPR-Cas9 IgH6 compared to controls (T2, EV and CTR) cells, showed the lack of the band of 60 KDa in IgH6 KO cells (**Supp. Figure 6C**). Moreover, Western blot analyses in reducing conditions with anti-IgKV of secretomes of LPS stimulated CRISPR-CAS9 IgH6 compared to controls (T2, EV and CTLR) cells, established the lack of the band at 60 KDa in IgH6 KO (**Supp. Figure 6C**). Moreover, shotgun proteomic analyses of the cell extracts from the 3 different constructs compared to control and EVs showed differential specific proteomic representation illustrated in the Venn diagram schematic (**Supp. Data 6, Supp. Figure 6D**). Forty-six common proteins to the 3 conditions have been identified compared to EV and control and forty-one between the two first conditions. Among these identified proteins, the Yap1 transcription factor is known to be implicated in astrocytic proliferation and is known to promote astrocytoma [28]. Similarly, enhanced activity of Crtc1 is implicated in cancers [29]. Moreover, the presence of the immunoglobulin superfamily (embigin) and the immunity related GTPase family reinforced the inflammatory and proliferative profile of the astrocytes. Altogether, overexpression of IgG2B constant chain (IgH6) reinforces the astrocyte fate but also switches it towards proliferation and astrocytoma.

IgG2B interactors proximal interactome uncovers CD98hc-like features

To get insight in IgG2B intracellular protein network, we performed a series of proximity-based biotin labeling experiments (**Figure 6A**). These experiments were designed to identify the intracellular proteins at the proximity of IgH6 in a constant heavy chain domain-dependent manner. We performed a series of BirA* alone controls and expressed the signal peptide (SP) fused to the IgG2B transmembrane (TM) domain with a C-terminal BirA*Flag tag (BF) to remove the BioID basal and the membrane protein processing-specific backgrounds, respectively. Both the SP-TM-BF and SP-Constant-TM-BF identified Signal Recognition Particle (SRP) receptor (SRPRB, SRPR, SRP14) and 32/159 structural constituent of the ribosome, supporting correct recognition of the SP and proper processing through the ER (**Figure 6B**). Comparing the SP-Constant IgG2B domain (C)-TM-BF data to both BirA* alone and SP-TM-BF controls, we identified 23 proximal high confidence SP-C-TM-BF interactors (i.e. proteins brought to SP-C-TM-BF through the Constant domain). Amongst those, we identified 6

components of the oligosaccharyltransferase complex (DDOST, MAGT1, RPN1, RPN2, STT3B and TUSC3) which suggest that SP-C-TM-BF is processed through the N-linked glycosylation pathway. Of note, SP-C-TM-BF harbors a single N-X-S/T glycosylation sequon located at the N183 (-S-T). We also identified three components of the proton-transporting two-sector ATPase complex (ATP5F1, ATP6AP1 and ATP6AP2) which catalyzes the synthesis or hydrolysis of ATP coupled to an H+ transport across membranes. Together, these proximal interactions strongly suggest a plasma, lysosomal or vesicular membrane addressing of SP-C-TM-BF. In line with this hypothesis, we detected TMEM57 (Macoilin), C2CD2L, ILKAP and SLC7A5 among the remaining 14 high confidence interactors (**Supp Data 7**). TMEM57 association is strongly dependent of the IgG2B constant domain. It is a poorly characterized protein which has solely been reported to regulate neuronal activity, resulting in Ca2+ imbalance [30, 31]. Of peculiar interest, the phospholipid transfer protein C2CD2L ensures the transit of phosphatidylinositol from ER to the plasma membrane in a Ca2+ dependent manner [32]. We hypothesize that the interactions between IgG2B, TMEM57 and C2CD2L may occur at the tethering sites between ER and plasma membrane and could link membrane embedded IgG2B to neuronal physiology through PIP and Ca2+ regulation. The large neutral amino acids transporter small subunit 1 (SLC7A5, LAT1) appears as another partner of membrane embedded IgG2B. LAT1 is crucial in transporting large neutral amino acids as well as drugs or metabolites (e.g. L-DOPA [33] across the blood-brain barrier (BBB). Beyond its function, SLC7A5 acts through heterodimerizing with SLC3A2 (CD98 heavy chain; hc). This is interesting regarding our study since CD98hc is a N-glycosylated protein [34] and SLC7A5 (LAT1) is one of its associated light chain ensuring amino acids transport . These data suggest that membrane embedded IgG2B could substitute SLC3A2 to form a membrane heterodimer with SLC7A5. In addition, the specific interaction with ILKAP (integrin-linked kinase associated phosphatase) potentially indicates a link between IgG2B and the PI3K/AKT pathway through its reported ability to dephosphorylate GSK3[35]. This pathway is downstream the canonical CD98hc-LAT1 complex. Our data thus sketch an alternative CD98 receptor where IgG2B could replace CD98hc and associate with LAT-1 to form a functional entity potentially impacting multiple pathways, *e.g.* PI3K/AKT, Wnt (through modulating GSK3b activity, thus b-catenin regulation) and mTORC1 (because of its amino acids transporter activity when associated with LAT-1). Of note, we did not detect integrins as IgG2B interactors, suggesting a partial recapitulation of CD98 organization.

Together, our proximal interactomics study suggests that IgG2B is: (i) N-glycosylated by the OST complex; (ii) addressed at the vesicle membrane through ATPase complex-containing vesicles; and (iii); partially behaves as CD98hc through its association with LAT1 and ability to recruit ILKAP which potentially regulates downstream signaling pathways. These experiments were performed in HEK293 and certainly present cell-type dependent limitations. However, LAT1 is expressed in astrocytes, and we believe this dataset uncovers a putative CD98hc-like function which represents a great interest for pharmaceutical research (because of the ability of CD98 to ensure BBB large molecule crossing). Further experiments are needed to characterize IgG2B-LAT1 interaction in astrocytes and could represent an interesting path for astrocytic neoplasms understanding [36]. Furthermore, it will be of peculiar interest to investigate whether the IgG2B-LAT1 proximal interaction occurs concomitantly with TMEM57 and C2CD2L, at the core of a potentially novel cell signaling platform.

Antigen recognition by astrocytes Ig

We established that aberrant Ig have been identified in astrocytes extracts. Their secretion must be demonstrated and their ability to recognize antigens and function as antibodies too. This supports the fact that all different free chains may associate to produce a structure functioning as a complete antibody (**Figure 7A**). To evaluate whether this IgG antibody can recognize antigens, Western blot of protein extracts from DI TNC1 cells was performed on 2D gels (**Figure 7B**)**.** All membranes were incubated with secretome of DI TNC1 cells stimulated with 200 ng/mL of LPS as a source of primary antibodies. Of note, these secretomes were collected after the culture of cells in DMEM without FBS for 24h. Then secondary antibody was added, and positive spots were detected (**Figure 7B**). Each recognized spot was then analyzed by shotgun proteomics. Their identification revealed, proteins involved in microtubule cytoskeleton organization (Tubulin alpha chain and beta chains, Vim) as well as PRSS1 (**Supp. Data 8**). PRSS1 is a factor known to be involved in the neuroprogenitor stem cell conversion and in astrocytoma [37]. PRSS1 is a ligand of the protease-activated receptor 1 (PAR1). PAR1 activation triggered action potentials through transient Ca^{2+} responses and induces a significant depolarization in neurons and in glial cells [38]. String protein analyses of the identified proteins confirmed that most of the proteins were involved in the intermediate filament cytoskeleton (**Figure 7C**). Reactome pathways analyses established proteins involved in Rho GTPases activity, Gap junction trafficking, autophagy, and developmental biology.

KEGGS pathways also highlighted proteins involved in Parkinson's disease. Taken together these results are in line with the CRISPR-Cas9 data. Intermediate filaments (IFs) are key players in the control of cell morphology and structure as well as in active processes such as cell polarization and migration. Previous studies have shown that IFs are major players in fetal brain development. Vimentin was observed in astrocytes and glial progenitor cells/glioblasts while tubulin beta II was only found in some glial progenitor cells/glioblasts and not at all in mature astrocytes [39]. *In vitro*, astrocytes lacking GFAP or vimentin were shown to be the substrate for increased neuronal plasticity [40]. Thus, regulation by aberrant IgG chains in astrocytes of IFs can also explain the control of the astrocyte-to-neuronal progenitor stem cell conversion as presented in (**Figure 8**).

Discussion

In the present study, we identified variable and constant heavy and light chain coding sequences in astrocytes. If some are from the CDS, others are considered pseudogenes. However, their translation was demonstrated by proteomic analysis. The use of pseudogenes to synthesize multiple IglV and IghV has already been observed in mice and chickens. Within the multiple IglV and IghV pseudogenes, the number of stop codons contained in the ‘‘coding’’ sequence is far lower than would be expected while nucleotide substitutions occurred at random. In fact, most stop codons introduced by point mutations are ‘‘corrected’’ and eliminated by further point mutations within the same codon [41-43]. In rodent B cells, the conservation of open reading frames plays a role in any putative function of pseudogenes involved in somatic gene arrangement [44] as we showed in astrocytes not only from pups but also from adult rats and human embryos. Similar results were already observed in human immunome. In fact, gene conversion with pseudogenic sequences like somatic hypermutation or class switch conversion or recombination (CSR) of the constant region increases the repertoire for a vast diversity of immunological recognition molecules starting from a limited number of gene segments [45, 46]. This ensures the detection of all possible foreign organisms and substances. Moreover, under inflammatory conditions, our results demonstrated the existence of a specific subpopulation of astrocytes displaying an expression of plasmocyte markers such as CD38 and CD138. This is consistent with their ability to synthesize a diversity of immunoglobulin subtypes such as IgG2B and IghM. We can rely upon these results with those depicting a glia subpopulation in the spleen [47]. Spleen glia differentially expresses genes

associated with an immune response such as cytokine-cytokine receptor interactions, phagocytosis, and the complement cascade. It thus can be envisaged that activated astrocytes share common features with this spleen glial population.

In the CNS, astrocytes present multiple important physiological functions such as maintenance of the blood-brain barrier, production of neurotrophic factors, adjustment of the density of ions in extracellular space, modulation of inflammation, regulation of neuronal activity, synaptic transmission, and neural circuit function [48]. Astrocyte proliferation stops after 1 month of age in rodents. However, in response to insults such as traumatic brain injury or Spinal cord injury (SCI), astrocytes proliferate [49] to perform astrogliosis [13, 19, 50-53]. Astrocytes and neurons originate from the same progenitor cells. Therefore, astrocytes might have kept intrinsic neuronal conversion potential. Supporting this fact, it has been observed in certain circumstances that astrocytes can dedifferentiate and switch their phenotype to become neuron-like cells [54]. It has even been speculated that glial cells might be a kind of NPC-like cells due to the observations that astrocytes can express certain NPC markers such as Nestin and Sox2, whereas certain glial markers such as GFAP are also observed in NPCs. However, it has recently been shown that only cortical astrocytes but not astrocytes from other brain regions such as the hippocampus and the cerebellum can be converted into neurons under the current condition [55, 56]. Pax6 was found as one of the key transcription factors that can reprogram astrocytes to neurons [57]. Other transcription factors (TFs) such as Ascl1, Lmx1a and Nurr1 (Nr4a2) so-called ALN TFs have also been used to switch astrocytes to dopaminergic neurons. Similarly, the combination of ALN with NG2 glia switches them into GABAergic neurons in mice [48]. These TFs seem to promote chromatin remodeling and activate the TGFβ, Sonic hedgehog (Shh) and Wnt signaling pathways [58]. NeuroD1, a bHLH pro-neural TF essential for embryonic development and adults' neurogenesis, is also involved with Sox2, Ngn2 and Ascl1 in the conversion of glia into neurons. According to these data, we can speculate that factors implicated downstream of neural TFs regulation of Shh and Wnt signaling pathways can participate in astrocytes to neuron conversion [59]. Accordingly, it has been demonstrated that astrocytes can be converted into neurons by the knockdown of *Ptbp1* [60]. Ptbp1 plays an essential role in pre-mRNA splicing and mediates several cellular processes in certain types of cells, including the activation of immune cells as well as the growth and differentiation of

neuronal cells. In such a line, our present study establishes that IgG2B also plays a role as gatekeepers of astrocytes to neural progenitor conversion.

Indeed, when we Knocked-out the rat *igg2b* gene by CRISPR-Cas9, we demonstrated that TFs such as YAP, TEAD and SMAD2/9 were more abundant. It is known that YAP and TEAD gain of function causes marked expansion of the neural progenitor population (**Figure 8**). This is partly linked to their ability to promote cell cycle progression by inducing cyclin D1 activity and to inhibit cell differentiation by suppressing NeuroM. Their loss of function results in increased apoptosis, whereas repressing their target genes leads to premature neuronal differentiation [23]. In accordance with these results, an over-proliferation profile of astrocytes was also observed after the KO of *Igg2b* gene. Besides, it has previously been demonstrated that these various proteins play a key role during neuronal differentiation by inhibiting the upstream kinases of the Hippo signaling pathway and the input for their conversion to neuronal progenitor stem cells [61] by triggering the TGF beta/BMP pathways. To better define IgG2B activity, we then performed its overexpression in HEK 293 cells and study its localization. We observed that it was synthesized as a free transmembrane constant chain through its Kozak sequence located upstream of its first exon and was addressed to vesicular structures such as endosomes or extracellular vesicles. Through proximal BioID studies we also found that IgG2B is: (i) N-glycosylated by the OST complex; (ii) addressed at the membrane of ATPase complex-containing vesicles; and (iii) partially behaves as CD98hc through its association with LAT1 and its ability to recruit ILKAP, which potentially regulates downstream signaling pathways (**Figure 8**). These experiments were performed in HEK293 and certainly present cell-type dependent limitations. However, LAT1 is expressed in astrocytes, and we believe this dataset uncovers a putative CD98hc-like function which represents a great interest for pharmaceutical research since CD98 ensures BBB crossing of large molecules. Further experiments are needed to characterize IgG2B-LAT1 interaction in astrocytes and could represent an interesting path to understand astrocytic neoplasms [36]. During these experiments, we also detected TMEM57 and C2CD2L as putative IgG2B interactors (**Figure 8**). It will be of peculiar interest to investigate whether the IgG2B-LAT1 proximal interaction occurs concomitantly with TMEM57 and C2CD2L, at the core of a potentially novel cell signaling platform. Indeed, it is worth noting that TMEM57 (MACO-1) is known in *C. elegans* to be involved in different neuronal functions. It regulates the forgetting of olfactory adaptation to isoamyl alcohol, which is an attractive

odorant perceived by different types of sensory neurons [62]. In Human, MACO-1 is expressed in neural progenitors particularly during memory consolidation in the hippocampus [63]. Moreover, it also acts in the ER to regulate assembly or traffic of ion channels or ion channel regulators to modulate neuronal excitability [64]. Based on these data and our results, it is tempting to speculate that IgG2B acts as a scaffold protein bringing together various regulators involved in the astrocytic phenotype.

In parallel of IgG2B, we also identified free variable heavy chains synthesized without the DJ sequences, free variable kappa light chains as well as a constant kappa light chain linked to a joining sequence. As suggested by our previous Western blot data and proteomic experiments [9], this does not exclude the possibility that these free variable chains may associate with their respective constant chains. The heavy and light chains formed independently may then interact to form a structure related to a BCR expressed at the membrane of endosomes/extravesicular vesicles or to be secreted to recognize some antigens or activate specific FcγR. In such a line, we recently demonstrated that neurons express CD16 and CD32b, which are linked to the antibody dependent neurite outgrowth modulation responses (A.D.N.M) [20]. Moreover, we demonstrated that these neural immunoglobulins can recognize antigens in astrocytes such as the PRSS1 protein, known to be involved in neuroprogenitor stem cell conversion[37]. This recognition of autoantigens may also constitute another way to stabilize the fate of astrocytes by blocking their conversion to neurons. Taken together, these results clearly demonstrate that astrocytes immunoglobulins coding by CDS or pseudogenes are aberrant IgG chains maintaining their fate and preventing their conversion to neuronal lineages. Thus, these proteins can clearly be novel therapeutic targets for *in vivo* direct conversion of astrocytes to neurons in neurodegenerative diseases such as TBI, SCI or stroke incidents.

Acknowledgments

This research was supported by funding from Ministère de l'Enseignement Supérieur, de la Recherche et de l'Innovation (MESRI), Institut National de la Santé et de la Recherche Médicale (Inserm), I-SITE ULNE (Nobody Project), Regional council Hauts de France, and Université de Lille. The authors thank the LIGAN-PM Genomics platform (Lille, France) which was supported

by the ANR EquipEx (ANR-10-EQPX-07-01; 'LIGAN-PM') and "France Génomique" consortium (ANR-10-INBS-009), APVV-19-0193, APVV-20-0585.

Author Contributions

Conceptualization, MS. Methodology, AC, OS, MAK, MZ, ARR, SA, EL, EC, DC, AB, FK, MD, MT, IEB, IF, FR and MS; Software MDe, AC, SA., FK; Validation, D.C., FR and M.S.; Formal analysis, DC, FR and MS; Investigation, DC, FR, MS; Resources, DC, DD, MT, IF and MS Data curation, MS, FR, AC. Writing – Original Draft Writing MS - Review and Editing, DC, MZ, DD, AB, MT, FK, IF, FR and MS Supervision, FR and MS; Project Administration, DD and MS; Funding Acquisition, DC, DD, IF and MS

Declaration of Interests

The authors declare no competing interests.

Materiel and Methods

Reagents

Flp-In™ T-REx™ HEK293 cells, DMEM media, Phosphate buffer saline (PBS), fetal bovine serum (FBS), puromycin, Alexa Fluor® 594-conjugated goat anti-rabbit, Streptavidin Alexa Fluor 488 conjugate, Alexa Fluor® 555-conjugated donkey anti-mouse, SuperScript® III kit, pcDNA5 FRT/TO N-ter BirA*Flag vectors, pOG44, biotin, hygromycin B, Streptavidin Ultralink Resin were purchased from Invitrogen Life Technologies (Milan, Italy). Rat Astrocytes-adult (RA-a) primary culture, Human Astrocytes-spinal cord (HA-sp) primary culture, Astrocyte Medium-animal and Astrocyte Medium were provided by Sciencell. Human NCH82 stage IV glioma cells were obtained from Dr. Regnier-Vigouroux. Water, formic acid (FA), trifluoroacetic acid (TFA), and acetonitrile (ACN) were from Biosolve B.V. (Valkenswaard, the Netherlands). Sodium dodecyl sulfate (SDS), DL-dithiothreitol (DTT), iodoacetamide (IAA), tetracycline, protease inhibitor cocktail, mouse anti-FLAG, Polybrene infection reagent, rat tail collagen type I, DMSO, FastDAB, astrocyte cell line DI TNC1 were provided by Sigma-Aldrich (Saint-Quentin Fallavier, France). Trypsin/Lys-C Mix, Trypsin Mass Spec Grade, MS-grade TPCK trypsin, DNase RQ1, Go Taq polymerase, pGEM-T easy were purchased from Promega (Charbonnieres, France). Papain Dissociation System was obtained from Worthington Biochem. Corporation (NJ, USA). Anti-GFAP used to assess the purity of astrocyte primary cultures was provided by Abcam. Alexa Fluor 700-conjugated mouse anti-GFAP was from Bio-Techne Corporation. FACS

Lysing Solution, BV421-conjugated mouse anti-rat CD45RA and PE-conjugated mouse anti-rat CD45R were provided by BD Biosciences. Rabbit anti-GFAP was used during immunofluorescence experiments, Mouse anti-GFAP was used during western blot experiments, Amicon ultracentrifugal filter 10K and ZipTip C18 were purchased from Millipore. Goat anti-rat IgG2a was obtained from Bethyl Laboratories, Inc. (Montgomery, TX). Vectashield mounting medium was purchased from Vector Laboratories. NucleoSpin RNA, Mini kit for RNA purification, NucleoSpin Gel and PCR clean up were obtained from Macherey-Nagel. SMARTer RACE 5'/3' Kit and SeqAmp DNA Polymerase were purchased from Clontech. Q5 High-Fidelity DNA Polymerase, Quick CIP, T4 DNA ligase, KpnI-HF and BsrGI-HF were provided by NEW ENGLAND BioLabs. LentiCRISPRv2-sgRNA, pVSVg and psPAX2 were from addgene. Mouse anti-CD20 (D-10) and peroxidase-conjugated mouse anti-IgGk BP were purchased from Santa Cruz Biotechnology. IgKV antiserum referred to as anti-Heimdall was produced in rabbits by Biotem (Apprieu, France) using the chemically synthesized immunogenic sequence KPGKSPQLLIYYASSLQD coupled to KLH. Rabbit anti-rat IgG, Peroxidase-conjugated donkey anti-goat, Peroxidase-conjugated goat anti-rabbit and peroxidase-conjugated goat anti-mouse were purchased from Jackson ImmunoResearch (West Grove, PA, USA). Mouse anti-Beta-actin was provided by Cell Signaling Technology. Turbonuclease was purchased from BPS Bioscience. Polyjet™ in vitro DNA Transfectionreagent was obtained from SignaGen Laboratories. Recombinant Human IL-2 (200-02), recombinant Human IL-1β (200-01B), recombinant Human TNF-α (300-01A), recombinant Human IL-12p70 (200-12), recombinant Human IFN-γ (300-02), recombinant Human IL-6 (200-06) and recombinant Human IL-4 (200-04) were purchased from Preprotech (Rocky Hill, NJ, USA).

Cell culture

DI TNC1 cell line was grown in DMEM supplemented with 10% Fetal bovine serum (FBS), 4 mM L-glutamine, 1 mM Sodium Pyruvate, 100 U/mL penicillin, and 100 µg/mL streptomycin. Rat Astrocytes-adult (RA-a) primary culture and Human Astrocytes-spinal cord (HA-sp) were cultured in Astrocyte Medium-animal and Astrocyte Medium, respectively. Human NCH82 stage IV glioma cells obtained from Dr. Regnier-Vigouroux were grown in DMEM supplemented with 10% FBS, 2 mM L-glutamine, 100 U/mL penicillin, and 100 µg/mL streptomycin. All cell lines were maintained at 37 °C in a humidified atmosphere containing 5% CO2.

Isolation and cultivation of rat primary astrocytes

Experiments on animals were carried out according to institutional animal care guidelines conforming to international standards and were approved by the State Veterinary and Food Committee of Slovak Republic (Ro-4081/17-221), and by the Ethics Committee of the Institute of Neuroimmunology, Slovak Academy of Science, Bratislava.

Cortex astrocytes: After cervical dislocation, cerebral cortices of 3–6-day-old rats were dissected, stripped of their meninges, and mechanically dissociated by repeated pipetting followed by passing through a nylon mesh (70 µm). Cells were plated in Petri dishes pre-coated with 20 µg/ml rat tail collagen, type I (Sigma-Aldrich, St. Louis, Missouri, USA) and cultivated in DMEM containing 10% FBS and 2 mM L-glutamine (all from Life Technologies Invitrogen, Carlsbad, USA) at 37°C, 5% CO2 in a water-saturated atmosphere. The medium was changed twice a week.

Spinal cord astrocytes: From the dissected spinal cord tissue, meninges were carefully removed. Afterward, 2ml of papain + DNase solution enzymes (Worthington Biochemical Corporation, USA) were added, gently mixed with 5 ml pipette, and incubated for 15 minutes at 37°C. The mixture was triturated and 2.7 ml of EBSS with 300 µl of albumin-ovomucoid inhibitor solution and 150 µl of DNase solution were added. The mixture was again gently triturated followed by centrifugation at 300 g for 5 minutes. Pelleted cells were resuspended in a fresh medium and plated at appropriate cell density.

Both astrocyte cultures (cortex astrocytes and spinal cord astrocytes) were cultivated and expanded for 20 days in special cultivation conditions with the aim to avoid the presence of B cells in culture [65]. The purity of astrocyte cell cultures isolated by this procedure was routinely around 95% by anti-GFAP antibody staining (Abcam, Cambridge, UK). The confluent astrocyte cultures were frozen in a freezing medium composed of 45% DMEM, 45% FBS and 10% DMSO.

Flow cytometry analysis to assess B-lymphocytes contamination in astrocyte cultures

One million of the cortex and spinal astrocyte cells were re-suspended in 50 µL of PBS and incubated with 5 µL of Alexa Fluor 700-conjugated mouse anti-GFAP (Bio-Techne, USA) BV421-conjugated mouse anti-rat CD45RA and PE-conjugated mouse anti-rat CD45R (Becton Dickinson, USA). After 30 min of incubation in the dark at RT, the cells were fixed with BD FACS Lysing Solution CD45R (Becton Dickinson, USA) and centrifuged at 300×g for 5 minutes. The

cell pellets were re-suspended in 400 µL of PBS and analyzed by flow cytometry (BD LSRFortessa™ II cell analyzer).

Control staining of rat blood B-lymphocytes. B-lymphocytes were detected by flow cytometry with BV421-conjugated mouse Anti-Rat CD45RA and PE-conjugated mouse Anti-Rat CD45R (high positivity for both markers) (green, double-positive cells).

B lymphocyte staining in spinal cord and cortex cell culture. Gates for positivity were set using an unstained sample, Alexa Fluor 700-conjugated mouse anti-GFAP, BV421-conjugated mouse Anti-Rat CD45RA and PE-conjugated mouse Anti-Rat CD45R were used for staining.

Immunofluorescence

Immunofluorescence experiments were carried out to detect IgG in DI TNC1 cells, rat primary cortex astrocytes and rat primary spinal astrocytes. After fixation with PFA 4% for 10 minutes at room temperature, cells were subjected to a cytospin on a glass slide. To block non-specific protein activity, they were then immersed in PBS 0.1 M; pH 7.4 containing 10% normal goat serum (NGS) and 0.2% Triton X-100 for 2 h at room temperature. This was followed by overnight incubation at 4 °C with rabbit anti-GFAP (1:500) and goat anti-rat IgG2A (1:500). Afterwards sections were washed three times in 0.1 M PBS pH 7.4 and incubated with Alexa Fluor® 488-conjugated goat anti-mouse and Alexa Fluor® 594-conjugated goat anti-rabbit at room temperature for 2 hours. After three additional washes with 0.1 M PBS pH 7.4, the nuclei were stained with 4-6-diaminidino-2-phenylindol (DAPI, 1:200). Finally, samples were again washed in 0.1 M PBS pH 7.4 and mounted with Vectashield mounting medium. To detect overexpressed IgH6 in HEK293 or DI TNC1 cells grown on coverslips, cells were fixed with PFA 4% for 10 minutes at room temperature. A blocking step was then performed in PBS 0.1 M; pH 7.4 containing 1% normal donkey serum (NDS), 1% BSA, 1% ovalbumin and 0.2% Triton X-100 for 1 h at room temperature. This was followed by overnight incubation at 4 °C with mouse anti-Flag (1:1000) or in the case of BioID experiments with Streptavidin Alexa Fluor 488 conjugate (1/10000) to detect proximal proteins that were biotinylated. Dilution of mouse anti-Flag and Streptavidin Alexa Fluor 488 conjugate was performed in the blocking solution. Afterward, sections were washed three times in 0.1 M PBS pH 7.4 and incubated at room temperature for 1 hour with Alexa Fluor® 555-conjugated donkey anti-mouse diluted at 2 µg/mL in the blocking buffer. After three additional washes with 0.1 M PBS pH 7.4, the nucleus

was stained with DAPI, washed in 0.1 M PBS pH 7.4 and mounted using Dako fluorescent mounting medium.

Immunocytochemistry

Rat primary cortex astrocytes were fixed with PFA 4% for 10 minutes at room temperature, cells were subjected to a cytospin on a glass slide. To block non-specific Ab binding, they were then immersed in PBS 0.1 M; pH 7.4 containing 10% normal goat serum (NGS) and 0.2% Triton X-100 for 2 h at room temperature. This was followed by overnight incubation at 4 °C with goat anti-rat IgG2a (1:500). Afterwards sections were washed three times in 0.1 M PBS pH 7.4 and incubated with Peroxidase-conjugated donkey anti-goat at room temperature for 2 hours. After three additional washes with 0.1 M PBS pH 7.4, DAB was added to visualize peroxidase activity. Finally, sections were again washed in 0.1 M PBS pH 7.4 and mounted with Vectashield mounting medium.

RT-PCR experiments.

RNA extraction was performed with NucleoSpin RNA, Mini kit from 2 million of DI TNC1 cells or rat primary cortex astrocytes or rat primary spinal astrocytes or rat primary adult astrocytes or Human primary spinal astrocytes following manufactory instructions. Two units of DNase RQ1 were used to treat 2 µg of RNA at 37 ° C for 30 minutes. To stop the enzymatic reaction, 2 µL of Stop solution were added and the samples were incubated for 10 minutes at 65°C. Reverse-transcription using random primers was then performed using the SuperScript® III kit. cDNAs were stored at -20°C. A "negative RT" without addition of the reverse transcriptase was also included as a control to assess gDNA contamination. RT-PCR reactions were then carried out using Go Taq polymerase and the primers listed in **Supp. Table 1** and according to the programs listed in **Supp. Table 2**. cDNA fragments of interest were then purified, subcloned into the pGEM-T easy vector, and then sequenced.

5'- RACE-PCR

To characterize the 5'-end of rat *Igg2b* cDNA, 5'-RACE-PCR was performed. Full-length cDNA was synthesized using SMARTer RACE 5'/3' Kit according to the manufacturer's instruction. PCR reactions were then carried out using SeqAmp DNA Polymerase, Universal Primer Short and the gene-specific primer 5'- -3'. The cycling parameters were described in (**Supp. Table 2**).

Illumina RNA sequencing.

Total RNAs were extracted using TRI Reagent (Invitrogen) from control and LPS-stimulated (24h, 48h) spinal and cortex primary astrocytes. Genomic DNA was removed by DNase I treatment (Sigma-Aldrich). RNAseq experiments were then performed in triplicate on Control or LPS-treated primary astrocytes either from the spinal cord or from the cortex. For each RNAseq sample, DNA-depleted total RNA was treated with the Ribo-Zero rRNA removal kit (Illumina) according to the manufacturer's recommendations. The rRNA-depleted RNA was then used to build the Illumina library using the TruSeq RNA library preparation kit, followed by sequencing on a flowcell S' de Novaseq a sequencer on Paired-End 25O. The RNAseq data of each sample were analyzed using both Rockhopper v2.0.3 and SPARTA with the default parameters to calculate the FPKM and TPM values for each coding sequence. The sequencing performed gave 646 million reads generated (323 M fragments) and 645 million reads (322.5 M fragments) for astrocytes from rat cortex and rat spinal cord respectively.

CRISPR-CAS9

sgRNAs were designed using the Biology software Benchling (https://benchling.com). Optimization of DNA target specificity and minimization of the off-target effects were obtained as described in [66] and in [67], respectively. sgRNAs were cloned into the plasmid LentiCRISPRv2 [68]. The corresponding lentiviruses were generated in HEK293T cells by co-transfection of LentiCRISPRv2-sgRNA with the packaging plasmids pVSVg [69] and psPAX2 [70]. Lentiviral particles were purified from the HEK293T culture supernatant and utilized for infection of the target cells. Stable knock-out of *IgH6* was obtained by selection in puromycin at 3 µg/ml. The sequences of the sgRNAs targeting IgH6 were as follows: *IgH6* CRISPR #1: 5'-TGTGACATGTAGGGCATGTA-3' (strand antisense); *IgH6* CRISPR #2: 5'-TGGTGATACAACCAGCTCCA-3' (strand sense). As a non-target control, the experiment was performed with a sgRNA targeting human Trop2: 5'- GCCACACGGCCGCGCAGGAC -3'. To evaluate the efficiency of the infection, a control, using the empty vector, was also added.

Western Blot

Total protein extracts from DI TNC1 cells, rat primary cortex, and spinal astrocytes were firstly obtained through cell lysis with RIPA buffer (150 mM NaCl, 50 mM Tris, 5 mM EGTA, 2 mM EDTA, 100 mM NaF, 10 mM sodium pyrophosphate, 1% Nonidet P-40, 1 mM PMSF, 1X

protease inhibitors). Lysates were then sonicated three times for 5 seconds with a step on the ice for 30 seconds between each sonication. After 20 minutes centrifugation at 14,000 g at 4°C, the supernatants containing the proteins were collected. Forty micrograms of proteins were reduced in Laemmli buffer containing β-Mercaptoethanol, 5 minutes denatured at 95°C and separated by SDS-PAGE. Afterward, proteins were transferred onto a nitrocellulose membrane and incubated for 1h with the blocking buffer (PBS,- 0.01% Tween 20 and 5% nonfat dry milk). The primary antibodies diluted in the blocking solution were then added and incubated overnight at 4°C. After three washes with PBS-Tween 0.01%, secondary antibodies were added and incubated for 1h at room temperature. Membranes were washed three times with PBS-Tween 0.01% and revealed with an enhanced chemiluminescence kit. Primary antibodies used were mouse anti-CD20 (1/1000), mouse anti-FLAG (1/1000), mouse anti-GFAP (1/1000), rabbit anti-Heimdall (1/1000), rabbit anti-rat IgG (1/500). The respective secondary antibodies used were HRP-conjugated goat anti-mouse (0.03 µg/mL), HRP-conjugated goat anti-rabbit (0.08 µg/mL) and HRP-conjugated mouse anti-IgGk BP. For Beta-actin Western blotting, membranes were first washed with PBS-Tween, stripped with 0.2 M citric acid for 30 minutes and washed with TBS-0.1% Tween. After saturation with blocking buffer (TBS-Tween containing 5% nonfat dry milk), mouse anti-Beta-actin diluted at 1/1000 in blocking buffer was added and incubated overnight at 4°C. After three washes with TBS-Tween, membranes were incubated with HRP-conjugated goat anti-mouse (0.03 µg/mL) for 1h at room temperature. Three washes with TBS-Tween were then performed and revelation with an enhanced chemiluminescence kit was carried out.

Two-dimensional gel electrophoresis

After 2 washes of LPS-treated DI TNC1 with an isotonic buffer (250 mM sucrose, 1 mM EDTA, 10 mM Tris HCl pH 7.5), cells were lysed in a final concentration buffer of 7 M urea, 2 M thiourea, 4% CHAPS, 40 mM DTT, 20 mM spermine base. After 30 min of incubation at RT, the lysate was centrifuged 15 min at 10,000 rpm to precipitate nucleic acids. The protein supernatant was then carefully collected, and the protein concentration estimated using a Bradford-type protein assay (Bio-Rad). Finally, 1% by volume of each carrier pharmalytes 3-10 and 4-7 (Bio-Rad) were added, and 200 µg protein aliquots were stored at -80°C until use. 2D electrophoresis was performed according to [71]. IEF was performed using 7 cm IPG Strips pH 3-10 (BioRad). IPG strips were first reswollen 30 minutes in 140 µL of solution containing 200 µg

of proteins and then incubated overnight with mineral oil. After IEF, the strips were equilibrated for 2x15 min in 6 M Urea, 30% w/v glycerol, 2% w/v SDS, 0.125 M Tris, 0.1 M HCl, containing either 50 mM DTT (first equilibration step) or 150 mM iodoacetamide (second equilibration step). The second separation was performed using 10% SDS–PAGE. After migration, the gels were fixed (50% ethanol; 0.2M orthophosphoric acid) and proteins were detected with colloidal blue staining (1 h in a mixture of 30% methanol, 0.2M orthophosphoric acid, and 170 g/l ammonium sulfate, before incubation in the same solution to which 0.66 g/L of G250 brilliant blue had been added). Then, membranes were used for Western blot.

Filter Aided Sample Preparation (FASP) protein digestion.

Forty micrograms of protein cell extracts were reduced using an equivalent volume of reduction buffer (Dithiothreitol-DTT 0.1 M) for 40 min at 56°C. After adjusting the volume to 200 µL with denaturing buffer 8M Urea, 0,1M Tris-HCL, H2O), the samples were centrifuged at 14,000 g for 30 minutes. Two hundred microliters of the denaturing buffer were again added and followed by centrifugation at 14,000 x g for 30 minutes. The filtrate was discarded and 100 µL of alkylation solution (0.05 M Iodoacetamide in denaturing buffer) was added. The samples were then incubated in the dark for 20 minutes at room temperature and centrifuged at 14,000 x g for 25 minutes. One hundred microliters of 50 mM Ammonium Bicarbonate Buffer were added and the samples were centrifuged at 14,000 g during 25 minutes. This step was repeated two times. One hundred microliters of Ammonium Bicarbonate buffer 50 mM wereadded and the samples were centrifuged at 14,000 x g during 25 minutes. This step was repeated twice. Filters were transferred into a new collection tube and 1.6 µg of Trypsin were loaded. After an overnight incubation at 37°C, samples were centrifuged at 14,000 g for 25 minutes and filters were washed with 50 µL of 0.5 M NaCl. After centrifugation at 14,000 x g for 25 minutes, 10 µL of H_2O-5% TFA were loaded to stop the digestion and samples were dried using SpeedVac. After their resuspension with 20 µL of H2O-0.1%TFA, samples were desalted using C18 Millipore ZipTip and eluted with 20 µl of elution solution (80% ACN / 20% H2O-0.1%TFA). The solution was then dried using the SpeedVac. Dried samples were solubilized in resuspension solution (2% ACN / 80% formic acid 0.1%) before LC-MS/MS analysis.

Shot-gun proteomics data analysis

RAW data obtained from the nLC-MS/MS run were treated using MaxQuant v1.6.1.0 using the LFQ annotation of the protein identified. Proteins were identified by searching MS and MS/MS data against the Decoy version of the complete proteome for *Rattus norvegicus* of the UniProt database (Release June 2014, 33,675 entries) combined with 262 commonly detected contaminants. Statistical analyses were carried out using Perseus software (version) after filtering for "reverse", and "contaminant" proteins. For the comparison between control and Forskolin-treated groups, a t-test was performed with a permutation-based FDR of 0.05, and p-values less than 0.05 were considered statistically significant. A heat-map of differentially expressed proteins across the two different groups was generated. Gene ontology (GO) analysis was performed using ClueGO [72], on Cytoscape v3.7.1 [73].

Proteogenomic analyses

The AltProt database of rat is a prediction of the possible start codon around the classical Open Reading Frame (ORF), permitting the prevision of proteins on UTR, overlapping between UTR and coding sequence (CDS, and shift of ORF in +2 and +3 and conserving an initiator AUG codon. This database was combined with the reference Uniprot database on the same FASTA file. Label-Free Quantification (LFQ) was performed by MaxQuant 1.5.6.5. During this analysis, principal parameters were assigned as follows: Trypsin digestion with maximum missed cleavage of 2, carbamidomethylation as a fixed modification, and oxidation as a variable modification. The first search peptide tolerance was adjusted at 20 ppm and the main search peptide at 6 ppm. Finally, the minimum peptide length was restricted to 6 amino acids. The length of this kind of protein, a mean of 50 to 100 amino acids, obliges to decrease the number of unique peptides identified at 1. Statistical analysis was performed with Perseus 1.5.5.3, log2(x) was then realized and results were filtrated to eliminate identification by site as well as reverse and potential contaminants. Significant variations between samples were assessed by t-test. Filtration for AltProt was applied to keep only the AltProt identified with a unique peptide and no classical protein redundancy on Majority ID. Variation of quantification was revealed by hierarchical clustering with Euclidian distance measurement. Identification of AltProt was performed using BlastP and non-redundant protein sequences to find their

sequence homology with cannonical and unknown proteins. The gene accession numbers were used to retrieve mRNA or ncRNA sequences from the Ensembl database.

Sub-network Enrichment Pathway Analysis.

Using Elsevier's Pathway Studio (version 11.0/ /Elsevier), all relationships between the differentially expressed proteins among all conditions were depicted based on the Ariadne ResNet ([74]. For proteins identified in the shotgun analysis, the Subnetwork Enrichment Analysis (SNEA) algorithm was used to detect the statistically significant altered biological pathways in which the identified proteins are involved. This algorithm uses Fisher's statistical test to detect any non-random associations between two categorical variables organized by a specific relationship. Also, this algorithm starts by creating a central "seed" from all the relevant identities in the database and builds connections with associated entities based on their relationship with the seed. SNEA compares the sub-network distribution to the background distribution using a one-sided Mann-Whitney U- Test and calculates a p-value; thus, representing a statistical significance between different distributions. In all analyses that we performed, the GenBank ID was used to form experimental groups based on the different conditions present for analysis. The pathway networks were reconstructed based on biological processes and molecular functions for every single protein, along with its associated targets.

Cloning of rat astrocyte IgG2B coding sequence in pcDNA5 FRT/TO C-ter BirA*Flag expression vector

Rat astrocyte IgH6 proteins coding sequences were cloned into pcDNA5 FRT/TO C-ter BirA*Flag vector. All clones were sequenced and verified before co-transfection with pOG44 in Flp-In™ T-REx™ HEK293 cells. The construction includes a signal peptide and the sequence coding the IgG2B transmembrane form (ATGGAGTTTGGGCTGAGCTGGGTTTTCCTTGTTGTTATTTTACAAGGTGTCCAGTGT**G** *CC CAAACAAC AGCCCCATCT GTCTATCCAC TGGCTCCTGG ATGTGGTGAT ACAACCAGCT CCACGGTGAC CCTGGGATGC CTGGTCAAGG GCTATTTCCC TGAGCCAGTC ACCGTGACCT GGAACTCTGGAGCCCTGTCC AGCGATGTGC ACACCTTCCC AGCTGTCCTG CAGTCTGGGC TCTACACTCT CACCAGCTCA GTGACCTCCA GCACCTGGCC CAGCCAGACC GTCACCTGCA ACGTAGCCCA CCCGGCCAGCAGCACCAAGG TGGACAAGAA AATTGAGCGC AGAAATGACA ACATTGGACA CAAAAGC CCTACATGCC CTACATGTCA CAAATGCCCA GCTCCTGAAC*

TCTTGGGTGG ACCATCCGTC TTCATCTTCCCCCCAAAGCC CAAGGACATC CTCTTGATCT CCCAGAACGC CAAGGTCACG TGTGTGGTGG TGGATGTGAG CGAGGAGGAG CCGGACGTCC AGTTCAGCTG GTTTGTGAAC AACGTAGAAG TACACACAGCTCAGACACAA CCCCGTGAGG AGCAGTACAA CAGCACCTTC AGAGTGGTCA GTGCCCTCCC CATCCAGCAC CAGGACTGGA TGAGCGGCAA GGAGTTCAAA TGCAAGGTCA ACAACAAAG CCCTCCCAAGCCCCATCGAG AAAACCATCT CAAAACCCAA AGGGCTAGTC AGAAAACCAC AGGTATACGT CATGGGTCCA CCGACAGAGC AGTTGACTGA GCAAACGGTC AGTTTGACCT GCTTGACCTC AGGCTTCCTCCCTAACGACA TCGGTGTGGA GTGGACCAGC AACGGGCATA TAGAAAAGAA CTACAAGAAC ACCGAGCCAG TGATGGACTC TGACGGTTCT TTCTTCATGT ACAGCAAGCT CAATGTGGAA AGGAGCAGGTGGGATAGCAG AGCGCCCTTC GTCTGCTCCG TGGTCCACGA GGGTCTGCAC AATCACCACG TGGAGAAGAG CATCTCCCGG CCTCCG

GGG CTAGAAGTGGA TGATGATTGT GCTGAGGCTC AGGACGGGGAGCTGGACGGG CTCTGGACGA CCATCACCAT CTTCATCAGC CTCTTCCTGC TCAGTGTGTG CTACAGTGCC TCCATCACAC TCTTCAAGGT AAAGTGGATC TTCTCCTCAG TGGTGGAGCT GAAGCAGACAATC TCCC CTGACTACAG AAACATGATT GGTCAAGGAG CC TAG). As a control, another construction displaying a signal peptide and the sequence coding for the Transmembrane domain only was built. (ATGGAGTTTGGGCTGAGCTGGGTTTTCCTTGTTGTTATTTTACAAGGTGTCCAGTGT GG G CTAGAAGTGGA TGATGATTGT GCTGAGGCTC AGGACGGGGAGCTGGACGGG CTCTGGACGA CCATCACCAT CTTCATCAGC CTCTTCCTGC TCAGTGTGTG CTACAGTGCC TCCATCACAC TCTTCAAGGT AAAGTGGATC TTCTCCTCAG TGGTGGAGCT GAAGCAGACAATC TCCC CTGACTACAG AAACATGATT GGTCAAGGAG CC TAG).

Overexpression of rat astrocyte IgG2b-Flag in DI TNC1 cells

DI TNC1 cells were plated in 6 well plates and grown in a complete medium until they reached about 80% confluence. One hour before the transfection, the medium was renewed. One microgram of the construct was mixed with 50 µL of DMEM-free medium and 3 µL of PolyJet were mixed with 50 µL of DMEM-free medium in another tube. The two solutions were mixed and after an incubation of 15 minutes at room temperature, the mixture was added to the cells. After an overnight incubation, the medium was replaced by fresh complete medium. After 24, 48, or 72 h western blots were carried out.

Characterization of IgG2B (IgH6) patterns in HEK293 cells

BioID samples were prepared as follows. Briefly, Flp-In™ T-REx™ HEK293 cells were grown in DMEM supplemented with 10% FBS GlutaMAX™ and Penicillin-Streptomycin (1x). Using the Flp-In system, Flp-In™ T-REx™ HEK293 stably expressing BirA*Flag alone and signal peptide with transmembrane domain (for control samples), or C-terminally tagged IgH bait proteins were generated co-transfecting pOG44 with pcDNA5 FRT/TO IgH BirA*Flag bait protein sequence plasmid. After selection (DMEM + 10% FBS + P/S + 200 µg/ml hygromycin B), three independent replicates of two 150 cm2 plates of sub-confluent (60%) cells were incubated for 24 h in complete media supplemented with 1 µg/ml tetracycline (Sigma), 50 µM biotin. Cells were collected and pelleted by centrifugation at 300 x g for 3 minutes. After two washes with PBS, dried pellets were snap frozen. Each cell pellet was resuspended in 5 ml of lysis buffer (50 mM Tris-HCl pH 7.5, 150 mM NaCl, 1 mM EDTA, 1 mM EGTA, 1% Triton X-100, 0.1% SDS, 1:500 protease inhibitor cocktail, 1:1,000 Turbonuclease and incubated on an end-over-end rotator at 4°C for 1 hour, briefly sonicated to disrupt any visible aggregates, then centrifuged at 45,000 x g for 30 minutes at 4°C. The supernatant was transferred to a fresh 15 mL conical tube. Twenty-five microliters of packed, pre-equilibrated Streptavidin Ultralink Resin was added, and the mixture was incubated for 3 hours at 4°C with end-over-end rotation. Beads were pelleted by centrifugation at 300 x g for 2 minutes and transferred with 1 mL of lysis buffer to a fresh tube. Beads were washed once with 1 mL of lysis buffer and twice with 1 mL of 50 mM ammonium bicarbonate (pH=8.3), then transferred in ammonium bicarbonate to a fresh centrifuge tube and washed two more times with 1 ml of ammonium bicarbonate buffer. Tryptic digestion was performed by incubating the beads with 1 µg MS-grade TPCK trypsin dissolved in 200 µl of 50 mM ammonium bicarbonate (pH 8.3) overnight at 37°C. The following morning, 0.5 µg MS-grade TPCK trypsin was added to the beads and incubated for 2 additional hours at 37°C. Following centrifugation at 2,000 x g for 2 min, the supernatant was collected and transferred to a fresh tube. Two additional washes were performed with 150 µL of 50 mM ammonium bicarbonate and pooled with the first eluate. The sample was lyophilized and resuspended in buffer A (2% ACN 0.1% formic acid). 1/3rd of each sample was analyzed per mass spectrometer run.

BioID data acquisition.

The samples were separated by online reversed-phase chromatography using a Thermo Scientific Easy-nLC1000 system equipped with a Proxeon trap column (75 µm ID x 2 cm, 3 µm, Thermo Scientific,) and a C18 packed-tip column (Acclaim PepMap, 75 µm ID x 50 cm, 2 µm, Thermo Scientific). The digested peptides were separated using an increasing amount of acetonitrile in 0.1% formic acid from 2 to 30% for 2 hours at a flow rate of 300 nL/min. A voltage of 2.4 kV was applied by the liquid junction to electrospray the eluent using the nanospray source. A high-resolution mass spectrometer Q-Exactive™ Thermo Scientific™ was coupled to the chromatography system to acquire the 10 most intense ions of MS1 analysis (Top 10) in a data-dependent mode. The MS analyses were performed in positive mode at a resolving power of 70,000 FWHM, using an automatic gain control target of 3e6, the default charge state was set at 2 and a maximum injection time at 120 ms. For full scan MS, the scan range was set between m/z 300 to 1600. For ddMS², the scan range was between m/z 200 to 2000, 1 Microscan was acquired at 17,500 FWHM, an AGC was set at 5e4 ions and an isolation window of m/z 4,0 was used.

BioID data analysis.

The proteins were identified by comparing all MS/MS data with the Homo sapiens proteome database (Uniprot, release March 2020, Canonical+ Isoforms, comprising 42,360 entries), using the MaxQuant software version 1.5.8.3. The digestion parameters were defined using trypsin with 2 maximum missed cleavages. The oxidation of methionine and N-terminal protein acetylation were defined as variable modifications. The Label-free quantification (LFQ) was done while keeping the default parameters of the software. As for initial mass tolerance, 6 ppm was selected for MS mode, and 20 ppm was set for fragmentation data to match MS/MS tolerance. The identification parameters of the proteins and peptides were performed with a false discovery rate (FDR) at 1%, and a minimum of 2 unique peptides per protein. The LFQ values from the 20 control runs (regrouping FlagBirA* and BirA*Flag alone samples), were collapsed to the three highest values for each given ID. These three values were defined as the control group for comparison. The statistical analysis was done using Perseus software (version 1.6.2.3). Briefly, the LFQ intensity of each sample was downloaded in Perseus and the data matrix was filtered by removing the potential contaminants, reverse, and only identified

by site. The data were then transformed using the log2(x) function. Only preys with detected values in all three replicates of a given the bait protein were kept for further analysis. Missing values (not detected) were then replaced by the minimal valid LFQ value separately for each column. Two-sample Student's T-test was then performed comparing all three biological replicates the bait against the three control runs. High confidence proximal labeling interactors were defined with a cut-off of $p<0.05$. Detailed experimental values are reported in Supplemental Data 7.

References

1. Rougon, G. & Hobert, O. New insights into the diversity and function of neuronal immunoglobulin superfamily molecules. *Annual review of neuroscience* **26**, 207-238 (2003).
2. Zinn, K. & Özkan, E. Neural immunoglobulin superfamily interaction networks. *Current opinion in neurobiology* **45**, 99-105 (2017).
3. Maness, P.F. & Schachner, M. Neural recognition molecules of the immunoglobulin superfamily: signaling transducers of axon guidance and neuronal migration. *Nature neuroscience* **10**, 19-26 (2007).
4. Williams, A.F. & Gagnon, J. Neuronal cell Thy-1 glycoprotein: homology with immunoglobulin. *Science* **216**, 696-703 (1982).
5. Avalos, A.M. *et al.* Neuronal Thy-1 induces astrocyte adhesion by engaging syndecan-4 in a cooperative interaction with αvβ3 integrin that activates PKCα and RhoA. *Journal of cell science* **122**, 3462-3471 (2009).
6. Tiveron, M.-C. *et al.* Selective inhibition of neurite outgrowth on mature astrocytes by Thy-1 glycoprotein. *Nature* **355**, 745-748 (1992).
7. Scheurer, L. *et al.* Expression of immunoglobulin constant domain genes in neurons of the mouse central nervous system. *Life science alliance* **4** (2021).
8. Capuz, A. *et al.* The Antibody Dependant Neurite Outgrowth Modulation Response Involvement in Spinal Cord Injury. *Front Immunol* **13**, 882830 (2022).
9. Osien, S. *et al.* Heimdall, a Ghost protein related to kappa light chain variable region, is a key player in Astrocyte-to-neuron reprogramming. *Submitted* (Submitted).
10. Devaux, S. *et al.* Proteomic analysis of the spatio-temporal based molecular kinetics of acute spinal cord injury identifies a time- and segment-specific window for effective tissue repair. *Mol Cell Proteomics* (2016).
11. Ankeny, D.P. & Popovich, P.G. B cells and autoantibodies: complex roles in CNS injury. *Trends Immunol* **31**, 332-338 (2010).
12. Holsapple, M.P., West, L.J. & Landreth, K.S. Species comparison of anatomical and functional immune system development. *Birth Defects Research Part B: Developmental and Reproductive Toxicology* **68**, 321-334 (2003).
13. Devaux, S. *et al.* RhoA Inhibitor Treatment At Acute Phase of Spinal Cord Injury May Induce Neurite Outgrowth and Synaptogenesis. *Molecular & cellular proteomics : MCP* **16**, 1394-1415 (2017).
14. Cizkova, D. *et al.* Modulation properties of factors released by bone marrow stromal cells on activated microglia: an in vitro study. *Scientific reports* **4**, 7514 (2014).

15. Battaglia, R.A. *et al.* Site-specific phosphorylation and caspase cleavage of GFAP are new markers of Alexander disease severity. *Elife* **8** (2019).
16. Barlow-Anacker, A.J., Fu, M., Erickson, C.S., Bertocchini, F. & Gosain, A.J.S.r. Neural crest cells contribute an astrocyte-like glial population to the spleen. **7**, 45645 (2017).
17. Danielyan, L., Gebhardt, R. & Buniatian, G. Expression of glial fibrillary acidic protein in the rat endocard, cardiac interstitial Cajal-like cells, and perivascular structures of the spleen. *Neurochemical Journal* **2**, 293-296 (2008).
18. Lefranc, M.-P. *et al.* IMGT unique numbering for immunoglobulin and T cell receptor constant domains and Ig superfamily C-like domains. *Developmental & Comparative Immunology* **29**, 185-203 (2005).
19. Devaux, S. *et al.* Proteomic Analysis of the Spatio-temporal Based Molecular Kinetics of Acute Spinal Cord Injury Identifies a Time- and Segment-specific Window for Effective Tissue Repair. *Molecular & cellular proteomics : MCP* **15**, 2641-2670 (2016).
20. Capuz, A. *et al.* The Antibody Dependant Neurite Outgrowth Modulation Response (ADNM) involvement in Spinal Cord Injury. *Frontiers Immunol.* **13** (2022).
21. Gerçel-Taylor, Ç., Bazzett, L.B. & Taylor, D.D. Presence of aberrant tumor-reactive immunoglobulins in the circulation of patients with ovarian cancer. *Gynecologic oncology* **81**, 71-76 (2001).
22. Owen, J.A., Punt, J. & Stranford, S.A. *Kuby immunology*. (WH Freeman New York, NY, USA:, 2013).
23. Cao, X., Pfaff, S.L. & Gage, F.H. YAP regulates neural progenitor cell number via the TEA domain transcription factor. *Genes & development* **22**, 3320-3334 (2008).
24. Ravid, S. The tumor suppressor Lgl1 regulates front-rear polarity of migrating cells. *Cell adhesion & migration* **8**, 378-383 (2014).
25. Laffita-Mesa, J.M., Paucar, M. & Svenningsson, P. Ataxin-2 gene: a powerful modulator of neurological disorders. *Current Opinion in Neurology* **34**, 578 (2021).
26. Subramanian, A. *et al.* Gene set enrichment analysis: a knowledge-based approach for interpreting genome-wide expression profiles. *Proceedings of the National Academy of Sciences* **102**, 15545-15550 (2005).
27. Smoot, M.E., Ono, K., Ruscheinski, J., Wang, P.-L. & Ideker, T. Cytoscape 2.8: new features for data integration and network visualization. *Bioinformatics* **27**, 431-432 (2011).
28. Orr, B.A. *et al.* Yes-associated protein 1 is widely expressed in human brain tumors and promotes glioblastoma growth. *J Neuropathol Exp Neurol* **70**, 568-577 (2011).
29. Kaye, F.J. Mutation-associated fusion cancer genes in solid tumors. *Mol Cancer Ther* **8**, 1399-1408 (2009).
30. de Melo Reis, R.A., Freitas, H.R. & De Mello, F.G. Cell calcium imaging as a reliable method to study neuron–glial circuits. *Frontiers in Neuroscience* **14**, 569361 (2020).
31. Miyara, A. *et al.* Novel and conserved protein macoilin is required for diverse neuronal functions in Caenorhabditis elegans. *PLoS genetics* **7**, e1001384 (2011).
32. Lees, J.A. *et al.* Lipid transport by TMEM24 at ER–plasma membrane contacts regulates pulsatile insulin secretion. *Science* **355**, eaah6171 (2017).
33. Kageyama, T. *et al.* The 4F2hc/LAT1 complex transports L-DOPA across the blood–brain barrier. *Brain research* **879**, 115-121 (2000).
34. Console, L. *et al.* N-glycosylation is crucial for trafficking and stability of SLC3A2 (CD98). *Scientific reports* **12**, 1-10 (2022).

35. Leung-Hagesteijn, C., Mahendra, A., Naruszewicz, I. & Hannigan, G.E. Modulation of integrin signal transduction by ILKAP, a protein phosphatase 2C associating with the integrin-linked kinase, ILK1. *The EMBO journal* **20**, 2160-2170 (2001).
36. Nawashiro, H. *et al.* The role of CD98 in astrocytic neoplasms. *Human cell* **15**, 25-31 (2002).
37. Staflin, K., Zuchner, T., Honeth, G., Darabi, A. & Lundberg, C. Identification of proteins involved in neural progenitor cell targeting of gliomas. *BMC cancer* **9**, 1-14 (2009).
38. Han, K.S. *et al.* Activation of protease activated receptor 1 increases the excitability of the dentate granule neurons of hippocampus. *Mol Brain* **4**, 32 (2011).
39. Nakamura, Y. *et al.* Expression of tubulin beta II in neural stem/progenitor cells and radial fibers during human fetal brain development. *Laboratory investigation* **83**, 479-489 (2003).
40. Desclaux, M. *et al.* A novel and efficient gene transfer strategy reduces glial reactivity and improves neuronal survival and axonal growth in vitro. *PloS one* **4**, e6227 (2009).
41. Schiff, C., Milili, M. & Fougereau, M. Functional and pseudogenes are similarly organized and may equally contribute to the extensive antibody diversity of the IgVHII family. *The EMBO journal* **4**, 1225-1230 (1985).
42. Rothenfluh, H.S., Blanden, R.V. & Steele, E.J. Evolution of V genes: DNA sequence structure of functional germline genes and pseudogenes. *Immunogenetics* **42**, 159-171 (1995).
43. Frank, M.B. & Gutman, G.A. Two pseudogenes among three rat immunoglobulin lambda chain genes. *Molecular immunology* **25**, 953-960 (1988).
44. Balakirev, E.S. & Ayala, F.J. Pseudogenes: are they “junk” or functional DNA? *Annual review of genetics* **37**, 123-151 (2003).
45. Pink, R.C. *et al.* Pseudogenes: pseudo-functional or key regulators in health and disease? *Rna* **17**, 792-798 (2011).
46. Vihinen, M. Contribution of pseudogenes to sequence diversity. *Pseudogenes*, 15-24 (2014).
47. Lucas, T.A., Zhu, L. & Buckwalter, M.S. Spleen glia are a transcriptionally unique glial subtype interposed between immune cells and sympathetic axons. *Glia* **69**, 1799-1815 (2021).
48. Wang, Y., Zhang, X., Chen, F., Song, N. & Xie, J. In vivo Direct Conversion of Astrocytes to Neurons Maybe a Potential Alternative Strategy for Neurodegenerative Diseases. *Frontiers in Aging Neuroscience*, 474 (2021).
49. Mallah, K. *et al.* Neurotrauma investigation through spatial omics guided by mass spectrometry imaging: Target identification and clinical applications. *Mass spectrometry reviews* (2021).
50. Cizkova, D. *et al.* Spinal Cord Injury: Animal Models, Imaging Tools and the Treatment Strategies. *Neurochem Res* (2019).
51. Cizkova, D. *et al.* Localized Intrathecal Delivery of Mesenchymal Stromal Cells Conditioned Medium Improves Functional Recovery in a Rat Model of Spinal Cord Injury. *Int J Mol Sci* **19** (2018).
52. Cizkova D. *et al.* Understanding molecular pathology along injured spinal cord axis: moving frontiers toward effective neuroprotection and regeneration. *InTech* (2017).
53. Cizkova, D. *et al.* Alterations of protein composition along the rostro-caudal axis after spinal cord injury: proteomic, in vitro and in vivo analyses. *Front Cell Neurosci* **8**, 105 (2014).

54. Zeng, P. *et al.* Neonatal cortical astrocytes possess intrinsic potential in neuronal conversion in defined media. *Acta Pharmacologica Sinica*, 1-12 (2021).
55. Doetsch, F., Caille, I., Lim, D.A., García-Verdugo, J.M. & Alvarez-Buylla, A. Subventricular zone astrocytes are neural stem cells in the adult mammalian brain. *Cell* **97**, 703-716 (1999).
56. Seri, B., Garcıa-Verdugo, J.M., McEwen, B.S. & Alvarez-Buylla, A. Astrocytes give rise to new neurons in the adult mammalian hippocampus. *Journal of Neuroscience* **21**, 7153-7160 (2001).
57. Heins, N. *et al.* Glial cells generate neurons: the role of the transcription factor Pax6. *Nature neuroscience* **5**, 308-315 (2002).
58. di Val Cervo, P.R. *et al.* Induction of functional dopamine neurons from human astrocytes in vitro and mouse astrocytes in a Parkinson's disease model. *Nature biotechnology* **35**, 444-452 (2017).
59. Yang, H. *et al.* Sonic hedgehog effectively improves Oct4-mediated reprogramming of astrocytes into neural stem cells. *Molecular Therapy* **27**, 1467-1482 (2019).
60. Qian, H. *et al.* Reversing a model of Parkinson's disease with in situ converted nigral neurons. *Nature* **582**, 550-556 (2020).
61. Lavado, A. *et al.* The Hippo Pathway Prevents YAP/TAZ-Driven Hypertranscription and Controls Neural Progenitor Number. *Dev Cell* **47**, 576-591 e578 (2018).
62. Kitazono, T. *et al.* Multiple signaling pathways coordinately regulate forgetting of olfactory adaptation through control of sensory responses in Caenorhabditis elegans. *Journal of Neuroscience* **37**, 10240-10251 (2017).
63. Poplawski, S.G. *et al.* Contextual fear conditioning induces differential alternative splicing. *Neurobiology of learning and memory* **134**, 221-235 (2016).
64. Arellano-Carbajal, F. *et al.* Macoilin, a conserved nervous system–specific ER membrane protein that regulates neuronal excitability. *PLoS genetics* **7**, e1001341 (2011).
65. Su, K.Y., Watanabe, A., Yeh, C.H., Kelsoe, G. & Kuraoka, M. Efficient Culture of Human Naive and Memory B Cells for Use as APCs. *J Immunol* **197**, 4163-4176 (2016).
66. Hsu, P.D. *et al.* DNA targeting specificity of RNA-guided Cas9 nucleases. *Nature biotechnology* **31**, 827-832 (2013).
67. Doench, J.G. *et al.* Optimized sgRNA design to maximize activity and minimize off-target effects of CRISPR-Cas9. *Nature biotechnology* **34**, 184-191 (2016).
68. Sanjana, N.E., Shalem, O. & Zhang, F. Improved vectors and genome-wide libraries for CRISPR screening. *Nature methods* **11**, 783-784 (2014).
69. Ryø, L.B., Thomsen, E.A. & Mikkelsen, J.G. Production and validation of lentiviral vectors for CRISPR/Cas9 delivery, in *CRISPR Gene Editing* 93-109 (Humana Press, New York, NY, 2019).
70. Ke, X. *et al.* A single mutation in the VP1 gene of enterovirus 71 enhances viral binding to heparan sulfate and impairs viral Pathogenicity in mice. *Viruses* **12**, 883 (2020).
71. Wilmet, J.P. *et al.* Proteome changes induced by overexpression of the p75 neurotrophin receptor (p75NTR) in breast cancer cells. *Int J Dev Biol* **55**, 801-809 (2011).
72. Lee, I.-Y., Ho, J.-M. & Chen, M.-S. in Fifth IEEE International Conference on Data Mining (ICDM'05) 4 pp. (IEEE, 2005).
73. Lopes, C.T. *et al.* Cytoscape Web: an interactive web-based network browser. *Bioinformatics* **26**, 2347-2348 (2010).

74. Yuryev, A., Kotelnikova, E. & Daraselia, N. Ariadne's ChemEffect and Pathway Studio knowledge base. *Expert Opin Drug Discov* **4**, 1307-1318 (2009).

Figures

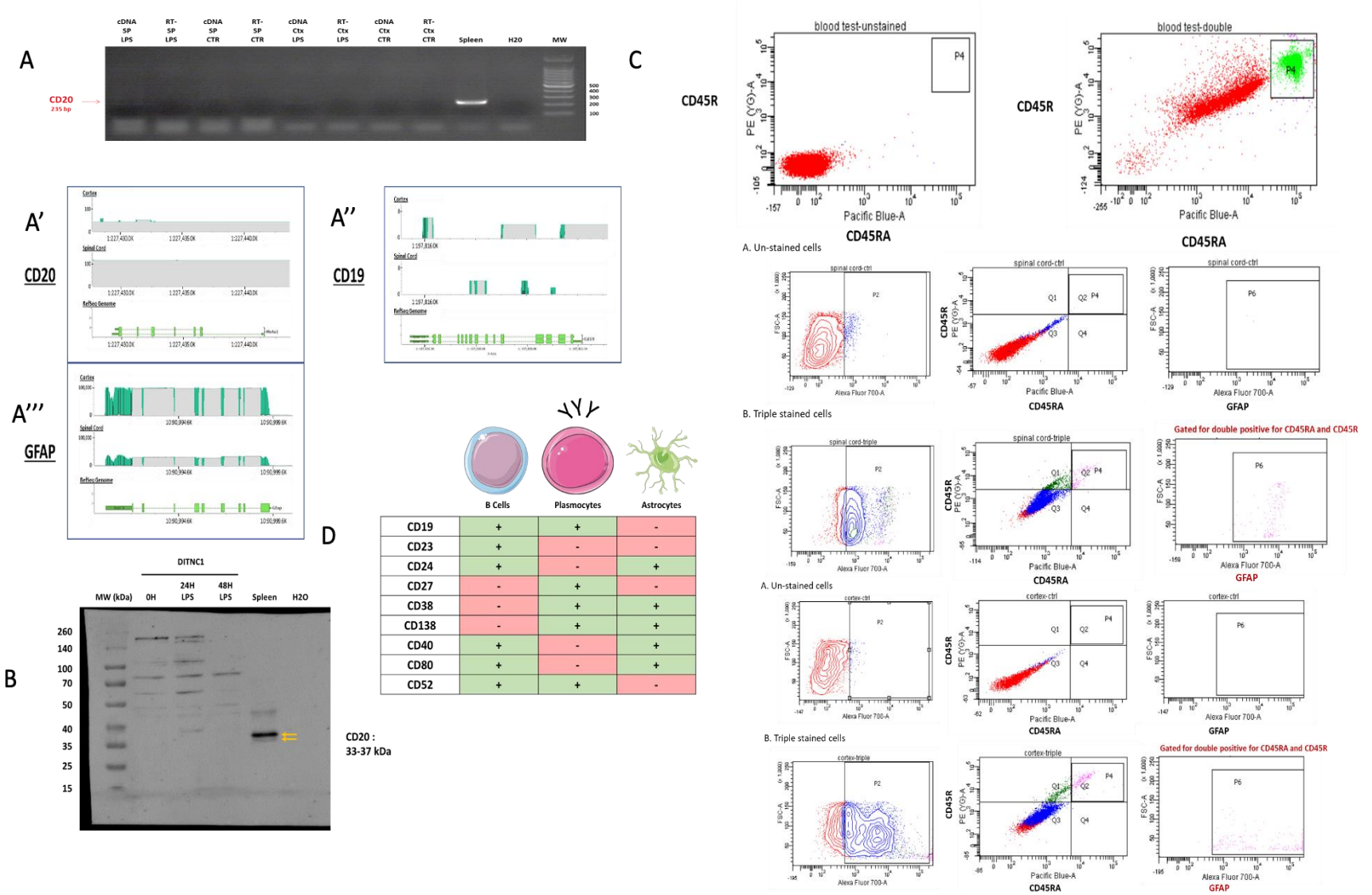
A
cDNA SP LPS
RT- SP LPS
cDNA SP CTR
RT- SP CTR
cDNA Ctx LPS
RT- Ctx LPS
cDNA Ctx CTR
RT- Ctx CTR
Spleen
H20
MW
CD20
235 bp
A'
CD20
A''
CD19
A'''
GFAP
B
DITNC1
MW (kDa)
0H
24H LPS
48H LPS
Spleen
H2O
260
140
100
70
50
40
35
25
15
CD20 :
33-37 kDa
C
CD45R
CD45RA
blood test-unstained
blood test-double
A. Un-stained cells
B. Triple stained cells
spinal cord-ctrl
spinal cord-triple
cortex-ctrl
cortex-triple
Gated for double positive for CD45RA and CD45R
GFAP
D
B Cells
Plasmocytes
Astrocytes
CD19 + + -
CD23 + - -
CD24 + - +
CD27 - + -
CD38 - + +
CD138 - + +
CD40 + - +
CD80 + - +
CD52 + + -

Figure 1 : **Validation that primary cultures of the cortex and spinal astrocytes are devoid of B cells**. **A)** RT-PCR amplification of *Cd20* in rat DI TNC1 astrocyte cell line and rat primary cortex and spinal astrocytes stimulated or not with 200 ng/mL of LPS. cDNA from the spleen served as a positive control. The experiment was also performed on a negative reverse transcriptase sample to rule out genomic DNA contamination. H_20: negative control. **A'** RNAseq analyses of *Cd20*, **A''** *Cd19* or **A'''** *Gfap* in rat primary cortex and spinal cord astrocytes. **B)** Western blot analyses of CD20 in spleen and DI TNC1 cells stimulated or not with 200 ng/mL of LPS during 24h and 48H. **C)** Flow cytometry analyses of primary cultures of the cortex and spinal astrocytes with CD45R - CD45RA double labeling and CD45R - CD45RA - GFAP triple labeling. Rat blood served as a positive control. **D**) Comparison of CD markers found in B lymphocytes, plasmocytes and astrocytes (RNAseq data).

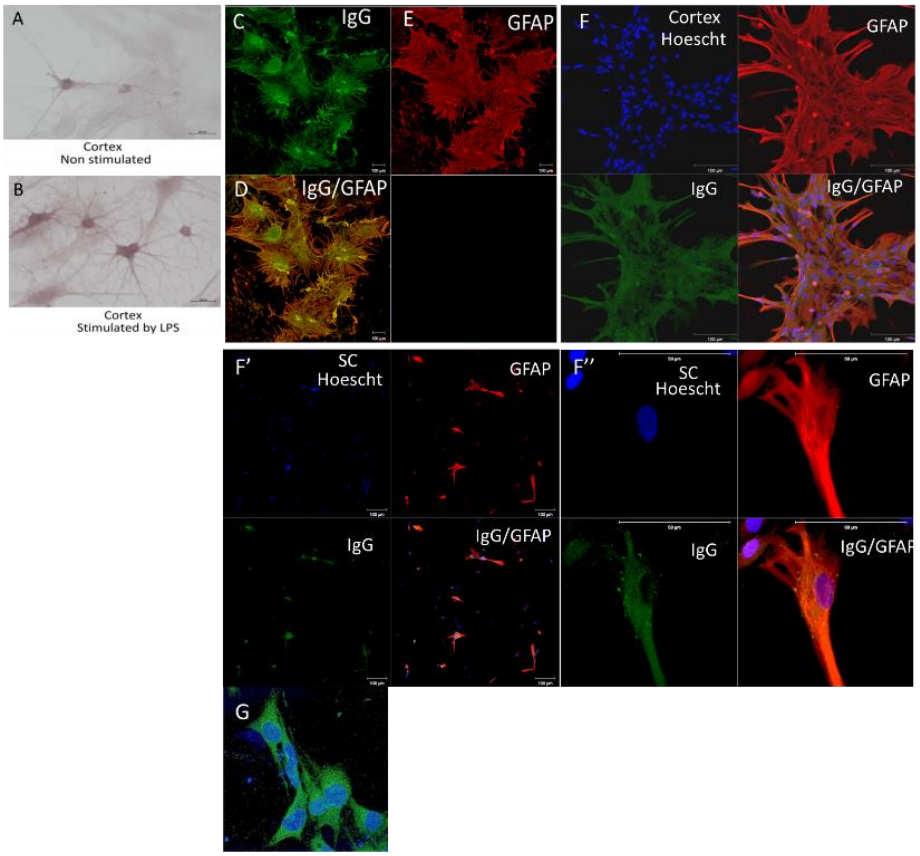
A
Cortex
Non stimulated
B
Cortex
Stimulated by LPS
C
IgG
E
GFAP
F
Cortex
Hoescht
GFAP
D
IgG/GFAP
IgG
IgG/GFAP
F'
SC
Hoescht
GFAP
F''
SC
Hoescht
GFAP
IgG
IgG/GFAP
IgG
IgG/GFAP
G

H

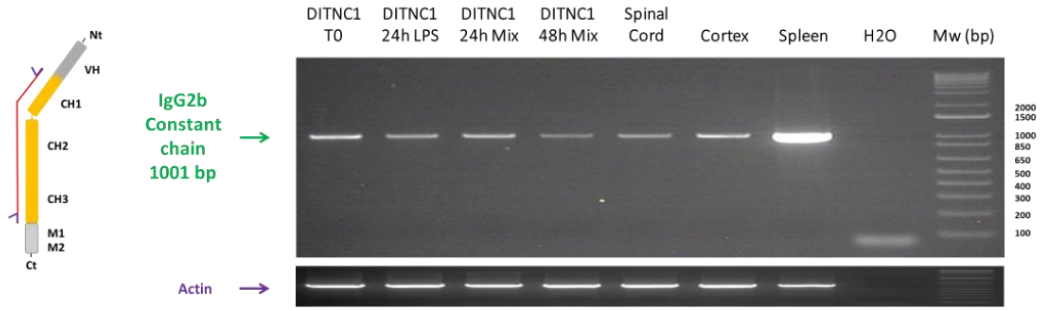
DITNC1 T0
DITNC1 24h LPS
DITNC1 24h Mix
DITNC1 48h Mix
Spinal Cord
Cortex
Spleen
H2O
Mw (bp)
Nt
VH
CH1
CH2
CH3
M1
M2
Ct
IgG2b Constant chain 1001 bp
Actin
2000
1500
1000
850
650
500
400
300
200
100

I

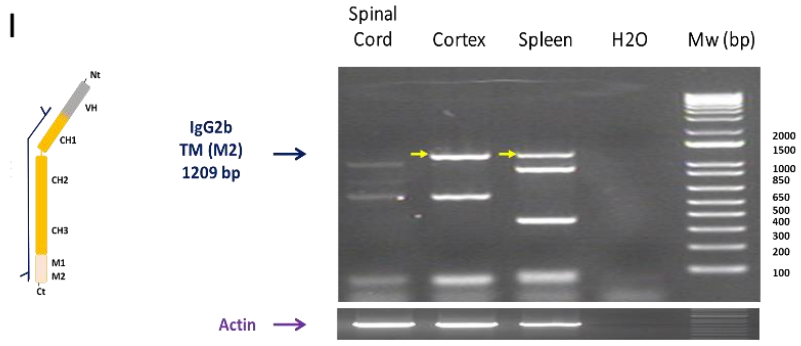
Spinal Cord
Cortex
Spleen
H2O
Mw (bp)
Nt
VH
CH1
CH2
CH3
M1
M2
Ct
IgG2b TM (M2) 1209 bp
Actin
2000
1500
1000
850
650
500
400
300
200
100

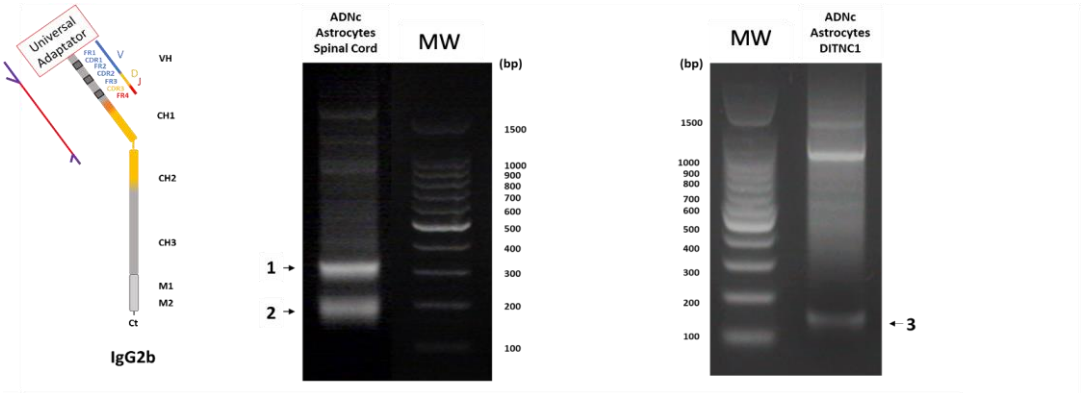
Universal Adaptator
VH
CH1
CH2
CH3
M1
M2
Ct
IgG2b
ADNc Astrocytes Spinal Cord
MW
(bp)
1500
1000
900
800
700
600
500
400
300
200
100
1
2
MW
ADNc Astrocytes DITNC1
(bp)
1500
1000
900
800
700
600
500
400
300
200
100
3

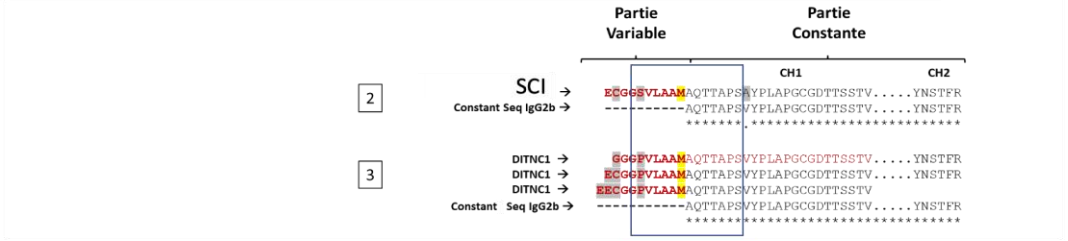
Partie Variable
Partie Constante
CH1
CH2
2
SCI
Constant Seq IgG2b
3
DITNC1
DITNC1
DITNC1
Constant Seq IgG2b

K

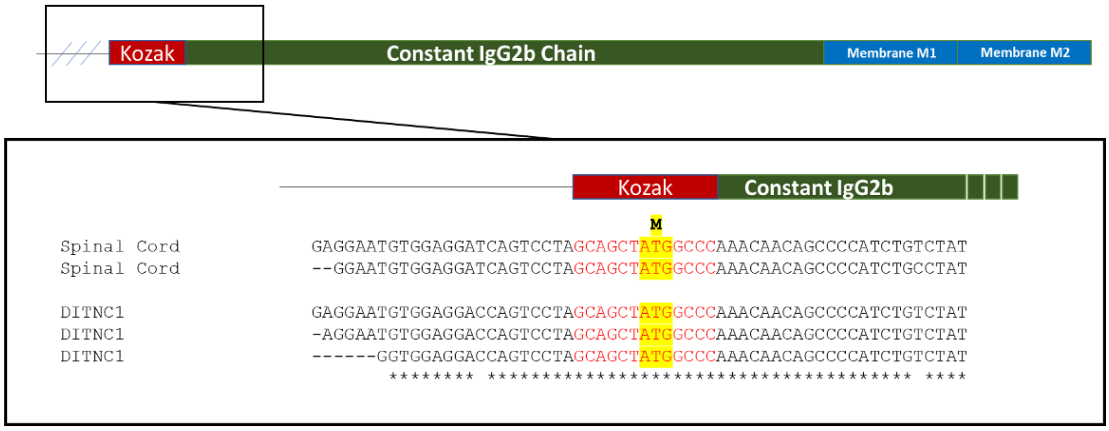
Kozak
Constant IgG2b Chain
Membrane M1
Membrane M2
Kozak
Constant IgG2b
M
Spinal Cord
Spinal Cord
DITNC1
DITNC1
DITNC1

L

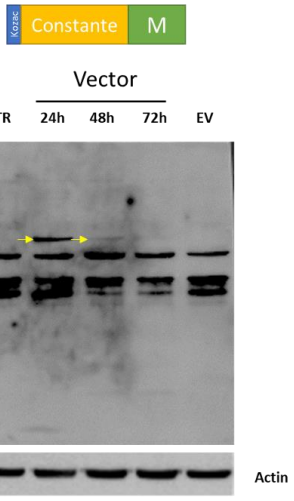
Kozac
Constante
M
Vector
Mw (kDa)
CTR
24h
48h
72h
EV
140
100
70
50
40
35
25
15
10
Actin

Figure 2 : **Identification of immunoglobulin constant heavy chain in astrocytes.** Immunocytochemical labeling of rat primary cortex astrocytes control **A)** or stimulated with 200 ng/mL of LPS **B)** using anti-IgG or **C-E**) Immunofluorescence with anti-GFAP and anti-IgG performed on rat primary cortex astrocytes controls. **F)** rat primary cortex astrocytes stimulated with 200 ng/mL of LPS during 48H **F')** rat primary spinal astrocytes stimulated with 200 ng/mL of LPS during 48H, **F'')** magnification of the double staining observed in rat primary spinal astrocytes, **G)** Immunofluorescence with anti-IgG carried out on DI TINC1 cells, **H)** RT-PCR amplification of the complete sequence coding IgG2B constant heavy chain in rat DI TNC1 astrocyte cell line stimulated or not with 200 ng/mL of LPS during 24h or a mix of cytokines for 24h and 48h as well as in rat primary cortex and spinal astrocytes. **I)** Amplification of the mRNA coding the IgG2B transmembrane form. cDNA from the spleen served as a positive control. The experiment was also performed on a negative reverse transcriptase sample to rule out genomic DNA contamination. H_20: negative control. **J)** 5'-RACE-PCR was performed on a cDNA library of DI TNC1 cells or astrocytes from the spinal cord to amplify the whole *IgG2B* mRNA. Three bands were amplified and sequenced. This revealed that no variable coding sequence was linked to IgG2B coding sequence. However, the presence of a Kozak sequence flanking the 5'-end of IgG2B coding sequence was identified in bands 2 and 3, indicating that this transcript encoded a free IgG2B constant chain. **K**) 5' Kozak sequence of the IgG2B sequence **L)** Overexpression of rat astrocyte IgG2B transmembrane form in fusion with Flag Tag in DI TNC1 cells. Western blot analysis using an antibody directed against the Flag tag was carried out 24h, 48h, or 72h after transfection. Non-transfected cells and transfection with an empty vector served as negative controls.

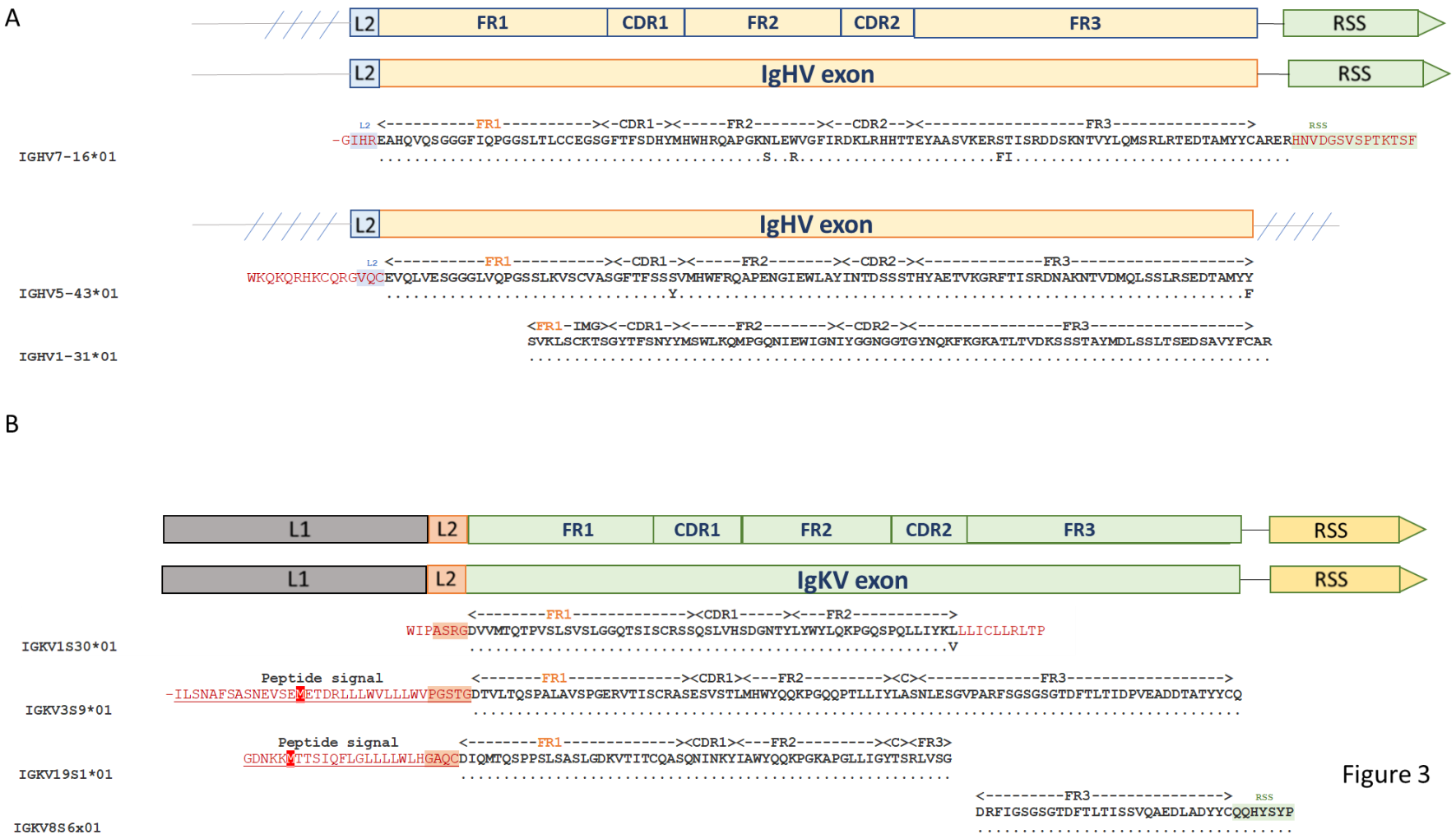
A
L2
FR1
CDR1
FR2
CDR2
FR3
RSS
IgHV exon
IGHV7-16*01
IGHV5-43*01
IGHV1-31*01
B
L1
IgKV exon
IGKV1S30*01
IGKV3S9*01
IGKV19S1*01
IGKV8S6x01
Peptide signal

Figure 3

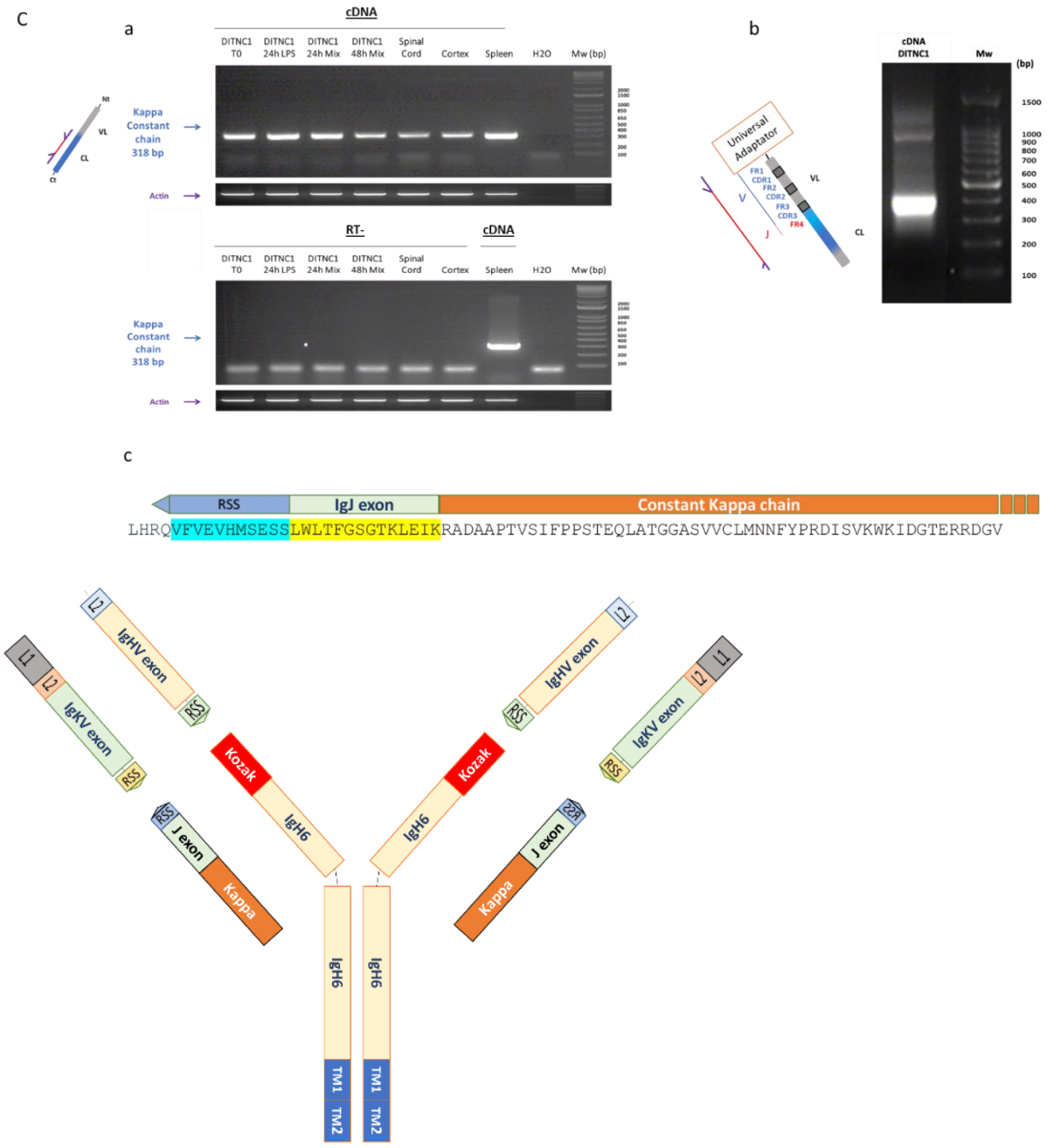
C
a
cDNA
DITNC1 T0
DITNC1 24h LPS
DITNC1 24h Mix
DITNC1 48h Mix
Spinal Cord
Cortex
Spleen
H2O
Mw (bp)
Kappa Constant chain 318 bp
Actin
RT-
cDNA
b
cDNA DITNC1
Mw
(bp)
Universal Adaptator
FR1
CDR1
FR2
CDR2
FR3
CDR3
FR4
VL
CL
c
RSS
IgJ exon
Constant Kappa chain
LHRQVFVEVHMSESSLWLTFGSGTKLEIKRADAAPTVSIFPPSTEQLATGGASVVCLMNNFYPRDISVKWKIDGTERRDGV
L1
L2
IgHV exon
IgKV exon
Kozak
IgH6
J exon
Kappa
TM1
TM2
D
a
cDNA Astrocytes Cortex LPS
cDNA Astrocytes Cortex CTR
Spleen
H2O
MW
(bp)
RT- Astrocytes Cortex LPS
RT- Astrocytes Cortex CTR
Lambda 282 bp
b
DITNC1 cDNA
DITNC1 RT-
LPS : 0H 3H 6H 14H 24H Spleen MW
LPS : 0H 3H 6H 14H 24H Spleen H2O MW
Lambda 282 bp
Actin

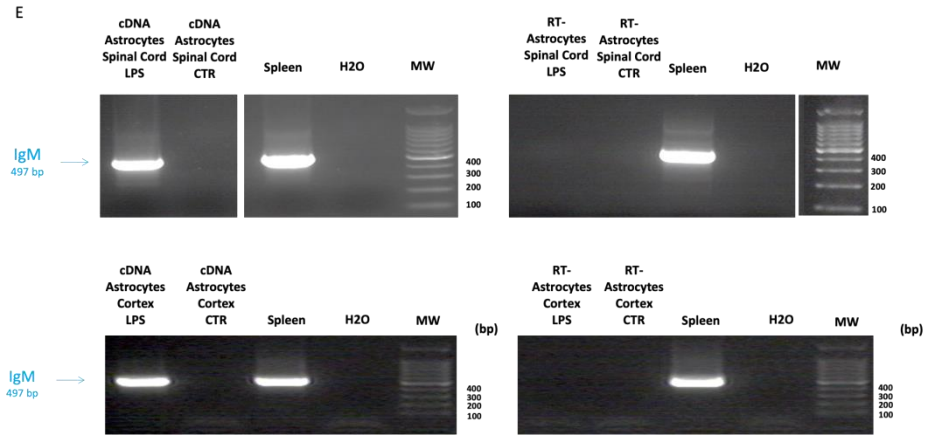

Figure 3: Characterization of mRNA coding variable chains in DI TNC1 cells and rat primary cortex and spinal astrocytes by transcriptomic approaches (RNAseq and RT-PCR) A) Schematic representation of the variable heavy chain transcripts (*IgHV7.16.01*, *IgHV5-43.01* and *IgHV1.31.01*) identified. The complete sequences are presented in **Supp. Figures 4A and 4B. B)** Schematic representation of the variable Kappa chain mRNA (IgKV) identified with the leader and the RSS sequences. **C) a)** RT-PCR amplification of the complete sequence coding IgK constant light chain in rat DI TNC1 astrocyte cell line stimulated or not with 200 ng/mL of LPS during 24h or a mix of cytokines for 24h or 48h as well as in rat primary cortex and spinal astrocytes. Upper panel : Amplification of the mRNA coding the IgG2B secreted form. cDNA from spleen served as a positive control. The experiment was also performed on a negative reverse transcriptase sample to rule out genomic DNA contamination. H_2O: negative control. **b)** 5' RACE-PCR amplification of *Igk*. The complete sequence is presented in **Supp. Figure 4A**. **c**) schematic representation of igKV, **C')** schematic presentation of the neural Immunoglobulin, **D)** RT-PCR amplification of *IgL* in rat primary cortex astrocytes and DI TNC1 cells stimulated or not with 200 ng/mL of LPS. cDNA from spleen served as a positive control. The experiment was also performed on a negative reverse transcriptase sample to rule out genomic DNA contamination. H_2O: negative control. **E**) RT-PCR amplification of ***Igh*m** in primary spinal and cortex astrocytes stimulated with 200 ng/mL of LPS. The complete sequence is presented in **Supp. Figure 4B.** cDNA from spleen served as a positive control. The experiment was also performed on a negative reverse transcriptase sample to rule out genomic DNA contamination. H_2O: negative control.

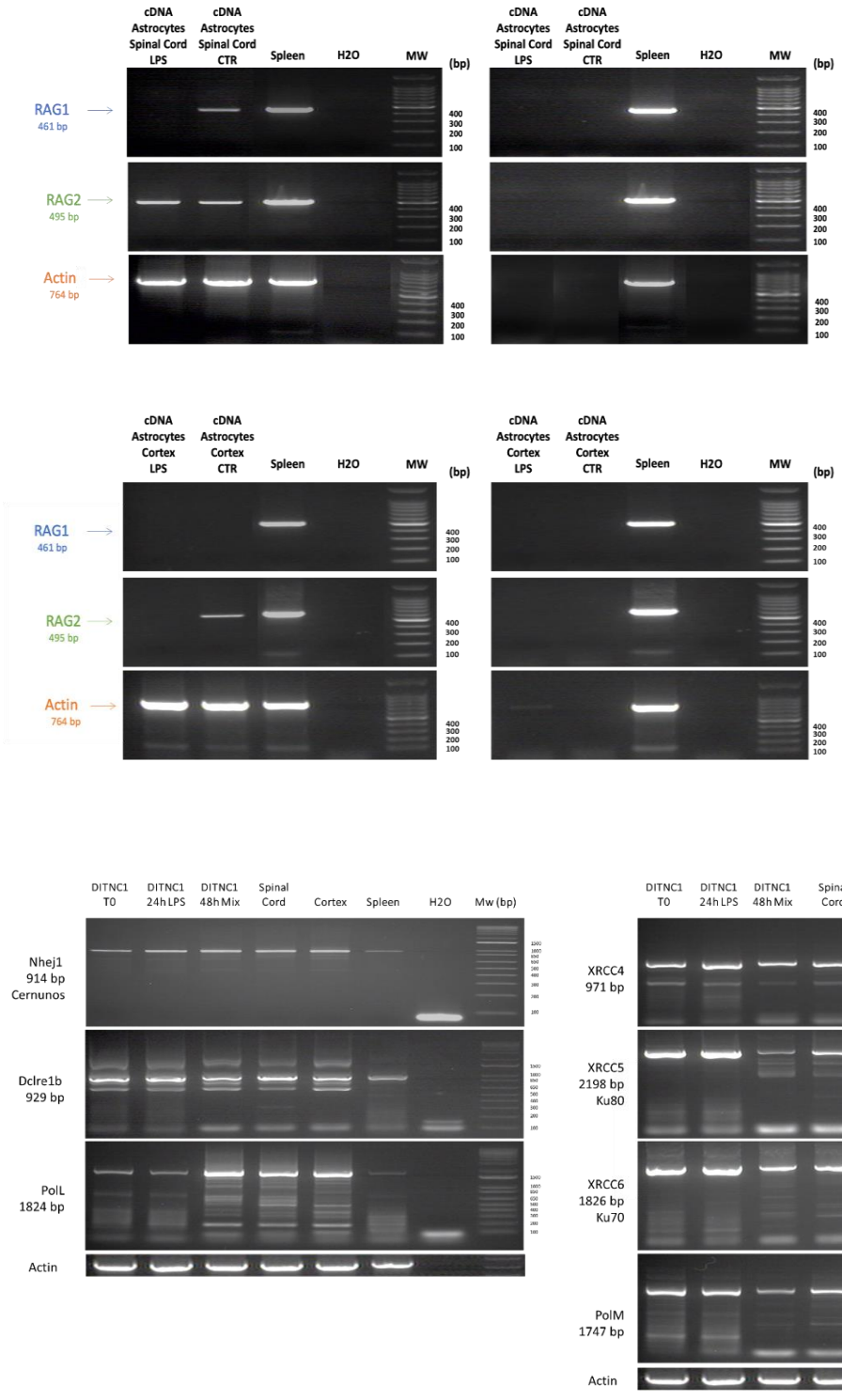

Figure 4 : RT-PCR amplification of the transcripts coding the enzymes of the enzymatic complex involved in V(D)J recombination. The experiments were performed on cDNA isolated from rat primary cortex and spinal astrocytes stimulated or not with 200 ng/mL of LPS as well as fromDI TNC1 cells stimulated or not with 200 ng/mL of LPS during 24h or a mix of cytokines for 24h and 48h. cDNA from spleen served as a positive control. The experiment was also performed on a negative reverse transcriptase sample to rule out genomic DNA contamination. H_2O: negative control.

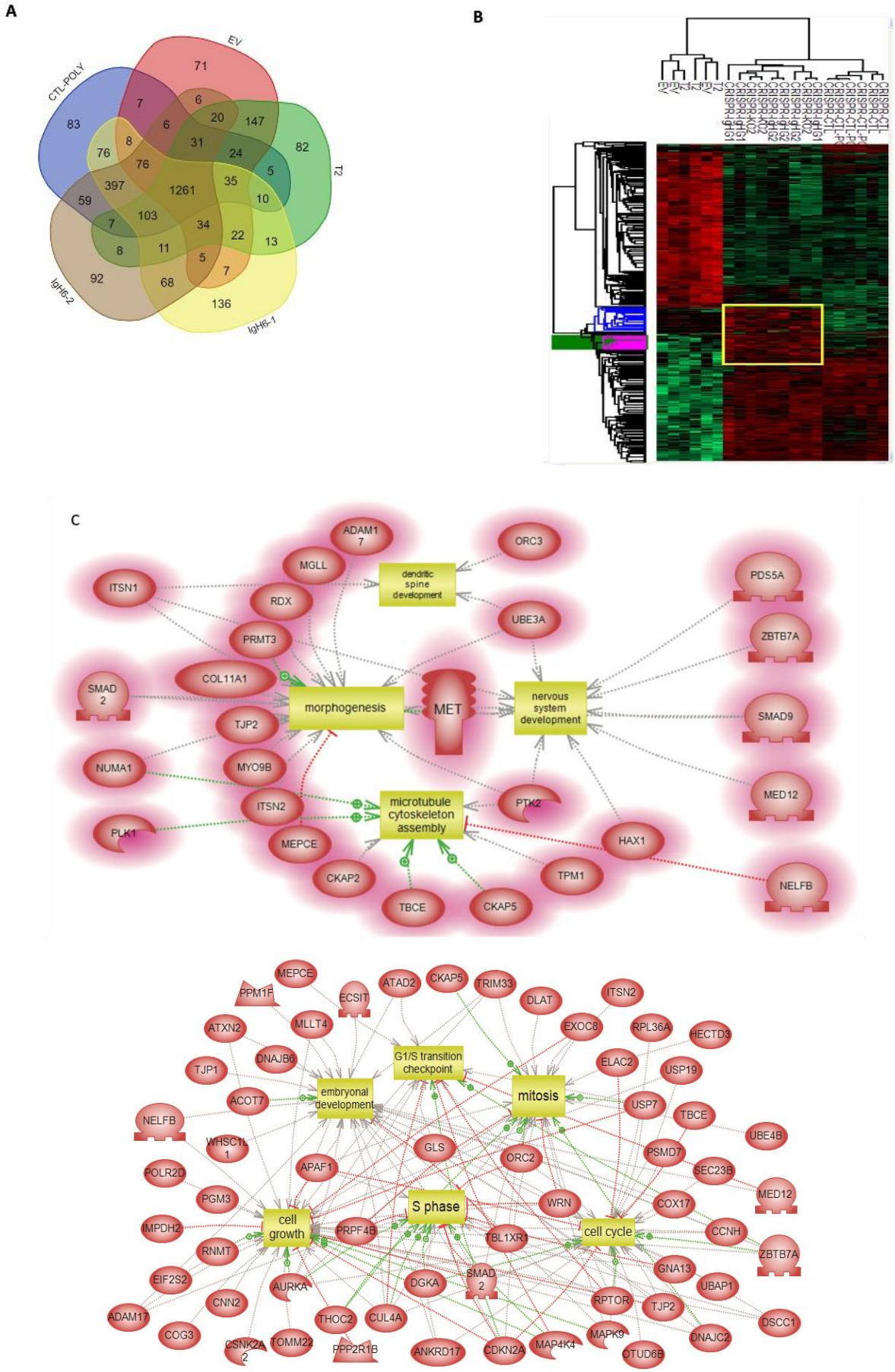
A
EV
CTL_POLY
T2
IgH6-2
IgH6-1
71
7
6
20
147
83
6
82
8
31
24
76
76
5
397
1261
35
59
10
103
34
22
7
13
8
11
5
92
68
7
136
B
C
ADAM17
MGLL
ORC3
ITSN1
dendritic spine development
RDX
UBE3A
PDS5A
PRMT3
ZBTB7A
COL11A1
SMAD2
morphogenesis
MET
nervous system development
SMAD9
TJP2
NUMA1
MYO9B
MED12
microtubule cytoskeleton assembly
ITSN2
PTK2
PLK1
MEPCE
HAX1
CKAP2
TPM1
NELFB
TBCE
CKAP5
MEPCE
PPM1F
ECSIT
ATAD2
CKAP5
TRIM33
DLAT
ITSN2
ATXN2
MLLT4
EXOC8
RPL36A
HECTD3
DNAJB6
G1/S transition checkpoint
ELAC2
TJP1
USP19
embryonal development
mitosis
ACOT7
USP7
TBCE
NELFB
UBE4B
WHSC1L1
GLS
ORC2
PSMD7
APAF1
SEC23B
POLR2D
MED12
PGM3
S phase
WRN
COX17
cell growth
PRPF4B
cell cycle
CCNH
IMPDH2
TBL1XR1
ZBTB7A
RNMT
GNA13
EIF2S2
DGKA
SMAD2
UBAP1
AURKA
RPTOR
CNN2
TJP2
ADAM17
THOC2
CUL4A
DSCC1
COG3
MAPK9
DNAJC2
CSNK2A2
TOMM22
PPP2R1B
ANKRD17
CDKN2A
MAP4K4
OTUD6B

Figure 5 : Proteomic study of the effect of rat *IgG2B* (*Igh6*) KO in DI TINC1 astrocyte cell line. **A)** Venn diagram of the specific proteins identified in DI TNC1 cells after *IgH6*-1 KO, *IgH6*-2 KO, infection with an empty vector (EV), control cells treated or not with polybrene and *Trop2* KO as a non-target control by Shotgun analyses (n=3). **B)** Heatmap representative of the proteins displaying a variation of abundance in DI TNC1 cells after I*gH6*-1 KO, *Igh6*-2 KO, *Heimdall* KO (KO2), control cells treated or not with polybrene, infection with EV and *Trop2* KO as a non-target control, (n=3).**C)** Systemic biology representative of the specific cluster common to *IgH6*-1 KO, *IgH6*-2 KO and *Heimdall* KO (KO2).

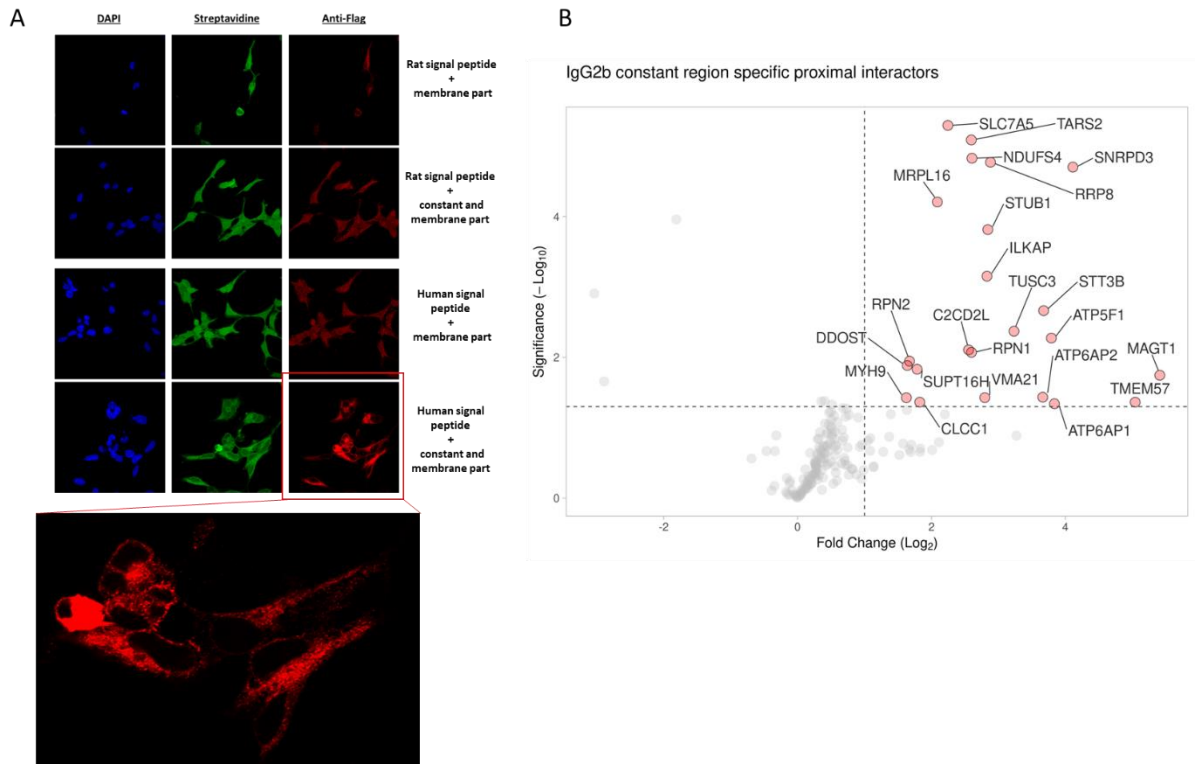

Figure 6 : Proximal labeling study in HEK 293 cells with rat IgG2B transmembrane form as a bait. A) Detection of biotinylated proteins (green, Streptavidin Alexa Fluor 488 conjugate) and rat IgG2B (red, anti-Flag) in HEK293 cells after overexpression of IgG2B in fusion with BirA*Flag. IgG2B was overexpressed with a rat or a human signal peptide. Nucleis were stained with DAPI (blue). A control consisting of the overexpression of the transmembrane domain itself fused to a rat or a human signal peptide has been included in the experiment. The inset represents a zoom of the results observed after detection of IgG2B with anti-Flag. **B)** Systemic biology representative of proximal interactome of rat IgG2B transmembrane form

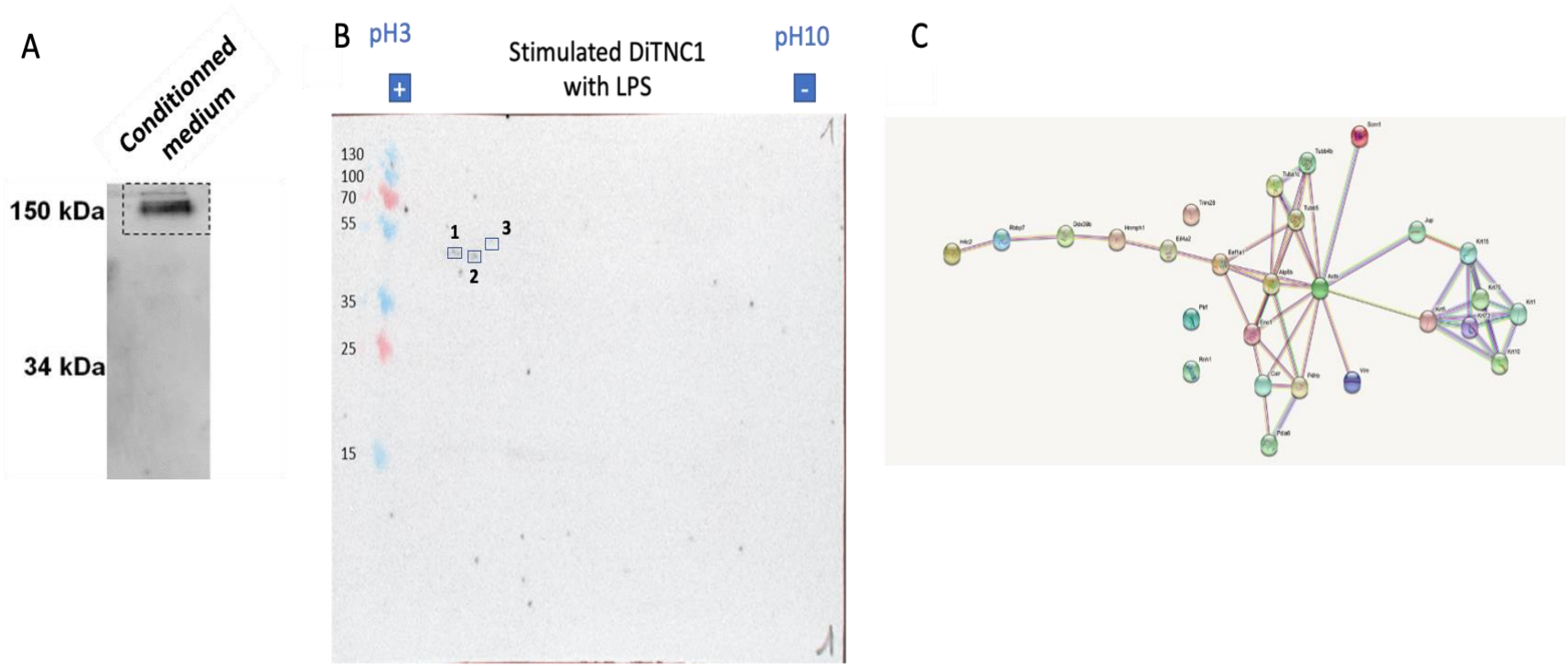

Figure 7: **A)** Detection of a complete secreted IgG2B by western blot in non-denaturing condition performed on secretome of DI TNC1 cells stimulated with 200 ng/mL of LPS. **B)** Western blot of 2D gel carried out on protein extracts of DI TNC1 astrocytes incubated with secretome of DI TNC1 astrocytes stimulated during 24h with 200 ng/mL of LPS. **C)** String of proteins identified during western blot performed on 2D gel and related to intermediate filaments cytoskeleton.

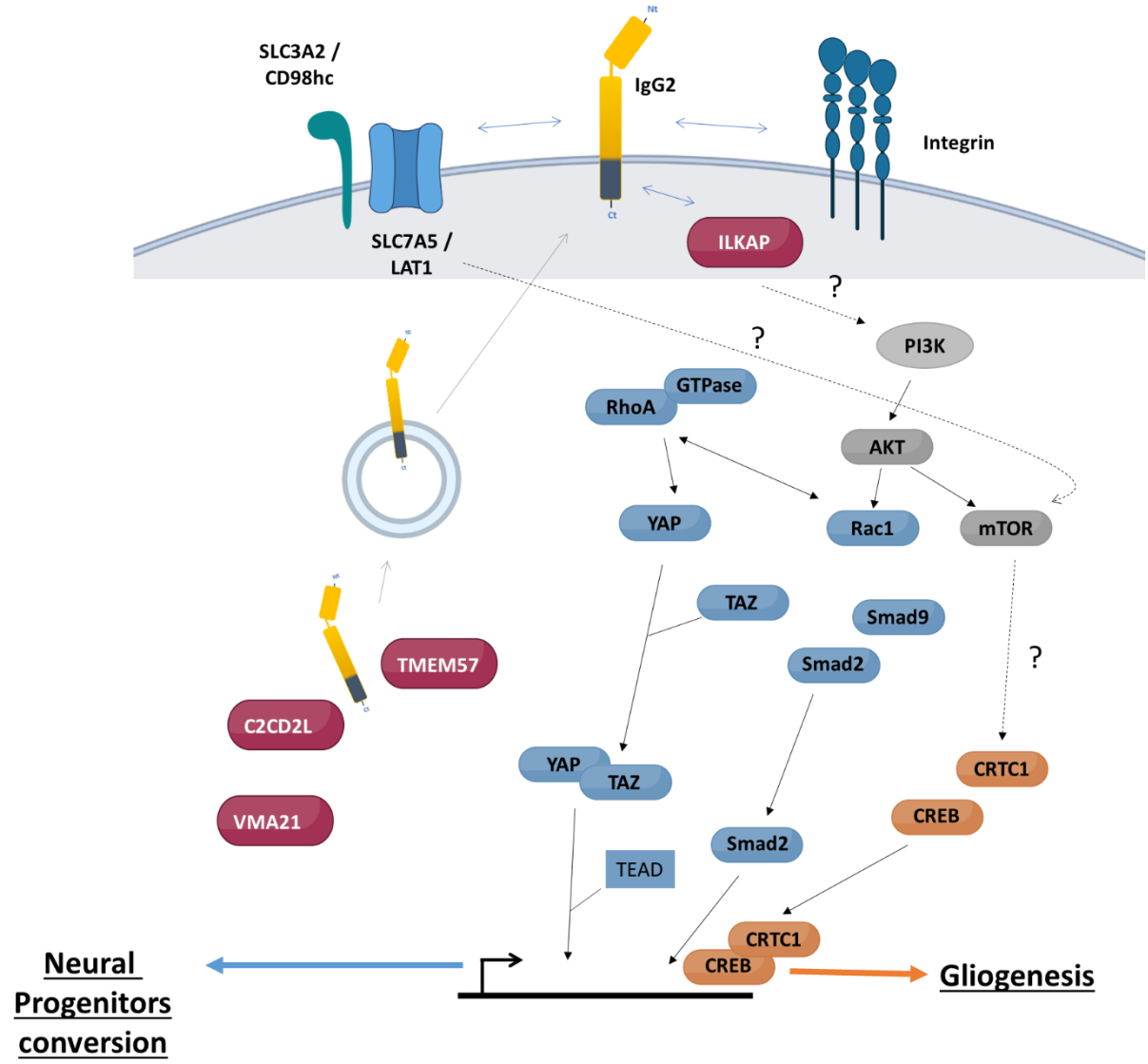

Figure 8 : Schematic representation of the potential intracellular role of IgG2B to preservation and conversion of the astrocyte phenotype. IgG2B can interact either with proteins from the endoplasmic reticulum, with LAT1 or integrins at the membrane surface. The blue pathway is found upon CRISPR-Cas9 invalidation of the IgG2B heavy chain while the orange pathway corresponds to identified upon overexpression. The proteins in red correspond proteins in proximal interaction with IgG2B. the ones in grey are related to proteins involved in ILKAP and CD98hc/LAT1/SLC7A5 signaling pathway.

SUPPLEMENTAL INFORMATION

Data S1: Complete sequences coding rat IgG2B and IgM heavy constant chains and the variable heavy and light chains

Data S2: Sequence and construct for overexpression of IgG2B with Kozak sequence, with or without the transmembrane domain

Data S3: Nucleic sequences coding all enzymes of the recombination V(D)J complex, CD20 and CD19. Sequences were identified in the spleen and astrocytes.

Data S4: List of exclusive proteins characterized by shotgun proteomic performed on extracts from DI TNC1 cells after *IgH6*-1 KO, *Igh6*-2 KO, *Heimdall* KO (KO2), control cells treated or not with polybrene, infection with an empty vector (EV) and *Trop2* KO as a non-target control, (n=3). Statistical significance was evaluated with the ANOVA test ($p<0.01$).

Data S5: List of proteins characterized in the clusters of the heatmap obtained after shotgun proteomic performed on extracts of DI TNC1 cells after *IgH6*-1 KO, *Igh6*-2 KO, *Heimdall* KO (KO2), control cells treated or not with polybrene, infection with an empty vector (EV) and *Trop2* KO as a non-target control, (n=3). Statistical significance was evaluated with the ANOVA test ($p<0.01$).

Data S6: List of proteins identified by shotgun proteomic after overexpression of the Kozak, IgG2B with or without the transmembrane domain or with only the Kozak sequencer and the transmembrane domain compared to empty vector and control.

Data S7: List of proteins identified by shotgun proteomic after proximal labeling carried out in HEK293 cells using rat IgG2B transmembrane form fused to BirA*Flag as a bait.

Data S8: List of proteins identified by shotgun proteomic performed on spots highlighted by western blot carried out on 2D gel. This western blot was conducted on protein extracts of DI TNC1 astrocytes using secretome of DI TNC1 astrocytes stimulated for 24h with 200 ng/mL of LPS.

Supplementary Figures

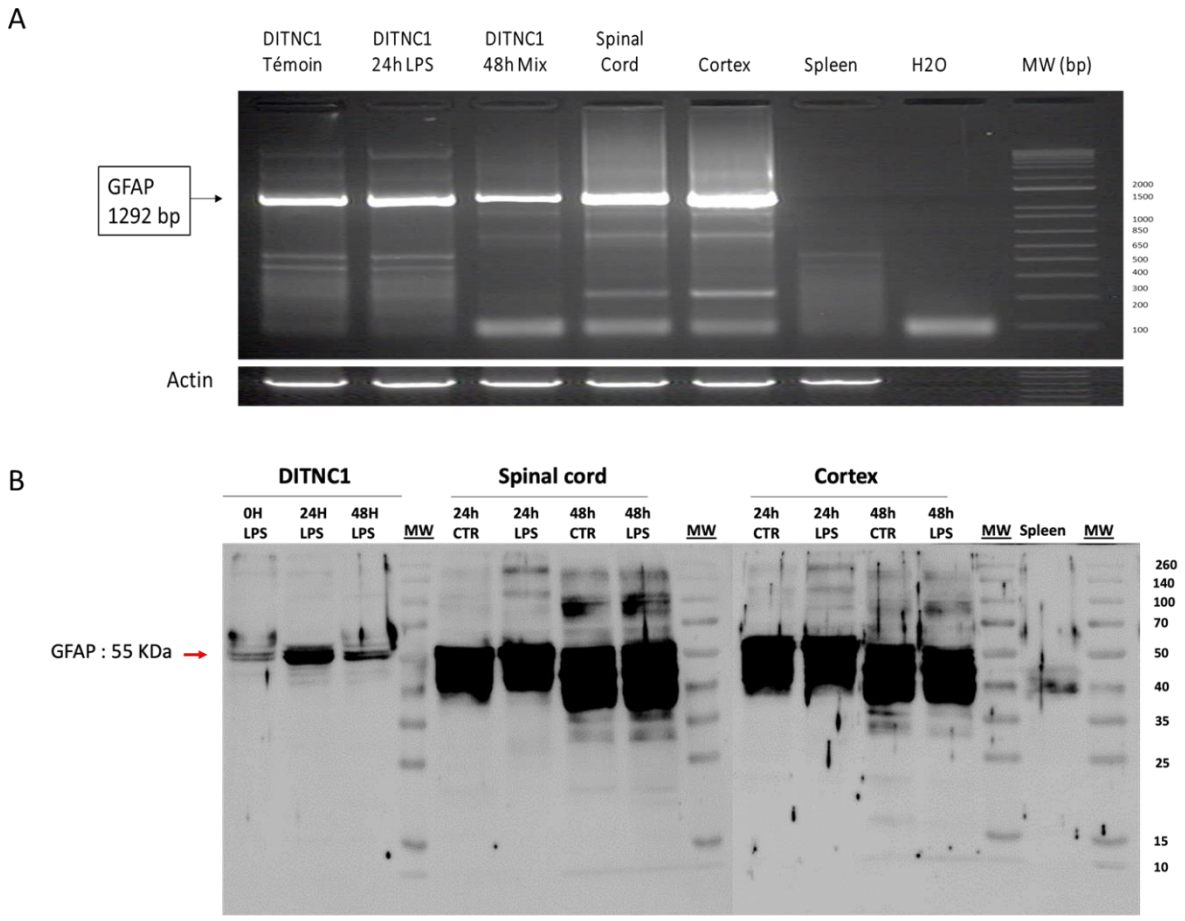

Supp. Figure 1 : **A)** RT-PCR amplification of *Gfap* in rat DI TNC1 astrocyte cell line and rat primary spinal astrocytes stimulated or not with 200 ng/mL of LPS during the time points indicated. H_2O: negative control. **B)** Western blot analyses of GFAP in DI TNC1 cells and rat primary cortex and spinal astrocytes stimulated or not with 200 ng/mL of LPS during 24h or 48H as well as in spleen.

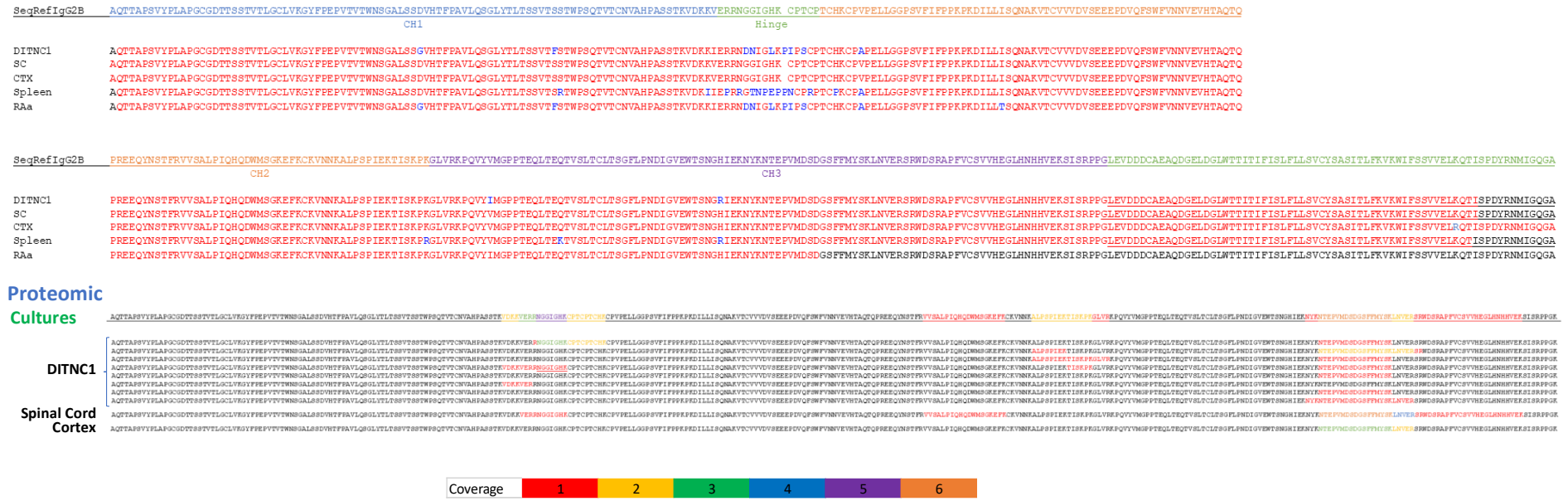

Supp. Figure 2 : Comparison of rat IgG2B sequences obtained from transcriptomic and proteomic analyses performed on DI TINC1 cells and rat primary cortex and spinal astrocytes with data obtained from spinal cord injury [8].

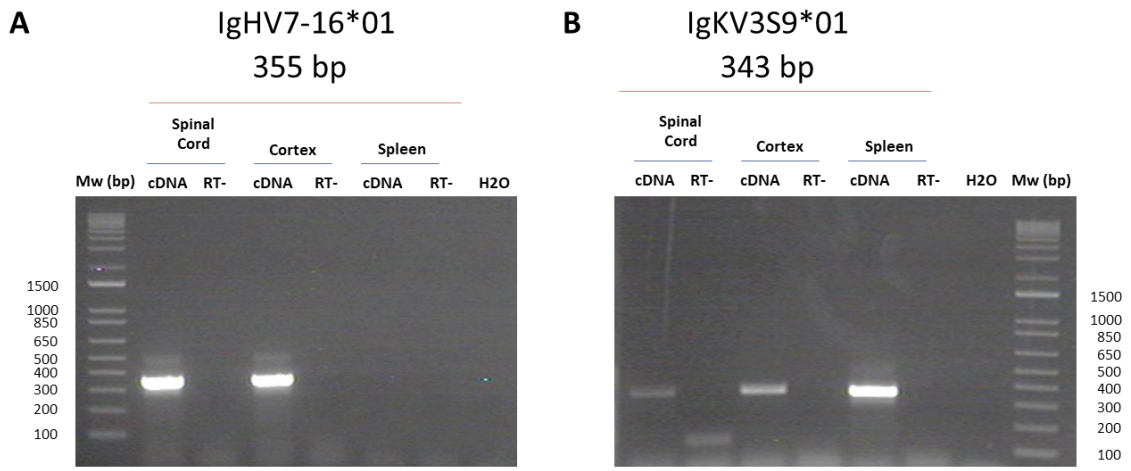

Supp. Figure 3 : RT-PCR amplification of IgHV and IgKV variable chains in rat primary spinal or cortex astrocytes. cDNA from spleen served as a positive control. H_2O and negative Reverse Transcriptase (RT-) serve as negative controls

A

Kappa constant Part

a

Allele A

Transcriptomic

Constante

```
Sequence      ADAAPTVSIFPPSMEQLTSGGATVVCFVNNFYPRDISVKWKIDGSEQRDGVLDSVTDQDSKDSTYSMSSTLSLTKVEYERHNLYTCEVVHKTSSSPVVKSFNRNEC
Spinal Cord   ADAAPTVSIFPPSMEQLTSGGATVVCFVNNFYPRDISVKWKIDGSEQRDGVLDSVTDQDSKDSTYSMSSTLSLTKVDYERHNLYTCEVVHKTSSSPVVKSFNRNEC
```

Mass spectrometry

```
              ADAAPTVSIFPPSMEQLTSGGATVVCFVNNFYPRDISVKWKIDGSEQRDGVLDSVTDQDSKDSTYSMSSTLSLTKVEYERHNLYTCEVVHKTSSSPVVKSFNRNEC
Spinal Cord   ADAAPTVSIFPPSMEQLTSGGATVVCFVNNFYPRDISVKWKIDGSEQRDGVLDSVTDQDSKDSTYSMSSTLSLTKVEYERHNLYTCEVVHKTSSSPVVKSFNRNEC
Cortex        ADAAPTVSIFPPSMEQLTSGGATVVCFVNNFYPRDISVKWKIDGSEQRDGVLDSVTDQDSKDSTYSMSSTLSLTKVEYERHNLYTCEVVHKTSSSPVVKSFNRNEC
```

b

Allele B

Transcriptomic

Constante

```
Sequence      ADAAPTVSIFPPSTEQLATGGASVVCLMNNFYPRDISVKWKIDGTERRDGVLDSVTDQDSKDSTYSMSSTLSLTKADYESHNLYTCEVVHKTSSSPVVKSFNRNEC
DITNC1        ADAAPTVSIFPPSTEQLATGGASVVCLMNNFYPRDISVKWKIDGTERRDGVLDSVTDQDSKDSTYSMSSTLSLTKADYESHNLYTCEVVHKTSSSPVVKSFNRNEC
Spinal Cord   ADAAPTVSIFPPSTEQLATGGASVVCLMNNFYPRDISVKWKIDGTERRDGVLDSVTDQDSKDSTYSMSSTLSLTKADYESHNLYTCEVVHKTSSSPVVKSFNRNEC
Cortex        ADAAPTVSIFPPSTEQLATGGASVVCLMNNFYPRDISVKWKIDGTERIAGVLDSVTDQDSKDSTYSMSSTLSLTKADYESHNLYTCEVVHKTSSSPVVKSFNRNEC
```

Mass spectrometry

```
Sequence      ADAAPTVSIFPPSTEQLATGGASVVCLMNNFYPRDISVKWKIDGTERRDGVLDSVTDQDSKDSTYSMSSTLSLTKADYESHNLYTCEVVHKTSSSPVVKSFNRNEC
Spinal Cord   ADAAPTVSIFPPSTEQLATGGASVVCLMNNFYPRDISVKWKIDGTERRDGVLDSVTDQDSKDSTYSMSSTLSLTKADYESHNLYTCEVVHKTSSSPVVKSFNRNEC
Cortex        ADAAPTVSIFPPSTEQLATGGASVVCLMNNFYPRDISVKWKIDGTERRDGVLDSVTDQDSKDSTYSMSSTLSLTKADYESHNLYTCEVVHKTSSSPVVKSFNRNEC
```

B

IgM constant Part

Trancriptomic

Proteomic

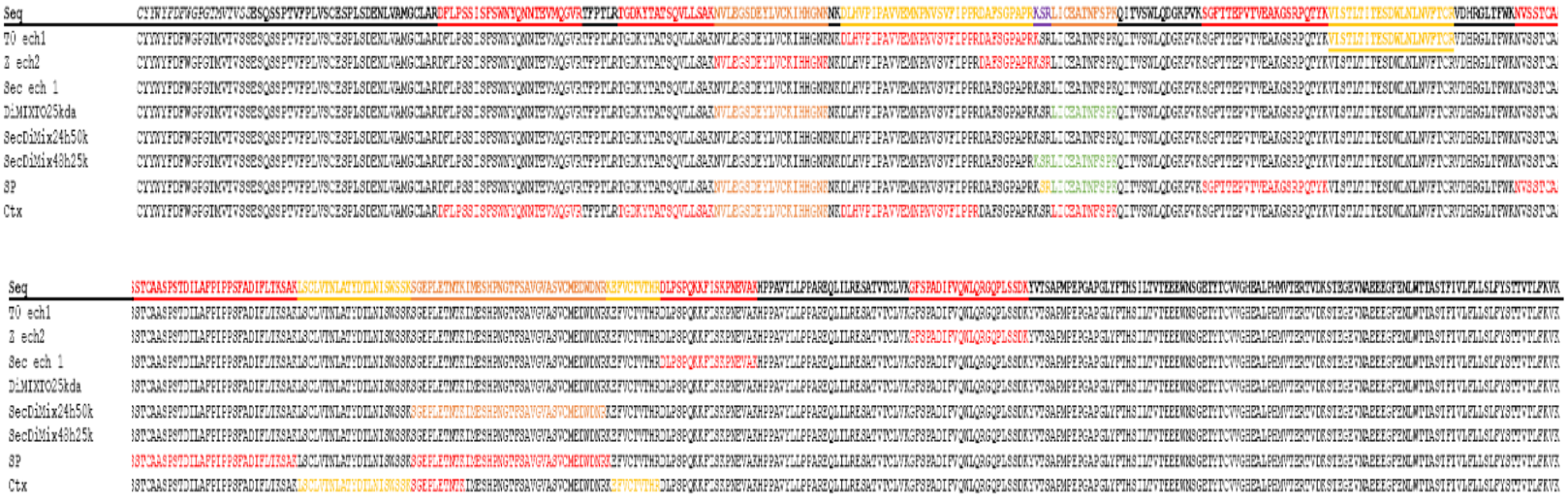

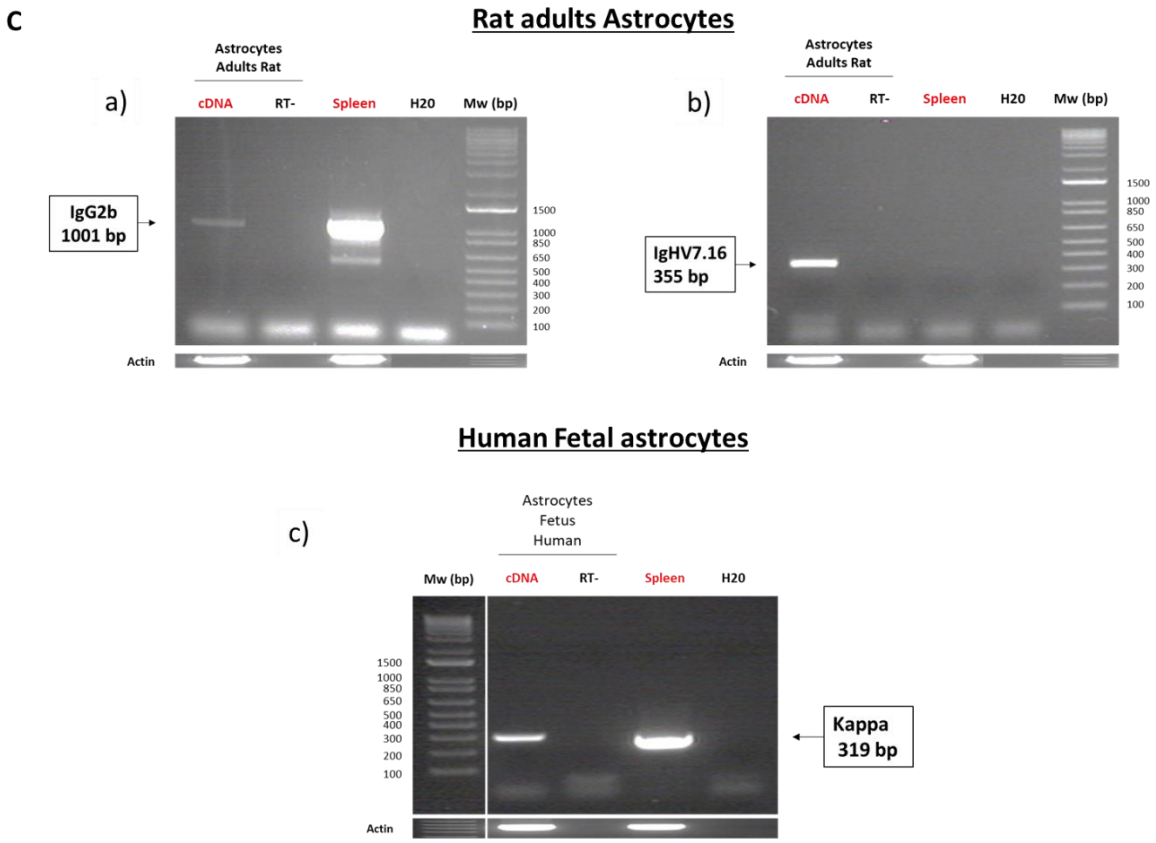

Supp. Figure 4 : **A)** Sequences alignment of different IgVH retrieved from RNAseq analyses performed on DI TNC1 cells and rat primary cortex and spinal astrocytes. These sequences were confirmed by RT-PCR amplification. **B)** Rat IgM sequence characterized by RNAseq, RT-PCR and proteomic analyses carried out on rat primary spinal and cortex astrocytes **C)** RT-PCR amplification of IgG2B constant **a**) and variable heavy chains **b**) coding sequences from primary astrocytes from adult rats. cDNA from spleen served as a positive control. **c**) RT-PCR amplification of *kappa* light constant chains and *kappa* light variable chain mRNA from embryonic primary culture of human astrocytes. The experiment was also performed on a negative reverse transcriptase sample to rule out genomic DNA contamination. H_20: negative control.

IgH6-1 KO IgH6-2 KO

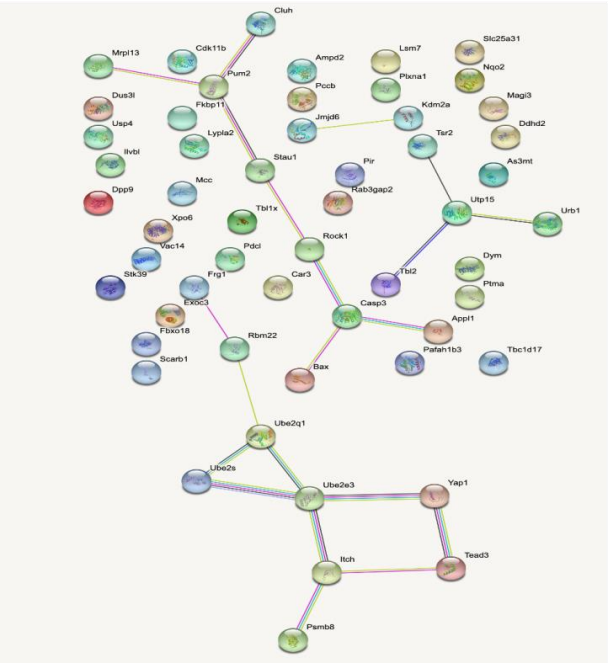

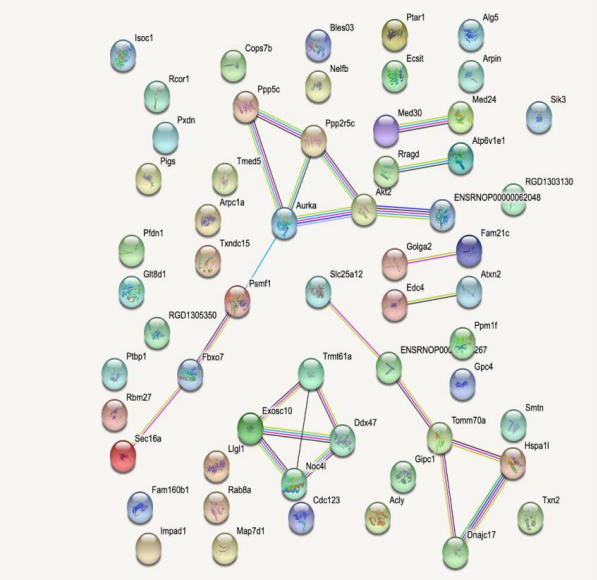

Supp. Figure 5 : String analyses of the specific proteins identified after *IgH6*-1 KO or *IgH6*-2 KO.

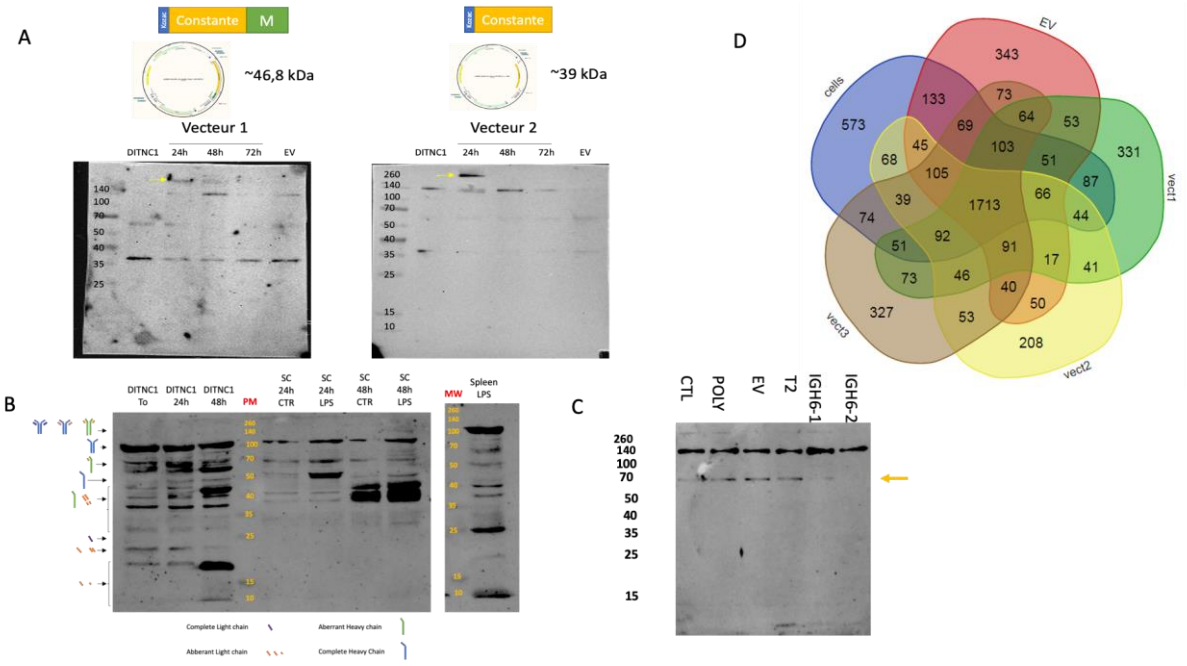

Supp. Figure 6: A) Anti-Flag Western blot analyses from Gel electrophoresis in non-reducing conditions of IgGH constructs with or without TM domain in DI TNC1, cells transduced with empty vector (EV) or LPS-stimulated for 24h, 48h or 72h. **B)** anti-IgKV Western blot analyses under reducing conditions of DI TNC1 cells as well as spinal and cortex primary astrocytes stimulated or not with LPS , **C)** Western blot analyses of secretome of LPS-stimulated CRIPSR-CAS 9 (IgH6-1, IgH6-2) DI TNC1 cells versus T2 (Trop2), control, polybrene and empty vector transfected cells with anti-Heimdall **D)** Venn diagram of the three conditions with controls and EV conditions.

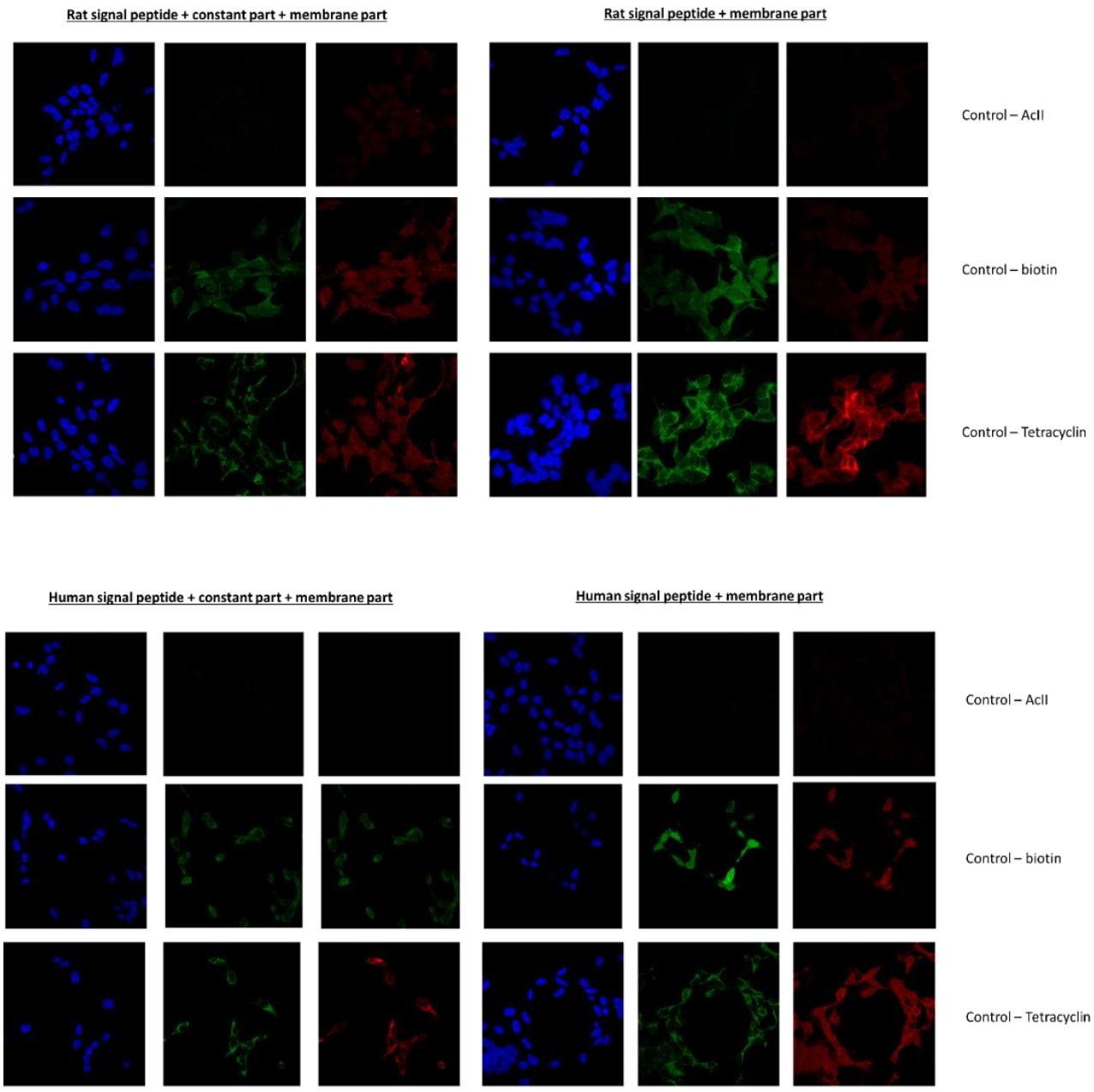

Supp. Figure 7 : Proximal labeling study in HEK 293 cells with rat IgG2B transmembrane form as a bait in control conditions. Detection of biotinylated proteins (green, Streptavidin Alexa Fluor 488 conjugate) and rat IgG2B (red, anti-Flag) in HEK293 cells after overexpression of IgG2B constant part in fusion with BirA*Flag. IgG2B was overexpressed with a rat or a human signal peptide. Nuclei were stained with DAPI (blue).

Supp. Table 1 : List of the primers used

Primers	Sequence	bp
Rat CD20 S	5'- ACA CAA AGC TTC TTC ATG AGG -3'	235 bp
Rat CD20 AS	5'- TCA CTT TCG CTT TGA CCA AAC -3'	
Rat GFAP S	5' CCC TGA GGC AGA AGC TCC -3'	349 bp
Rat GFAP AS	5' – CTG TGA GGT CTG CAA ACT TGG -3'	
Rat actine S	5'-TTGTAACCAACTGGGACGATATGG-3'	764 bp
Rat actine AS	5'-GATCTTGATCTTCATGGTGCTAGG-3'	
Rat IgG2b entier S	5'-GCC CAA ACA ACA GCC CCA TCT G-3'	1209 bp
Rat IgG2b entier Asm	5'-CTA GGC TCC TTG ACC AAT CAT G-3'	
Rat IgG2b entier S	5'-GCC CAA ACA ACA GCC CCA TCT G-3'	1209 bp
Rat IgG2b entier Asm	5'-CTA GGC TCC TTG ACC AAT CAT G-3'	
Rat IgG2b entier S	5'-GCC CAA ACA ACA GCC CCA TCT G-3'	1170 bp
Rat IgG2b entier M AS3	5'-GAT TGT CTG CTT CAG CTC C -3'	
Rat IgG2b entier S	5'-GCC CAA ACA ACA GCC CCA TCT G-3'	1170 bp
Rat IgG2b entier M AS3	5'-GAT TGT CTG CTT CAG CTC C -3'	
Rat Kappa-entier-S1	5'-CTG ATG CTG CAC CAA CTG-3'	318 bp
Rat Kappa-entier-AS1	5'-GCT TCA ACA GGA ATG AGT GA-3'	
Rat Lambda S1	5'-ACA CTC ACA GTA TTT CCA CC-3'	282 bp
Rat Lambda AS1	5'-AGG AGA CAG ACT CTT TTC C-3'	
Rat IghM MS S2	5'- AAC AGA TCA CAG TAT CCT GG -3'	497 bp
Rat IghM MS AS1	5'-GTG AGT CAC AGT GCA TAC-3'	
Rat RAG1 S2	5'-GGCCATCCGTGTCAATACCT-3'	461 bp
Rat RAG1 AS2	5'-ACCGAACTGCCTTTTCTGGA-3'	
Rat RAG2 S1	5'-GCCTTCTACCCAAAGAACCAC-3'	495 bp
Rat RAG2 AS1	5'-ACAGTCCCGTTTCCCATGTT-3'	
Oligo9-Vartrinity-RNAseq_Ctx	5'- ATT CAC CGT GAA GCA CAT CAG G -3'	355 bp
OligoAS9-Vartrinity-RNAseq_Ctx	5'- AGG AAG TTT TTG TTG GGC TGA C -3'	
Oligo11-Vartrinity-RNAseq_Ctx	5'- TCT AAT GAG GTC TCA GAG ATG G -3'	343 bp
OligoAS11-Vartrinity-RNAseq_Ctx	5'- 5'- GCT GAC AGT AAT AGG TTG CAG -3'	
Rat_DNApol-L_entier_S1	5'- TCA TTG GCT CCC ATG AAA GG -3'	1824 bp
Rat_DNApol-L_entier_AS1	5'- AAG AGG GTG GCA GAT GAG G -3'	
Rat_DNA-Pol-M_entier_S1	5'- TGC CTT CCT TCG TTC TGC -3'	1747 bp
Rat_DNA-Pol-M_entier_AS1	5'- AAG AGC ACC TGA CTG TGA GG -3'	
Rat-Dclre1b_AscI_Fwd	5'- tataGGCGCGCCa atgaacggggtcgtaatcc ccc -3'	914 bp
Rat-Dclre1b_NotI_Rev	5'- ttaaGCGGCCGCa ctatcctgaaaaaactctccac -3'	
Rat-Xrcc4_AscI_Fwd	('- tataGGCGCGCCa a tggaaaggaaagtcagcaga atc -3'	971 bp
Rat-Xrcc4_NotI_Rev	5'- ttaaGCGGCCGCa ctagtcaaagaggtcttctgggc -3'	
Rat-Xrcc5_AscI_Fwd	5'- tataGGCGCGCCa atggcgtggtccggtaataagg -3'	2198 bp
Rat-Xrcc5_NotI_Rev	5'- ttaaGCGGCCGCa ctatatcatgtccagtaaatcatcc -3'	
Rat-Xrcc6_AscI_Fwd	5'- tataGGCGCGCCa atgtca gagtgggaat cctactac -3'	1826 bp
Rat-Xrcc6_NotI_Rev	5'- ttaaGCGGCCGCa tcagttcttctccaagtgtctgc -3'	
Rat-Nhej1_AscI_Fwd	5'- tataGGCGCGCCa atgga ggaactagagcaaggcc -3'	930 bp
Rat-Nhej1_NotI_Rev	5'- ttaaGCGGCCGCa ctaactgaagagtcccctgggc -3'	
RACE Long primer	5'–CTAATACGACTCACTATAGGGCAAGCAGTGGTATCAACGCAGAGT–3'	x
RACE Short primer	5'–CTAATACGACTCACTATAGGGC–3'	
Rat Kappa AS2	5'-AGGACACCATCTCGTCGTTC-3'	x
Rat Iggam2B MS AS11	5'- CAG GAG CCA GTG GAT AGA CAG ATG GG -3'	x
Rat Iggam2B MS AS12	5'- CAC CGT GGA GCT GGT TGT ATC ACC -3'	
Kappa-entier-Human-S1	5'- GAACTGTGG *CTGCACCATC TG* -3'	319 bp
Kappa-entier-Human-AS1	5'- CACTCTCCCCTGTTGAAGCTC -3'	

Supp. Table 2 : RT-PCR and RACE_PCR parameters

Steps		Actin	Igs / / V(D)J enzymes	RACE
Initial denaturation		95°C - 2 minutes	95°C - 2 minutes	95°C - 2 minutes
Denaturation		95°C - 30 secondes	95°C - 30 secondes	95°C - 30 secondes
Annealing	x40	51°C - 30 secondes	60°C - 1 minute	60°C - 1 minute
Extension		72°C - 30 secondes	72°C - 1 or 2 minutes	72°C - 2 minutes
Final extension		72°C - 10 minutes	72°C - 10 minutes	72°C - 10 minutes

Conclusion

Nous avons montré lors de cette étude que les astrocytes de rat synthétisent différentes Igs. Bien que nous ne puissions pas totalement exclure que des Igs conventionnelles puissent être produites, nous avons démontré que celles-ci sont majoritairement synthétisées sous forme tronquée comme celles synthétisées par différentes cellules tumorales (Hu et *al.,* 2011). De plus, les expériences de Western-blot réalisées montrent que ces chaînes pourraient s'associer entre elles pour former un anticorps aberrant. Il est désormais important de déterminer les différentes conformations que présentent ces complexes protéiques. Pour ce faire, des analyses par protéomique de type Top-down ou Middle-down couplé à des analyses bio-informatiques permettront de caractériser leurs paratopes. Des études par résonance magnétique nucléaire (RNM) ou radiocristallographie permettront de valider leurs structures (Sela-Culang, Kunik and Ofran, 2013; Liberis *et al.,* 2018; den Boer *et al.,* 2022; Fernández-Quintero *et al.,* 2022). Par ailleurs, notre travail a montré que les enzymes de la recombinaison V(D)J nécessaires au réarrangement génique sont retrouvées tant au niveau transcriptomique que protéomique. Cependant, nous n'avons pas encore démontré l'implication de ce complexe enzymatique pour créer la diversité des paratopes. En effet, les transcrits identifiés ne présentent pas de segments V(D)J recombinés. Plusieurs hypothèses peuvent être émises. Les astrocytes utilisés ayant été isolés de pups âgées de 3 jours, il est possible que le mécanisme de genèse de diversité d'Igs ne soit pas encore fonctionnel. Autre possibilité, les astrocytes ne produisent que des immunoglobulines aberrantes avec un nombre limité de paratope. Outre l'*Igg2B*, l'expression du gène de la partie constante de la chaîne lourde IgM a également été observée dans ces cellules stimulées aux lipopolysaccharides. La présence de ces différents isotypes suggère que les astrocytes sont capables de commutation isotypique ou l'existence de différentes populations astrocytaires exprimant des isotypes différents. En effet, il existe une grande hétérogénéité d'astrocytes en fonction de leurs rôles et de leurs localisations dans le SNC (Schitine et *al.,* 2015; Buosi et *al.,* 2018; Cuevas-Diaz Duran et *al.,* 2019). C'est pourquoi, nous pouvons émettre l'hypothèse que la production d'un type de chaîne lourde et de parties variables spécifiques dépende soit de sous-population d'astrocytes soit de l'environnement dans lequel ceux-ci se trouvent. Des études protéomiques ont montré que les astrocytes sécrètent des Igs capables de reconnaitre un ou plusieurs antigènes astrocytaires tels que les filaments intermédiaires ou encore PRSS1. Ces Igs seraient donc impliquées dans la régulation de l'organisation du cytosquelette, ou

encore, de la morphologie de la cellule lors de la polarisation et migration cellulaire ou encore de l'identité astrocytaire. Afin de mieux comprendre le rôle de l'IgG2B, des expériences de surexpression et d'immunofluorescence ont été réalisées. Celles-ci ont permis de déterminer sa localisation cellulaire ainsi que la caractérisation de ses partenaires. Ainsi, l'IgG2B pourrait agir au niveau de la membrane vésiculaire et ce, en interagissant avec des protéines impliquées dans le transport des ions, la régulation des métabolites, le repliement des protéines, le trafic vésiculaire entre le RE et l'appareil de Golgi ou encore dans la reprogrammation et la différenciation cellulaire. En outre, l'analyse bio-informatique des données a révélé que certaines des protéines identifiées sont liées à des voies de prolifération et de croissance cellulaire, mais aussi au traitement et à la maturation des ARN. Il a également été observé qu'une partie de ces partenaires est impliquée dans le traitement et l'épissage des ARN pré-messagers. Dans la littérature, le trafic vésiculaire intracellulaire peut être corrélé avec la voie Hippo qui contrôle la prolifération cellulaire ainsi que la promotion de l'apoptose (Verghese et Moberg, 2019). Les astrocytes pour lesquels l'invalidation du gène *Igg2b* a été réalisée présentent une abondance plus importante de protéines caractéristiques des cellules hématopoïétiques (FRG1, PIR), des cellules souches neurales (YAP1, TEAD3, SMAD2/9, MCC, KDM2A et DDHD2) et la régulation de la neuritogénèse (PLXNA1, ROCK1, MAGI3, TBL1).

Les résultats tendent donc à montrer que l'IgG2B serait un gardien de l'identité du phénotype astrocytaire et qu'en son absence, l'astrocyte s'orienterait vers un phénotype de cellules souches neurales. Cependant, à ce stade, d'autres expériences sont nécessaires pour démontrer cette conversion. Dans un premier temps, il serait intéressant d'évaluer celle-ci en montrant que les astrocytes convertis perdent les marqueurs astrocytaires au profit des marqueurs de cellules souches neurales. Parallèlement, des études *in vitro* pourront être entreprises dans le but de montrer que la cellule convertie peut être orientée vers un phénotype de progéniteur neuronal puis de neurone. Pour cela, plusieurs caractéristiques neuronales seront étudiées, à savoir la synthèse de neurotransmetteurs, la capacité à établir et à s'intégrer dans des réseaux synaptiques ou encore de véhiculer un message nerveux. À la vue de l'hétérogénéité astrocytaires observée au sein du SNC, ces analyses seront réitérées sur des astrocytes isolées de différentes régions de celui-ci afin de déterminer si toutes les sous-populations astrocytaires produisent cette chaîne lourde IgG2B et ont la même capacité

de conversion. De plus, il sera aussi pertinent de prouver que cette conversion à la suite de l'inhibition de l'IgG2B peut être reproduite *in vivo*. L'ensemble de ces données pourrait permettre une meilleure compréhension des mécanismes mis en jeu lors de l'édification du SNC ainsi que la mise en place de différentes stratégies thérapeutiques dans divers cas pathologiques tels que les maladies de Parkinson ou d'Alzheimer.

Parallèlement, nous avons pu confirmer que l'IgG2B et la chaîne variable IgHV7.16.01 sont toutes deux produites par les astrocytes de rats adultes. De plus, lors de cette étude, l'expression de la chaîne légère Kappa ainsi qu'une Ig Lambda-like de substitution a été retrouvée dans les astrocytes de fœtus humains. Dans la littérature, l'Ig Lambda-like est synthétisée dans les cellules pré-B avant qu'une chaîne légère ne soit sélectionnée. Or, l'expression de cette chaîne Lambda-like a également été observée dans les astrocytes de rats âgés de 3 jours. Ainsi, ceci renforce l'hypothèse que les cellules astrocytaires présentent différents stades de différenciation pour les chaînes Igs, tout comme les lymphocytes B. Dans ces conditions, les astrocytes de fœtus humains sont peut-être à un stade trop précoce pour que l'expression des gènes codant les chaînes lourdes soit observée. Il reste à savoir si les différentes chaînes d'Igs sont bien retrouvées au niveau protéique et de déterminer si celles-ci sont aberrantes ou non. Il est aussi important de savoir si ces chaînes ont le même rôle dans le maintien du phénotype astrocytaire dans le SNC au cours du développement et chez l'adulte.

Chapitre 3 : L'ARN non codant Heimdall code une protéine alternative apparentée à une région variable de la chaîne légère kappa et joue un rôle clé dans la reprogrammation des astrocytes.

Introduction

Nous avons démontré lors de nos deux précédentes études que les neurones comme les astrocytes produisent des immunoglobulines. Certaines d'entre elles, telle que l'IgG2b, semblent être impliquées dans le maintien du phénotype astrocytaire et être impliquées dans la régulation de la croissance neuritique chez les neurones. L'ensemble de ces résultats tendent donc à montrer que le système nerveux exprime des éléments immunitaires qui jouent un rôle dans son développement et non un rôle immunitaire. Lors de nos études de protéomique spatio-temporelle, nous avons identifié une protéine alternative relative à la partie variable de la chaine légère Kappa. Cette chaîne semble être produite lors de l'inflammation à la suite de la LME et ressemble à la chaîne légère produite lors d'une pathologie, la maladie de Bence Jones qui surproduit cette chaîne(Perry et Kyle, 1975). Dans ce contexte, nous nous sommes focalisés sur cette chaîne en particulier. Cependant lors de notre étude, il s'est avéré que cette chaîne est codée par un ARN non-codant, remettant en cause le dogme de la séquence Kozak (Kozak, 1989). En effet, le dogme établi depuis très longtemps stipule qu'un ARNm ne code qu'une seule et unique protéine et que la traduction démarre uniquement au niveau du site d'initiation de la traduction défini par la séquence Kozak (Kozak, 1989). La traduction se fait donc alors dans le cadre de lecture ouvert de référence (Open Reading Frame, ORF) pour conduire à la synthèse d'une protéine de référence (**Figure 22**). Ainsi, toutes les banques bio-informatiques établies n'incluaient que ces protéines. Néanmoins, des études de protéomique à haut débit réalisées par PRISM ont révélé la présence d'un grand nombre de protéines qui n'étaient pas référencées dans ces banques de données (Vanderperre et *al.,* 2013). Ceci a ainsi permis de mettre en évidence la présence d'un protéome caché (Cardon et *al.,* 2021). Des études fonctionnelles telles que le ribosome profiling réalisées ensuite ont permis de démontrer comment se faisait la synthèse de ces protéines (Cardon et *al.,* 2021). Ainsi, celle-ci ne se fait pas selon la « règle Kozak » mais à partir des régions 5'UTR et 3' UTR de certains transcrits ou encore selon un cadre de lecture +2 et +3. Ces protéines ont donc été qualifiées de protéines alternatives (Altprot) (Delcourt et *al.,* 2018; Brunet et *al.,* 2021; Cardon et *al.,* 2021). De plus, ce protéome caché s'est avéré

bien plus riche encore puisque des études ont également montré que des protéines alternatives pouvaient également être synthétisées à partir d'ARN non codants (Cardon et *al.,* 2021a, 2021b). Néanmoins, à l'heure actuelle, il est évident que le nombre de protéines alternatives restant à identifier reste conséquent et que la complexité réelle de ce protéome caché reste à être déterminée, ce à quoi PRISM s'est engagé depuis quelques années(Cardon et *al.,* 2020; Cardon et *al.,* 2021a).

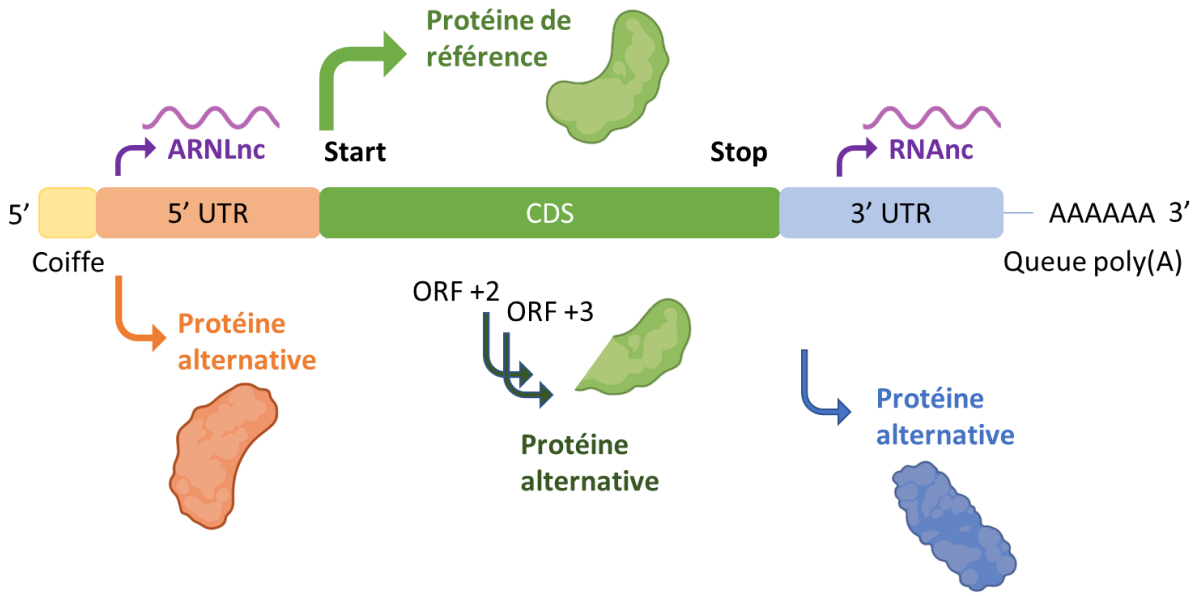

Figure 22 : Schéma des régions d'expression des protéines alternatives (AltProt). Chez les eucaryotes, l'expression de la protéine de référence (RefProt) provient du premier codon de départ 'AUG' avec une séquence d'ADN codante (CDS) encadrée par une région non traduite UTR 5' et 3. Les 5' et 3' UTR peuvent également être le lieu de fixation du ribosome, permettant la traduction de AltProt 5'-UTR ou AltProt 3'-UTR. De plus, le ribosome peut également déplacer le cadre de lecture en se fixant à +2 ou +3 du codon de départ de référence, ce qui permet la traduction de AltProt CDS+2 ou AltProt CDS+3. La dernière source de traduction d'AltProt est l'ARN non codant (ARNnc) et le long ARN non codant (lncARN).

Objectifs

Le premier objectif de cette troisième partie a donc été de caractériser les cellules produisant la protéine alternative Heimdall et de déterminer sa fonction.

Résultats

Pour cette étude, les données obtenues lors des expériences de protéomique réalisées sur les sécrétomes d'explants de moelle épinière 12h après la lésion ont été réanalysées à l'aide d'une banque de protéines alternatives, Openprot (Brunet *et al.,* 2021). Les résultats obtenus

montrent que la protéine alternative IP_1304334 est plus fortement libérée dans le sécrétome d'explant de moelle épinière localisé au niveau du site lésionnel. Cette AltProt présente un domaine immunoglobuline (Ig) apparenté à celui d'une région variable de la chaîne légère kappa et qu'elle est codée par l'ARN non codant (lncRNA) AABR07051592.290. La consultation de la banque d'Altprot révèle la présence d'une deuxième isoforme IP_1304331.1 qui présente 90% d'identité avec IP_1304334. Cette protéine particulière a été nommée « Heimdall ». Dans un premier temps, nous avons voulu déterminer qu'elle était l'origine cellulaire d'Heimdall. Une étude par immunofluorescence a permis de mettre en évidence sa présence au sein des astrocytes qui a été validée par transcriptomique et par protéomique sur la lignée astrocytaire de rat DI TNC1 et à partir de cultures primaires d'astrocytes (cortex et moelle épinière). Ces analyses ont montré que cette chaîne variable de type Kappa est synthétisée seule. L'étude de sa séquence révèle la présence d'un peptide signal en amont de la région FR1 suggérant ainsi qu'Heimdall est traduit en protéine (**Figure 12**). Par la suite, des analyses conformationnelles montrent qu'Heimdall présente une conformation semblable aux protéines intrinsèquement désordonnées (IPD). Ces protéines ont la particularité de s'auto-assembler et sont retrouvées dans différentes pathologies telles que la maladie de Bence Jones, la maladie d'Alzheimer ou encore les astrocytomes. La capacité d'Heimdall à s'auto-associer a pu alors être vérifiée par Western-blot. En effet, outre la forme monomérique d'Heimdall de 11 kDa, une forme dimérique de22 kDa a également été observée. De plus, des bandes présentant des poids moléculaires plus élevés de 34 kDa, 50 kDa, 60 kDa et 140 kDa suggèrent qu'Heimdall peut s'associer à d'autres partenaires protéiques dont des chaines lourdes d'immunoglobulines que nous avons identifiées dans le chapitre 2. Des résultats similaires ont été obtenus sur le sécrétome de ces astrocytes démontrant qu'Heimdall est sécrétée sous forme de multimère ou associé à ses partenaires protéiques. Afin de déterminer la fonction d'Heimdall, des études ont été réalisées via l'ajout de l'anticorps anti-Heimdall dans le milieu de culture des astrocytes. À la suite de cette neutralisation d'Heimdall, les astrocytes présentent alors des extensions semblables à des neurites. Afin de comprendre l'impact moléculaire exercé par cette neutralisation d'Heimdall, des analyses protéomiques de type shot gun ont ensuite été réalisées. Celles-ci révèlent l'abondance de facteurs impliqués dans la pluripotence cellulaire, la régulation de l'épissage alternatif, la croissance cellulaire, la prolifération cellulaire et la différenciation cellulaire. Fait intéressant, certains d'entre eux sont connus pour être indispensables au maintien de

l'identité astrocytaire et jouent un rôle dans la conversion entre phénotype astrocytaire et neuronal. Ceci suggère donc qu'Heimdall puisse réguler l'état de différenciation astrocytaire. Cette hypothèse a pu être confirmée à la suite de l'invalidation génique d'*Heimdall* par CRISPR-Cas9 réalisée dans les astrocytes. En effet, les résultats obtenus révèlent que les cellules DI TNC1 KO produisent spécifiquement des facteurs normalement synthétisés par les cellules neuroprogénitrices. Ceux-ci sont impliqués dans la neuritogenèse, l'excroissance des neurites et le développement cérébral. Ce rôle d'Heimdall est corroboré par des expériences d'immunoprécipitation qui montrent qu'Heimdall interagirait notamment avec des protéines impliquées dans la croissance ou la pluripotence des neurites ainsi que le maintien de l'identité astrocytaire. Afin de vérifier que ces astrocytes ont bien été convertis vers un phénotype neuronal à la suite du KO d'*Heimdall*, des études d'électrophysiologie ont été réalisées. Les résultats obtenus montrent que les cellules KO présentent une dépolarisation membranaire par rapport aux astrocytes normaux suggérant leur capacité à déclencher un potentiel d'action. Afin de définitivement confirmer le rôle d'Heimdall, sa surexpression a cette fois ci été entreprise dans les astrocytes. Celle-ci révèle la présence de protéines impliquées dans la signalisation MAPK et dans le maintien du phénotype dans les astrocytes surexprimant Heimdall. Or, cette voie est indispensable dans la gliogenèse. L'ensemble de ces résultats montre qu'Heimdall joue un rôle clé dans le maintien du phénotype astrocytaire et empêche sa conversion vers un phénotype neuronal.

Heimdall, an alternative protein issued from a ncRNA related to kappa light chain variable region, is a key player in Astrocyte-to-neuron reprogramming

Sylvain Osien[1*], Alice Capuz[1*], Tristan Cardon[1*], Mélodie Anne Karnoub[1], Soulaimane Aboulouard[1], Antonella Raffo-Romero[1], Marie Duhamel[1], Dasa Cizkova[1,2], Marco Trerotola[4], David Devos[5], Firas Kobeissy[6], Fabien Van den Abelle[7], Amélie Bonnefond[8], Isabelle Fournier[1,9], Franck Rodet[1**], Michel Salzet[1,9**]

[1]Univ. Lille, Inserm, U-1192 - Laboratoire Protéomique, Réponse Inflammatoire et Spectrométrie de Masse-PRISM, F-59000 Lille, France

[2]Institute of Neuroimmunology, Slovak Academy of Sciences, Dúbravská cesta 9, 845 10 Bratislava, Slovakia

[3]Centre for Experimental and Clinical Regenerative Medicine, University of Veterinary Medicine and Pharmacy in Kosice, Kosice, Slovakia

[4]Laboratory of Cancer Pathology, Center for Advanced Studies and Technology (CAST), University 'G. D'Annunzio', Chieti, Italy; Department of Medical, Oral and Biotechnological Sciences, University 'G. d'Annunzio', Chieti, Italy.

[5] Université de Lille, INSERM, U1172, CHU-Lille, Lille Neuroscience Cognition Research Centre, 1 place de Verdun, 59000, Lille, France.

[6] Department of Biochemistry and Molecular Genetics, Faculty of Medicine, American University of Beirut, Beirut, Lebanon.

[7]Université de Lille, INSERM U1003, Laboratory of Cell Physiology, 59650 Villeneuve d'Ascq, France.
[8]Univ. Lille, Inserm UMR1283, CNRS UMR8199, European Genomic Institute for Diabetes (EGID), Institut Pasteur de Lille, CHU de Lille, 1 place de Verdun, 59000 Lille, France.

[9]Institut Universitaire de France, 75005 Paris.

Key words: Spinal cord lesion, Proteogenomic, *In vivo* studies, Kappa chain, Astrocytes, Neuronal progenitor, Neurites outgrowth, Ghost Proteome, Small pep, Alternative protein

***Authors contributed equally to the work.**

**** Co-Last and Co-Corresponding author**: Pr. Michel Salzet, [1]Univ. Lille, INSERM, U1192 - Laboratoire Protéomique, Réponse Inflammatoire et Spectrométrie de Masse-PRISM, F-59000 Lille, France, Email: Michel.salzet@univ-lille1.fr Tel.: +33-320-4194; Fax: +33-320-4354.

Dr. Franck Rodet (franck.rodet@univ-lille.fr) [1]Univ. Lille, INSERM, U1192 - Laboratoire Protéomique, Réponse Inflammatoire et Spectrométrie de Masse-PRISM, F-59000 Lille, France

Abstract

Alternative proteins originate from the 5'- and 3'- UTR mRNA regions, frameshifts of mRNA ORFs or from non-coding RNAs. Longtime considered as non-coding, recent *in-silico* translation prediction methods enriched the protein databases allowing the identification of new target structures that have not been identified previously. To gain insight into the role of these newly identified alternative proteins in the regulation of cellular functions, it is crucial to assess their dynamic modulation within a framework of altered physiological modifications such as experimental spinal cord injury (SCI). Here, we carried out a longitudinal proteomic study on rat SCI. Based on the alternative protein predictions, it was possible to identify a plethora of newly predicted protein hits. Among these proteins, one presented a special interest due to its function and high homology with a kappa light chain variable region. We demonstrated that this protein named “Heimdall” was expressed by astrocytes and was secreted under inflammatory conditions. Immunoprecipitation experiments showed that the Heimdall interactome contained proteins related to astrocyte fate keepers such as “NOTCH1, EPHA3, IPO13” as well as membrane receptor protein including “CHRNA9; TGFBR, EPHB6, and TRAM”. However, when Heimdall protein was neutralized utilizing a specific antibody or its gene knocked out by CRISPR-Cas9, sprouting elongations were observed in the corresponding astrocytes. Interestingly, depolarization assays and intracellular calcium measurements confirmed a phenotype switch from astrocytes to neuron-like phenotype. Proteomic analyses performed under injury conditions as well as under lipopolysaccharides (LPS) stimulation, revealed the expression of neuronal factors, stem cell proteins, and neurogenesis of astrocyte convertor factors such as EPHA4, NOTCH2, SLIT3, SEMA3F, suggesting a role of Heimdall to regulate astrocytic fate. Heimdall represents the first established astrocytic alternative protein that plays a key role in defining astrocyte phenotype and could be a potential therapeutic target in neurodegenerative diseases such as SCI, stroke or brain injury.

Introduction

Spinal cord injury (SCI) is considered a major public disorder of the central nervous system (CNS) [1]. In this work, an experimental balloon-compressive SCI model was performed at

thoracic Th8-9 spinal level in adult rat [1]. Spatial and temporal events occurring in acute phase post-SCI were evaluated with an advanced spatio-temporal shot-gun proteomic analysis complemented with 3D MALDI Imaging, confocal imaging along with *in vitro* and *in vivo* tests [1, 2]. In this context, comparative analysis between the caudal and rostral segments was performed and revealed a high-discrepancy in the nature of the cytokines and cellular components present at these sites and defined the caudal segment as a potential therapeutic target [1, 2]. Indeed, T regulators were detected in the first 3 days at the rostral segment and only a week later at the caudal side secreting inflammatory cytokines, glycoproteins and other factors involved in the RhoA pathway [2]. Then, we assessed the *in vivo* impact of a sustained RhoA inhibitor (RhoAi) administration in a rat SCI model via functionalized-alginate scaffold [3]. Fine mapping of the spatio-temporal molecular events that occurred during this treatment was assessed around the lesion site [3]. To further analyze these changes, an *in vitro* neuroproteomic-systems biology platform was developed. For this purpose, the pan-proteomic profile of the dorsal root ganglia (DRG) cell line ND7/23 was assessed in a large array of culture conditions using RhoAi and/or conditioned media obtained from *ex-vivo* cultures of injured spinal cord slices [3]. Notably, results showed a time-dependent alteration of the transcription factors profile along with the synthesis of growth cone-related factors (receptors, ligands, and signaling pathways) in the RhoAi treated DRG cells [3]. Furthermore, we demonstrated that during the inflammatory response, immunoglobulins (Igs) were also released and could bind to their specific receptors, *i.e.* CD16 and CD32b, on DRG cells [4]. Concomitantly, neuritogenesis induction was observed upon RhoAi treatment and the transactivation of these receptors during IgG treatment modulated the neurite outgrowth process [4].

Based on these results, bone marrow stem cells were treated with the secretome of the rostral, lesion and caudal segments [5] prior to their intrathecal injection [6] with alginate functionalized with growth factors [7]. Results clearly established better neurogenesis and synaptic contacts as well as an increase in the Basso, Beattie and Bresnahan (BBB) locomotor score from 0 to 18.4 ± 1.4 [6]. To further assess the underlying mechanism involved, we relied on “deep proteomic data mining” focusing on Ghost protein as potential culprits in such events as described recently by our group [8]. Indeed, the spatio-temporal study of these Ghost proteins observed post-SCI highlighted the contribution of this sub-proteome and its

involvement in the outcome regulation in SCI pathology. The ghost proteins identified represent proteins translated from the 3'- or 5'- UTR regions, frameshifts of mRNA ORFs or from non-coding RNAs [9, 10, 11]. While they were described as non-coding during a long time, *in silico* translation allowed the enrichment of the databases with these novel proteins [12, 13, 14, 15]. When we deeply re-analyzed our proteomic data, based on these alternative protein predictions, we identified several interesting candidate hits. One of these alternative proteins, named "Heimdall", was found to share high homology with a kappa light chain variable region identified in amyloidosis disease [16]. We first demonstrated its expression in astrocytes, which play a key role in the physiopathology of SCI. interestingly, when we investigated Heimdall's function in these cells via advanced neuroproteomics platforms supported with molecular cell biology assays, we found that Heimdall is a novel member of the gatekeeping astrocyte-to-neuron conversion factors, along with Notch [17] and PTBP [18] protein families as described later.

Materiel and Methods

Reagents

Dulbecco's modified Eagle's medium (DMEM), fetal bovine serum (FBS), Sodium Pyruvate, HEK293TREx, Flp-In, L-glutamine, penicillin and streptomycin, puromycin, Tetracycline Hydrochloride, Phosphate buffer saline (PBS), DiSBAC2, DSSO, SuperScript® III kit, Random primers, pcDNA™5/FRT/TO Vector, enhanced chemiluminescence kit, Dynabeads® Protein A, Hoechst 33,342, Alexa Fluor® 488-conjugated donkey anti-rabbit and Alexa Fluor® 555-conjugated donkey anti-mouse were all purchased from Life Technologies (Milan, Italy). Water, formic acid (FA), trifluoroacetic acid (TFA), and acetonitrile (ACN) were obtained from Biosolve B.V. (Valkenswaard, the Netherlands). DI TNC1 cell line, Sodium dodecyl sulfate (SDS), DL-dithiothreitol (DTT), iodoacetamide (IAA), Polybrene and mouse anti-FLAG, rat tail collagen type I were purchased from Sigma Aldrich (Saint-Quentin Fallavier, France). DNase RQ1, deoxyribonucleotides (dNTPs), RNAsin® ribonuclease inhibitor, RNase H, GoTaq® G2 Hot Start Taq polymerase kit, molecular weight markers, PGEM-T Easy Vector System II®, T4 DNA ligase, *E. coli* strain JM109, Trypsin/Lys-C Mix and Trypsin Mass-Spec Grade was purchased from Promega (Charbonnières-les-Bains, France). Q5 High-Fidelity DNA Polymerase, Quick CIP, T4 DNA ligase, KpnI-HF, and BsrGI-HF were provided by NEW ENGLAND BioLabs.

Nucleospin® RNA Plus® kit, Nucleospin® gel, and PCR clean up, NucleoSpin® Plasmid kit, and NucleoBond® Xtra MAXI Plus EF were obtained from Macherey Nagel. Polyjet DNA Transfection™ was purchased from SignaGen Laboratories. LentiCRISPRv2-sgRNA, pVSVg and psPAX2 were from addgene. Mouse anti-GFAP, Amiconultra centrifugal filter 10K, and ZipTip C18were purchased from Millipore. Ultrapure Lipopolysaccharides (LPS-EB) were obtained from In vivo Gen (Toulouse, France). Peroxidase-conjugated goat anti-rabbit and peroxidase-conjugated goat anti-mouse were purchased from Jackson Immuno Research (West Grove, PA, USA). Mouse anti-Beta-actin was obtained from Cell Signaling Technology. Alt IgG-kappa-V antiserum referred to as anti-Heimdall was produced in rabbits by Biotem (Apprieu, France) using the chemically synthesized immunogenic sequence KPGKSPQLLIYYASSLQD coupled to KLH. Rabbit isotype control was purchased from BioLegend. Dako fluorescent mounting medium was obtained from Agilent (Santa Clara CA, USA).

Experimental Design and Statistical Rational

For the collection of the conditioned media n = 3 control rats (no balloon inflation, 0 day) and n=3 rats 3 days after SCI were sacrificed. All the experiments were performed in experimental replicates. Statistical analysis: For the proteomic statistical analysis of conditioned media, as a criterion of significance, we applied an ANOVA significance threshold of $P<0.05$, and heat maps were generated. Normalization was achieved using a Z-score with matrix access by rows. Data obtained from tissue analyses and behavioral testing were reported as mean ± SEM. Mean values among different experimental groups were statistically compared by one-way ANOVA and Tukey's post-hock tests using Graph pad PRISM software. p values < 0.05 were considered statistically significant (*$p < 0.05$, **$p< 0.01$, ***$p < 0.001$).

Spinal cord trauma

This study was carried out with the approval and according to the guidelines of the Institutional Animal Care and Use Committee of the Slovak Academy of Sciences and with the European Communities Council Directive (2010/63/EU) regarding the use of animals in research and Slovak Law for Animal Protection 377/2012 and 436/2012. All experiments were approved by the State Veterinary and Food Committee of the Slovak Republic (Ro-4081/17-221), and by the Institutional Ethics Committee. The SCI was induced using the modified

balloon compression technique according to our previous study[2]. Manual bladder extraction was required for 5 days after the injury. In the sham group (control) a 2-French Fogarty catheter was inserted at the same level of the spinal cord, but the balloon was not inflated and no lesion was made.

Collection of conditioned media (CM) from control and lesioned spinal cord segments

Experimental SCI rats (n=3) at 12h, 1D, 3D, 7D and 10 days were sacrificed by isoflurane anesthesia followed by decapitation. The spinal cord was pressure extracted by injection of 10ml of sterile saline buffer throughout the vertebrate canal, along the caudo-rostral axis. Each spinal cord was macroscopically observed to check that lesion was well centered at the Th8-Th9 level on the longitudinal axis. Entire spinal cord was divided into transversally sectioned slides (approximately 1.0 cm thick each) obtained from the lesion site (Th7-Th11) and from the rostral (C1-Th6) and caudal (Th12-L6) segments to the site of injury. Slides were then chopped into 0.5 cm thick sections (2 sections per segment) and deposited into a 12-well culture plate containing 1ml DMEM without FBS. After 24 hours of incubation at 37°C in a humidified atmosphere with 5% CO_2, 1 ml of SCI-derived conditioned media CM (CM-SCI) were collected (rostral, lesion, caudal segments) and centrifuged for 30 minutes at 15,000 g at 4°C. The same procedure was performed to obtain CM from control spinal cord tissue (n=3). Segments were stored at -80°C.

Voltage-sensitive Dye (Electrophysiology experiments)

The experiments were performed on control DI TNC1 cells (CTL), *Heimdall* KO DI TNC1 cells (KO) and DI TNC1 cells infected with the empty-vector used during CRISPR Cas9 (EV). Cells were plated onto 30-mm glass coverslips and grown for 3 days. Cells were loaded with 0.5 µM DisBAC2(3) at 37°C for 20 min in the HBSS medium to ensure dye distribution across the membrane (HBSS: 140 mM NaCl, 5 mM KCl, 1 mM MgCl2, 2 mM CaCl2, 0.3 mM Na2HPO3, 0.4 mM KH2PO4, 4 mM NaHCO3, 5 mM glucose and 10 mM HEPES adjusted to pH 7.4 with NaOH). Resting membrane potential was measured at 37°C using a temperature controller associated with the imaging platform (incubator box combined with a precision air heater: LIFE IMAGING SERVICES; Efringer strasse 79; CH-4057 Basel; Switzerland). Fluorescence was excited using an illumination DG4 system (Sutter) fitted with a xenon lamp (300 W). All recordings of

fluorescence were acquired using objective 20× in the Superfluor Nikon Eclipse Ti-series inverted microscope coupled to an EMCCD camera Rolera EM-C2 (Qimaging) and processed using Metafluor 7.7.5.0 software. Typically, we measured individually between 60-80 cells per experiment, and we repeated this at least 3 times and a representative figure is presented. Changes in DisBAC2(3) fluorescence were measured within an hour following incubation to ensure that the dye signal reached a steady state at excitation and emission wavelengths of 488 and 520 nm, respectively.

Patch Clamp

Membrane currents were recorded in the whole-cell configuration of the patch-clamp techniques using the Axopatch 200B amplifier (Molecular Devices, Union City, CA). The resistance of the patch pipettes, fabricated from borosilicate glass capillaries (World Precision Instruments, Sarasota, FL), when filled with the intracellular solution, was 2–3 megaohms for the whole-cell recordings. In the whole-cell experiments, series resistance was compensated for by ~70%. Currents were filtered at 1 or 2 kHz and sampled at 10 kHz. For current-clamp experiments, the pipette solution contained 140 mM KCl, 1 mM EGTA, 1 mM MgCl2, 5 mM HEPES. Osmolarity and pH were adjusted to 290 mOsm liter−1 and 7.2, respectively. Bath medium used for current-clamp experiments contained 140 mM NaCl, 5 mM KCl, 1 mM MgCl2, 2 mM CaCl2, 10 mM HEPES, and 5 mM glucose. The osmolarity and pH of external buffers were adjusted to 310 mOsm liter−1 and 7.4, respectively.

Secretome Protein Digestion

One hundred microliters of secretome were collected for each condition. Secretome digestion was performed as previously described [18]. In brief, the cell supernatants were denatured with 2 M urea in 10 mM HEPES, pH 8.0 and sonication performed on ice. The proteins were reduced with 10 mM DTT for 40 minutes followed by alkylation with 55 mM iodoacetamide conducted for 40 minutes in the dark. The iodoacetamide was quenched with 100 mM thiourea. The proteins were digested with 20 µg/mL LysC/Trypsin mixture overnight at 37°C. The digestion was stopped with 0.5% TFA. The peptides were desalted with a Millipore ZipTip device in a final volume of 20 µl of 80% ACN elution solution. The solution was then dried using the

SpeedVac. Dried samples were solubilized in 98% water+0.1% formic acid / 2% ACN before LC-MS/MS analysis.

Tissue protein extraction

Spinal cord injury segments (R1, L and C1) were collected 12 h, 1D, 3D,7D and 10D after the lesion. Each segment was cut in 10 slices of 1 mm thickness with a scalpel before being ground and proteins were extracted with CHAPS buffer 3.5% containing 50 mM dithiothreitol (DTT), 40 mM Tris/HCL buffer; pH 7.5. Samples were then vortexed, spun, sonicated for 20 min, and centrifuged at 15,000 x g. The supernatant was then collected. From each supernatant, 30µL of the sample were placed on 10 kDa amicons, to which 200 µL of UA buffer (8 M Urea, 0.1 M Tris, pH 8.5) were added before centrifugation for 15 minutes at 15000 x g. The procedure was repeated twice, before discarding the filtrate. The samples were then alkylated by adding 100 µL of 0.05 M iodoacetamide conducted for 40 minutes in the dark. These steps were repeated 3 times. The iodoacetamide was quenched with 100 mM thiourea. The proteins were digested with 20 µg/mL LysC/Trypsin mixture overnight at 37°C. The digestion was stopped with 0.5% TFA. The samples were then dried with speedvac, resuspended in 20 µL of 0.1% TFA water. The samples were then purified by Zip Tip before separation by reverse phase chromatography and analysis for shot gun proteomic.

Cells protein extraction

To extract the proteins, DI TNC1 or cortex primary astrocytes were resuspended in RIPA buffer (150 mM NaCl, 50 mM Tris, 5 mM EGTA, 2 mM EDTA, 100 mM NaF, 10 mM sodium pyrophosphate, 1% Nonidet P-40, 1 mM PMSF, 1X protease inhibitors) and subjected to three sonications of 5 seconds with a step on the ice for 30 seconds between each sonication. Then the samples were centrifuged at 14,000 x g for 20 minutes at 4°C. The supernatant containing the proteins was collected. To determine protein concentration in the samples, Bradford assay was used.

LC-MS/MS analysis

Samples were separated by online reversed-phase chromatography using a Thermo Scientific Proxeon Easy-nLC1000 system equipped with a Proxeon trap column (100 µm ID x 2 cm,

Thermo Scientific) and a C18 packed-tip column (Acclaim PepMap, 75 µm ID x 15 cm, Thermo Scientific). Peptides were separated using an increasing amount of acetonitrile (5%-35% over 120 minutes) at a flow rate of 300 nL/min. The LC eluate was electrosprayed directly from the analytical column and a voltage of 1.7 kV was applied via the liquid junction of the nanospray source. The chromatography system was coupled to a Thermo Scientific Q-Exactive mass spectrometer programmed to acquire in a data-dependent mode the Top 10 most intense ion method. The survey scans were done at a resolving power of 70,000 FWHM (m/z 400), in positive mode and using an AGC target of 3^{e6}. Default charge state was set at 2, unassigned and +1 charge states were rejected, and dynamic exclusion was enabled for 25s. The scan range was set to 300-1600 m/z. For ddMS², the scan range was between 200-2000m/z, 1 Microscan was acquired at 17,500 FWHM and an isolation window of 4.0 m/z was used.

MS Data Analysis of protein extract from the secretome

All the MS data were processed with MaxQuant (version 1.5.6.5) [19] using the Andromeda [20] search engine. The Secretome was processed in two different files. Proteins were identified by searching MS and MS/MS data against the Decoy version of the complete proteome for *Rattus norvegicus* of the UniProt database [21] (Release June 2014, 33,675 entries) combined with 262 commonly detected contaminants. Trypsin specificity was used for the digestion mode with N-terminal acetylation and methionine oxidation selected as the variables. Carbamidomethylation of cysteines was set as a fixed modification, with up to two missed cleavages. For the MS spectra, initial mass accuracy of 6 ppm was selected, with a minimum of 2 peptides and at least 1 unique peptide per protein, and the MS/MS tolerance was set to 20 ppm for HCD data. For identification, the FDR at the peptide spectrum matches (PSMs) and protein level was set to 0.01. Relative label-free quantification of proteins was performed using the MaxLFQ algorithm [22] integrated into MaxQuant with the default parameters. The data sets, the Perseus result files used for analysis, and the annotated MS/MS spectra were deposited at the ProteomeXchange Consortium [23](http://proteomecentral.proteomexchange.org) via the PRIDE partner repository[24]with the dataset identifier PXD004639 (for review: Username: reviewer60033@ebi.ac.uk Password: 7O08FxXe) for secretomes (12h and 24h) and PXD003375 for the ones from 3 days to 10 days. Analysis of the proteins identified was performed using Perseus software (http://www.perseus-framework.org/) (version 1.5.6.0). The file containing the information

from identification was used with hits to the reverse database, and proteins only identified with modified peptides and potential contaminants were removed. Then, the LFQ intensity was logarithmized (log2[x]). Multiple-samples tests were performed using an ANOVA test with a FDR of 5% and preserving grouping in randomization. Normalization was achieved using a Z-score with a matrix accessed by rows. For the statistical analysis, only proteins presented as significant by the ANOVA test were used for statistical analysis. Hierarchical clustering depending on protein extracts or secretomes was first performed using the Euclidean parameter for distance calculation and average option for linkage in a row and column trees using a maximum of 300 clusters. For visualization of the variation of the protein expression depending on the condition, the profile plot tool was used with a reference profile and an automatic selection of the 10 or 15 correlated profiles. To quantify fold changes of proteins across samples, we used MaxLFQ. To visualize these fold changes in the context of individual protein abundances in the proteome, we projected them onto the summed peptide intensities normalized by the number of theoretically observable peptides. Specifically, to compare relative protein abundances between and within samples, protein lengths normalized to log 2 protein intensities (termed “iBAQ” value in MaxQuant) were added to the MaxLFQ differences. Functional annotation and characterization of identified proteins were obtained using PANTHER software (version 9.0, http://www.pantherdb.org) and STRING (version 9.1, http://string-db.org).

Proteogenomic analyses

The AltProt database of rat is a prediction of the possible start codon around the classical Open Reading Frame (ORF), permitting the prevision of proteins on UTR, overlapping between UTR and CDS, and shift of ORF in +2 and +3 and conserving an initiator AUG codon. This database was combined with the reference Uniprot database on the same FASTA file. Label-Free Quantification (LFQ) was performed by MaxQuant 1.5.6.5. During this analysis, principal parameters were assigned as follows: Trypsin digestion with maximum missed cleavage of 2, carbamidomethylation as a fixed modification, and oxidation as a variable modification. The first search peptide tolerance was adjusted at 20 ppm and the main search peptide at 6 ppm. Finally, the minimum peptide length was restricted to 6 amino acids. The length of this kind of protein, a mean of 50 to 100 amino acids, obliges to decrease the number of unique peptides identified at 1. Statistical analysis was performed with Perseus 1.5.5.3, log2(x) was

then realized and results were filtrated to eliminate identification by site as well as reverse and potential contaminants. Significant variations between samples were assessed by t-test. Filtration for AltProt was applied to keep only the AltProt identified with a unique peptide and no classical protein redundancy on Majority ID. Variation of quantification was revealed by hierarchical clustering with Euclidian distance measurement. Identification of AltProt was performed using BlastP and non-redundant protein sequences to find their sequence homology with classic and unknown proteins. The gene accession numbers were used to retrieve mRNA or ncRNA sequences from the Ensembl database.

Sub-network Enrichment Pathway Analysis.

Using Elsevier's Pathway Studio (version 11.0/ /Elsevier), all relationships between the differentially expressed proteins among all conditions were depicted based on the Ariadne ResNet[19]. For proteins identified in the shotgun analysis, the Subnetwork Enrichment Analysis (SNEA) algorithm was used to detect the statistically significant altered biological pathways in which the identified proteins are involved. This algorithm uses Fisher's statistical test to detect any non-random associations between two categorical variables organized by a specific relationship. Also, this algorithm starts by creating a central "seed" from all the relevant identities in the database and builds connections with associated entities based on their relationship with the seed. SNEA compares the sub-network distribution to the background distribution using one-sided Mann-Whitney U-Test and calculates a p-value; thus, representing a statistical significance between different distributions. In all analyses that we performed, the GenBank ID was used to form experimental groups based on the different conditions present for analysis. The pathway networks were reconstructed based on biological processes and molecular functions for every single protein, along with its associated targets.

Astrocytes cell line

DI TNC1 cell line was grown in DMEM supplemented with 10% Fetal bovine serum (FBS), 4 mM L-glutamine, 1 mM Sodium Pyruvate, 100 U/ml penicillin, and 100 µg/ml streptomycin at 37°C in a humidified atmosphere containing 5% CO_2.

Isolation and cultivation of rat cortex primary astrocytes

After cervical dislocation, cerebral cortices of 3–6-day-old rats were dissected, stripped of their meninges, and mechanically dissociated by repeated pipetting followed by passing through a nylon mesh (70 µm). Cells were plated in Petri dishes pre-coated with 20 µg/ml rat tail collagen, type I and cultivated in DMEM containing 10% FBS and 2 mM L-glutamine at 37°C, 5% CO_2 in a water-saturated atmosphere. The medium was changed twice a week. The astrocyte cells were cultivated and expanded for 20 days. The purity of astrocyte cell cultures isolated by this procedure was routinely around 95% (anti-GFAP antibody staining). The confluent astrocyte cultures were frozen in a freezing medium: 45% DMEM, 45% FBS, and 10% DMSO.

Transcriptomic

RNA extractions were performed using Nucleospin RNA Plus® kit according to the manufacturer's instructions. Two micrograms of RNA were treated with DNase RQ1 (1U/µg total RNA) and retro-transcribed using the SuperScript® III kit. RT-PCR was then carried out using primers encompassing coding as well as 5' and 3' non-coding sequences: Rat *Heimdall* forward primer: 5'- AAT GAA CCC TGC AGC TCT GC -3' and reverse primer: 5'- GCT GGG GCA CCC TGT ACT CTC -3'), GoTaq polymerase and 40 cycles at 95°C/1 min, 60°C/1 min and 72°C/2 min. Products were then purified, subcloned into pGEM-T easy vector and sequenced.

Immunofluorescence

During immunofluorescence experiments, 19 000 normal DI TNC1 or DI TNC1 overexpressing Heimdall-Flag were grown on cover slips. After fixation with paraformaldehyde 4% (PFA) for 10 min, cells were washed in PBS 1X (phosphate-buffered sodium 1X) and quenched with glycine 50mM for 10 min. Cells were then permeabilized with 0.2% Triton X-100 for 10 min and treated in a blocking buffer (PBS 1x containing 1% bovine serum albumin, 1% ovalbumin, 1% NDS) for 1 hour. Overnight incubation was then carried out at 4°C with rabbit Anti-Heimdall (15.6 ng/µL) or mouse anti-FLAG (1/1000). Primary antibodies were diluted in the blocking buffer. After 3 washes with PBS 1X, cells were incubated for 1h at 37°C with respective secondary antibodies, *i.e.*, Alexa Fluor® 488-conjugated donkey anti-rabbit or Alexa Fluor® 555-conjugated donkey anti-mouse diluted at 2 µg/mL in the blocking buffer. After 3

washes with PBS 1X, nuclei were stained with Hoechst 33,342 (1:10 000). A final wash in PBS 1X was performed and cover slips were mounted using Dako fluorescent mounting medium. Samples without the addition of primary antibodies were used as a negative control. The pictures presented are representative of independent triplicates. Observations were then performed using a confocal microscope (Zeiss LSM700).

Effect of Heimdall neutralization with rabbit anti-Heimdall added in the culture medium of DI TNC1 cells.

DI TNC1 cells were plated at a density of 18 000 cells/per well in 35 mm wells plate. After overnight starvation with DMEM medium supplemented with 2% FBS, 4 mM L-glutamine, 1 mM Sodium Pyruvate, 100 U/ml penicillin and 100 µg/ml streptomycin, cells were placed in serum-free medium. Rabbit anti-Heimdall or rabbit isotype control at 1 µg/mL was then added to the medium. Live images of cells incubated or not in the presence of the antibodies were captured after 24 h or from 0 to 7 days of treatment. Images were captured with a camera mounted on a phase-contrast microscope (Nikon Eclipse TS100). During the treatment with rabbit anti-Heimdall, neurite-like structures were observed. To determine their length, measurements were performed by ImageJ software and statistical significance was evaluated with One-Way ANOVA followed by Tukey Kramer Test (GraphPadInStat 3.0). Total protein cell extracts were also obtained after lysis with RIPA buffer (see “cell protein extraction” section) and digested with trypsin before shot-gun proteomics analysis.

CRISPR-Cas9

The various sgRNAs were designed using the Biology software Benchling (https://benchling.com). Optimization of DNA target specificity and minimization of the off-target effects were obtained as described previously[26]. The sgRNAs were cloned into the plasmid LentiCRISPRv2 [27]. The corresponding lentiviruses were generated in HEK293T cells by co-transfection of LentiCRISPRv2-sgRNA with the packaging plasmids pVSVg[28] and psPAX2 [29]. Lentiviral particles were purified from the HEK293T culture supernatant and utilized for infection of the target cells. Polybrene was used as an infection reagent. Infected cells were selected by treatment with puromycin at 3 µg/ml. The sequences of the sgRNAs targeting *Heimdall* were as follows: 5'- CATCGAATGTCGAGCAAGTG -3' (strand sense) and 5’-

CTCACTTGCTCGACATTCGA -3' (strand antisense). As a non-target control, the experiment was performed with a sgRNA targeting *Trop2*, a human gene that is not expressed in astrocytes, *Trop2*: 5'- GCCACACGGCCGCGCAGGAC -3'.

Western Blots

During the experiments performed to detect Heimdall or assess the efficiency of *Heimdall* KO by CRISPR-Cas9, 2 million control or *Heimdall* KO DI TNC1 cells were plated on sterile 6-well plates. In the case of LPS stimulation, cells were starved overnight in DMEM medium supplemented with 2% FBS, placed in serum-free medium and treated or not with 200 ng/mL of LPS. Protein extraction was also conducted on primary cultures of astrocytes isolated from the cortex of pups 3 Days, known to be depleted of B Cells. To detect Heimdall-Flag during overexpression studies, cell extracts from HEK293 and DI TNC1 astrocytes transfected with the construct were also prepared. Total cell extracts were obtained after lysis with RIPA buffer as described in the "cell protein extraction" section. When secretomes were collected, protein concentrations were determined using the Bradford assay. Forty micrograms of proteins from total cell extracts or secretomes were reduced in Laemmli buffer containing β-Mercaptoethanol and denatured at 95°C for 5 minutes. During western blots performed in non-reducing and non-denaturing conditions β-Mercaptoethanol and the 95°C step were omitted. Proteins were then separated by SDS-PAGE. After transfer onto a nitrocellulose membrane, a blocking step was performed for 1h in blocking buffer 1 (PBS-Tween 0.1% containing 5% BSA). According to the studies performed, an overnight incubation at 4°C was then carried out with rabbit anti-Heimdall (1/1000) or mouse anti-GFAP (1/500) or mouse anti-FLAG (1/500). After extensive washes with PBS-Tween 0.1%, membranes were respectively incubated for 1h with peroxidase-conjugated goat anti-rabbit (0.08 µg/mL) or peroxidase-conjugated goat anti-mouse (0.03 µg/mL) diluted in blocking solution 1. Extensive washes with PBS-Tween 0.1% were again performed and revelation was carried out using an enhanced chemiluminescence kit. When Beta-actin detection was also carried out, membranes were washed with PBS-Tween 0.1% and stripped with 0.2 M citric acid for 30 min. After extensive washes with TBS-Tween 0.1%, a blocking step was performed for 1h in blocking buffer 2 (TBS-Tween 0.1% containing 5% nonfat dry milk). Membranes were then incubated with mouse anti-Beta-actin diluted at 1/1000 in blocking buffer 2. After extensive washes with TBS-Tween 0.1%, incubation with peroxidase-conjugated goat anti-mouse (0.03

µg/mL) diluted in blocking solution 2 was performed for 1h. Washes steps with TBS-Tween 0.1% were repeated and the revelation was conducted using an enhanced chemiluminescence kit. Band quantification was performed using ImageJ software.

Immunoprecipitation

One and a half micrograms of Dynabeads Protein A were resuspended according to the manufacturer's instructions. Then 7.8 µg of rabbit Anti-Heimdall or 7.8 µg of rabbit Anti-Heimdall pre-incubated overnight at 4°C with 15.6 µg of peptides used for the immunization (control condition referred in the figure as "PEP") were added to the beads. The samples were incubated under agitation for 1h at room temperature. The supernatants were removed, and beads were washed 3 times with 250 µL of PBS 0.1 M pH 8.0. Then samples were incubated under agitation for 1h at room temperature with 500 µg of proteins from cell extracts of DI TNC1 astrocytes treated or not with 200 ng/mL of LPS. After 3 washes with 250 µL of PBS 0.1M pH 8.0, an elution with 50 µL of Glycine 100 mM pH 2.8 was performed under agitation for 15 minutes at room temperature. The supernatants were collected and stored in a collection tube. The elution step was repeated 2 times. The pH of the samples was then adjusted to pH 7.4 with Tris 500 mM and they were dry with SpeedVac before trypsin digestion and shot gun proteomic analyses.

Trypsin digestion of proteins immunoprecipitated with rabbit anti-Heimdall.

Vacuum dried samples were resuspended with Ammonium Bicarbonate 20 mM and reduced with DTT 10 mM for 30 minutes at 60°C. An equal volume of Iodoacetamide 15 mM was added and samples were incubated in the dark for 30 minutes at room temperature. Fifty microliters of DTT 15 mM were again added and tryptic digestion was conducted overnight at 37°C with 50 ng of Trypsin. Digestion was stopped with 10 µL of H_2O-TFA 5% and the samples were dried using the SpeedVac. They were resuspended with 20 µL of H_2O-TFA 0.1%, desalted with a Millipore ZipTip C18 device and eluted in a final volume of 20 µl of elution solution (80% ACN / 20% H_2O-TFA 0.1%). The solution was then dried using the SpeedVac. Dried samples were solubilized in resuspension solution (2% ACN / 80% formic acid 0.1%) before LC-MS/MS analysis.

Filter Aided Sample Preparation (FASP) protein digestion.

Forty micrograms of protein cell extracts from control or *Heimdall* KO DI TNC1 cells were loaded on Amicon ultracentrifugal filter 10K and the volume was adjusted at 200 µL with denaturing buffer (Urea 8M, Tris-HCL 0,1M, H2O) before centrifugation at 14,000 x g for 30 minutes. Two hundred microliters of the denaturing buffer were again loaded, and the samples were centrifuged at 14,000 x g for 30 minutes. The filtrate was discarded and 100 µL of alkylation solution (Iodoacetamide 0.05 M in denaturing buffer) was loaded. The samples were then incubated in the dark for 20 minutes at room temperature and centrifuged at 14,000 x g for 25 minutes. One hundred microliters of denaturing buffer were loaded, and the samples were centrifuged at 14,000 x g for 25 minutes. This step was repeated two times. One hundred microliters of Ammonium Bicarbonate Buffer 50 mM were loaded, and the samples were centrifuged at 14,000 x g for 25 minutes. This step was repeated two times. Amicon ultracentrifugal filter 10K was transferred to a new collection tube and 1.6 µg of Trypsin were loaded. After overnight incubation at 37°C, samples were centrifuged at 14,000 x g for 25 minutes and filters were washed with 50 µL of NaCl 0.5 M. After centrifugation at 14,000 x g for 25 minutes, 10 µL of H_2O-TFA 5% were loaded to stop the digestion and samples were dried using SpeedVac. After their resuspension with 20 µL of H_2O-TFA 0.1%, samples were desalted using a Millipore ZipTip C18 device and eluted with 20 µl of elution solution (80% ACN / 20% H_2O-TFA 0.1%). The solution was then dried using the SpeedVac. Dried samples were solubilized in resuspension solution (2% ACN / 80% formic acid 0.1%) before LC- MS/MS analysis.

Overexpression of Heimdall in DI TNC1 cell line.

Heimdall coding sequence was amplified using the following primers: Forward primer: 5'-TATAGGTACCAGGCGCGCCGCCACCATGGCTGTGCCCACTCAGC -3'; reverse primer: 5'-TTAATGTACAGGCGCGCCTTACGCTGCTTTATCATCATCATCTTTATAATCCGCTGCTGTCATGGCTTG AATCACTGTGG -3'. KpnI restriction site was added in the forward primer and BsrGI restriction site as well as Flag-Tag coding sequence were included in the reverse primer. During PCR experiment, 1 ng of PGEM-T vector in which, *Heimdall* cDNA has been subcloned served as a template. Amplification was carried out using Q5 High-Fidelity DNA Polymerase. Purified PCR products and 2 µg of pcDNA™5/FRT/TO vector were then digested with KpnI-HF and BsrGI-HF. Digested vector was also dephosphorylated using Quick CIP. After gel and column

purification of digested products, ligation of *Heimdall* cDNA fused to Flag-Tag coding sequence into processed pcDNA™5/FRT/TO vector was conducted using T4 DNA ligase. Maxipreparation of the plasmid was prepared and the construct was transfected into HEK293 or DI TNC1. For this purpose, 300 000 HEK293 or DI TNC1 cells were plated in 6 well plates and grown in a complete medium until they reached about 80% confluence. One hour before the transfection, the medium was renewed. One microgram of the construct was mixed with 50 µL of DMEM-free medium and 3 µL of PolyJet were mixed with 50 µL of DMEM-free medium in another tube. The two solutions were mixed and after an incubation of 15 minutes at room temperature, the mixture was added to the cells. After an overnight incubation, the medium was replaced by the complete medium. For HEK293 overexpression, it was induced by treatment with tetracycline 1X. After 24, 48 and 72 h immunofluorescence and western blots were carried out.

Modeling and prediction of interactions

Structure modeling of Heimdall was performed with the I-Tasser software [30]. For both the Kappa variable light chain and Heimdall, the most stable models (C-Score between -5 and +2) were retained. The prediction of PPIs was performed with the ClusPro software [31]. The Kappa light chain was identified as a receiver and Heimdall as a ligand. The interaction model was carried out by docking the ligand onto the receiver without crosslinker size restriction. ClusPro then generated multiple interaction models ranked in the order of stability. The selected models were still part of the Top5 "balanced" models considering the best compromise of stability. The selected interactions were then illustrated with Chimera to measure the distance between the atoms observed during XL-MS analysis[32].

Results

Spatio-temporal shotgun proteomic analyses were performed on the secretome of spinal cord segments obtained on days 1, 3, 7 or 10 post-SCI. A set of 17 Ghost proteins was identified at the lesion site with at least 1peptide per protein recognized and with a percentage of false positive (FDR) of 0.01. Hierarchical clustering indicated two main branches *i.e.*, one for the 1-day lesion segment and the second one regrouped control segment, 3 days, 7 days, and 10 days lesion segments (**Figure 1A**). Two clusters were computated according to

the relative abundance of the proteins. Cluster 1 represented proteins that are more abundant at 1 day after the lesion and Cluster 2, those less abundant at 1 day after the lesion and which, were also mostly over-abundant at 10 days (**Figure 1A**). Four Ghost Proteins from each of these clusters were identified. Since the branch at 1 day is the most variable condition according to the hierarchical division of the sample, we focused on the spatial distribution of these proteins at the lesion site and at the lesion proximity *i.e.* Rostral 2 and Caudal 2 segments (**Figure 1B**). It is interesting to note that among the 9 proteins observed as more abundant at 1 day (**Figure 1A**) only 2 were detected at the lesion site. Most of them were in higher levels in the Rostral and Caudal segments than in the lesion segment (**Figure 1B**). This suggests a specificity in the function of these Ghost Proteins between lesion, rostral and caudal segments. We have previously demonstrated that 12h after injury, inflammation is not activated at the rostral-caudal regions [3]. Thus, we also pursued our investigation at 12h after SCI by considering all segments from Rostral 2 to Caudal 2 and identified additional 30 Ghost proteins (**Supp. Data 1 & 2, Table 1**). Proteins were characterized according to the MaxQuant and Perseus software. As a criterion of significance, we applied ANOVA significance threshold of p-value of 0.05, and a heat map was generated (**Figure 1C**). Data from this analysis revealed that fourteen Ghost proteins exhibited a specific expression in terms of segments. Only 2 proteins were almost always more abundant whatever the segments *i.e.* IP_1315648.1 and IP_1255506.1 (**Figure 1C**).

Immunoglobulin-like proteins identification

Interestingly, two Ghost proteins (IP_1304334 and IP_1282467), identified at the lesion site at 12h displayed an immunoglobulin (Ig) domain (**Supp. Data 1 & 2, Figure 1C**). However, only IP_1304334 was more abundant in the lesion segment at 12h. Time course analysis per segment, confirmed its expression in the control group in the R1, C2, at 3 days and in the R2, then in C3 at 10 days (**Supp. Figure 1**). This Ghost protein showed homology with the predicted protein rCG53372 and was described in the archive Ensembl database as being derived from the long non-coding RNA (lincRNA) AABR07051592.2 **(Supp. Data 2**). Tandem mass spectrometry (MS/MS) allowed the identification of the protein from amino acids 45 to its C-terminal residue based on tryptic digested peptides (**Figure 2A**). These peptides contained an Ig superfamily sequence. AltProt database survey revealed the presence of two

isoforms *i.e.* IP_1304331.1 and IP_1304334.1 (**Figure 2A**). The major difference between the two amino acid sequences was in residues 70-73 from GASS to AANR (**Supp. Figure 2).** Our previous results on SCI showed the presence of immunoglobulins in astrocytes despite a preliminary treatment with anti-CD20[2]. In addition, a survey of "Geodatasets" (https://www.ncbi.nlm.nih.gov/gds/), the NIH-compiled bank of mRNA expression studies that focused specifically on the mRNA profile of spinal cord astrocytes under inflammatory conditions showed that astrocytes can be a second source of neural IgGs. Moreover, when we evaluated the supplementary data provided in the transcriptomic work performed by Itoh and collaborators[33] on astrocytes from a mouse model of multiple sclerosis, we found that the mRNA species showing the highest fold changes in the EAE spinal astrocytes were indeed mRNAs coding for IgG2c, kappa chains and junction chains to control spinal astrocytes [33]. Thus, we suspected that these cells may also synthesize IP_1304331.1 protein. Therefore, cDNA was synthesized from rat astrocytes DI TNC1 cell line, and RT-PCR was performed with primers designed from AABR07051592.2 and encompassing coding as well as 5' and 3' non-coding sequences (**Figure 2Ba**). A fragment of interest at the expected size of 540 bp was amplified and sequencing confirmed that this amplicon encoded IP_1304331.1 (**Figure 2B**). We, then, decided to name this protein "Heimdall". Sequence analysis of Heimdall revealed the presence of a leader sequence corresponding to a signal peptide at regions 1 to 21 before the FR1 region to the CD3 segments and confirmed that this protein was close to a kappa light chain variable region (**Figure 2C; Supp. Figure 3**). A prediction using PrDOS software also indicated that Heimdall sequence contained intrinsically misformed parts in positions 1-6, 81-88 and 100-123 (**Figure 2C)**. This sequential mis-conformation feature is unique to proteins commonly referred to as Intrinsically Disordered Proteins (IDPs) [34]. These proteins can self-assemble into fibrils [35]. They are involved in several pathologies such as Bence Jones disease, Alzheimer's disease and astrocytomas[35]. The 3D representation of Heimdall confirmed that this alternative protein displayed similarities with the kappa V chain found in amyloidosis [16] (**Figure 2D**). In Bence Jones disease, the over-expression of the kappa V chain leads to the formation of multimers [16]. To determine if Heimdall was also able to form multimers, we synthesized a polyclonal antibody directed against the following sequence KSGKSPQLLIYAANRLQDG (red) (**Figure 2D'**).To validate that Heimdall was specifically detected by the antibody, Western blots were performed on protein extracts from DI TNC1 cells (**Figure 2E**). The experiments were conducted in reducing conditions with anti-Heimdall alone or anti-

Heimdall pre-incubated with its antigenic peptides (**Figure 2E**). A control with the secondary antibody alone was also added. No signal was observed after incubation with the secondary antibody. Therefore, all the various bands detected were specific to the fixation of anti-Heimdall antibody. In addition, all the various bands detected with anti-Heimdall antibody disappeared or strongly decreased when anti-Heimdall was incubated with the Heimdall peptides. A decrease of band intensities and not a complete loss can be explained by the fact that the raised antibody has a very strong affinity with Heimdall and the incomplete saturation of anti-Heimdall with its antigenic peptides. Considering the different specific bands observed with anti-Heimdall, the one at 11 kDa corresponded to Heimdall without signal peptides, the one at 22 kDa to Heimdall dimer and the one at 26 kDa to Heimdall dimer with the signal peptide. Similarly, to what is observed during pre-antibodies synthesis, the higher bands at 34 kDa, 50 kDa, 60 kDa and 140 kDa may correspond to Heimdall associated with its protein partners. To confirm this hypothesis, MS/MS experimental analyses were performed and confirmed the presence of IGVK or IgHV chains (**Supp. Data 3**). According to the sizes detected, this suggests the association of Heimdall with aberrant forms of IgG such as the truncated forms identified in different cancers [36]. To mimic the inflammatory condition observed at the lesion site after SCI, Western blot experiments were performed on protein cell extracts from DI TNC1 cells stimulated or not with 200 ng/mL of LPS for 24h and 48h (**Figure 2F**). To validate our results, these experiments were also carried out on protein cell extracts from primary astrocytes isolated from the cortex of 3 days pups, known to be depleted of B Cells [37]. Before protein extraction, these cells were also treated or not with 200 ng/mL of LPS for 24h and 48h (**Figure 2F**). Western blot analyses were conducted in reducing and denaturing conditions. At 48h post-LPS stimulation, the presence of the 11 kDa band corresponding to the predicted size of Heimdall without the leader sequence was detected in DI TNC1 cells and in primary cortex astrocytes. At this time point, the band at 22 kDa was highly abundant in DI TNC1 cells while the one at 26 kDa decreased. In primary cortex astrocytes, bands at 22 kDa and 26 kDa appeared at 48h with or without LPS treatment (**Figure 2F**). This experiment also revealed the presence of higher forms between 40 kDa and 140 kDa. To study the intracellular localization of Heimdall, we performed an immunofluorescence experiment and established its presence in the endoplasmic reticulum, Golgi apparatus, and cytoplasm but not at the membrane level which is in line with the presence of the leader sequence and therefore its secretion (**Figure 2G**). Western blot analyses carried out on the

secretome of astrocytes stimulated with LPS confirmed the presence of Heimdall monomer and revealed the presence of two bands at 75 kDa and 110 kDa in control and LPS conditions. A third band at 52 kDa was also observed only in LPS conditions (**Figure 2H**). Interestingly, the overexpression of Heimdall in HEK293 cells confirmed the size of Heimdall at 11kDa (**Figure 2I**). Of note, as mentioned previously, the two isoforms *i.e.* IP_1304331.1 and IP_1304334.1 exhibited very close sequences including the one used as an antigenic peptide. Altogether, this reinforced the fact that astrocytes contained several IGKV light chains forming multimers or associated with truncated or complete heavy chains. Moreover, the presence of aberrant IgG could be reinforced by other ghost proteins identified in our data such as the Ghost protein IP_1282467 (**Figure 1C**). Indeed, it also originated from the lincRNA AABR07065780.1 (**Supp. Data 2**), synthesized from the gene AAA41368, and described in the IMGT database () as homologous to a IGHV11*4 (**Supp. Figure 4**). The IGVH-like protein was also identified in the lesion segment 12h after SCI and after RhoAi treatment which is known to activate neurogenesis (**Supp. Figure 5**). However, the role of these molecules remains currently unknown. Homology with reference proteins and immunoglobulin-like sequences suggest that these proteins originate from regions described as non-coding and have a much more important role than expected. More than a simple regulator, the presence of the Ig domains suggests that alternative proteins may interact with receptors and other proteins and could play an integral role in a cell signaling pathway. It is interesting to note that the Heimdall protein also shares 90% sequence homology with the PrevB1 light chain. Our results revealed that the Heimdall protein would have the ability to form multimers but also to associate with other IgG chains. Therefore, this process is close to what is observed during an early stage of somatic maturation of B cells with the expression of a heavy chain linked to a pseudo light chain[38]. Moreover, if the current debate on the ability of lncRNAs to code proteins is keen, finding a protein from one of them and possessing Ig domain seems to prove it.

Heimdall function investigation

Since DI TNC1 astrocytes secreted Heimdall even in resting conditions, we decided to assess if it may exert an autocrine effect. Thus, we tested the impact of the addition of anti-Heimdall to the astrocytes culture medium. The treatment with a rabbit isotype control was also included to ensure that the effect observed was due to the neutralization of Heimdall and not to the fixation of the antibody to the FC gamma receptor through its constant region. After

24h of incubation in presence of anti-Heimdall, astrocytes showed extensions that were similar to neurite-like structures which were not observed with the control isotype treatment (**Figure 3A**). The significance of this observation was confirmed by the measurement of the astrocytic extension between 0 and 1 day (**Figure 3B**). Moreover, a time course experiment performed from 0 to 7 days revealed that the size of the extensions was significantly longer in the presence of anti-Heimdall than in the isotype condition up to 3 days (**Figure 3B'**). From 4 to 7 days, no clear difference was detected suggesting that the cells continued to proliferate and secrete Heimdall. Therefore, the amount of anti-Heimdall added to the medium was probably not sufficient to permanently induce the change of cell phenotype.

To characterize the impact induced by the neutralization of Heimdall, we carried out shotgun proteomics on protein cell extracts from DI TNC1 astrocytes incubated with anti-Heimdall or treated with LPS to mimic the inflammatory conditions observed at the lesion site after SCI. A multiple sample ANOVA-test with a $p<0.05$ was applied and 3 clusters were identified (**Figure 3C, Supp. Data 4**). **Cluster 1** was specific to proteins more abundant under anti-Heimdall treatment whereas **Cluster 2** corresponded to those more abundant under LPS stimulation. Proteins identified in **Cluster 1** were related to pluripotency (Pfa1, phf5a), alternative splicing (Hrnpa1b2, Khsrp, Srsf1, Srsf2), cell growth, cell proliferation, and cell differentiation (**Figure 3C, See inset Pathway analysis, Supp. Data 4**). **Cluster 3** was common to both LPS and anti-Heimdall conditions. To rule out non-specific effects due to FcγR activation by the Fc antibody itself, we then compared treatment with anti-Heimdall to treatment with the isotype control antibody. Venn diagram revealed 92 specific proteins detected only after incubation with anti-Heimdall versus 124 and 220 in control and isotype conditions, respectively (**Figure 3D, Supp. Data 5)**.

Among the proteins detected after treatment with anti-Heimdall, some of them were known as gatekeepers of astrocyte-neuronal conversion such as RNA-binding proteins PTBP3, CD166, Dead-end homolog 1, Rho GTPase-activating protein 1, Twinfilin-1, Tachykinin 4 and Huntingtin interacting protein 2 (**Supp. Data 5**). Pathway analysis (**Figure 3D'**) revealed that the specific proteins modulated by the various treatments were involved in common processes such as cell proliferation or cell survival. However, after Heimdall blockage or treatment with isotype control antibody, proteins involved in embryonal development were

popping out (**Figure 3D'**). MaxLFQ algorithm was then used to perform label-free quantification of proteins. A Heatmap was then obtained based on the average of the triplicate from anti-Heimdall and isotype treatments, followed by a t-test with a p-value <0.05. This pointed out two specific clusters (**Figure 3E**). In **Cluster 1**, proteins more abundant in the isotype condition were identified. and some of them were linked to neuroinflammation (Lyar, Svil, Lzic, Leng1, Ikbkg proteins) or involved in neural development (Nedd8, S100a6, Phf3) (**Supp. Data 6**). **Cluster 2** highlighted the proteins more abundant under anti-Heimdall treatment and included proteins involved in pluripotency (Ube2k, Plrg1), notch pathway (Kdelc2), differentiation and development (Dhx15, Nsun2), neuronal progenitor (Ywhah, Ctsb, Stoml2), RUNX3 expression (Psmc4, Psmb4, Psme2, Psmd5, Ap2m1, Ap2a1) (**Supp. Data 6**). Similarly, to what was observed, pathways analysis confirmed that proteins found in **Cluster 1** were involved in cell survival, proliferation, cell growth, alternative RNA splicing, and transcription activation. In **Cluster 2** proteins were involved in embryonal development, cell growth, protein synthesis and regulation of apoptosis (**Figure 3E**).

To identify the putative Heimdall interactors, an immunoprecipitation with anti-Heimdall was then carried out on total protein extracts from DI TNC1 cells treated or not with LPS **(Figure 3F**). As a control condition, anti-Heimdall was pre-incubated with its antigenic peptides before the addition of total protein extracts (IP PEP) (**Figure 3F**). Characterization of immunoprecipitated proteins was conducted using shotgun proteomics. Twenty-four specific proteins were identified from cell extracts of DI TNC1 stimulated with LPS and immunoprecipitated with anti-Heimdall (**Figure 3F**). String proteins analysis revealed that some proteins were involved in neurites outgrowth or pluripotency (**Figure 3F'**). Among these proteins, EphA3, EphB6, Notch 1, ChRNA9, TRAM, Ndrg2, angiomotin, Snta1, Ipo13, Hdac4 and Src were identified and known to be involved in astrocyte fate. Notch 1 is a key factor protein that mediates cell fate safeguarding mechanism in astrocytes, and acts as an essential barrier for lineage conversion [15]. Moreover, Epha3 is also involved in control of astrocytes fate. In fact, EphA3 acts via EphA4 to suppress Wnt/β-catenin signaling to inhibit the neurogenic potential of retinal stem cells [39]. Finally, IPO13 has a key role in ESC neuronal differentiation, through the nuclear transport of Pax6 [40]. Hdac4 is also a key factor involved in astrocytes reprogramming [41]. An average Heatmap followed by a t-test with p<0.05 revealed that in resting conditions, seven phosphoproteins were overexpressed upon

treatment with anti-Heimdall (**Figure 3F''**). Six of them are known to be critical in Parkinson's disease such Ndufs3 [42], Dnm1L[43, 44], Gstp1[45], Psmd11 [46], Blvra[47] or in Epilepsia (Nmt1) [48] (**Figure 3F'', Supp. Data 7**). Funrich analysis revealed that the proteins immunoprecipitated with anti-Heimdall after LPS treatment (IP LPS) were mostly implicated in neuronal differentiation, axon guidance, Notch signaling pathway and astrocyte differentiation (**Figure 3F'''**). To definitively confirm our results, CRISPR-Cas9 was then performed to knock out *Heimdall* in DI TNC1 cells. Phenotypic analysis of the astrocytes by microscopy, demonstrated that compared to control, *Heimdall* KO astrocytes showed elongations after 7 days of culture (**Figure 4Aa, Supp. Data 8**) as it was observed during incubation with anti-Heimdall (**Figures 3B', 3B''**). To validate the KO of *Heimdall,* Western blot analyses were conducted (**Figure 4Ab**). As expected, a total loss of the dimeric form of Heimdall (in non-reducing conditions) and several other bands from 40 kDa to 100 kDa corresponding to its association with heavy chains truncated or not were registered for *Heimdall* KO samples. Interestingly, the remaining bands could correspond to the second isoform since it possesses a sequence close to the epitope recognized by the antibody. Moreover, such close sequences can also be found in IGKV. Therefore, we cannot also exclude that this signal could be linked to IGKV recognition. We then performed Western blot analysis on secretome from control DI TNC1 cells or *Heimdall* KO DI TNC1 cells. (**Figure 4Ab'**). Since transfection via lentiviruses may trigger an immune reaction and a secretory profile, we decided to consolidate the control panel by using DI TNC1 cells transfected with an empty vector. During these experiments, all the cells were stimulated or not with LPS. In non-stimulated cells, two bands were detected at 90 kDa and 140 kDa. By contrast, under LPS stimulation, the previous two bands were absent and two bands were observed at 55 kDa and 110 kDa. However, only the protein at 55 kDa disappeared in *Heimdall* KO DI TNC1 cells and not in other conditions, confirming its specificity. These results confirmed that *Heimdall* was secreted not as a monomer but associated with another protein such as an IgH protein. Since, *Heimdall* KO astrocytes displayed a neuronal-like phenotype, we investigated the expression of GFAP, a specific maker of astrocytes (**Figure 4Ac**). This revealed that its expression decreased under *Heimdall* KO, consistently with astrocyte phenotype changes (**Figure 4Ad**). The depolarization state of *Heimdall* KO DI TNC1 cells, control DI TNC1 cells and DI TNC1 cells infected with the empty vector (EV) was then evaluated. While a fluorescence of 600 A.U. was observed in control and EVs conditions, it reached 2200 A.U. in *Heimdall* KO, establishing a depolarization effect of *Heimdall* KO on

astrocyte membranes (**Figure 4Ae**). Moreover, we measured the resting membrane potential of DITNC1 cells in the whole-cell configuration of the patch-clamp techniques. Control cells had a resting membrane potential of −25 ± 1.7 mV (n = 8), whereas KO-2 cells had a resting membrane potential of −11 ± 1.2 mV (n = 8) (**Figure 4Af**), confirming that KO2 are more likely to trigger an action potential compared to CTL which is line with depolarization experiments. Thus, to assess the effect of *Heimdall* KO at the molecular level, shot gun proteomic analyses were conducted. To rule out off-target effects, we included a negative control sgRNA targeting human *Trop2*, known to be non-expressed in the brain. A comparison with control DI NTC1 cells treated or not with polybrene, the cationic polymer used to enhance lentiviral infection, was also performed. A Venn diagram was generated and revealed 38 proteins detected exclusively in *Heimdall* KO cells (**Figure 4B**). Among these proteins, some of them are known to be involved in neurite outgrowth (Camkk2, Musashi RNA-binding protein 2 [49], Spastin[50], Cactin[51], Mapkapk2 [52], Angpt4 [53], Akt2 [54], Lin7a [55], Mark2 [56]) or neuronal progenitor phenotype (Cnot2, Dis3l2, Musashi 2). Systems biology analysis performed through Reactome pathways analyses revealed proteins involved in cell cycle and embryonic development, metabolism (lipids, RNA, and proteins), cytokines signaling molecules, neuronal system, signal transduction, apoptosis, neddylation and amyloid fiber formation pathways (**Supp. Figure 6**). By contrast, for *Trop2* KO (T2), signaling by FGFR2 was the most prevalent pathway detected by Reactome pathways analysis (**Supp. Data 9**). Shotgun proteomic experiments followed by statistical analysis using ANOVA with a p-value <0.05 revealed two branches that separate *Trop2* KO (T2) and EV, from the other conditions which were subdivided in one branch for *Heimdall* KO and the other one for controls (**Figure 4C, Supp. Data 10**). Two clusters specific to the *Heimdall* KO were identified *i.e.* **Cluster 1** displaying proteins under-represented and **Cluster 2**, those over-represented (**Figure 4C, Supp. Data 10**). Among proteins identified in **Cluster 1**, some are of particular interest. For example, the involvement of Tgfβ3 is well characterized during brain injury. Indeed, TGFβ signaling can be neuroprotective, but promote glial scarring and fibrosis[57]. TGF-β family is also specifically present in the early phases of human fetal brain development. It suppresses proliferation and enhances neuronal and glial differentiation [58]. Concerning Trip6, it is known to regulate neural stem cell maintenance through Notch signaling, a pathway required for NSC self-renewal [59]. Similarly, Phf6 which is a Neurog2-regulated gene [20], can be directly linked to the control of astrocytes switch to glutamatergic or GABAergic neurons. In fact, Neurog2 or Ascl1 are known to

generate such types of neurons from postnatal mouse astrocytes [60]. Trip6 is also known to be involved in neuronal progenitors and not in adult astrocytes [21], leading astrocytes conversion to neuronal progenitors. Rap1a is known to inhibit mitogenic Ras pathway signaling in astrocytes and thus regulates their proliferation [62]. In **Cluster 2**, systems biology analyses revealed proteins that were more abundant. Some of them were involved in astrocytic differentiation (Rptor[22], Arhgef12[23], Mina [24], Cadm1 [25]), neuronal progenitor expression (Camk1d, Arhgap29) or cell reprogramming (AATF) (**Figure 4C'**). Gene ontology also established that some proteins in this **Cluster 2** were involved in RNA and non-coding RNA processing and metabolism (Tut1, Elac2, Rpl7l1, Wdr12, Wdr43, Wdr75, Utp3, Utp20, Ddx52, Thada, Mettl1, Qtrtd1, Plus10, Ints10 and thumpd3) (**Figure 4C'**) confirming the results obtained with anti-Heimdall treatment (**Figure 3F'**). We also performed this proteomic analysis under LPS treatment and exclusive proteins identified in *Heimdall* KO were related to axon guidance such as the receptor Plexin C1 [64], Pdgfrb[65], Collapsin response mediator protein 1 [66];BRICK1 [67],Glioblastoma amplified sequence [68],Prosaposin[69], Eph receptor A4 [70], Retinoblastoma binding protein 6 [71], Thrombospondin 1[72], Rho-associated coiled-coil containing protein kinase 1 [73], Notch2 [74], interferon-related developmental regulator 2 [75] (**Supp. Data 11**). These results established that under inflammatory conditions, *Heimdall* KO DI TNC1 cells expressed neuronal progenitor proteins (receptors, intracellular signaling factors) and switched their phenotype from astrocytes to neuronal stem cells.

Astrocytes deprived of Heimdall secrete neuronal progenitor factors

We decided to assess the effect of *Heimdall* KO on DI TNC1 secretion. Shotgun proteomics was performed, and differential proteins were revealed compared to controls. Several proteins in *Heimdall* KO DITNC1 cells treated with LPS were involved in neuritogenesis and growth such as Slit guidance ligand 3[76], Semaphorin 3F [77], Transforming growth factor beta-3[78], Receptor for opioid growth factor[79], Actinin alpha 1[80], striatin 4 [81] (**Supp. Data 11**). All these factors are produced by neuroprogenitors during brain development. Compared to no treatment conditions, *Heimdall* KO cells also produced some factors that are known to be involved in neuronal brain development such as Profilin 2 [82] or Huntingtin interacting protein 1 which is known to be linked to Notch-mediated neurogenesis[83] (**Supp. Data 11**). Taken together, this show that under LPS stimulation, DI TNC1 cells deprived of Heimdall produced factors which are known to be synthesized by neuroprogenitor cells and which stimulate

neuritogenesis, neurite outgrowth and brain development. This confirms that Heimdall inhibition allows astrocyte conversion to neuronal stem cells.

Overexpression of Heimdall in astrocytes sustains the astrocyte fate

Shotgun proteomics was also performed on protein extracts from DI TNC1 cells overexpressing Heimdall or transfected with an empty vector as a control. This led to the identification of 125 exclusives proteins under Heimdall overexpression condition (**Supp. Figure 7A**). Among the protein identified some are interest such as molecules involved in the MAPK signaling like bin 1, Fgfr4, Pdgfrb, Raf1, Ppp3ca, Gng12, Gna12 **(Supp. Data 12**). The MAPK signaling is essential for survival and proliferation of astrocytes[26]. After an ANOVA test with a p value <0.01, a heatmap with specific clusters was retrieved (**Supp. Figure 7B, Supp. Data 13**). **Cluster 1** contained proteins less abundant in cells overexpressing Heimdall such as Myadm, Sorting nexin-5, DNA primase, Sorbs3, Athl1 and Hagh (**Supp. Figure 7B, Supp. Data 13**). By contrast, **Cluster 2** corresponded to proteins more abundant in cells overexpressing Heimdall (**Supp. Figure 7B, Supp. Data 13**). Among the proteins identified, some are of particular interest since they reinforce the role of Heimdall as a gate keeper of the astrocyte to neuronal conversion. It is the case of the nuclear scaffold protein promyelocytic leukemia (PML) known as a regulator of forebrain development [84]. PML controls cell migration via Polycomb repressive complex 2 (PRC2)-mediated repression of Slits, which are key regulators of axon guidance [84]. Another example is PRP19. It suppresses neuronal differentiation and conversely promotes astrocyte differentiation as a neuron/glia switch molecule. Overexpression of PRP19 conferred astrocyte properties at a certain level and induced more astrocyte markers, glial fibrillary acidic protein (GFAP) and S100β by activating the gp130/Janus kinase (JAK)/STAT signaling via PTP1B ubiquitination[85]. Other factors such as, the N-acylethanolamine acid amidase (NAAA) are also present in **Cluster 2**. NAAA is implicated in deactivating hydrolysis of palmitoylethanolamide (PEA), a lipid-derived agonist of the transcriptional regulator. Another factor, the peroxisome proliferator-activated receptor-α (PPAR-α) is known to exert a role in the modulation of neuroinflammation such as multiple sclerosis[86]. Finally, the global analysis between *Heimdall* KO, anti-Heimdall treatment compared to Heimdall overexpression (**Supp. Figure 7Ca, Supp. Data 14**) clearly established two clusters. **Cluster 1** highlighted the common proteins more abundant in *Heimdall* KO and after its neutralization with anti-heimdall (**Supp. Figure 7Cb**) and **Cluster 2**, the mirror of

Cluster 1, those more abundant after Heimdall overexpression (**Supp. Figure 7Cb**). Pathways analyses of **Cluster 1** revealed a protein pattern involved in cell differentiation, cell growth, cell proliferation, and cell migration common to neuronal progenitors whereas **Cluster 2** is mostly turned in regulation of apoptosis, cell survival, cell proliferation with transcriptomic factors such like STAT1/STAT2 link to JAK/STAT, TGF and Notch signaling pathway known to maintain the astrocytes fate[27]. Interestingly, the splicing regulators TRA2B known to exert its function in neuroprogenitor cells has been identified in our cells overexpressing Heimdall[28]. TRA2B seems implicated in astrocyte differentiation regulation specifically in astrocytoma[29]. IF135 were also detected and is known to regulate the innate immune response in astrocytoma [30]. Surprisingly, the FK506 binding protein 51 (FKBP5) which is a negative regulator of the glucocorticoid receptor involved in stress and normally absent in astrocytes[31] was also found in astrocytes overexpressing Heimdall. Taken together, the results show that overexpression of Heimdall may modify the astrocytes phenotype to astrocytoma whereas its inhibition leads to neuronal conversion.

Discussion

Thy-1 was the first protein related to a free variable heavy chain of immunoglobulin discovered in neurons. This protein, also named CD90, is a glycophosphatidylinositol-linked glycoprotein expressed at the surface of neurons. Several observations associate Thy-1 with the resolution of neuronal injury. Thy-1 expression in the nervous system is predominantly neuronal, but some human glial cells also express Thy-1, especially at later stages of their differentiation [87]. Neurons express high levels of Thy-1, which interacts with αvβ3 integrin present on astrocytes [88]. In astrocytes, Thy-1 interacts with the HSPG syndecan-4. The interaction with αvβ3 integrin inhibits neuritogenesis and causes retraction of neurites through the Thy-1/C-terminal Src kinase (Csk)-binding protein (CBP)/Csk complex. Src-RhoA-ROCK axis [89]. Injury to the sciatic nerve in young adult rats causes an initial decline of Thy-1 expression followed by an increase in dorsal root ganglion neurons that coincides with recovery of sensory function [90]. Thus, Thy-1 was the foundation of the Immunoglobulin superfamily. In the present study, we discovered other members of such families close to the variable chain of immunoglobulins, except for the fact that these chains are issued from long noncoding RNA. Therefore, they can be considered ghost proteins as we previously discovered and defined [10, 91]. Among them, Heimdall shares high homology with the variable

part of the kappa light chain. Heimdall like its isoform and the variable heavy chain are overexpressed during spinal cord injury and thus during inflammation. We established that Heimdall was involved in the astrocyte phenotype switch back to neuron-like phenotype. Heimdall neutralization by anti-Heimdall added in the culture medium of astrocytes or *Heimdall* KO using CRISPR-Cas9 was found to stimulate the expression of neuronal progenitor stem cell factors and neurite outgrowth. It is well known that during mammalian neocortical development, neural precursor cells generate neurons first and astrocytes later. The cell fate switch from neurons to astrocytes is a key process generating proper numbers of neurons and astrocytes. Although the intracellular mechanisms regulating this cell fate switch have been well characterized, extracellular regulators are still largely unknown. We thus propose Heimdall as one of these factors. Indeed, Heimdall inhibition triggered neuritogenesis and neurite outgrowth from astrocytes by limiting astrocytes factor expression like GFAP. All neural progenitor factors identified when Heimdall was inhibited and more clearly under LPS stimulation reinforced such hypothesis. The partners identified by immunoprecipitation strengthened the fact that Heimdall controlled the level of transcription factors involved in neuronal pluripotency and secretion of axon guidance factors. In fact, among the factors found in the interactome of Heimdall, IPO13 is known to play a critical role in early embryonic development through nuclear transport of key regulators, such as transcription factors Pax6, Pax3, and ARX[40]. Similarly, we detected erythropoietin-producing hepatocellular (Eph) receptors (EPHA3), which is known to inhibit the Wnt/β-catenin pathway involved in neurogenesis. The Notch signaling pathway has long been known to influence cell fate in the developing nervous system [92]. Inhibition of NOTCH1 signaling resulted in upregulated expression of transcription factors, including NeuroD1, NeuroD2, Pax6, Lmx1a and Lhx6, in astrocytes and converted them into neurons. It is interesting to note that *in vivo*, the expression of NOTCH1 was detected in astrocytes, which was significantly increased after SCI. Of note, NOTCH1 was found in the interactome of Heimdall during an inflammation mimicked by LPS treatment. In this condition, HDAC4 which is known to be a key element in astrocytes epigenetic reprogramming[41] was also observed. Altogether, these results showed that Heimdall through its association with NOTCH1, HDAC4 and IPO13 plays a key role to determine astrocytes fate.

This regulatory role of Heimdall was confirmed by our CRISPR-Cas9 experiment. Indeed, after *Heimdall KO* and LPS stimulation, the axon guidance factors (SLIT3, SEMA3F) have been identified. Moreover, the PTBP factors known to convert astrocytes to neurons is overexpressed when anti-Heimdall is added to the culture medium[93]. Taken together, Heimdall seems to exert with Notch 1 and other fate keepers such as the PTBP factor an important role in gliogenesis and its inhibition switch astrocytes to neurogenesis (**Figure 6**). Moreover, we and others groups have recently demonstrated that according to their nature, neurons differentially expressed at the level of the spinal cord IgGM, IgG2a, IgG2B and IgG3 isotypes with a transmembrane domain [94]. Previously, another group showed that oligodendrocyte precursors expressed the IgM receptor Fcα/μR (encoded by the *Fcmar* gene) [95] and we established the presence of CD16 and CD32b at the surface of sensory neurons linked to neurite outgrowth [4]. CD97 has been shown to be the receptor of the secreted form of V immunoglobulin Thy-1 suggesting that Heimdall can also have its own receptor. But we cannot exclude that Heimdall can bind the heavy constant chains present at the surface of neurons to form an aberrant antinomy like in cancer [36] but with the ability to form a fragment antigen binding. Interestingly like Heimdall, Thy1 protein has been detected in the hippocampus, followed by the neocortex, cerebellum, and spinal cord. This similarity of localization also suggests an involvement of such Immunoglobulin variable chains in neuritogenesis modulation in course of brain development. Taken together, Heimdall, Thy-1, and neuronal IgGs issued from pseudogenes are novel members of a large family of immunoglobulins. It will be now necessary to determine if these proteins are members of a larger list and if the variability of these chains also occurs in neurons and/or astrocytes as it occurs in B lymphocytes. In this context, we will open the pandorabox of multi-variable brain IgGs and it will be necessary to understand their functions in the crosstalk between neurons and astrocytes.

Acknowledgments

This research was supported by funding from ministère de l'Enseignement Supérieur, de la Recherche et de l'Innovation (MESRI), Institut National de la Santé et de la Recherche Médicale (Inserm), I-SITE ULNE (Nobody Project), Regional council Hauts de France, and Université de Lille. The authors would like to thank Zarah Laouby, and Estelle Laurent for their contribution to this manuscript.

Author Contributions

Conceptualization, M.S. Methodology, O.S, A.C., T.C., S.A., M.D., A. RR., M.A.K., M.T, D.C, I.F., F.R. and M.S.; Software, M.S. and T.C.; Validation, T.C., D.C., F.R. and M.S.; Formal analysis, M.S., F.R., and D.C. Investigation, F.R., D.C. and M.S.; Resources, D.C., I.F., M.T., D.D. and M.S.; Data curation, M.S., F.R., A.C., O.S., and T.C. Writing – Original Draft, M.S. Writing - Review and Editing, I.F., D.C., F.R. and M.S.; Supervision, F.R., D.C. and M.S.; Project Administration, D.D. and M.S.; Funding Acquisition, D.C., I.F., M.T., D.D. and M.S.

Declaration of Interests

The authors declare no competing interests.

References

1. Cizkova D*, et al.*Alterations of protein composition along the rostro-caudal axis after spinal cord injury: proteomic, in vitro and in vivo analyses. *Front Cell Neurosci***8**, 105 (2014).
2. Devaux S*, et al.* Proteomic Analysis of the Spatio-temporal Based Molecular Kinetics of Acute Spinal Cord Injury Identifies a Time- and Segment-specific Window for Effective Tissue Repair. *Molecular & cellular proteomics : MCP***15**, 2641-2670 (2016).
3. Devaux S*, et al.* RhoA Inhibitor Treatment At Acute Phase of Spinal Cord Injury May Induce Neurite Outgrowth and Synaptogenesis. *Molecular & cellular proteomics : MCP***16**, 1394-1415 (2017).
4. Capuz A*, et al.* The Antibody Dependant Neurite Outgrowth Modulation Response (ADNM) involvement in Spinal Cord Injury. *Frontiers Immunol***13**, 882830 (2022).
5. Cizkova D*, et al.* Modulation properties of factors released by bone marrow stromal cells on activated microglia: an in vitro study. *Scientific reports***4**, 7514 (2014).
6. Cizkova D*, et al.* Localized Intrathecal Delivery of Mesenchymal Stromal Cells Conditioned Medium Improves Functional Recovery in a Rat Model of Spinal Cord Injury. *Int J Mol Sci***19**, (2018).
7. Grulova I*, et al.* Delivery of Alginate Scaffold Releasing Two Trophic Factors for Spinal Cord Injury Repair. *Scientific reports***5**, 13702 (2015).
8. Delcourt V, Staskevicius A, Salzet M, Fournier I, Roucou X. Small Proteins Encoded by Unannotated ORFs are Rising Stars of the Proteome, Confirming Shortcomings in Genome Annotations and Current Vision of an mRNA. *Proteomics***18**, e1700058 (2018).
9. Delcourt V*, et al.* The protein coded by a short open reading frame, not by the annotated coding sequence is the main gene product of the dual-coding gene MIEF1. *Molecular & cellular proteomics : MCP*, (2018).
10. Vanderperre B*, et al.* Direct detection of alternative open reading frames translation products in human significantly expands the proteome. *PLoS One***8**, e70698 (2013).

11. Brunet MA*, et al.*OpenProt: a more comprehensive guide to explore eukaryotic coding potential and proteomes. *Nucleic acids research*, (2018).

12. Samandi S*, et al.* Deep transcriptome annotation enables the discovery and functional characterization of cryptic small proteins. *Elife***6**, (2017).

13. Mouilleron H, Delcourt V, Roucou X. Death of a dogma: eukaryotic mRNAs can code for more than one protein. *Nucleic acids research***44**, 14-23 (2016).

14. Vanderperre B, Lucier JF, Roucou X. HAltORF: a database of predicted out-of-frame alternative open reading frames in human. *Database : the journal of biological databases and curation***2012**, bas025 (2012).

15. Magnusson JP*, et al.* A latent neurogenic program in astrocytes regulated by Notch signaling in the mouse. *Science***346**, 237-241 (2014).

16. Cooper A, Berninger B. Brain Repair: Gatekeeping astrocyte identity. *Elife***11**, e80232 (2022).

17. Vanicky I, Urdzikova L, Saganova K, Cizkova D, Galik J. A simple and reproducible model of spinal cord injury induced by epidural balloon inflation in the rat. *Journal of neurotrauma***18**, 1399-1407 (2001).

18. Meissner F, Scheltema RA, Mollenkopf HJ, Mann M. Direct proteomic quantification of the secretome of activated immune cells. *Science***340**, 475-478 (2013).

19. Cox J, Mann M. MaxQuant enables high peptide identification rates, individualized p.p.b.-range mass accuracies and proteome-wide protein quantification. *Nat Biotechnol***26**, 1367-1372 (2008).

20. Cox J, Neuhauser N, Michalski A, Scheltema RA, Olsen JV, Mann M. Andromeda: a peptide search engine integrated into the MaxQuant environment. *Journal of proteome research***10**, 1794-1805 (2011).

21. UniProt C. Reorganizing the protein space at the Universal Protein Resource (UniProt). *Nucleic acids research***40**, D71-75 (2012).

22. Cox J, Hein MY, Luber CA, Paron I, Nagaraj N, Mann M. Accurate proteome-wide label-free quantification by delayed normalization and maximal peptide ratio extraction, termed MaxLFQ. *Molecular & cellular proteomics : MCP***13**, 2513-2526 (2014).

23. Vizcaino JA*, et al.*ProteomeXchange provides globally coordinated proteomics data submission and dissemination. *Nat Biotechnol***32**, 223-226 (2014).

24. Vizcaino JA*, et al.* The PRoteomicsIDEntifications (PRIDE) database and associated tools: status in 2013. *Nucleic acids research***41**, D1063-1069 (2013).

25. Hsu PD*, et al.* DNA targeting specificity of RNA-guided Cas9 nucleases. *Nature biotechnology***31**, 827-832 (2013).

26. Doench JG*, et al.* Optimized sgRNA design to maximize activity and minimize off-target effects of CRISPR-Cas9. *Nature biotechnology***34**, 184-191 (2016).

27. Sanjana NE, Shalem O, Zhang F. Improved vectors and genome-wide libraries for CRISPR screening. *Nature methods***11**, 783-784 (2014).

28. Ryø LB, Thomsen EA, Mikkelsen JG. Production and validation of lentiviral vectors for CRISPR/Cas9 delivery. In: *CRISPR Gene Editing*). Humana Press, New York, NY (2019).

29. Ke X*, et al.* A single mutation in the VP1 gene of enterovirus 71 enhances viral binding to heparan sulfate and impairs viral Pathogenicity in mice. *Viruses***12**, 883 (2020).

30. Yang J, Yan R, Roy A, Xu D, Poisson J, Zhang Y. The I-TASSER Suite: protein structure and function prediction. *Nature methods***12**, 7-8 (2015).

31. Kozakov D*, et al.* The ClusPro web server for protein–protein docking. *Nature protocols***12**, 255-278 (2017).

32. Goddard TD, Huang CC, Ferrin TE. Software extensions to UCSF chimera for interactive visualization of large molecular assemblies. *Structure***13**, 473-482 (2005).

33. Itoh N*, et al.* Cell-specific and region-specific transcriptomics in the multiple sclerosis model: Focus on astrocytes. *Proc Natl Acad Sci U S A*, (2017).

34. Shigemitsu Y, Hiroaki H. Common molecular pathogenesis of disease-related intrinsically disordered proteins revealed by NMR analysis. *The Journal of Biochemistry***163**, 11-18 (2018).

35. Oldfield CJ, Dunker AK. Intrinsically disordered proteins and intrinsically disordered protein regions. *Annual review of biochemistry***83**, 553-584 (2014).

36. Hu D*, et al.* Heterogeneity of aberrant immunoglobulin expression in cancer cells. *Cellular & molecular immunology***8**, 479-485 (2011).

37. Holsapple MP, West LJ, Landreth KS. Species comparison of anatomical and functional immune system development. *Birth Defects Research Part B: Developmental and Reproductive Toxicology***68**, 321-334 (2003).

38. Winkler TH, Mårtensson I-L. The role of the pre-B cell receptor in B cell development, repertoire selection, and tolerance. *Frontiers in immunology***9**, 2423 (2018).

39. Fang Y*, et al.* Ephrin-A3 suppresses Wnt signaling to control retinal stem cell potency. *Stem Cells***31**, 349-359 (2013).

40. Gajewska KA, Haynes JM, Jans DA. Nuclear Transporter IPO13 Is Central to Efficient Neuronal Differentiation. *Cells***11**, 1904 (2022).

41. Vasan L, Park E, David LA, Fleming T, Schuurmans C. Direct neuronal reprogramming: Bridging the gap between basic science and clinical application. *Frontiers in Cell and Developmental Biology***9**, (2021).

42. Poewe W*, et al.* Parkinson disease. *Nature reviews Disease primers***3**, 1-21 (2017).

43. Wang X*, et al.* DLP1-dependent mitochondrial fragmentation mediates 1-methyl-4-phenylpyridinium toxicity in neurons: implications for Parkinson's disease. *Aging cell***10**, 807-823 (2011).

44. Hoekstra JG*, et al.* Astrocytic dynamin-like protein 1 regulates neuronal protection against excitotoxicity in Parkinson disease. *The American journal of pathology***185**, 536-549 (2015).

45. Menegon A, Board PG, Blackburn AC, Mellick GD, Le Couteur DG. Parkinson's disease, pesticides, and glutathione transferase polymorphisms. *The Lancet***352**, 1344-1346 (1998).

46. Bi M, Du X, Jiao Q, Chen X, Jiang H. Expanding the role of proteasome homeostasis in Parkinson's disease: Beyond protein breakdown. *Cell Death & Disease***12**, 1-16 (2021).

47. Gazzin S, Vitek L, Watchko J, Shapiro SM, Tiribelli C. A novel perspective on the biology of bilirubin in health and disease. *Trends in molecular medicine***22**, 758-768 (2016).

48. Lakshmikuttyamma A, Selvakumar P, Tuchek J, Sharma RK. Myristoyltransferase and calcineurin: novel molecular therapeutic target for epilepsy. *Progress in neurobiology***84**, 77-84 (2008).

49. Sakakibara S-i, Nakamura Y, Satoh H, Okano H. Rna-binding protein Musashi2: developmentally regulated expression in neural precursor cells and subpopulations of neurons in mammalian CNS. *Journal of Neuroscience***21**, 8091-8107 (2001).

50. Zhang C*, et al.* Role of spastin and protrudin in neurite outgrowth. *Journal of cellular biochemistry***113**, 2296-2307 (2012).

51. Miller KE, Suter DM. An integrated cytoskeletal model of neurite outgrowth. *Frontiers in cellular neuroscience***12**, 447 (2018).

52. Schmid R-S, Pruitt WM, Maness PF. A MAP kinase-signaling pathway mediates neurite outgrowth on L1 and requires Src-dependent endocytosis. *Journal of Neuroscience***20**, 4177-4188 (2000).

53. Li L*, et al.* Neuroglobin promotes neurite outgrowth via differential binding to PTEN and Akt. *Molecular Neurobiology***49**, 149-162 (2014).

54. Jin E-J*, et al.* Akt regulates neurite growth by phosphorylation-dependent inhibition of radixin proteasomal degradation. *Scientific reports***8**, 1-12 (2018).

55. Crespi A*, et al.* LIN7 regulates the filopodium-and neurite-promoting activity of IRSp53. *Journal of Cell Science***125**, 4543-4554 (2012).

56. Zuo Y-C, Xiong N-X, Shen J-Y, Yu H, Huang Y-Z, Zhao H-Y. MARK2 rescues Nogo-66-induced inhibition of neurite outgrowth via regulating microtubule-associated proteins in neurons in vitro. *Neurochemicalresearch***41**, 2958-2968 (2016).

57. Doyle KP, Cekanaviciute E, Mamer LE, Buckwalter MS. TGFβ signaling in the brain increases with aging and signals to astrocytes and innate immune cells in the weeks after stroke. *Journal of neuroinflammation***7**, 1-13 (2010).

58. Meyers EA, Kessler JA. TGF-β family signaling in neural and neuronal differentiation, development, and function. *Cold Spring Harbor perspectives in biology***9**, a022244 (2017).

59. Lai YJ, Li MY, Yang CY, Huang KH, Tsai JC, Wang TW. TRIP6 regulates neural stem cell maintenance in the postnatal mammalian subventricular zone. *Developmental Dynamics***243**, 1130-1142 (2014).

60. Masserdotti G*, et al.* Transcriptional mechanisms of proneural factors and REST in regulating neuronal reprogramming of astrocytes. *Cell stem cell***17**, 74-88 (2015).

61. Dermentzaki G*, et al.* Deletion of Ripk3 prevents motor neuron death in vitro but not in vivo. *Eneuro***6**, (2019).

62. Apicelli AJ*, et al.* Role of the Rap1 GTPase in astrocyte growth regulation. *Glia***42**, 225-234 (2003).

63. D'Ambrosi N, Milani M, Apolloni S. S100A4 in the Physiology and Pathology of the Central and Peripheral Nervous System. *Cells***10**, 798 (2021).

64. Limoni G, Niquille M. Semaphorins and Plexins in central nervous system patterning: the key to it all? *Current opinion in neurobiology***66**, 224-232 (2021).

65. Funa K, Sasahara M. The roles of PDGF in development and during neurogenesis in the normal and diseased nervous system. *Journal of Neuroimmune Pharmacology***9**, 168-181 (2014).

66. Nakamura F, Ohshima T, Goshima Y. Collapsin response mediator proteins: their biological functions and pathophysiology in neuronal development and regeneration. *Frontiers in cellular neuroscience*, 188 (2020).

67. Brick RM, Sun AX, Tuan RS. Neurotrophically induced mesenchymal progenitor cells derived from induced pluripotent stem cells enhance neuritogenesis via neurotrophin and cytokine production. *Stem cells translational medicine***7**, 45-58 (2018).

68. Sabelström H*, et al.* Driving neuronal differentiation through reversal of an ERK1/2-miR-124-SOX9 axis abrogates glioblastoma aggressiveness. *Cell Reports***28**, 2064-2079. e2011 (2019).

69. Nabeka H*, et al.* Interneurons secrete prosaposin, a neurotrophic factor, to attenuate kainic acid-induced neurotoxicity. *IBRO reports***3**, 17-32 (2017).

70. Khodosevich K, Watanabe Y, Monyer H. EphA4 preserves postnatal and adult neural stem cells in an undifferentiated state in vivo. *Journal of cell science***124**, 1268-1279 (2011).

71. Jaafar C*, et al.* Role of Rb during neurogenesis and axonal guidance in the developing olfactory system. *Frontiers in Molecular Neuroscience***9**, 81 (2016).

72. Lu Z, Kipnis J. Thrombospondin 1—a key astrocyte-derived neurogenic factor. *The FASEB Journal***24**, 1925-1934 (2010).

73. Shi J, Wei L. Rho Kinases in Embryonic Development and Stem Cell Research. *ArchivumImmunologiae et TherapiaeExperimentalis***70**, 1-22 (2022).

74. Solecki DJ, Liu X, Tomoda T, Fang Y, Hatten ME. Activated Notch2 signaling inhibits differentiation of cerebellar granule neuron precursors by maintaining proliferation. *Neuron***31**, 557-568 (2001).

75. Konishi S, Maeda S, Watanabe M, Nakamichi N, Takarada T, Yoneda Y. Predominant expression of ifrd1 by neural progenitor cells in adult mouse hippocampus. In: *journal of neurochemistry*). Wiley-blackwell publishing, inc commerce place, 350 main st, malden 02148, (2009).

76. Lin L, Isacson O. Axonal growth regulation of fetal and embryonic stem cell-derived dopaminergic neurons by Netrin-1 and Slits. *Stem cells***24**, 2504-2513 (2006).

77. Ng T*, et al.* Class 3 semaphorin mediates dendrite growth in adult newborn neurons through Cdk5/FAK pathway. *PloS one***8**, e65572 (2013).

78. Jason JY, Barnes AP, Hand R, Polleux F, Ehlers MD. TGF-β signaling specifies axons during brain development. *Cell***142**, 144-157 (2010).

79. Tsai N-P, Tsui Y-C, Pintar JE, Loh HH, Wei L-N. Kappa opioid receptor contributes to EGF-stimulated neurite extension in development. *Proceedings of the National Academy of Sciences***107**, 3216-3221 (2010).

80. Fu C*, et al.* Neuronal migration is mediated by inositol hexakisphosphate kinase 1 via α-actinin and focal adhesion kinase. *Proceedings of the National Academy of Sciences***114**, 2036-2041 (2017).

81. Lin L, Lo LH-Y, Lyu Q, Lai K-O. Determination of dendritic spine morphology by the striatin scaffold protein STRN4 through interaction with the phosphatase PP2A. *Journal of Biological Chemistry***292**, 9451-9464 (2017).

82. Di Domenico M, Jokwitz M, Witke W, PiloBoyl P. Specificity and Redundancy of Profilin 1 and 2 Function in Brain Development and Neuronal Structure. *Cells***10**, 2310 (2021).

83. White JK*, et al.* Huntingtin is required for neurogenesis and is not impaired by the Huntington's disease CAG expansion. *Nature genetics***17**, 404-410 (1997).

84. Amodeo V*, et al.* A PML/Slit Axis Controls Physiological Cell Migration and Cancer Invasion in the CNS. *Cell Rep***20**, 411-426 (2017).

85. Yamada T, Urano-Tashiro Y, Hashi Y, Sakumoto M, Akiyama H, Tashiro F. The U-box-type ubiquitin ligase PRP19beta regulates astrocyte differentiation via ubiquitination of PTP1B. *Brain Res***1524**, 12-25 (2013).

86. Pontis S*, et al.* N-Acylethanolamine Acid Amidase contributes to disease progression in a mouse model of multiple sclerosis. *Pharmacol Res***160**, 105064 (2020).

87. Kemshead JT, Ritter MA, Cotmore SF, Greaves MF. Human Thy-1: Expression on the cell surface of neuronal and and glial cells. *Brain research***236**, 451-461 (1982).

88. Herrera-Molina R*, et al.* Astrocytic αVβ3 integrin inhibits neurite outgrowth and promotes retraction of neuronal processes by clustering Thy-1. *PLoS One***7**, e34295 (2012).

89. Lagos-Cabré R*, et al.*α V β 3 Integrinregulatesastrocytereactivity. *Journal of neuroinflammation***14**, 1-13 (2017).

90. Chen CH, Wang SM, Yang SH, Jeng CJ. Role of Thy-1 in in vivo and in vitro neural development and regeneration of dorsal root ganglionic neurons. *Journal of cellular biochemistry***94**, 684-694 (2005).

91. Cardon T, Fournier I, Salzet M. Shedding Light on the Ghost Proteome. *Trends Biochem Sci***46**, 239-250 (2021).

92. Gaiano N, Fishell G. The role of notch in promoting glial and neural stem cell fates. *Annual review of neuroscience***25**, 471-490 (2002).

93. Contardo M*, et al.* Targeting PTB for Glia-to-Neuron Reprogramming In Vitro and In Vivo for Therapeutic Development in Neurological Diseases. *Biomedicines***10**, 399 (2022).

94. Scheurer L*, et al.* Expression of immunoglobulin constant domain genes in neurons of the mouse central nervous system. *Life science alliance***4**, (2021).

95. Nakahara J*, et al.* Signaling via immunoglobulin Fc receptors induces oligodendrocyte precursor cell differentiation. *Developmental cell***4**, 841-852 (2003).

96. Howe KL*, et al.*Ensembl 2021. *Nucleic acids research***49**, D884-D891 (2021).

97. Pathan M*, et al.*FunRich: An open access standalone functional enrichment and interaction network analysis tool. *Proteomics***15**, 2597-2601 (2015).

98. Ye J, Ma N, Madden TL, Ostell JM. IgBLAST: an immunoglobulin variable domain sequence analysis tool. *Nucleic acids research***41**, W34-W40 (2013).

99. Lefranc M-P*, et al.*IMGT unique numbering for immunoglobulin and T cell receptor constant domains and Ig superfamily C-like domains. *Developmental & Comparative Immunology***29**, 185-203 (2005).

Table 1 : Whole AltProt identified from all spinal cord segments after 12 h to 10 days of injury.

protein accession	gene symbol	transcript accession	type	localization
IP_1255506	AABR07039092.1	ENSRNOT00000036763.4	ncRNA	-
IP_1389396	Cyfip2	NM_001106996.1	mRNA	5'UTR
		ENSRNOT00000059496.4	mRNA	5'UTR
IP_1296106	RGD1563294	ENSRNOT00000073655.2	ncRNA	-
IP_1372316	AC126486.2	ENSRNOT00000092705.1	ncRNA	-
IP_1369985	AABR07021586.1	ENSRNOT00000076665.1	ncRNA	-
IP_1369659	Prdx6	ENSRNOT00000076989.1	ncRNA	-
IP_1365940	Slit2	ENSRNOT00000005477.7	mRNA	3'UTR
		XM_017599277.1	mRNA	3'UTR
		XM_017599272.1	mRNA	3'UTR
		XM_017599271.1	mRNA	3'UTR
		NM_022632.2	mRNA	3'UTR
		XM_017599278.1	mRNA	3'UTR
		XM_017599269.1	mRNA	3'UTR
		XM_017599270.1	mRNA	3'UTR
		XM_017599275.1	mRNA	3'UTR
		XM_017599276.1	mRNA	3'UTR
		XM_017599273.1	mRNA	3'UTR
		XM_017599274.1	mRNA	3'UTR
		ENSRNOT00000081601.1	mRNA	3'UTR
IP_1375305	Zbed5	XM_006249235.3	mRNA	CDS
		ENSRNOT00000001220.7	mRNA	CDS
		NM_001105924.1	mRNA	CDS
IP_1329311	LOC100360791	ENSRNOT00000044222.4	ncRNA	-
		XR_589869.1	misc_RNA	-
IP_1304331	AABR07051642.1	ENSRNOT00000084373.1	ncRNA	-
IP_1304334	AABR07051592.2	ENSRNOT00000089977.1	ncRNA	-
IP_1282467	AABR07065780.1	ENSRNOT00000084080.1	ncRNA	-
IP_1294056	Mfsd2a	XM_006238792.3	mRNA	CDS
		NM_001106683.1	mRNA	CDS
		ENSRNOT00000019080.7	mRNA	CDS
IP_1380263	Clic6	ENSRNOT00000084412.1	mRNA	3'UTR
IP_1315648	AC099304.1	ENSRNOT00000076041.1	ncRNA	-
IP_1372374	AABR07035345.1	ENSRNOT00000092473.1	ncRNA	-
IP_1286060	LOC690435	NM_001047975.2	mRNA	CDS
		ENSRNOT00000046749.1	mRNA	CDS
IP_1081314	Cluap1	ENSRNOT00000064964.2	mRNA	CDS
		XM_017597417.1	mRNA	CDS
		NM_001014225.1	mRNA	CDS
		XM_008767515.2	mRNA	CDS
		ENSRNOT00000078577.1	mRNA	CDS
		XM_006245832.3	mRNA	CDS
IP_1257188	Col4a6	ENSRNOT00000079180.1	mRNA	CDS
		XM_017602361.1	mRNA	3'UTR
IP_1257457	Armcx4	ENSRNOT00000040476.5	mRNA	CDS
IP_1261339	Capn10	NM_031673.2	mRNA	CDS
		ENSRNOT00000074160.1	mRNA	CDS
IP_1274687	Ddn	XM_008765672.2	mRNA	CDS
		ENSRNOT00000089060.1	mRNA	CDS
		NM_030993.1	mRNA	CDS
IP_1283121	Tmem121	XR_001838593.1	misc_RNA	-
		ENSRNOT00000006872.2	mRNA	CDS
		XR_001838594.1	misc_RNA	-
		XM_006240674.3	mRNA	CDS
		XM_001079243.6	mRNA	CDS
IP_1284174	Ylpm1	ENSRNOT00000006492.7	mRNA	CDS
		ENSRNOT00000089683.1	mRNA	CDS
		NM_001271258.1	mRNA	3'UTR
		ENSRNOT00000080038.1	mRNA	CDS
IP_1291962	Slc35d1	NM_001106668.2	mRNA	3'UTR
		ENSRNOT00000032126.5	mRNA	3'UTR
IP_1344128	Adgb	ENSRNOT00000082415.1	mRNA	CDS
IP_1345979	Ankrd11	ENSRNOT00000031389.7	mRNA	CDS
		XM_008772666.2	mRNA	CDS
		XM_008772667.2	mRNA	CDS
		XM_017601456.1	mRNA	CDS
		XM_017601455.1	mRNA	CDS
IP_1347636	AABR07042668.1	ENSRNOT00000091435.1	ncRNA	-
	Cdh11	XM_017601373.1	mRNA	5'UTR
IP_1361001	Lcp1	XM_017599708.1	mRNA	3'UTR
		XM_006252320.3	mRNA	3'UTR
		XM_017599707.1	mRNA	3'UTR
		ENSRNOT00000082191.1	mRNA	3'UTR
		XM_006252322.3	mRNA	3'UTR
		XM_006252319.2	mRNA	3'UTR
		XM_006252318.3	mRNA	3'UTR
		XM_017599709.1	mRNA	3'UTR
		NM_001012044.1	mRNA	3'UTR
		ENSRNOT00000014502.5	mRNA	3'UTR
IP_1366843	Hnrnpdl	NM_001033696.1	mRNA	5'UTR
		ENSRNOT00000003106.6	mRNA	5'UTR

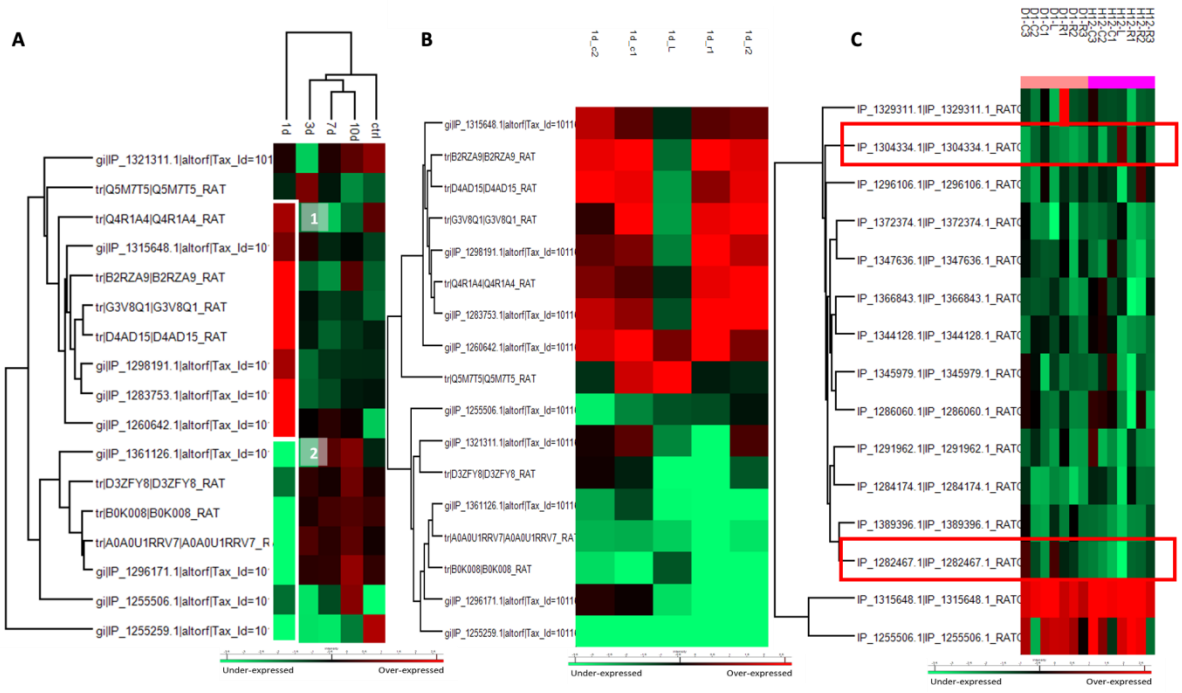

Figure 1 : A) Heatmap representing the variation in the average abundance from triplicate of the Ghost-proteins identified at the lesion site from 1 day to 10 days after SCI and compared to control ($p<0.05$). B) Spatial proteomic study at 1 day after SCI. Heatmap was performed on identified Ghost proteins: C for caudal and R for rostral regions. Most AltProt were less abundant (cluster 1) at the lesion site compared to the other parts. C) Spatio-temporal study from 12h to 24h after SCI. Heatmap represents the Ghost proteins identified.

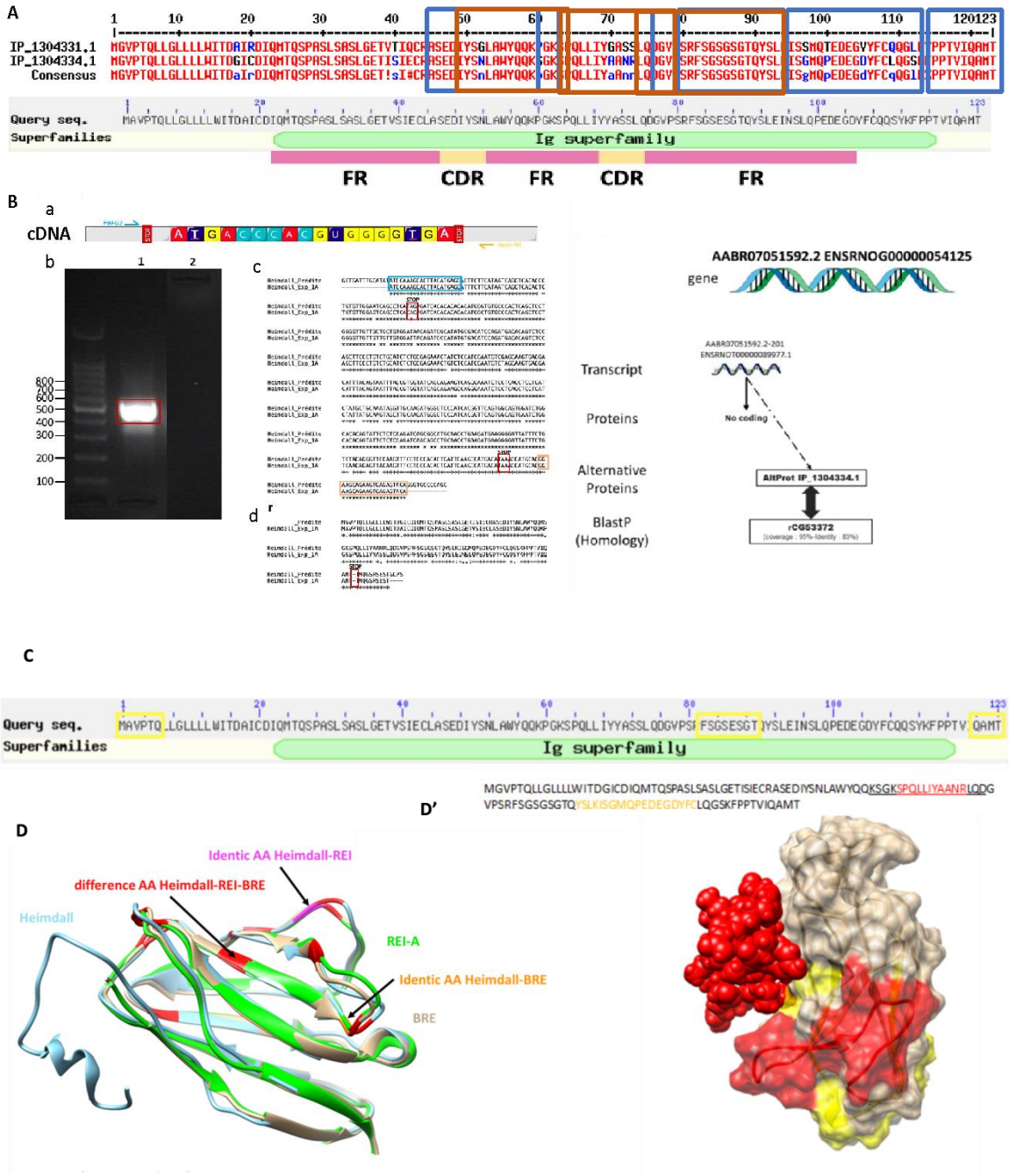
A
IP_1304331.1
IP_1304334.1
Consensus
Query seq.
Superfamilies
Ig superfamily
FR
CDR
FR
CDR
FR
B
a
cDNA
b
c
d
AABR07051592.2 ENSRNOG00000054125
gene
Transcript
Proteins
Alternative Proteins
BlastP (Homology)
No coding
AltProt IP_1304334.1
rCG53372
C
Query seq.
Superfamilies
Ig superfamily
D'
D
Identic AA Heimdall-REI
difference AA Heimdall-REI-BRE
Heimdall
REI-A
Identic AA Heimdall-BRE
BRE

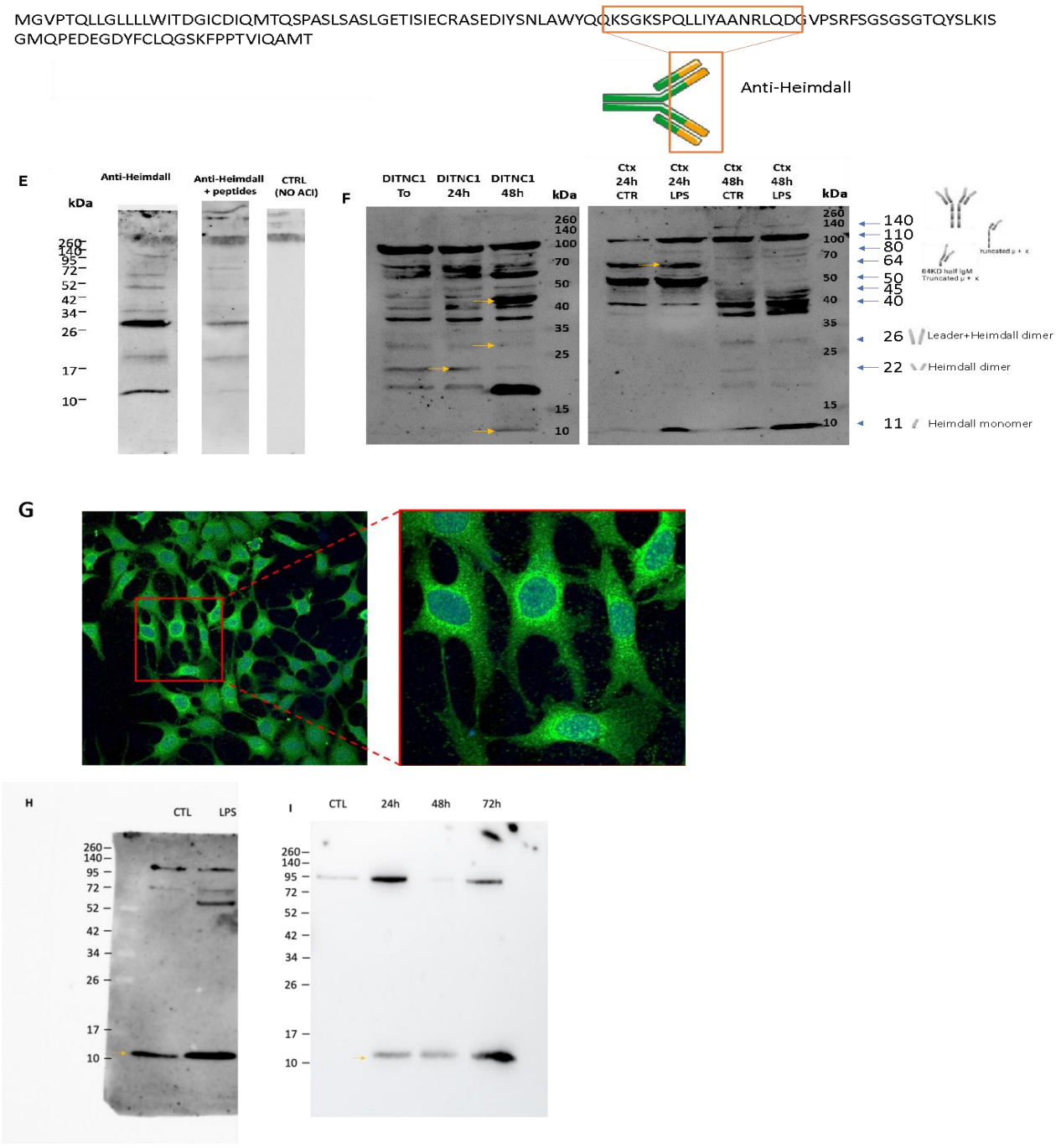

Figure 2: Transcriptomic and proteomic characterization of Heimdall. **A)** Identification by shot gun proteomic of Heimdall and its isoform. Peptides covering Heimdall sequence are presented in blue (for IP_1304331.1and brown. IP_1304334.1). A sequence comparison with the variable kappa light chain is presented. **B)** Amplification of *Heimdall* transcript. **(a)** Localization of the two primers used during RT-PCR experiment **(b)** Amplification by RT-PCR of a fragment at 540 bp

corresponding to *Heimdall* transcript was performed (1) on cDNA synthesized from DI TNC1 Astrocytes (2) As a control to exclude genomic DNA contamination, the experiment was also carried out on a negative reverse transcriptase sample. **(c)** Alignment of the nucleic acid sequence coding Heimdall obtained by RT-PCR with the long non-coding RNA AABR07051592.2 retrieved from Ensembl database [96]. **(d)** Alignment of the deduced amino acid sequence of Heimdall with the predicted sequence IP-1304343.1 coded by the noncoding RNA AABR07051592.2. **C)** The 3 yellow boxes indicate the IDP sequences in Heimdall. The orange box highlights the immunogenic peptide used to synthesized rabbit polyclonal anti-Heimdall. **D)** I-Taser representation. Heimdall was compared to the variable Kappa light chain found in Bence Jone diseases. **D')** Localization of the antigenic peptide (red) used to perform the immunization to get the anti-Heimdall and I-Taser representation with the localization of the pocket interaction. **E)** To validate the specificity of anti-Heimdall, western blot analyses in reducing and denaturating conditions were carried out on protein cell extracts from DI TNC1 astrocytes with anti-Heimdall pre-incubated or not with the peptides used for the immunization. A control with the secondary antibody alone was also added **F)** Western blot experiments in reducing and denaturing conditions using anti-Heimdall were performed on protein cell extracts from DI TNC1 cells or primary cortex astrocytes stimulated or not with 200 ng/mL of LPS for 24 h and 48 h. **G**) Detection of Heimdall in DI TNC1 cells by immunofluorescence **H**) Western blot analyses with anti-Heimdall performed on the secretomes of DI TNC1 Astrocytes treated or not without LPS. **I**) Overexpression of Heimdall in HEK293 cells, confirmed its size.

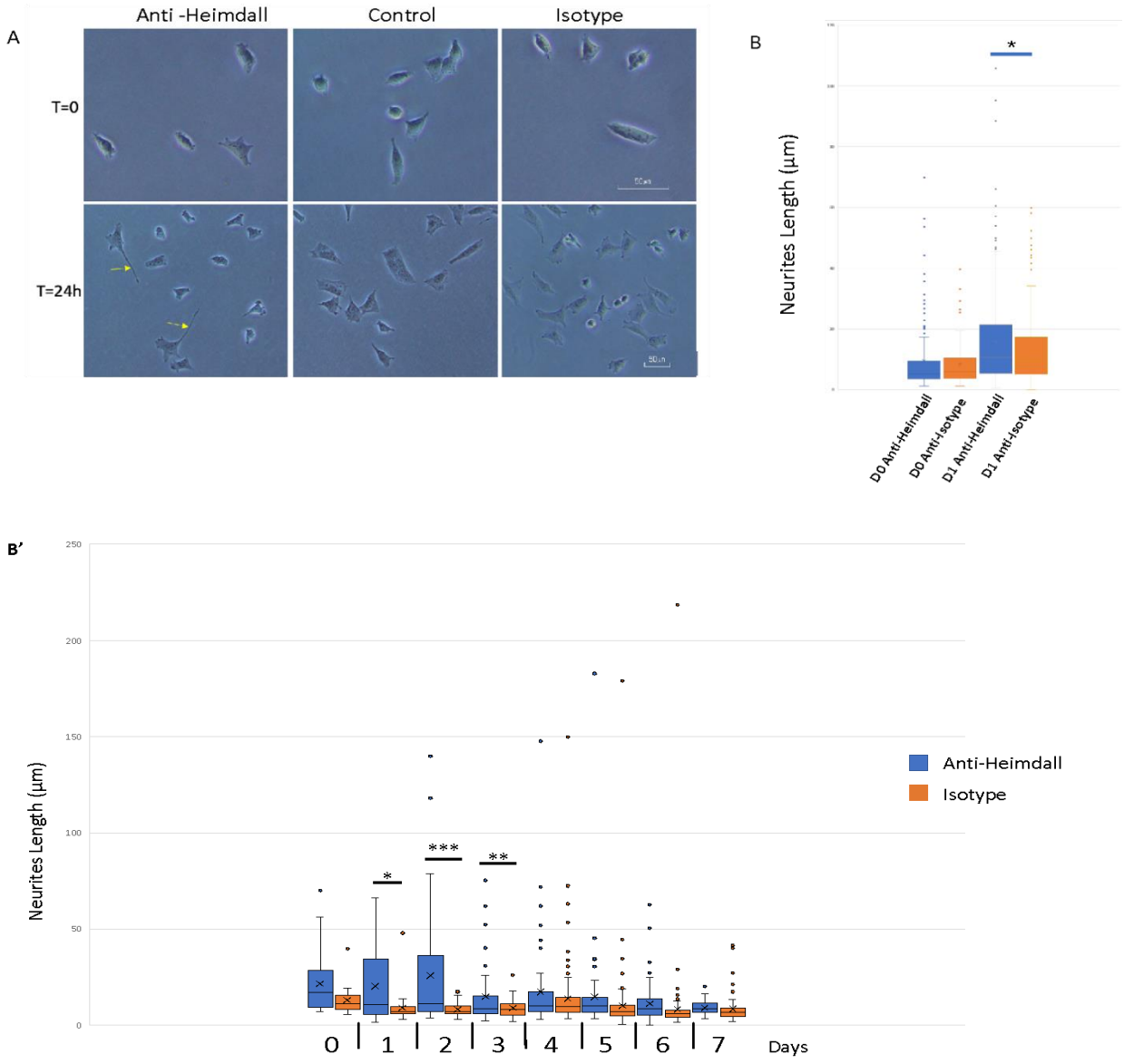
A
Anti -Heimdall
Control
Isotype
T=0
T=24h
B
Neurites Length (µm)
*
D0 Anti-Heimdall
D0 Anti-Isotype
D1 Anti-Heimdall
D1 Anti-Isotype
B'
Neurites Length (µm)
250
200
150
100
50
0
*
***
**
0
1
2
3
4
5
6
7
Days
Anti-Heimdall
Isotype

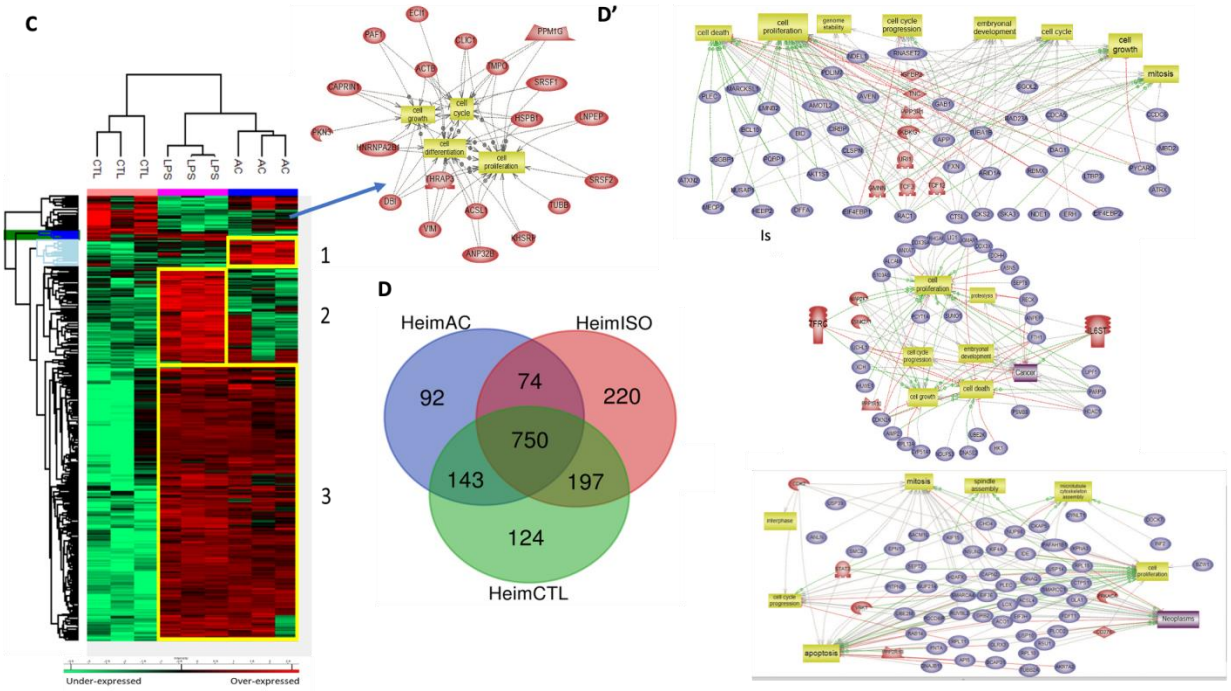
C
CTL
CTL
CTL
LPS
LPS
LPS
AC
AC
AC
Under-expressed
Over-expressed
1
2
3
D
HeimAC
HeimISO
HeimCTL
92
74
220
750
143
197
124
D'
cell death
cell proliferation
genome stability
cell cycle progression
embryonal development
cell cycle
cell growth
mitosis
ls
cell proliferation
proteolysis
cell cycle progression
embryonal development
cell death
cell growth
Cancer
mitosis
spindle assembly
microtubule cytoskeleton assembly
interphase
cell cycle progression
cell proliferation
Neoplasms
apoptosis

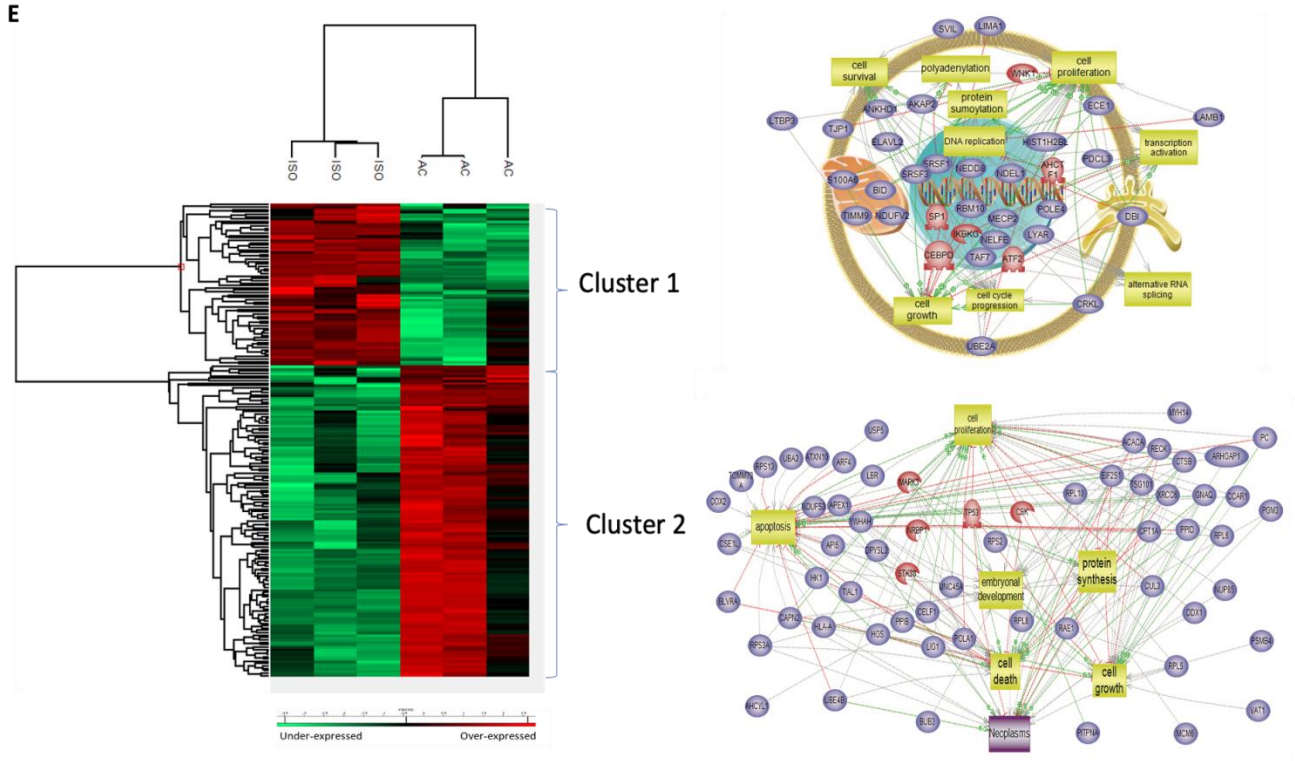
E
ISO
ISO
ISO
AC
AC
AC
Cluster 1
Cluster 2
Under-expressed
Over-expressed
cell survival
polyadenylation
cell proliferation
protein sumoylation
DNA replication
transcription activation
alternative RNA splicing
cell growth
cell cycle progression
cell proliferation
apoptosis
protein synthesis
embryonal development
cell death
cell growth
Neoplasms

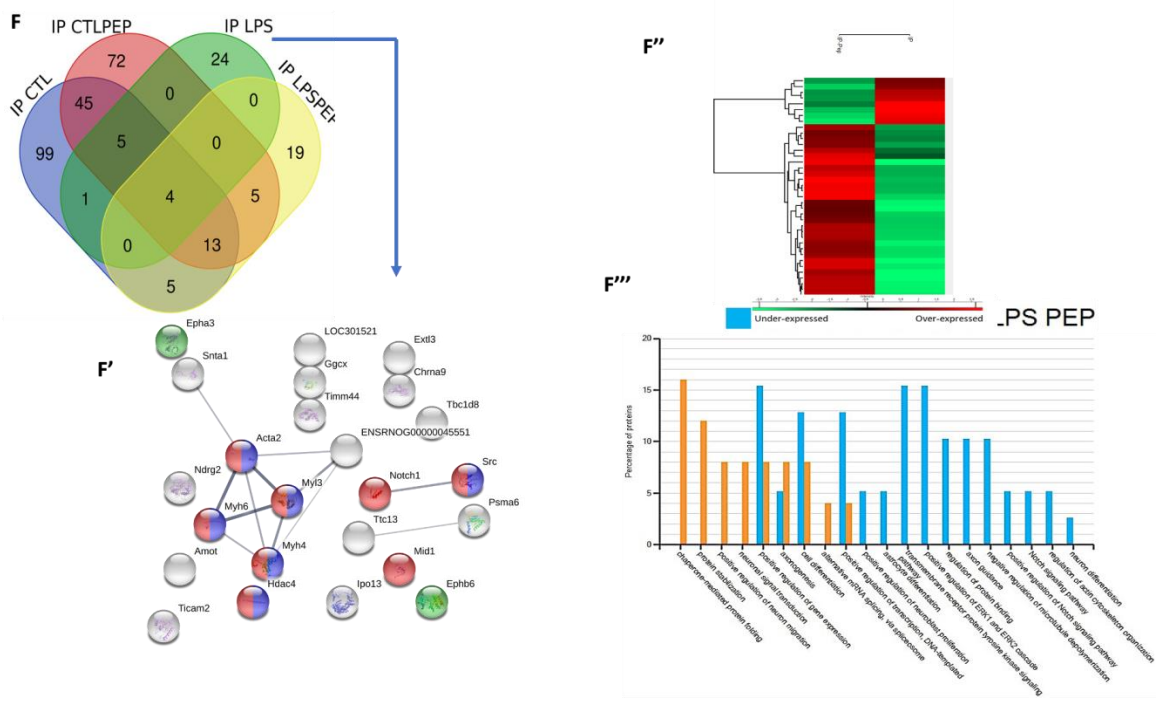

Figure 3: Heimdall neutralization by anti-Heimdall modulated the growth of neurite-like extensions in astrocytes DI TNC1 cell line A) Images of DI TNC1 cells depicting the growth of neurite-like extensions after 24h of incubation with anti-Heimdall compared to isotype control antibody and no treatment (control). Scale bars: 50 µm. **B)** Box plot representation of the length of neurite-like extensions after one day of treatment with anti-Heimdall compared to isotype control antibody treatment. An equal number of cells was analyzed for each experimental group (n = 3). **B')** Measurement of neurite-like extensions length performed from 0 to 7 days after anti-Heimdall treatment (Blue) compared to isotype control antibody (orange) treatment. To assess the significance of the results, the multiple sample ANOVA test was carried out with a significance threshold of $p < 0.01$. **C)** Heatmap corresponding to shot gun analyses performed on cell extracts of DI TNC1 astrocytes incubated with anti-Heimdall (Ac) or stimulated (LPS) or not (CTL) with 200 ng/mL of LPS. String analyses carried out on proteins more abundantly represented after anti-Heimdall treatment (Cluster 1) established the presence of progenitor stem cells factors and proteins involved in cytoskeleton organization. **D)** Venn diagram highlighted specific proteins detected in cell extracts from DI TNC1 astrocytes treated with anti-Heimdall compared to isotype control antibody and no treatment (control). **D')** Pathways analyses of proteins detected specifically in control DI TNC1 cells or after treatment with anti-Heimdall or isotype control

antibody**. E)** Heatmap representing the variation in the abundance of proteins identified after treatment with anti-Heimdall or isotype control antibody (n=3). Two specific clusters were observed. In **Cluster 1** proteins identified were linked to the neuroinflammation and neural development. In **Cluster 2** proteins identified were involved in pluripotency, notch pathway, differentiation and development, neuronal progenitor and RUNX3 expression. Pathways analyses revealed that the proteins found in **Cluster 1** are involved in cell survival, proliferation, cell growth, alternative RNA splicing, transcription activation and cell growth, while **Cluster 2** proteins are involved in embryonal development, cell growth, protein synthesis and regulation of apoptosis. **F)** Immunoprecipitation experiments with anti-Heimdall and with anti-Heimdall pre-incubated with the peptides used for the immunization were conducted on cell extracts from DI TNC1 astrocytes treated or not with 200 ng/mL of LPS. Venn diagram revealed proteins specifically immunoprecipitated for each condition. **F')** String analysis conducted on proteins immunoprecipitated with anti-Heimdall from cell extract of DI TNC1 astrocytes treated with LPS is also presented. **F'')** Average Heatmap performed with the average of the triplicate. Significant differences in abundance between proteins immunoprecipitated with anti-Heimdall and with anti-Heimdall pre-incubated with the peptides used for the immunization were established by t-test with a p-value <0.05. **F''')** Funrich[97] enrichment and biological processes comparison was also applied to compare these proteins with those specifically immunoprecipitated with anti-Heimdall pre-incubated with the peptides used for the immunization.

A

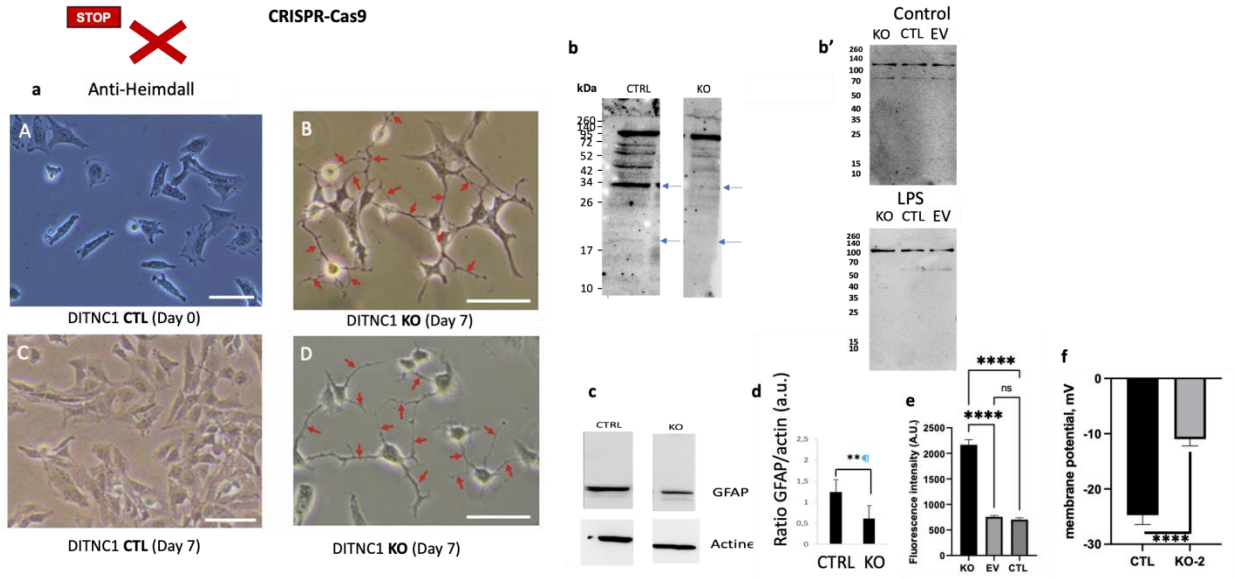
STOP
CRISPR-Cas9
a
Anti-Heimdall
A
B
C
D
DITNC1 CTL (Day 0)
DITNC1 KO (Day 7)
DITNC1 CTL (Day 7)
DITNC1 KO (Day 7)
b
kDa
CTRL
KO
260
140
95
72
52
42
34
26
17
10
b'
Control
KO CTL EV
LPS
KO CTL EV
c
CTRL
KO
GFAP
Actine
d
Ratio GFAP/actin (a.u.)
**
CTRL KO
e
Fluorescence Intensity (A.U.)
****
ns
****
KO EV CTL
f
membrane potential, mV
CTL
KO-2

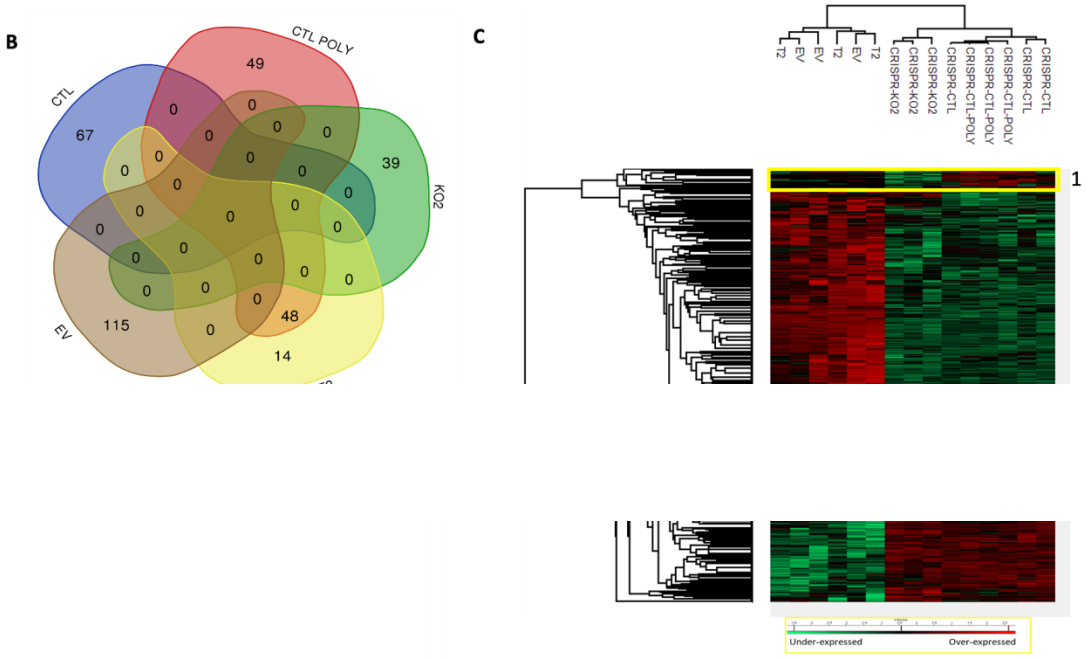
B
CTL
CTL POLY
KO2
EV
49
67
39
115
48
14
C
T2
EV
T2
EV
T2
CRISPR-KO2
CRISPR-KO2
CRISPR-CTL
CRISPR-CTL-POLY
CRISPR-CTL-POLY
CRISPR-CTL
CRISPR-CTL
1
Under-expressed
Over-expressed

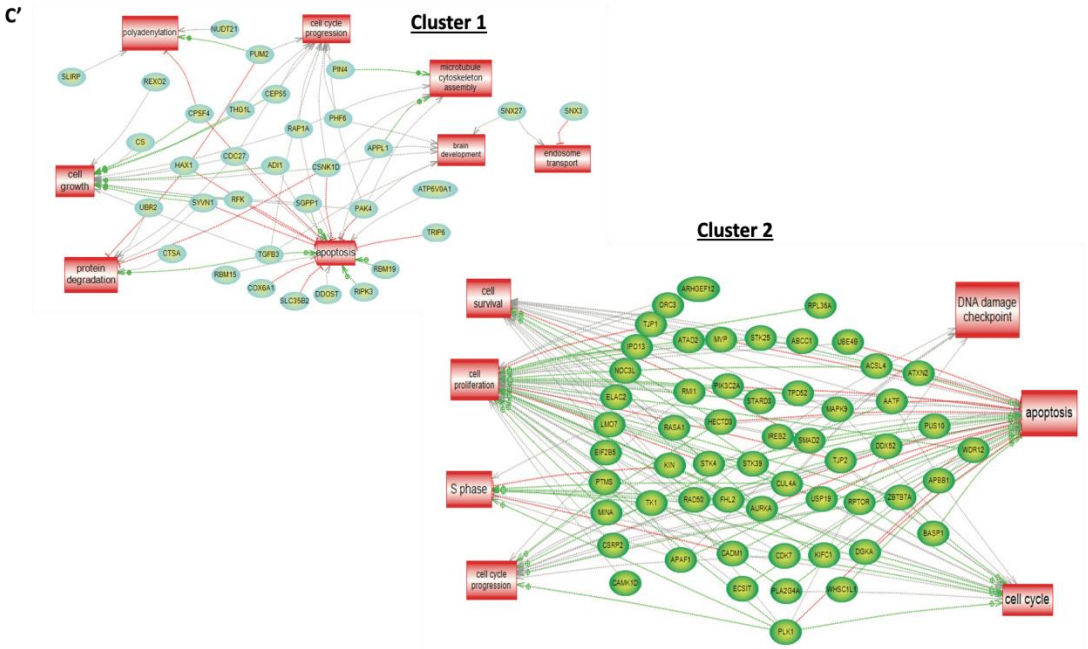

Figure 4: *Heimdall* knockout using CRISPR-CAS9 technology. A) a) Phenotype analyses of normal DI TNC1 astrocytes and *Heimdall* KO astrocytes revealed that *Heimdall* KO astrocytes triggered the growth of neurite-like extensions as revealed in time course from 1 day to 7 days. Scale bars: 50 µm **b**) Western blot analyses performed with anti-Heimdall, on cell extracts from control DI TNC1 astrocytes (CTRL) or *Heimdall* KO DI TNC1 astrocytes stimulated with 200 ng/mL of LPS or not (LPS) **b')** Western blot analyses performed with anti-Heimdall, on cell secretome from control astrocytes (CTRL) or DI TNC1 infected with empty vector (EV) or *Heimdall* KO DI TNC1 astrocytes stimulated or not with 200 ng/mL of LPS **c)** Western blot analyses of GFAP and **d**) its quantification after normalization with those of Actin. **e)** Heimdall KO DI TNC1 astrocytes exhibit 4-fold higher depolarization state compared to control and EV condition (ANOVA p<0.0001) **f**) Heimdall KO DI TNC1 astrocytes exhibit 2-fold lesser rest membrane potential (mV) compared to control (ANOVA p<0.0001) **B)** Venn diagram highlighted specific proteins identified in *Heimdall* KO DI TNC1 astrocytes (KO), in DI TNC1 cells infected with a sgRNA targeting human *Trop2* (T2) as a non-target control, and in DI TNC1 control cells incubated or not with polybrene, a cationic polymer used to enhance lentiviral infection (CTL and Poly CTL, respectively). **C)** Heatmap representing the variation in the abundance of proteins identified in the various conditions by shot gun analyses. Significant changes were assessed by ANOVA test with a p value of P<0.005. Two

specific clusters were observed in *Heimdall* KO (n=3). **C')** String analyses of the proteins found in these clusters are presented. Proteins identified in cluster 1 are involved in cell growth and proliferation, cytoskeletal remodeling for vesicle transport, and brain development. Proteins identified in cluster 2 are involved in cell cycle regulation.

`

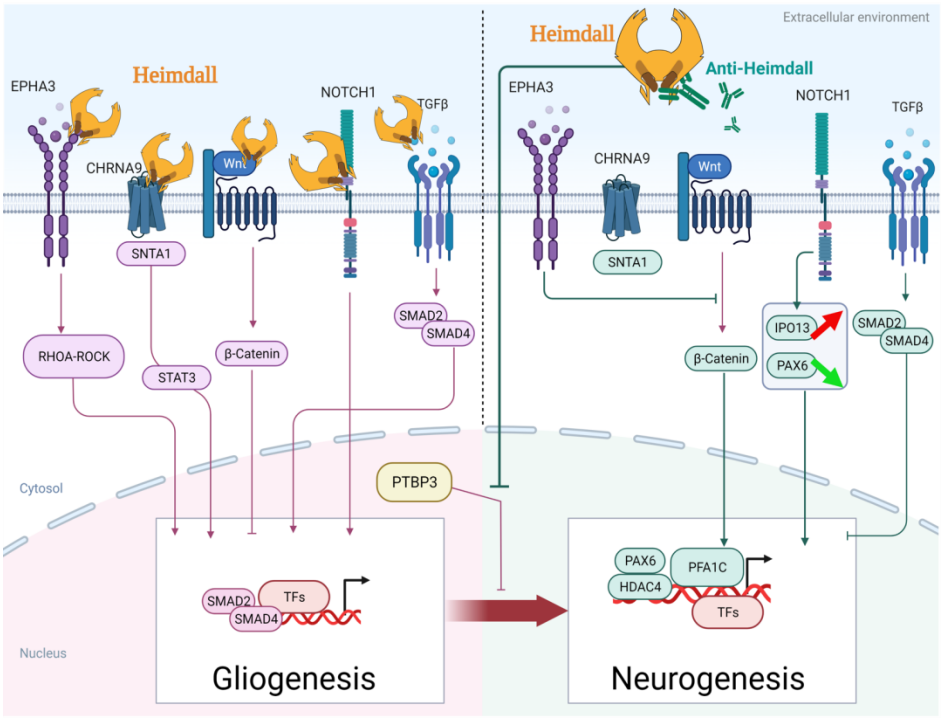

Figure 6 : Schematic representation of Heimdall action in astrocytes to maintain the fate of astrocytes. When inhibited through anti-Heimdall or CRISPR-Cas9, the astrocytes neuronal conversion take place.

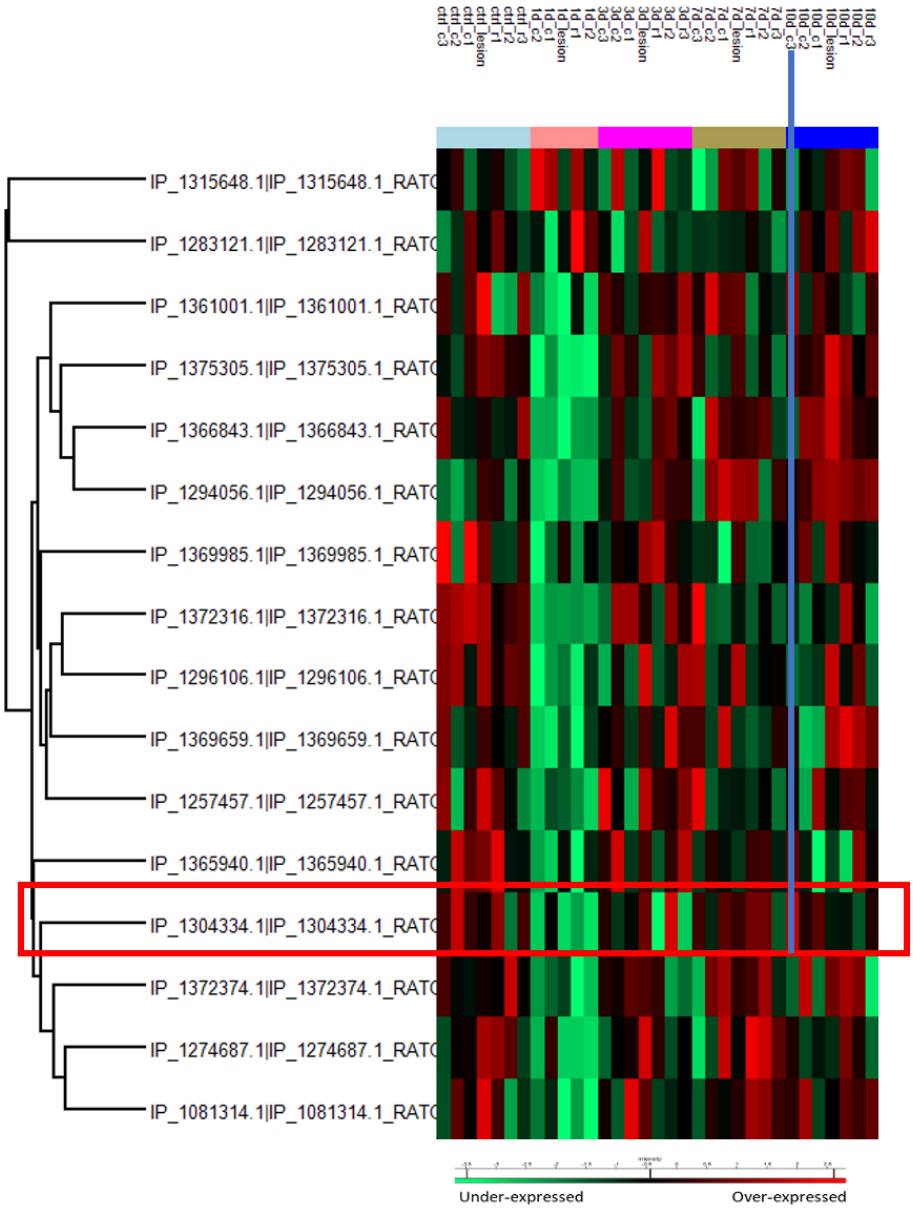

Supp. Figure 1 : Heatmap representing the variation in the abundance of proteins identified in the secretomes of rostral, Lesion and caudal segments after 12 h to 10 days of Spinal cord injury (SCI).

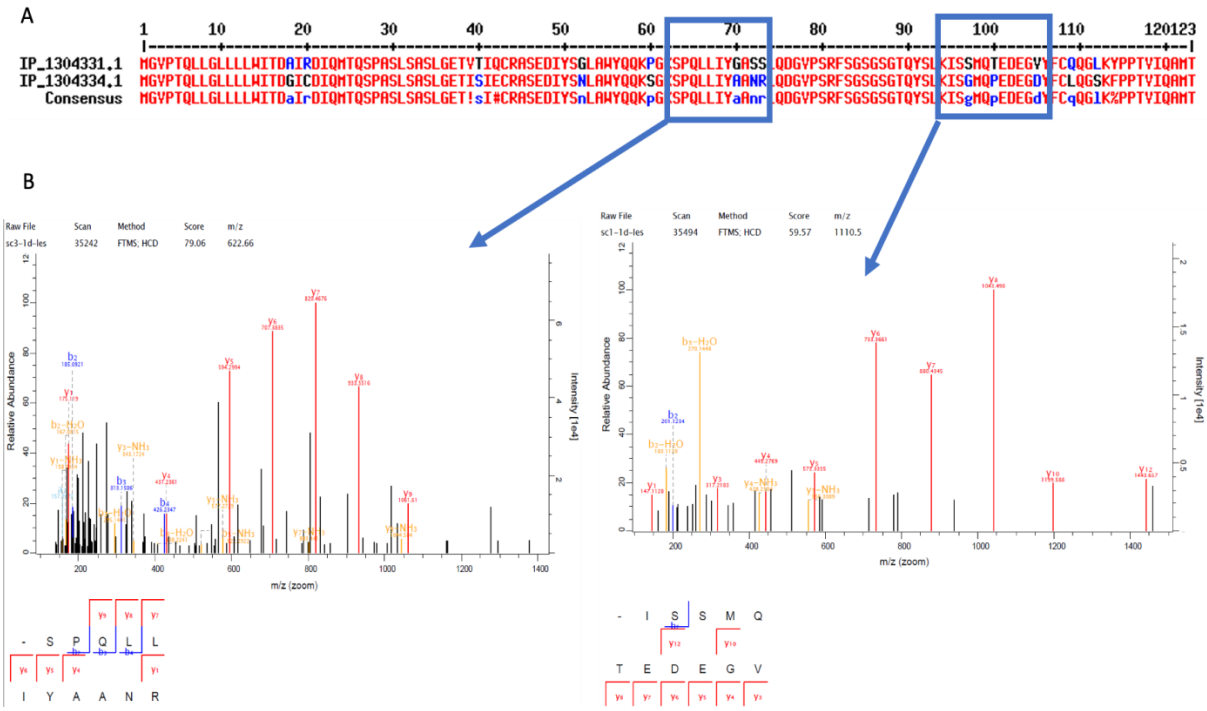

Supp. Figure 2 : **A**) Sequence alignment between the two isoforms of Heimdall. Blue boxes represent the amino acid residues the most different between the two proteins. B) MS/MS spectra corresponding to the two sequences highlighted with blue boxes

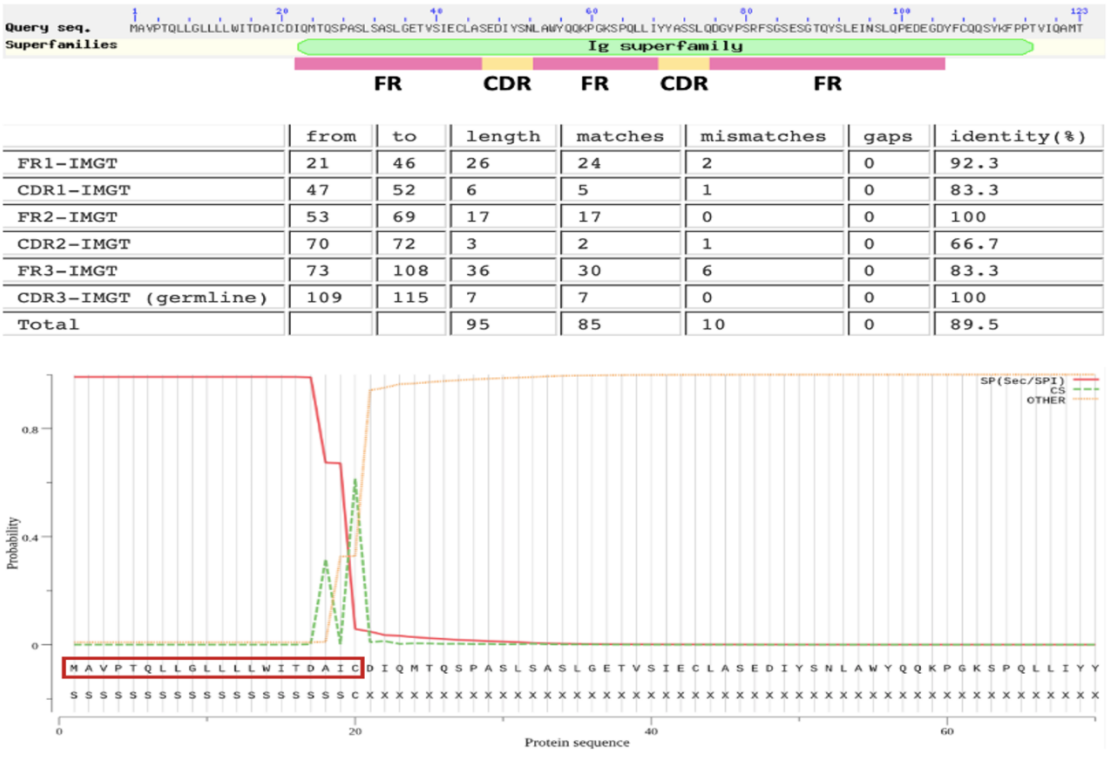

	from	to	length	matches	mismatches	gaps	identity(%)
FR1-IMGT	21	46	26	24	2	0	92.3
CDR1-IMGT	47	52	6	5	1	0	83.3
FR2-IMGT	53	69	17	17	0	0	100
CDR2-IMGT	70	72	3	2	1	0	66.7
FR3-IMGT	73	108	36	30	6	0	83.3
CDR3-IMGT (germline)	109	115	7	7	0	0	100
Total			95	85	10	0	89.5

Supp. Figure 3 : IgBlast[98] analyses of Heimdall sequence confirming its homology with the variable Kappa chain. Heimdall sequence contains a signal peptide leading to its secretion.

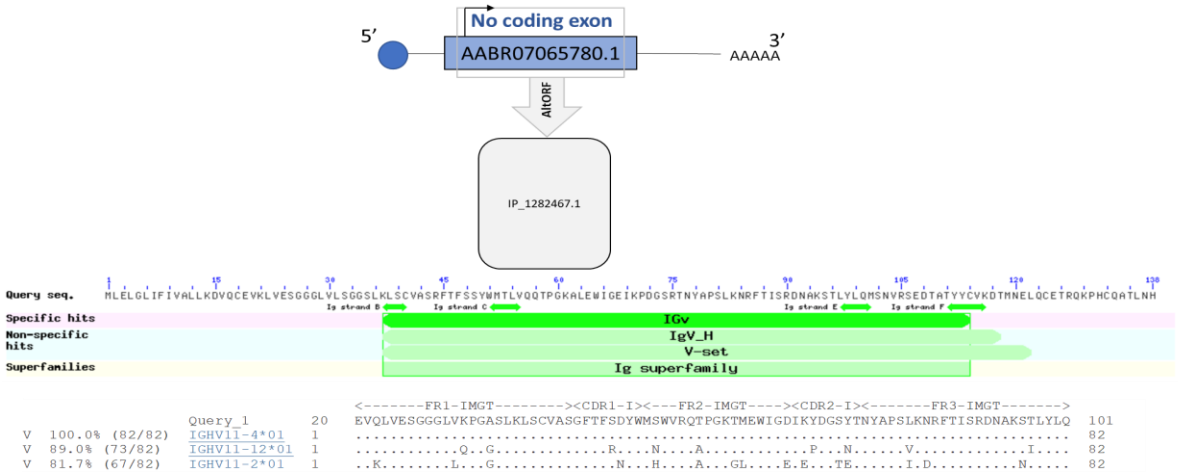

Supp. Figure 4 : Third long non coding RNA (AABR07065780.1) encoding a protein (IP_1282467.1) related to variable heavy chain. IGMT [99] analyses confirm the homology of this Alternative protein with the somatic IGHV11-8*01.

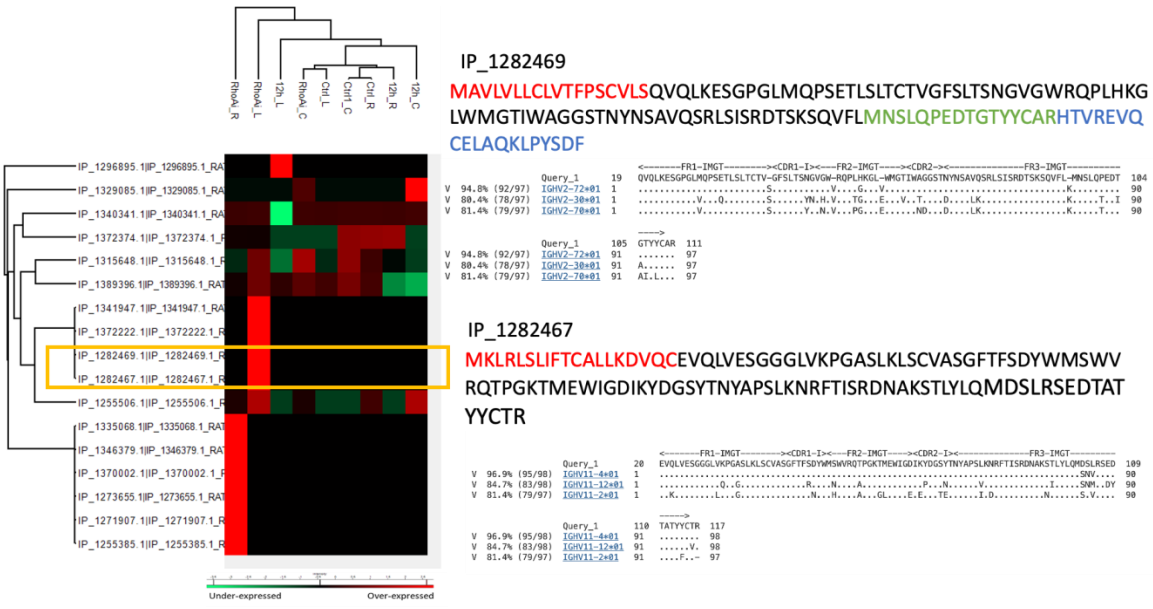

Supp. Figure 5 : Heatmap represents the Ghost proteins related to IGVH and identified at Lesion segment 12 h after SCI and RhoAi treatment.

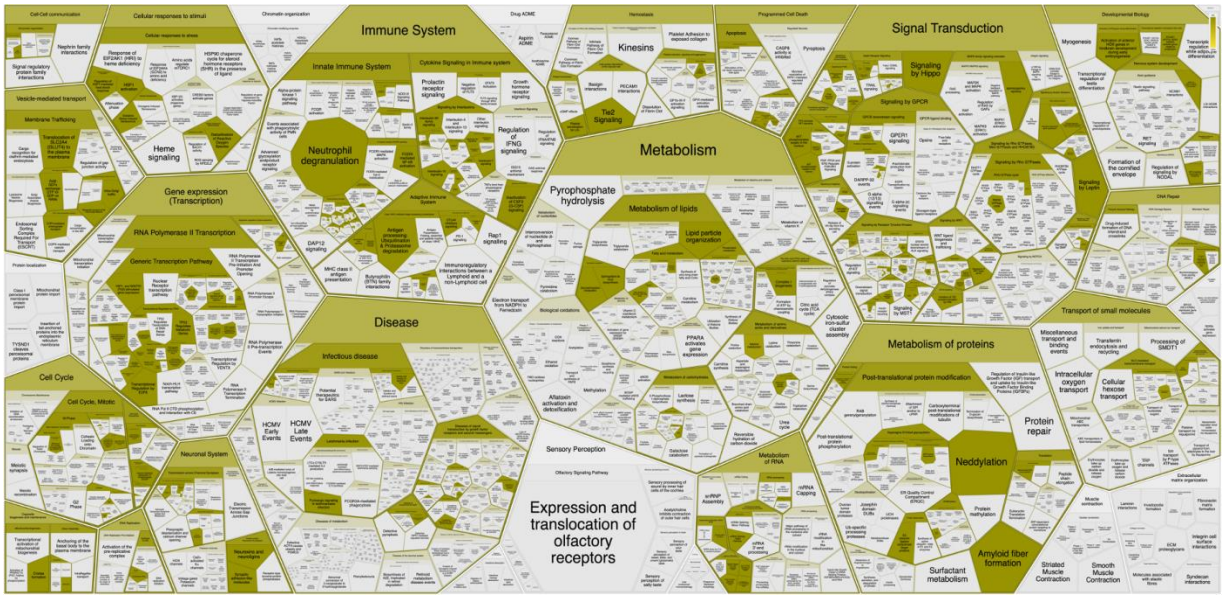

Supp. Figure 6 : Reactome analysis of specific proteins found in *Heimdall* KO DI TNC1 astrocytes.

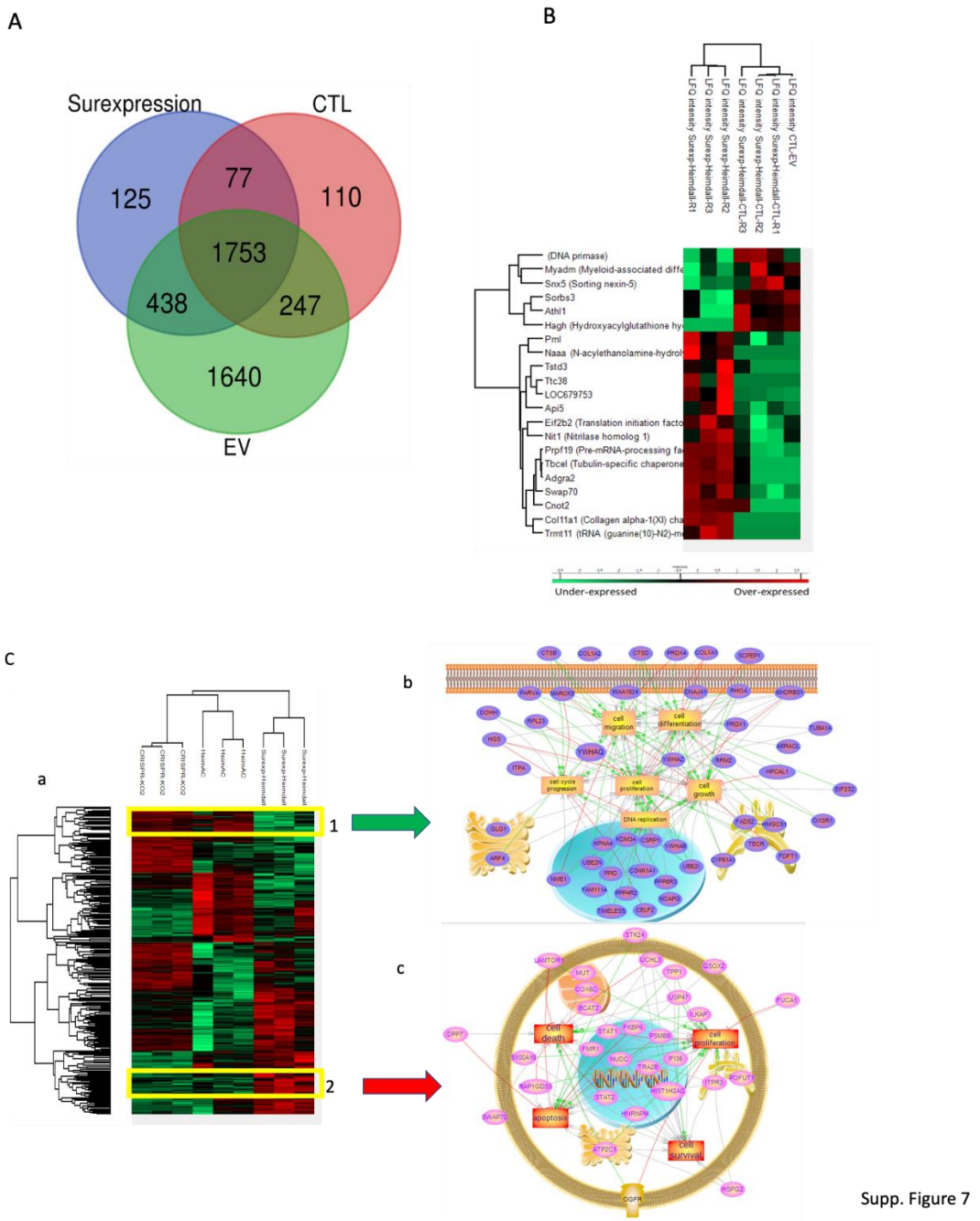

Supp. Figure 7

Supp. Figure 7 : A) Venn diagram and **B)** Heatmap comparison between DI TNC1 cells overexpressing Heimdall, DI TNC1 cells infected with the empty vector and DI TNC1 control cells **C**) a)Heatmap construct based on the comparison between *Heimdall* KO DI TNC1 cells DI TNC1 cells incubated with anti-Heimdall and DI TNC1 cells overexpressing Heimdall. Systemic biology analyses of the two Clusters (1,2) are presented in b and c.

SUPPLEMENTAL INFORMATION (A REVOIR)

Data S1: Significative list of alternative proteins identified by shotgun proteomic in secretome of (rostral, lesion, and caudal) segments of spinal cord after 12h and 24 h of injury after Perseus with a P value 0.05.

Data S2 Description of alternative proteins identified by shotgun proteomic in secretome of rostral, lesion, and caudal segments of spinal cord after 12h and 24 h of injury as presented in Figure 1C.

Data S3: List of identified immunoglobulin chains (constant and variable) identified in DiTNC1, B cells and primary culture of astrocytes from cortex.

Data S4: List of total proteins and from clusters (1 & 2) obtained after shot gun proteomic performed on cell extracts from DI TNC1 astrocytes stimulated or not with 200 ng/mL of LPS or incubated with anti-Heimdall ANOVA with a p value <0.05. The experiments were carried out in triplicate

Data S5 : List of exclusives proteins obtained after shot gun proteomic performed on cell extracts from control DI TNC1 astrocytes or incubated with anti-Heimdall or the isotype control antibody ANOVA with a p value <0.05. ANOVA with a p vale <0.05.

Data S6: List of proteins identified in clusters (1 and 2) of the heatmap obtained after shot gun analyses conducted on cell extracts from DI TNC1 astrocytes incubated with anti-Heimdall ANOVA with a p value <0.05. The experiments were carried out in triplicate.

Data S7: List of identified proteins through shot gun proteomic in average clusters (1 and 2) from the ones immunoprecipitated with anti-Heimdall or anti-Heimdall pre-incubated with the peptides used for the immunization from LPS stimulated cell extracts of DI TNC1 cells ANOVA with a p value <0.05. The experiments were carried out in triplicate.

Data S8 : Pictures of *Heimdall* KO and normal DI TNC1 astrocyte cultures.

Data S9 : List of Exclusives proteins identified after shot gun proteomic performed on cell extracts from DI TNC1 astrocytes treated or not with polybrene (Poly), *Heimdall* KO (KO), *Trop2* KO (T2),

Empty vector (EV). List of proteins characterized in clusters (1 and 2) of the heatmap obtained after shot gun analyses conducted on these cell extracts after ANOVA with a p value <0.05. The experiments were carried out in triplicate.

Data S10 : List of proteins identified in clusters (1 & 2) after shot gun proteomic performed on cell extracts from DI TNC1 astrocytes treated or not with polybrene (Poly), *Heimdall* KO (KO), *Trop2* KO (T2), Empty vector (EV) after ANOVA with a p value <0.05. The experiments were carried out in triplicate.

Data S11: List of Exclusives proteins identified after shot gun proteomic performed on secretome from DI TNC1 cells transduced with lentiviruses containing an empty vector (EV) or control DI TNC1 cells after stimulation or not with 200 ng/mL of LPS after ANOVA with a p value <0.05. The experiments were carried out in triplicate.

Data S12 : List of Exclusives proteins identified after shot gun proteomic performed on extracts from cells overexpressing Heimdall or control or transduced with an empty vector after ANOVA with p value <0.05. The experiments were carried out in triplicate.

Data S13 : List of proteins in Clusters identified after shot gun proteomic performed on extracts from cells overexpressing Heimdall or control or transduced with an empty vector after ANOVA with p value <0.05. The experiments were carried out in triplicate.

Data S14 : List of proteins in Clusters identified after shot gun proteomic performed on extracts from cells overexpressing Heimdall or CRISPR CAS9 Heimdall or with anti-Heimdall after ANOVA with p value <0.05. The experiments were carried out in triplicate.

Conclusion

Au cours de cette étude, nous avons pu montrer qu'un protéome alternatif spécifique est retrouvé lors d'une lésion de la moelle épinière. Parmi ces protéines alternatives, certaines ont été retrouvées de façon plus abondante au niveau de la lésion, comme IP_1304334 qui est une petite Altprot correspondant à une région variable d'une chaîne légère Kappa. De plus, nous avons pu identifier également que celle-ci présente une isoforme dans les astrocytes. Des analyses protéomiques de type shot-gun réalisées suite à la neutralisation de cette protéine dans le milieu de culture de ces cellules ou le KO de son gène révèle que cette protéine alternative joue un rôle dans le maintien de l'identité astrocytaire. En effet, son inhibition entraîne une dédifférenciation des astrocytes vers un phénotype neuronal alors que sa surexpression favorise le phénotype astrocytaire.

Lors d'une lésion de la moelle épinière, Heimdall pourrait donc jouer un rôle clé pour la mise en place de l'astrogliose expliquant ainsi sa sécrétion à un temps si précoce. En effet, au cours de cette astrogliose, les astrocytes réactifs vont s'activer et proliférer pour former une cicatrice gliale. C'est pourquoi, la sécrétion de cette région variable Kappa pourrait conduire à l'activation notamment de la voie MAPK comme le montre nos travaux de surexpression. Ceci permettrait de maintenir le phénotype astrocytaire et induire la prolifération ainsi que la survie des astrocytes. Bien que cette barrière empêche la propagation de la lésion aux sites avoisinants, celle-ci empêche la régénération neuronale et une récupération des fonctions motrices et sensorielles de la moelle épinière. Inhiber Heimdall au niveau du site lésionnel pourrait donc réduire la survenue d'une cicatrice gliale et permettre la conversion des astrocytes en neurones favorisant ainsi la repousse neuronale. En ce sens, Heimdall serait donc une cible thérapeutique à envisager tout comme NeuroD1 ou Ascl1qui s'avèrent être des facteurs impliqués dans la reconversion astrocytes – neurones (Griffiths et *al.,* 2019; Puls et *al.,* 2020; Tai et *al.,* 2021; Ma, et *al.,* 2022)

Afin de poursuivre ce projet, nous déterminerons tout d'abord quel est le mode d'action d'Heimdall. Pour ce faire des expériences de pull-down seront réalisées sur des extraits

membranaires d'astrocytes afin d'identifier le récepteur auquel se lierait Heimdall. Les voies de signalisation correspondantes pourront être également caractérisées. L'association d'Heimdall avec des protéines spécifiques et / ou des chaînes lourdes et légères d'immunoglobulines sera également évaluée. De plus, l'étude du changement phénotypique des astrocytes en phénotype neuronal lors d'une inhibition d'Heimdall sera poursuivie en recherchant la présence de marqueurs et facteurs de transcription neuronaux. La recherche de contacts synaptiques entre neurones et astrocytes convertis sera également entreprise. Par la suite, il serait pertinent de déterminer à quel moment du développement est synthétisée cette protéine ainsi que son rôle dans l'édification du SNC. De plus, une étude pourrait être entreprise sur le rôle d'Heimdall au cours d'une lésion de la moelle épinière et voir quel serait l'impact de son inhibition sur la formation de la cicatrice gliale et la régénération de la ME.

Discussion Générale

L'un des plus grands dogmes de l'immunologie est que seuls les lymphocytes B sont capables de produire des anticorps. Pourtant, de nos jours, celui-ci est largement controversé. Comme nous avons pu le voir précédemment, nous démontrons avec ce travail l'existence d'une nouvelle source cellulaire pour leur synthèse *i.e.* les astrocytes et les neurones.

Dans un premier temps, nous avons montré que la chaîne lourde IgG2C et les récepteurs FcγRII (CD32) et FcγRIII (CD16) sont synthétisés par la lignée neurale N27 non différenciée. De plus, l'activation du récepteur CD16 induit la croissance neuritique, alors que l'ajout de façon concomitante de l'isotype IgG2 bloque la croissance neuritique via l'activation du récepteur CD32b. Le récepteur CD16 est connu pour avoir une plus grande affinité pour l'IgG1. Or, celle-ci et des IgG2 sont détectées dans le sécrétome d'explants de LME dès les premiers instants post lésion. Il est donc possible qu'il existe une balance entre les isotypes et l'activation de leurs récepteurs respectifs. Cet équilibre varie au cours du temps post-lésion *i.e.* favorable à la repousse neuritique dans les premières heures puis défavorable après 24h (Cizkova *et al.,* 2014; Devaux *et al.,* 2016). L'origine des isotypes est pour l'instant non tranchée. En effet, les cellules neurales non différenciées semblent produire des IgG2C, alors que les astrocytes de l'IgG2B et de l'IgM. En ce qui concerne l'IgG1 et les autres sous-types d'IgG2 pourraient être issus d'une commutation de classe en fonction de l'environnement neurotrophique ou inflammatoire. De plus, un contrôle de la réparation pourrait être lié à des effets autocrines et paracrine avec notamment un dialogue croisé entre les neurones et les astrocytes. De plus nos travaux d'invalidation génique montrent que les Igs interviennent pour maintenir le phénotype astrocytaire. Leurs productions à la suite de la LME pourraient également conditionner la mise en place de la cicatrice gliale et ainsi de la réparation nerveuse ou non.

Par ailleurs, le laboratoire PRISM a démontré que la voie RhoA est fortement activée par différents facteurs tel que le protéoglycane de sulfate de chondroïtine (CPSG) produit par les astrocytes (**Figure 23**) (Devaux et *al.,* 2018). L'activation de cette voie est cependant associée à une diminution de la croissance neuritique, une excitotoxicité et une mort neuronale. Son

inhibition a été corrélée avec une amélioration de la régénération axonale et la repousse neuritique. Dans ce contexte, l'hypothèse de l'implication des Igs dans le contrôle de la neuritogenèse est renforcée par nos résultats montrant que l'inhibition de la voie RhoA au cours de la LME entraîne une augmentation des taux d'IgG1 et d'IgG2. Par ailleurs, l'activation de la voie RhoA peut être modulée par la protéine C3 de la voie du complément (**Figure 23**). L'inhibition de celle-ci dans les cellules souches neurales entraîne une diminution de l'activité de Rac1 et une stimulation de la voie RhoA. De plus, l'absence de C3 est corrélée avec une diminution des marqueurs progéniteurs et l'expression de marqueurs neuronaux suggérant que cette protéine du complément joue un rôle dans la conservation du phénotype progéniteur (Gorelik *et al.,* 2018). De même, l'étude de Shinjyo montre également que la protéine du complément C3a influence la différenciation et la migration des cellules progénitrices neurales sous une stimulation par du SDF-1α. En effet, ces cellules ainsi stimulées se différencient en cellules neuronales alors que l'ajout de la protéine C3a inhibe cette différenciation (Shinjyo *et al.,* 2009). Ainsi, la C3 inhibe la voie RhoA et empêche la différenciation cellulaire. Dans ce contexte, des études au laboratoire ont montré que les protéines Rac1 et C3 sont plus abondantes au niveau de la lésion et de la région caudale (Devaux et *al.,* 2018). De plus, les analyses par RNAseq réalisées sur des cultures primaires d'astrocytes d'embryons humains stimulées pendant 24 et 48 heures par du LPS ou un mixte de cytokines montrent que l'expression du gène codant la protéine C3 du complément est induite. Ceci soutient que la C3 est produite à un stade précoce du développement et serait impliquée dans le contrôle de la circuiterie neuronale. D'autres études ont également montré que la C3 est majoritairement produite par les astrocytes et régule la prolifération des progéniteurs neuronaux, la migration neuronale et l'élagage synaptique (Chen *et al.,* 2022). A ce stade, les mécanismes moléculaires et intracellulaires restent inconnus. Néanmoins, il est possible d'émettre l'hypothèse que la C3 serait libérée par les astrocytes afin d'inhiber la voie RhoA neuronale et, favoriser la production d'Igs neuraux (**Figure 23**).

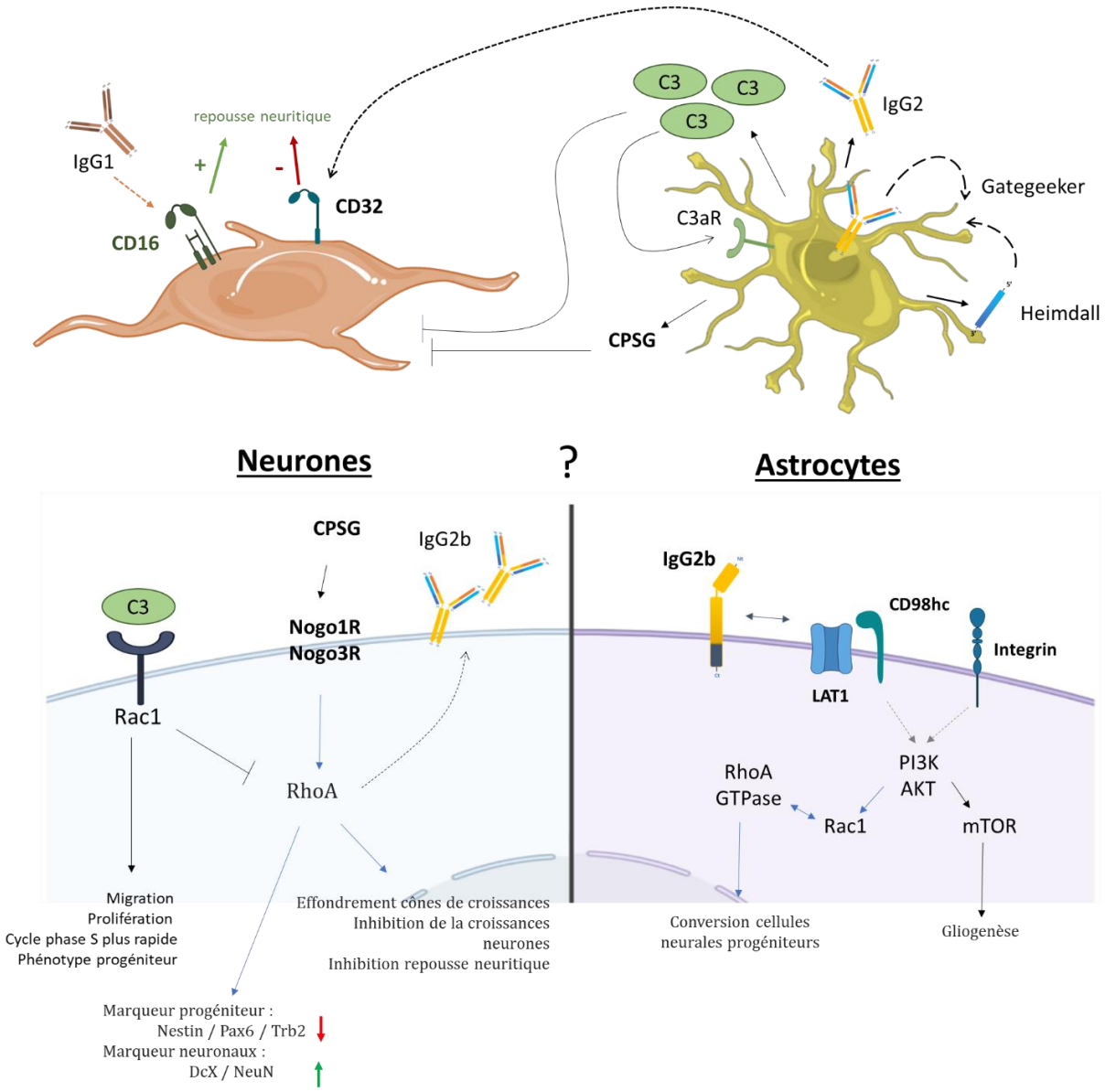

<u>Figure 23 :</u> Schéma hypothétique de la fonction des IgG sur les astrocytes et les neurones lors d'une lésion de la moelle épinière.

Parallèlement, au cours de cette thèse, nous avons confirmé que les astrocytes produisent des chaînes variables seules, ne présentant que la région V. Celles-ci sont codées par des gènes de références ou des ORF alternatifs. L'inhibition de l'une d'entre elles, Heimdall, induit une reconversion des astrocytes en cellules neuronales. Ces nouvelles cellules converties présentent une diminution du potentiel de membrane comme observé dans les neurones ainsi que la présence d'extensions cellulaires rappelant des neurites. Les parties variables

d'immunoglobulines ont la particularité de reconnaitre des antigènes spécifiques. Heimdall sécrété pourrait piéger des ligands spécifiques impliqués dans le maintien du phénotype astrocytaire. Nous démontrons à nouveau que des molécules immunitaires pouvaient présenter une plasticité fonctionnelle en étant soit immunitaires, soit régulatrices des voies de différenciation neurale eut égard aux cellules qui les produisent. Leurs modes d'actions impliqueraient également les mêmes récepteurs *i.e.* FcGR. L'ADNM du système nerveux est donc le miroir l'ADCC du système immunitaire.

A long terme, ces études pourraient mener à ouvrir de nouveaux axes de recherche, non seulement pour le traitement de la lésion de la moelle épinière, mais aussi dans différentes conditions pathologies du SNC (maladie de Parkinson, Alzheimer, sclérose en plaque, cancers cérébraux…). Mais un autre champ ambitieux serait de comparer la mémoire cognitive et la mémoire immunologique. En effet, nous savons que les immunoglobulines sont les messagers de la mémoire immunitaire, or le rôle de telles molécules au sein du système nerveux questionne surtout si l'on considère la forte présence des astrocytes au sein de l'un des sièges de la mémoire, *i.e.* l'hippocampe. La présence du complexe enzymatique de recombinaison génétique que nous avons caractérisé au sein des astrocytes s'apparente à celui présent dans les lymphocytes B. L'inactivation des gènes RAG1 ou RAG2 impacte la mémoire spatiale et la mémoire de reconnaissance sociale (McGowan et *al.,* 2011; Sacks et *al.,* 2018). Peut-on émettre l'hypothèse que ces Immunoglobulines neurales participent à la mémoire cognitive. Est-ce que l'association que nous faisons entre notre Grand-Mère et sa merveilleuse tarte aux pommes comme l'indiquait Proust avec sa madeleine, ne serait pas en fait une association entre éléments volatiles (volatilome) liés à des récepteurs odorants. Ceci conduirait à des voies de signalisation permettant la production de facteurs reconnus comme des antigènes et permettant ainsi l'édification de paratopes qui seront conservés au sein du système nerveux par des astrocytes porteurs de ces paratopes, des astrocytes mémoires en quelque sorte afin d'édifier une mémoire spécifique. Peut-être est-ce des conjectures, ou l'inverse un vrai champ d'investigation, plein de perspectives sont alors à envisager.

Bibliographie

Akdemir, E.S., Huang, A.Y.-S. and Deneen, B. (2020) 'Astrocytogenesis: where, when, and how', *F1000Research*, 9, p. F1000 Faculty Rev-233. Available at: https://doi.org/10.12688/f1000research.22405.1.

Alizadeh, A., Dyck, S.M. and Karimi-Abdolrezaee, S. (2019) 'Traumatic Spinal Cord Injury: An Overview of Pathophysiology, Models and Acute Injury Mechanisms', *Frontiers in Neurology*, 10, p. 282. Available at: https://doi.org/10.3389/fneur.2019.00282.

Allaman, I., Bélanger, M. and Magistretti, P.J. (2015) 'Methylglyoxal, the dark side of glycolysis', *Frontiers in Neuroscience*, 9. Available at: https://www.frontiersin.org/article/10.3389/fnins.2015.00023 (Accessed: 27 May 2022).

Allen, N.J. and Eroglu, C. (2017) 'Cell biology of astrocyte-synapse interactions', *Neuron*, 96(3), pp. 697–708. Available at: https://doi.org/10.1016/j.neuron.2017.09.056.

Aloisi, F. (2001) 'Immune function of microglia', *Glia*, 36(2), pp. 165–179. Available at: https://doi.org/10.1002/glia.1106.

Andoh, T. and Kuraishi, Y. (2004) 'Direct action of immunoglobulin G on primary sensory neurons through Fc gamma receptor I', *FASEB journal: official publication of the Federation of American Societies for Experimental Biology*, 18(1), pp. 182–184. Available at: https://doi.org/10.1096/fj.02-1169fje.

Arellano-Carbajal, F. *et al.* (2011) 'Macoilin, a conserved nervous system-specific ER membrane protein that regulates neuronal excitability', *PLoS genetics*, 7(3), p. e1001341. Available at: https://doi.org/10.1371/journal.pgen.1001341.

Arnold, S.A. and Hagg, T. (2011) 'Anti-inflammatory treatments during the chronic phase of spinal cord injury improve locomotor function in adult mice', *Journal of Neurotrauma*, 28(9), pp. 1995–2002. Available at: https://doi.org/10.1089/neu.2011.1888.

Babbage, G. *et al.* (2006) 'Immunoglobulin Heavy Chain Locus Events and Expression of Activation-Induced Cytidine Deaminase in Epithelial Breast Cancer Cell Lines', *Cancer Research*, 66(8), pp. 3996–4000. Available at: https://doi.org/10.1158/0008-5472.CAN-05-3704.

Bagriyanik, H.A. *et al.* (2008) 'Neuroprotective effects of ketorolac tromethamine after spinal cord injury in rats: an ultrastructural study', *Advances in Therapy*, 25(2), pp. 152–158. Available at: https://doi.org/10.1007/s12325-008-0018-x.

Beard, E. *et al.* (2022) 'Astrocytes as Key Regulators of Brain Energy Metabolism: New Therapeutic Perspectives', *Frontiers in Physiology*, 12, p. 825816. Available at: https://doi.org/10.3389/fphys.2021.825816.

Beseler, C. *et al.* (2017) 'The complex relationship between oligoclonal bands, lymphocytes in the cerebrospinal fluid, and immunoglobulin G antibodies in multiple sclerosis: Indication of serum contribution', *PLoS ONE*, 12(10), p. e0186842. Available at: https://doi.org/10.1371/journal.pone.0186842.

den Boer, M.A. *et al.* (2022) 'Comparative Analysis of Antibodies and Heavily Glycosylated Macromolecular Immune Complexes by Size-Exclusion Chromatography Multi-Angle Light Scattering, Native Charge Detection Mass Spectrometry, and Mass Photometry', *Analytical Chemistry*, 94(2), pp. 892–900. Available at: https://doi.org/10.1021/acs.analchem.1c03656.

Boross, P. and Leusen, J.H.W. (2012) 'Mechanisms of action of CD20 antibodies', *American Journal of Cancer Research*, 2(6), pp. 676–690.

Brunet, M.A. *et al.* (2021) 'OpenProt 2021: deeper functional annotation of the coding potential of eukaryotic genomes', *Nucleic Acids Research*, 49(D1), pp. D380–D388. Available at: https://doi.org/10.1093/nar/gkaa1036.

Buosi, A.S. *et al.* (2018) 'Heterogeneity in Synaptogenic Profile of Astrocytes from Different Brain Regions', *Molecular Neurobiology*, 55(1), pp. 751–762. Available at: https://doi.org/10.1007/s12035-016-0343-z.

Bushong, E.A. *et al.* (2002) 'Protoplasmic Astrocytes in CA1 Stratum Radiatum Occupy Separate Anatomical Domains', *The Journal of Neuroscience*, 22(1), pp. 183–192. Available at: https://doi.org/10.1523/JNEUROSCI.22-01-00183.2002.

Cardon, T. *et al.* (2020) 'Alternative proteins are functional regulators in cell reprogramming by PKA activation', *Nucleic Acids Research*, 48(14), pp. 7864–7882. Available at: https://doi.org/10.1093/nar/gkaa277.

Cardon, T., Fournier, I. and Salzet, M. (2021a) 'Shedding Light on the Ghost Proteome', *Trends in Biochemical Sciences*, 46(3), pp. 239–250. Available at: https://doi.org/10.1016/j.tibs.2020.10.003.

Cardon, T., Fournier, I. and Salzet, M. (2021b) 'Unveiling a Ghost Proteome in the Glioblastoma Non-Coding RNAs', *Frontiers in Cell and Developmental Biology*, 9. Available at: https://www.frontiersin.org/articles/10.3389/fcell.2021.703583 (Accessed: 27 September 2022).

Casha, S. *et al.* (2012) 'Results of a phase II placebo-controlled randomized trial of minocycline in acute spinal cord injury', *Brain*, 135(4), pp. 1224–1236. Available at: https://doi.org/10.1093/brain/aws072.

Chandrasekaran, A. *et al.* (2016) 'Astrocyte Differentiation of Human Pluripotent Stem Cells: New Tools for Neurological Disorder Research', *Frontiers in Cellular Neuroscience*, 10, p. 215. Available at: https://doi.org/10.3389/fncel.2016.00215.

Chen, Y. *et al.* (2022) 'The Complement System in the Central Nervous System: From Neurodevelopment to Neurodegeneration', *Biomolecules*, 12(2), p. 337. Available at: https://doi.org/10.3390/biom12020337.

Chen, Z. and Gu, J. (2007) 'Immunoglobulin G expression in carcinomas and cancer cell lines', *FASEB journal: official publication of the Federation of American Societies for Experimental Biology*, 21(11), pp. 2931–2938. Available at: https://doi.org/10.1096/fj.07-8073com.

Chung, W.-H. *et al.* (2013) 'Improved rat spinal cord injury model using spinal cord compression by percutaneous method', *Journal of Veterinary Science*, 14(3), pp. 329–335. Available at: https://doi.org/10.4142/jvs.2013.14.3.329.

Cizkova, D. *et al.* (2014) 'Alterations of protein composition along the rostro-caudal axis after spinal cord injury: proteomic, in vitro and in vivo analyses', *Frontiers in Cellular Neuroscience*, 8, p. 105. Available at: https://doi.org/10.3389/fncel.2014.00105.

Cizkova, D. *et al.* (2018) 'Correction: Cizkova, D., et al. Localized Intrathecal Delivery of Mesenchymal Stromal Cells Conditioned Media Improves Functional Recovery in A Rat Model of Contusive Spinal Cord Injury. Int. J. Mol. Sci. 2018, 19, 870', *International Journal of Molecular Sciences*, 19(7), p. E1942. Available at: https://doi.org/10.3390/ijms19071942.

Cizkova, D. *et al.* (2020) 'Spinal Cord Injury: Animal Models, Imaging Tools and the Treatment Strategies', *Neurochemical Research*, 45(1), pp. 134–143. Available at: https://doi.org/10.1007/s11064-019-02800-w.

Crescioli, S. *et al.* (2016) 'IgG4 Characteristics and Functions in Cancer Immunity', *Current Allergy and Asthma Reports*, 16, p. 7. Available at: https://doi.org/10.1007/s11882-015-0580-7.

Cuevas-Diaz Duran, R. *et al.* (2019) 'Brain Region-Specific Gene Signatures Revealed by Distinct Astrocyte Subpopulations Unveil Links to Glioma and Neurodegenerative Diseases', *eNeuro*, 6(2), p. ENEURO.0288-18.2019. Available at: https://doi.org/10.1523/ENEURO.0288-18.2019.

Cui, M. *et al.* (2021) 'Immunoglobulin Expression in Cancer Cells and Its Critical Roles in Tumorigenesis', *Frontiers in Immunology*, 12, p. 613530. Available at: https://doi.org/10.3389/fimmu.2021.613530.

Delcourt, V. *et al.* (2018) 'Small Proteins Encoded by Unannotated ORFs are Rising Stars of the Proteome, Confirming Shortcomings in Genome Annotations and Current Vision of an mRNA', *Proteomics*, 18(10), p. e1700058. Available at: https://doi.org/10.1002/pmic.201700058.

Devaux, S. *et al.* (2016) 'Proteomic Analysis of the Spatio-temporal Based Molecular Kinetics of Acute Spinal Cord Injury Identifies a Time- and Segment-specific Window for Effective Tissue Repair', *Molecular & Cellular Proteomics : MCP*, 15(8), pp. 2641–2670. Available at: https://doi.org/10.1074/mcp.M115.057794.

Devaux, S. *et al.* (2017) 'RhoA Inhibitor Treatment At Acute Phase of Spinal Cord Injury May Induce Neurite Outgrowth and Synaptogenesis', *Molecular & Cellular Proteomics : MCP*, 16(8), pp. 1394–1415. Available at: https://doi.org/10.1074/mcp.M116.064881.

Dong, L., Smith, J.R. and Winkelstein, B.A. (2013) 'Ketorolac reduces spinal astrocytic activation and PAR1 expression associated with attenuation of pain after facet joint injury', *Journal of Neurotrauma*, 30(10), pp. 818–825. Available at: https://doi.org/10.1089/neu.2012.2600.

Duan, L. and Pomerantz, R.J. (1994) 'Elimination of endogenous aberrant kappa chain transcripts from sp2/0-derived hybridoma cells by specific ribozyme cleavage: utility in genetic therapy of HIV-1 infections', *Nucleic Acids Research*, 22(24), pp. 5433–5438. Available at: https://doi.org/10.1093/nar/22.24.5433.

EMSLEY, J.G. and MACKLIS, J.D. (2006) 'Astroglial heterogeneity closely reflects the neuronal-defined anatomy of the adult murine CNS', *Neuron glia biology*, 2(3), pp. 175–186. Available at: https://doi.org/10.1017/S1740925X06000202.

van Erp, E.A. *et al.* (2019) 'Fc-Mediated Antibody Effector Functions During Respiratory Syncytial Virus Infection and Disease', *Frontiers in Immunology*, 10, p. 548. Available at: https://doi.org/10.3389/fimmu.2019.00548.

Fanger, N.A. *et al.* (1996) 'Type I (CD64) and type II (CD32) Fc gamma receptor-mediated phagocytosis by human blood dendritic cells', *Journal of Immunology (Baltimore, Md.: 1950)*, 157(2), pp. 541–548.

Farhy-Tselnicker, I. and Allen, N.J. (2018) 'Astrocytes, neurons, synapses: a tripartite view on cortical circuit development', *Neural Development*, 13, p. 7. Available at: https://doi.org/10.1186/s13064-018-0104-y.

Fernández-Quintero, M.L. *et al.* (2022) 'Paratope states in solution improve structure prediction and docking', *Structure*, 30(3), pp. 430-440.e3. Available at: https://doi.org/10.1016/j.str.2021.11.001.

Ginhoux, F. and Garel, S. (2018) 'The mysterious origins of microglia', *Nature Neuroscience*, 21(7), pp. 897–899. Available at: https://doi.org/10.1038/s41593-018-0176-3.

Gorelik, A. *et al.* (2018) 'Complement C3 Affects Rac1 Activity in the Developing Brain', *Frontiers in Molecular Neuroscience*, 11, p. 150. Available at: https://doi.org/10.3389/fnmol.2018.00150.

Gorina, R. *et al.* (2011) 'Astrocyte TLR4 activation induces a proinflammatory environment through the interplay between MyD88-dependent NFκB signaling, MAPK, and Jak1/Stat1 pathways', *Glia*, 59(2), pp. 242–255. Available at: https://doi.org/10.1002/glia.21094.

Griffiths, B.B., Bhutani, A. and Stary, C.M. (2019) 'Adult neurogenesis from reprogrammed astrocytes', *Neural Regeneration Research*, 15(6), pp. 973–979. Available at: https://doi.org/10.4103/1673-5374.270292.

Han, R.T. *et al.* (2021) 'Astrocyte-immune cell interactions in physiology and pathology', *Immunity*, 54(2), pp. 211–224. Available at: https://doi.org/10.1016/j.immuni.2021.01.013.

Hasel, P. and Liddelow, S.A. (2021) 'Astrocytes', *Current Biology*, 31(7), pp. R326–R327. Available at: https://doi.org/10.1016/j.cub.2021.01.056.

Hsieh, Y.-C. *et al.* (2005) 'Intrathecal Ketorolac Pretreatment Reduced Spinal Cord Ischemic Injury in Rats', *Anesthesia & Analgesia*, 100(4), pp. 1134–1139. Available at: https://doi.org/10.1213/01.ANE.0000146962.91038.15.

Hu, D. *et al.* (2011) 'Heterogeneity of aberrant immunoglobulin expression in cancer cells', *Cellular & Molecular Immunology*, 8(6), pp. 479–485. Available at: https://doi.org/10.1038/cmi.2011.25.

Huang, J. *et al.* (2008) 'Expression of immunoglobulin gene with classical V-(D)-J rearrangement in mouse brain neurons', *The International Journal of Biochemistry & Cell Biology*, 40(8), pp. 1604–1615. Available at: https://doi.org/10.1016/j.biocel.2007.12.004.

Huang, Z. *et al.* (2016) 'YAP stabilizes SMAD1 and promotes BMP2-induced neocortical astrocytic differentiation', *Development (Cambridge, England)*, 143(13), pp. 2398–2409. Available at: https://doi.org/10.1242/dev.130658.

Jiang, H. *et al.* (2019) 'Cancer IgG, a potential prognostic marker, promotes colorectal cancer progression', *Chinese Journal of Cancer Research*, 31(3), pp. 499–510. Available at: https://doi.org/10.21147/j.issn.1000-9604.2019.03.12.

Kaeser, G. and Chun, J. (2020) 'Brain cell somatic gene recombination and its phylogenetic foundations', *Journal of Biological Chemistry*, 295(36), pp. 12786–12795. Available at: https://doi.org/10.1074/jbc.REV120.009192.

Kaptanoglu, E. *et al.* (2003) 'Effect of magnesium sulphate in experimental spinal cord injury: evaluation with ultrastructural findings and early clinical results', *Journal of Clinical Neuroscience: Official Journal of the Neurosurgical Society of Australasia*, 10(3), pp. 329–334. Available at: https://doi.org/10.1016/s0967-5868(03)00031-6.

Karmodiya, K. *et al.* (2012) 'H3K9 and H3K14 acetylation co-occur at many gene regulatory elements, while H3K14ac marks a subset of inactive inducible promoters in mouse embryonic stem cells', *BMC Genomics*, 13(1), p. 424. Available at: https://doi.org/10.1186/1471-2164-13-424.

Kimoto, Y. (1998) 'Expression of heavy-chain constant region of immunoglobulin and T-cell receptor gene transcripts in human non-hematopoietic tumor cell lines', *Genes, Chromosomes & Cancer*, 22(1), pp. 83–86. Available at: https://doi.org/10.1002/(sici)1098-2264(1998)22:1<83::aid-gcc12>3.0.co;2-o.

Kitazono, T. *et al.* (2017) 'Multiple Signaling Pathways Coordinately Regulate Forgetting of Olfactory Adaptation through Control of Sensory Responses in Caenorhabditis elegans', *The Journal of Neuroscience: The Official Journal of the Society for Neuroscience*, 37(42), pp. 10240–10251. Available at: https://doi.org/10.1523/JNEUROSCI.0031-17.2017.

Kozak, M. (1989) 'The scanning model for translation: an update', *The Journal of Cell Biology*, 108(2), pp. 229–241. Available at: https://doi.org/10.1083/jcb.108.2.229.

Kucukdereli, H. *et al.* (2011) 'Control of excitatory CNS synaptogenesis by astrocyte-secreted proteins Hevin and SPARC', *Proceedings of the National Academy of Sciences of the United States of America*, 108(32), pp. E440–E449. Available at: https://doi.org/10.1073/pnas.1104977108.

Kwon, D. (2022) 'Guardians of the brain: how a special immune system protects our grey matter', *Nature*, 606(7912), pp. 22–24. Available at: https://doi.org/10.1038/d41586-022-01502-8.

Li, L. *et al.* (2016) 'Overexpression of cancer cell-derived immunoglobulin G correlates with poor prognosis in gastric cancer patients', *Translational Cancer Research*, 5(3). Available at: https://doi.org/10.21037/8033.

Li, M. *et al.* (2012) 'Promotion of cell proliferation and inhibition of ADCC by cancerous immunoglobulin expressed in cancer cell lines', *Cellular & Molecular Immunology*, 9(1), pp. 54–61. Available at: https://doi.org/10.1038/cmi.2011.40.

Liberis, E. *et al.* (2018) 'Parapred: antibody paratope prediction using convolutional and recurrent neural networks', *Bioinformatics (Oxford, England)*, 34(17), pp. 2944–2950. Available at: https://doi.org/10.1093/bioinformatics/bty305.

Liddelow, S.A. and Barres, B.A. (2017) 'Reactive Astrocytes: Production, Function, and Therapeutic Potential', *Immunity*, 46(6), pp. 957–967. Available at: https://doi.org/10.1016/j.immuni.2017.06.006.

Linnerbauer, M., Wheeler, M.A. and Quintana, F.J. (2020) 'Astrocyte crosstalk in CNS inflammation', *Neuron*, 108(4), pp. 608–622. Available at: https://doi.org/10.1016/j.neuron.2020.08.012.

Ma, N.-X., Puls, B. and Chen, G. (2022) 'Transcriptomic analyses of NeuroD1-mediated astrocyte-to-neuron conversion', *Developmental Neurobiology*, 82(5), pp. 375–391. Available at: https://doi.org/10.1002/dneu.22882.

MacVicar, B.A. and Newman, E.A. (2015) 'Astrocyte Regulation of Blood Flow in the Brain', *Cold Spring Harbor Perspectives in Biology*, 7(5), p. a020388. Available at: https://doi.org/10.1101/cshperspect.a020388.

Mallah, K. *et al.* (2021) 'Neurotrauma investigation through spatial omics guided by mass spectrometry imaging: Target identification and clinical applications', *Mass Spectrometry Reviews*, n/a(n/a). Available at: https://doi.org/10.1002/mas.21719.

Marquardt, T. *et al.* (2005) 'Coexpressed EphA Receptors and Ephrin-A Ligands Mediate Opposing Actions on Growth Cone Navigation from Distinct Membrane Domains', *Cell*, 121(1), pp. 127–139. Available at: https://doi.org/10.1016/j.cell.2005.01.020.

McGowan, P.O. *et al.* (2011) 'Impaired social recognition memory in recombination activating gene 1-deficient mice', *Brain Research*, 1383, pp. 187–195. Available at: https://doi.org/10.1016/j.brainres.2011.02.054.

Metz, G.A. *et al.* (2000) 'Validation of the weight-drop contusion model in rats: a comparative study of human spinal cord injury', *Journal of Neurotrauma*, 17(1), pp. 1–17. Available at: https://doi.org/10.1089/neu.2000.17.1.

Mohamed, H.A. *et al.* (2002) 'Immunoglobulin Fc gamma receptor promotes immunoglobulin uptake, immunoglobulin-mediated calcium increase, and neurotransmitter release in motor neurons', *Journal of Neuroscience Research*, 69(1), pp. 110–116. Available at: https://doi.org/10.1002/jnr.10271.

Molofsky, A.V. *et al.* (2014) 'Astrocyte-encoded positional cues maintain sensorimotor circuit integrity', *Nature*, 509(7499), pp. 189–194. Available at: https://doi.org/10.1038/nature13161.

Nimmerjahn, F. and Ravetch, J.V. (2006) 'Fcgamma receptors: old friends and new family members', *Immunity*, 24(1), pp. 19–28. Available at: https://doi.org/10.1016/j.immuni.2005.11.010.

Niu, N. *et al.* (2012) 'IgG Expression in Human Colorectal Cancer and Its Relationship to Cancer Cell Behaviors', *PLoS ONE*, 7(11), p. e47362. Available at: https://doi.org/10.1371/journal.pone.0047362.

Noriega-Prieto, J.A. and Araque, A. (2021) 'Sensing and Regulating Synaptic Activity by Astrocytes at Tripartite Synapse', *Neurochemical Research*, 46(10), pp. 2580–2585. Available at: https://doi.org/10.1007/s11064-021-03317-x.

Oberheim, N.A. *et al.* (2009) 'Uniquely Hominid Features of Adult Human Astrocytes', *The Journal of Neuroscience*, 29(10), pp. 3276–3287. Available at: https://doi.org/10.1523/JNEUROSCI.4707-08.2009.

Perez-Catalan, N.A., Doe, C.Q. and Ackerman, S.D. (2021) 'The role of astrocyte-mediated plasticity in neural circuit development and function', *Neural Development*, 16, p. 1. Available at: https://doi.org/10.1186/s13064-020-00151-9.

Perry, M.C. and Kyle, R.A. (1975) 'The clinical significance of Bence Jones proteinuria', *Mayo Clinic Proceedings*, 50(5), pp. 234–238.

Poplawski, S. (2014) 'The Regulation of Gene Expression During Memory Consolidation in the Hippocampus', *Publicly Accessible Penn Dissertations* [Preprint]. Available at: https://repository.upenn.edu/edissertations/1408.

Puls, B. *et al.* (2020) 'Regeneration of Functional Neurons After Spinal Cord Injury via in situ NeuroD1-Mediated Astrocyte-to-Neuron Conversion', *Frontiers in Cell and Developmental Biology*, 8, p. 591883. Available at: https://doi.org/10.3389/fcell.2020.591883.

Qiu, X. *et al.* (2003) 'Human epithelial cancers secrete immunoglobulin g with unidentified specificity to promote growth and survival of tumor cells', *Cancer Research*, 63(19), pp. 6488–6495.

Quanico, J. *et al.* (2018) '3D MALDI mass spectrometry imaging reveals specific localization of long-chain acylcarnitines within a 10-day time window of spinal cord injury', *Scientific Reports*, 8(1), p. 16083. Available at: https://doi.org/10.1038/s41598-018-34518-0.

Raghavan, M. and Bjorkman, P.J. (1996) 'Fc receptors and their interactions with immunoglobulins', *Annual Review of Cell and Developmental Biology*, 12, pp. 181–220. Available at: https://doi.org/10.1146/annurev.cellbio.12.1.181.

Raju, T.S. (2008) 'Terminal sugars of Fc glycans influence antibody effector functions of IgGs', *Current Opinion in Immunology*, 20(4), pp. 471–478. Available at: https://doi.org/10.1016/j.coi.2008.06.007.

Reemst, K. *et al.* (2016) 'The Indispensable Roles of Microglia and Astrocytes during Brain Development', *Frontiers in Human Neuroscience*, 10. Available at: https://www.frontiersin.org/articles/10.3389/fnhum.2016.00566 (Accessed: 21 August 2022).

Reiber, H., Ungefehr, S. and Jacobi, C. (1998) 'The intrathecal, polyspecific and oligoclonal immune response in multiple sclerosis', *Multiple Sclerosis (Houndmills, Basingstoke, England)*, 4(3), pp. 111–117. Available at: https://doi.org/10.1177/135245859800400304.

Sacks, D. *et al.* (2018) 'Multisociety Consensus Quality Improvement Revised Consensus Statement for Endovascular Therapy of Acute Ischemic Stroke', *International Journal of Stroke: Official Journal of the International Stroke Society*, 13(6), pp. 612–632. Available at: https://doi.org/10.1177/1747493018778713.

Scallon, B.J. *et al.* (2007) 'Higher levels of sialylated Fc glycans in immunoglobulin G molecules can adversely impact functionality', *Molecular Immunology*, 44(7), pp. 1524–1534. Available at: https://doi.org/10.1016/j.molimm.2006.09.005.

Schitine, C. *et al.* (2015) 'Astrocyte heterogeneity in the brain: from development to disease', *Frontiers in Cellular Neuroscience*, 9, p. 76. Available at: https://doi.org/10.3389/fncel.2015.00076.

Schlachetzki, F., Zhu, C. and Pardridge, W.M. (2002) 'Expression of the neonatal Fc receptor (FcRn) at the blood-brain barrier', *Journal of Neurochemistry*, 81(1), pp. 203–206. Available at: https://doi.org/10.1046/j.1471-4159.2002.00840.x.

Sela-Culang, I., Kunik, V. and Ofran, Y. (2013) 'The Structural Basis of Antibody-Antigen Recognition', *Frontiers in Immunology*, 4. Available at: https://www.frontiersin.org/articles/10.3389/fimmu.2013.00302 (Accessed: 27 September 2022).

Serwanski, D.R., Jukkola, P. and Nishiyama, A. (2017) 'Heterogeneity of astrocyte and NG2 cell insertion at the node of Ranvier', *The Journal of comparative neurology*, 525(3), pp. 535–552. Available at: https://doi.org/10.1002/cne.24083.

Shinjyo, N. *et al.* (2009) 'Complement-derived anaphylatoxin C3a regulates in vitro differentiation and migration of neural progenitor cells', *Stem Cells (Dayton, Ohio)*, 27(11), pp. 2824–2832. Available at: https://doi.org/10.1002/stem.225.

Sofroniew, M.V. (2020) 'Astrocyte Reactivity: Subtypes, States, and Functions in CNS Innate Immunity', *Trends in Immunology*, 41(9), pp. 758–770. Available at: https://doi.org/10.1016/j.it.2020.07.004.

Staflin, K. *et al.* (2009) 'Identification of proteins involved in neural progenitor cell targeting of gliomas', *BMC Cancer*, 9, p. 206. Available at: https://doi.org/10.1186/1471-2407-9-206.

Tai, W. *et al.* (2021) 'In vivo reprogramming of NG2 glia enables adult neurogenesis and functional recovery following spinal cord injury', *Cell stem cell*, 28(5), pp. 923-937.e4. Available at: https://doi.org/10.1016/j.stem.2021.02.009.

Takahashi, S. (2022) 'Metabolic Contribution and Cerebral Blood Flow Regulation by Astrocytes in the Neurovascular Unit', *Cells*, 11(5), p. 813. Available at: https://doi.org/10.3390/cells11050813.

Tang, J. *et al.* (2018) 'Lung squamous cell carcinoma cells express non-canonically glycosylated IgG that activates integrin-FAK signaling', *Cancer Letters*, 430, pp. 148–159. Available at: https://doi.org/10.1016/j.canlet.2018.05.024.

Tao, Y. and Zhang, S.-C. (2016) 'Neural Subtype Specification from Human Pluripotent Stem Cells', *Cell Stem Cell*, 19(5), pp. 573–586. Available at: https://doi.org/10.1016/j.stem.2016.10.015.

Upender, M. b. *et al.* (1997) 'Immunoglobulin molecules are present in early-generated neuronal populations in the rat cerebral cortex and retina', *Journal of Comparative Neurology*, 384(2), pp. 271–282. Available at: https://doi.org/10.1002/(SICI)1096-9861(19970728)384:2<271::AID-CNE7>3.0.CO;2-Z.

Vanderperre, B. *et al.* (2013) 'Direct Detection of Alternative Open Reading Frames Translation Products in Human Significantly Expands the Proteome', *PLOS ONE*, 8(8), p. e70698. Available at: https://doi.org/10.1371/journal.pone.0070698.

Verghese, S. and Moberg, K. (2019) 'Roles of Membrane and Vesicular Traffic in Regulation of the Hippo Pathway', *Frontiers in Cell and Developmental Biology*, 7, p. 384. Available at: https://doi.org/10.3389/fcell.2019.00384.

Vidarsson, G., Dekkers, G. and Rispens, T. (2014) 'IgG Subclasses and Allotypes: From Structure to Effector Functions', *Frontiers in Immunology*, 5, p. 520. Available at: https://doi.org/10.3389/fimmu.2014.00520.

Vikartovska, Z. *et al.* (2020) 'Stem Cell Conditioned Medium Treatment for Canine Spinal Cord Injury: Pilot Feasibility Study', *International Journal of Molecular Sciences*, 21(14), p. 5129. Available at: https://doi.org/10.3390/ijms21145129.

Wang, Z. *et al.* (2020) 'Cancer-derived sialylated IgG promotes tumor immune escape by binding to Siglecs on effector T cells', *Cellular and Molecular Immunology*, 17(11), pp. 1148–1162. Available at: https://doi.org/10.1038/s41423-019-0327-9.

Wilde, C. *et al.* (2002) 'Interaction of the Rho-ADP-ribosylating C3 Exoenzyme with RalA *', *Journal of Biological Chemistry*, 277(17), pp. 14771–14776. Available at: https://doi.org/10.1074/jbc.M201072200.

Wu, X. and Xu, X. (2016) 'RhoA/Rho kinase in spinal cord injury', *Neural Regeneration Research*, 11(1), pp. 23–27. Available at: https://doi.org/10.4103/1673-5374.169601.

Yang, B. *et al.* (2013) 'Correlation of immunoglobulin G expression and histological subtype and stage in breast cancer', *PloS One*, 8(3), p. e58706. Available at: https://doi.org/10.1371/journal.pone.0058706.

Yeo, S.J. *et al.* (2004) 'Development of a Rat Model of Graded Contusive Spinal Cord Injury Using a Pneumatic Impact Device', *Journal of Korean Medical Science*, 19(4), pp. 574–580. Available at: https://doi.org/10.3346/jkms.2004.19.4.574.

Zaoui, K. *et al.* (2008) 'Memo–RhoA–mDia1 signaling controls microtubules, the actin network, and adhesion site formation in migrating cells', *The Journal of Cell Biology*, 183(3), pp. 401–408. Available at: https://doi.org/10.1083/jcb.200805107.

Zhang, J. *et al.* (2013) 'Neuron-derived IgG protects dopaminergic neurons from insult by 6-OHDA and activates microglia through the FcγR I and TLR4 pathways', *The International Journal of Biochemistry & Cell Biology*, 45(8), pp. 1911–1920. Available at: https://doi.org/10.1016/j.biocel.2013.06.005.

Zheng, J. *et al.* (2009) 'Immunoglobulin Gene Transcripts Have Distinct VHDJH Recombination Characteristics in Human Epithelial Cancer Cells', *The Journal of Biological Chemistry*, 284(20), pp. 13610–13619. Available at: https://doi.org/10.1074/jbc.M809524200.